

**Anti-infectives for Novel Targets:  
Development of Inhibitors targeting  
CYP121 from *Mycobacterium tuberculosis*  
and  
LasB from *Pseudomonas aeruginosa***

**Dissertation**

Zur Erlangung des Grades  
des Doktors der Naturwissenschaften  
der Naturwissenschaftlich-technischen Fakultät  
der Universität des Saarlandes

von

**M. Sc. Isabell Walter**

Saarbrücken

2019

Tag des Kolloquiums: 05.07.2019

Dekan: Prof. Dr. Guido Kickelbick

Berichterstatter: Prof. Dr. Rolf W. Hartmann

Prof. Dr. Christian Ducho

Akad. Mitglied: Dr. Jessica Hoppstädter

Vorsitz: Prof. Dr. Claus-M. Lehr

Die vorliegende Arbeit wurde von Dezember 2015 bis Dezember 2018 unter Anleitung von Herrn Univ.-Prof. Dr. Rolf W. Hartmann in der Fachrichtung Pharmazeutische und Medizinische Chemie der Naturwissenschaftlich-Technischen Fakultät der Universität des Saarlandes sowie am Helmholtz-Institut für Pharmazeutische Forschung Saarland (HIPS) in der Abteilung Drug Design and Optimization (DDOP) angefertigt.



‘Only those who will risk going too far can possibly find out how far one can go’

T. S. Eliot

## Summary

Infectious diseases remain a serious threat to human health. The rise of antibiotic resistances in combination with the low output of novel antibiotics in the last decades poses a severe challenge to anti-infective treatment. There are two main strategies in the fight against pathogens: the traditional approach to attack bacterial survival or the blockade of bacterial virulence without killing the bacteria by pathoblockers. In this thesis these two approaches are utilized for the development of inhibitors against CYP121 from *Mycobacterium tuberculosis* and LasB from *Pseudomonas aeruginosa*.

A screening approach led to the identification of a class of biaryl imidazoles as potent inhibitors of the essential CYP121. The elucidation of the relationship of structure to affinity and antimycobacterial activity shed light on the complex correlation of both properties. Different mode of action studies supported that CYP121 inhibition is the main reason for the antimycobacterial activity of the novel compounds.

For the virulence factor LasB, structure-based approaches were used to optimize inhibitors in the class of N-aryl mercaptoacetamides. Synthesized inhibitors of the  $\alpha$ -benzyl mercaptoacetamides showed a significant increase in activity. Furthermore, a potent hydroxamate derivative could prove that LasB inhibition is an effective method to reduce virulence.

## Zusammenfassung

Infektionskrankheiten bleiben eine ernsthafte Bedrohung für die menschliche Gesundheit. Der Anstieg der Antibiotikaresistenzen sowie die geringe Zahl neuer Antibiotika in den letzten Jahrzehnten stellt die Behandlung von Infektionen vor schwere Herausforderungen. Es gibt zwei Hauptstrategien im Kampf gegen Pathogene: die traditionelle Herangehensweise, das Überleben der Bakterien zu verhindern oder die bakterielle Virulenz mit Pathoblockern zu reduzieren ohne die Bakterien zu töten. In dieser Dissertation wurden beide Methoden verwendet um neue Inhibitoren gegen CYP121 von *Mycobacterium tuberculosis* und LasB von *Pseudomonas aeruginosa* zu entwickeln.

Ein Screening-Ansatz führte zur Identifizierung einer Klasse von Biaryl-Imidazolen als Inhibitoren des essentiellen CYP121. Die Aufklärung der Beziehung zwischen Struktur und Affinität beziehungsweise Aktivität beleuchtete den komplexen Zusammenhang beider Eigenschaften. Verschiedene Studien zur Wirkungsweise verdeutlichen, dass die Inhibition von CYP121 hauptverantwortlich für die antimykobakterielle Aktivität ist.

Für den Virulenzfaktor LasB wurden Struktur-basierte Ansätze genutzt um Inhibitoren vom N-Aryl Mercaptoacetamid-Typ zu optimieren. Die synthetisierten  $\alpha$ -Benzyl Mercaptoacetamide zeigten eine deutlich gesteigerte Aktivität. Des Weiteren, konnten potente Hydroxamat-Derivate zeigen, dass die Inhibition von LasB eine effektive Methode zur Reduzierung der Virulenz ist.

## **Publications included in this Thesis**

### **Publication A:**

Biophysical Screening of a Focused Library for the Discovery of CYP121 Inhibitors as Novel Antimycobacterials

Christian Brengel, Andreas Thomann, Alexander Schiffrin, Giuseppe Allegretta, Ahmed A. M. Kamal, Jörg Haupenthal, Isabell Schnorr, Sang Hyun Cho, Scott G. Franzblau, Martin Empting, Jens Eberhard, Rolf W. Hartmann

*ChemMedChem* **2017** 12 (19), 1616-1626

DOI: 10.1002/cmdc.201700363

### **Publication B:**

Tackling *Pseudomonas aeruginosa* Virulence by a Hydroxamic Acid-Based LasB Inhibitor

Andreas M. Kany, Asfandyar Sikandar, Samir Yahiaoui, Jörg Haupenthal, Isabell Walter, Martin Empting, Jesko Köhnke, and Rolf W. Hartmann

*ACS Chemical Biology* **2018** 13 (9), 2449-2455

DOI: 10.1021/acscchembio.8b00257

## **Contribution Report**

### **Publication A**

The author was involved in heterologous expression and purification of CYP121, determination of  $K_D$  and  $MIC_{50}$  values and in manuscript preparation.

### **Publication B**

The author performed and analyzed experiments to determine the Michaelis-Menten constant of LasB.

**Abbreviations**

ADAM	A disintegrin and metalloproteinase
AMP	antimicrobial peptide
BCG	Bacillus Calmette-Guérin
CDI	carbonyldiimidazole
CDP	cyclodipeptide
CDPS	cyclodipeptide synthase
CF	cystic fibrosis
CFU	colony forming unit
CYP	cytochrome P450
cYY	cyclo-di-L-tyrosine
Da	Dalton
DKP	diketopiperazine
DNA	deoxyribonucleic acid
DOPA	3,4-dihydroxyphenylalanine
DPhG	Deutsche Pharmazeutische Gesellschaft
eDNA	extracellular DNA
EDTA	ethylenediaminetetraacetic acid
FDA	Food and Drug Administration
FRET	Förster resonance energy transfer
HCV	hepatitis C virus
HDAC	histone deacetylase
HIV	human immunodeficiency virus
HPLC	high-performance liquid chromatography
IPTG	isopropyl- $\beta$ -D-thiogalactopyranoside
LB	lysogenic broth medium
LC	liquid chromatography
MDR	multiple-drug-resistance
MMP	matrix metalloprotease
MRSA	methicillin-resistant <i>Staphylococcus aureus</i>
MS	mass spectrometry
Mtb	<i>Mycobacterium tuberculosis</i>
MWCO	molecular weight cut-off

NADH	nicotinamide adenine dinucleotide
NADPH	nicotinamide adenine dinucleotide phosphate
NDK	nucleoside-diphosphate kinase
NRPS	nonribosomal peptide synthetase
PCET	proton-coupled electron-transfer
PDB	protein Data Bank
RNA	ribonucleic acid
SAR	structure-activity relationship
SDS-PAGE	sodium docecylsulphate polyacrylamidegelelectrophoresis
SPR	surface plasmon resonance
TB	tuberculosis
TB-medium	terrific broth medium
TDR	totally-drug-resistance
TLC	thin layer chromatography
WHO	World Health Organization
XDT	extensive drug resistance

## Table of Contents

Summary .....	VI
Zusammenfassung .....	VII
Publications included in this Thesis .....	VIII
Contribution Report.....	IX
Abbreviations .....	X
Table of Contents .....	XII
1 Introduction .....	1
1.1 Bacterial Infections and Anti-Infective Development.....	1
1.1.1 Antibiotics and Resistances .....	1
1.1.2 Strategies to Combat Bacterial Infections.....	2
1.1.3 Drug Discovery Approaches .....	3
1.2 <i>Mycobacterium tuberculosis</i> .....	5
1.2.1 Tuberculosis and Characteristics of <i>Mycobacterium tuberculosis</i> .....	5
1.2.2 Mycobacterial Cytochrome P450s as Potential Targets .....	6
1.2.3 CYP121: Properties and Inhibitors .....	7
1.3 <i>Pseudomonas aeruginosa</i> .....	10
1.3.1 Characteristics of <i>Pseudomonas aeruginosa</i> .....	10
1.3.2 Virulence Factors as Potential Targets.....	10
1.3.3 LasB: Properties and Inhibitors .....	11
2 Aim of the Thesis .....	14
3 Results .....	16
3.1 Chapter A: Biophysical Screening of a Focused Library for the Discovery of CYP121 Inhibitors as Novel Antimycobacterials <sup>186</sup> .....	16
3.2 Chapter B: Structure-Activity Relationship and Mode of Action Studies Highlight 1-(4-Biphenylmethyl)-1H-imidazole Derived Small Molecules as Potent <i>Mycobacterium tuberculosis</i> CYP121 Inhibitors .....	28
3.3 Chapter C: Fragment-based Design of $\alpha$ -substituted Mercaptoacetamides as Inhibitors of the Virulence Factor LasB from <i>Pseudomonas aeruginosa</i> .....	47
3.4 Chapter D: Tackling <i>Pseudomonas aeruginosa</i> Virulence by a Hydroxamic Acid-Based LasB Inhibitor <sup>215</sup> .....	66
4 Final Discussion .....	74
4.1 CYP121 .....	74
4.1.1 Biological Function.....	75

4.1.2 Library Screening.....	76
4.1.3 Binding Mode .....	77
4.1.4 Affinity vs. Activity .....	78
4.1.5 Mode of action studies .....	80
4.1.6 Intracellular Replication in Macrophages .....	81
4.2 LasB.....	82
4.2.1 Structure-based Approaches .....	82
4.2.2 Binding Mode .....	83
4.2.3 SAR.....	84
4.2.4 Selectivity & Cytotoxicity .....	85
4.2.5 Cellular Activity.....	86
4.3 Conclusion and Outlook .....	86
5 References .....	88
6 Acknowledgement.....	103
7 Appendix .....	105
7.1 Supporting Information .....	105
7.1.1 Supporting Information for Chapter 3.1 .....	105
7.1.2 Supporting Information for Chapter 3.2 .....	133
7.1.3 Supporting Information for Chapter 3.3 .....	148
7.1.4 Supporting Information for Chapter 3.4 .....	153
7.2 Conference Contributions.....	160



# 1 Introduction

## 1.1 Bacterial Infections and Anti-Infective Development

### 1.1.1 Antibiotics and Resistances

Bacteria are ubiquitous and most of the people see them as a threat. However, the main part of the bacteria does no harm.<sup>1</sup> They are useful and essential for the human survival. They colonize the inside and outside of the human body and ideally coexist happily with their host.<sup>2-6</sup> However, bacteria can cause infections.

Nowadays, we are increasingly confronted with the topic of severe and life-threatening bacterial infections and resistant pathogens.<sup>7</sup> There are reports about epidemics in hospitals or health care facilities all around the world and deaths caused by bacteria which do not respond to any known antibiotic.<sup>8-10</sup> Additionally, there are still local outbreaks of hazardous diseases such as cholera and Ebola in parts of Africa.<sup>11,12</sup> The awareness that not each infection can be easily cleared by swallowing a pill is slowly awakening. However, among scientists it is well known that the 'golden era' of antibiotics is long gone.<sup>13,14</sup>

The rise of the antibiotics began around 1930 to 1940 with the discovery of the antibacterial activity of sulfonamides.<sup>15</sup> These were followed by the first use of penicillin in 1942 which was discovered by Alexander Fleming in 1928.<sup>16-18</sup> It was the life-saver for many soldiers in the Second World War and soon after that was used as standard medication for infections caused by gram-positive bacteria.<sup>19</sup> However, already in 1945, more than 20 % of *Staphylococcus aureus* hospital isolates showed resistance to the  $\beta$ -lactam antibiotic.<sup>16</sup>

The mode of action of  $\beta$ -lactam antibiotics, to which penicillin belongs, is based on the inhibition of the cell wall biosynthesis caused by the binding to DD-transpeptidase<sup>20,21</sup> However, some bacteria possess enzymes called  $\beta$ -lactamases which are able to cleave the lactam structure and thereby inactivate these drugs.<sup>22</sup> This kind of resistance may be suppressed by the simultaneous administration of  $\beta$ -lactamase inhibitors.<sup>23</sup> However, there are other resistance mechanisms. For example, the bacteria can express a modified target – in this case the transpeptidase - which is not inhibited by the administered drug.<sup>24</sup>

In the following decades there were more and more antibiotics discovered such as for example streptomycin, gentamicin (both aminoglycosides), tetracycline and vancomycin. However, resistant strains were in most cases observed immediately or after a few years except for vancomycin. It was rarely used in the first decade after its development (1958) in order to preserve it as back-up antibiotic. But soon after its rising use in the 1980s, also vancomycin-resistant strains occurred.<sup>16</sup>

Interestingly, resistances do not only evolve within one strain but can be transferred to other strains through plasmids that carry the respective resistance genes.<sup>25,26</sup> The possibility of this relatively quick transfer led to the development of strains with accumulated resistances against different antibiotics.<sup>26,27</sup> One of the most popular representatives of these is the methicillin-resistant *Staphylococcus aureus* (MRSA).<sup>16</sup>

However, nowadays there are resistant strains known for almost all pathogens.<sup>28</sup> The WHO recently prioritized the so called ESKAPE pathogens as the most critical ones due to the threatening lack of available treatment options.<sup>29</sup> Currently, these pathogens are the leading causative agents of nosocomial infections.<sup>30</sup> Furthermore, there are infections which are widespread (although latent) among the world's population such as tuberculosis (TB) caused by *Mycobacterium tuberculosis* (Mtb).<sup>31</sup> Although there are still treatment options available for TB, they are often ineffective and rising resistances additionally complicate the situation.<sup>32,33</sup>

### **1.1.2 Strategies to Combat Bacterial Infections**

The human body is an expert in the fight against bacteria. First of all, it has several barriers that non-specifically prevent their entrance.<sup>34</sup> The most obvious is probably the skin, which not only poses a mechanical barrier but is also to some extent bactericidal due to its acid mantle.<sup>35-37</sup> Another well-known barrier is the system of mucus and ciliated epithelium in the respiratory tract. It scavenges incoming bacteria of the breathing air preventing a deeper invasion into the throat or lung.<sup>38</sup> Trapped in the mucus the invaders can be neutralized by the most effective defensive system of the human body: the immune system. The human immune system is highly complex and due to its relevance also extensively scientifically explored. Nevertheless, there are still some weakly understood or unknown mechanisms, processes and interactions.

Despite all defensive mechanisms of the human body, bacteria can and do cause infections. These affect both, healthy and immuno-compromised individuals. The latter group comprises humans with autoimmune diseases or genetic disorders or individuals infected with HIV for example.<sup>39</sup> Bacteria often enter the host through impaired barriers caused by wounds or disturbed mucous membranes. Furthermore, infections may establish in case of a weakened or disordered immune system.

Bacterial infections are usually treated with antibiotics. In the ideal situation, the administered drug will eradicate the infection by killing the bacteria or impairing their replication. The decreased number of bacteria can be eliminated by the immune system.<sup>40</sup> However, as described beforehand, individual bacteria of a population (or the whole population) can be resistant to the used antibiotic or become resistant in the course of the treatment. These will

continue replication and subsequently constitute the majority of the population. The result is an ongoing infection which has to be treated with a different drug to achieve the desired therapeutic effect. During the time needed to identify a suitable antibiotic, the bacteria may cause irreparable damage or the death of the patient.

In some cases, bacteria carry too many resistances so that no effective drug can be found.<sup>16</sup> Furthermore, some infections need increased treatment duration due to weak drug efficacy. The prolonged bacterial survival (statistically) increases the occurrence of resistances.<sup>26</sup> An additional disadvantage of the administration of antibiotics is the destruction of the patients gut microbiome which may lead to serious health problems.<sup>41</sup>

A different strategy to fight bacterial infections is called anti-virulence approach. This strategy aims at disarming the bacteria rather than killing them and is based on the fact that bacteria produce virulence factors. Bacteria use them to damage their host or to ensure or facilitate survival. Some virulence factors can deconstruct tissue or immune system components while others are used for the communication between bacteria.<sup>42-45</sup> The idea behind the anti-virulence approach is the inhibition of the production or the inactivation of one or several virulence factors. In this way, the overall virulence of the bacteria is reduced and the infection can be cleared by the immune system.

The anti-virulence approach has some advantages over the classical antibiotic strategy. Firstly, the risk of resistance development is significantly decreased as the therapy will not target an essential bacterial target. Additionally, as the virulence factors are unique it is unlikely that occurring resistances will be transferred to other species. Another important factor is that the intestinal flora of the host will probably not be affected by the drug.<sup>42-45</sup>

However, there are also some disadvantages of this strategy. It may be necessary to combine several anti-virulence drugs or to co-administer an antibiotic to achieve a significant effect. As some virulence factors are only active in a distinct stage of the infection, the time of drug administration must coincide with the time that the virulence factor is actively involved in the infection.<sup>42,43</sup>

### **1.1.3 Drug Discovery Approaches**

In the field of drug discovery there are basically two strategies applied: the structure-based or the ligand-based approach.

The structure-based approach can be used if the structure of the target is known. The structure may be in form of an experimentally determined 3D structure of the target protein (via X-Ray crystal structure analysis for example).<sup>46,47</sup> If there is no such 3D structure available a homology

model can be prepared. This possibility is dependent on whether there is a 3D structure of a similar or related protein available which can serve as template. In this case, the sequences of both proteins are superimposed to analyze differences. Ideally, the sequence parts which constitute the binding pocket should be identical (conserved) or at least highly similar. With the aid of a special software, the 3D structure of the target protein can be modelled according to the template. The higher the similarity between the two proteins the more accurate and reliable the homology model will be.<sup>48,49</sup>

With a 3D structure in hand there are again two possibilities. In case of known ligands (either through co-crystallization or docking studies with known inhibitors) the ligand can be rationally modified. For example, functional groups can be exchanged, removed, added or shifted. The ligand can be enlarged in one or more directions or substituents can be exchanged or added.<sup>46,47</sup> In the case of no known ligands, virtual screening (of a compound library) can be applied to identify other potential ligands.<sup>50</sup> Another possibility is to design ligands 'by hand'. This so-called *de novo* design is based on the connection of small fragments inside the binding pocket and is typically performed with the aid of computer programs.<sup>51,52</sup> In both cases the binding of the identified or created ligands to the target should be confirmed experimentally before further optimization processes.<sup>46,53</sup>

In contrast, the ligand-based approach relies on the existence of one or several ligands of the same structural class. The affinity, for example in form of an  $IC_{50}$  or  $K_D$  value, is compared to the molecular weight and the ligand may be downsized until an acceptable coefficient is achieved.<sup>54</sup> With this starting point in hand the ligand can be modified as described beforehand for the structure-based approach. Additionally, ligands with similar features can be identified through the screening of a database.<sup>55,56</sup>

If several diverse ligands of the target protein are known, a pharmacophore model can be created. Therefor the ligands are superimposed and essential molecular features as well as their spatial position to each other are identified. This model can be used for the creation of new ligands or the screening of a database. If several ligands with different affinities are known it may be possible to prioritize the molecular features. Additionally, in case of known inactive ligands it may be possible to define 'forbidden' areas which are probably occupied by the protein itself.<sup>57,58</sup>

## **1.2 *Mycobacterium tuberculosis***

### **1.2.1 Tuberculosis and Characteristics of *Mycobacterium tuberculosis***

*Mycobacterium tuberculosis* (Mtb) is the causative agent of the disease tuberculosis (TB). According to the WHO, TB is the infectious disease that causes the most deaths worldwide. In 2017, the WHO announced about 10 million new infections and 1.6 million deaths related to the disease.<sup>59</sup> The estimated amount of infected people is as high as one third of the world's population. Most of the infections are located in the lung (pulmonary tuberculosis); however, also other organs or tissues can be infected.<sup>59,60</sup>

Upon infection, the mycobacteria may be eliminated by the immune system or cause an acute or latent infection. Mtb can survive and replicate inside macrophages and induces the formation of so-called granulomas.<sup>61,62</sup> These consist of infected macrophages, T cells, B cells and giant cells. In this assembly, the mycobacteria can rest, in a dormant state, for several years or decades inside their host (latent infection). From this state, the infection may eventually be reactivated to an acute infection.<sup>61</sup> In principal, such a reactivation is caused by circumstances which lead to a general weakening of the immune system for example through a HIV infection.<sup>63</sup>

The current treatment options comprise a number of so-called first-line and second-line drugs.<sup>64</sup> These are typically administered in a combination therapy for several months.<sup>65</sup> However, latent infections are extremely difficult to treat due to granuloma formation and the dormant state of the bacteria.<sup>66,67</sup> Additionally, Mtb has developed various resistances which further complicate TB treatment.<sup>64,68</sup>

Mtb cannot be classified into the groups of gram-positive or gram-negative bacteria as the staining method is not applicable in this case.<sup>69,70</sup> However, it can be stained with other, acid-fast methods for example the Ziehl-Neelsen stain.<sup>71</sup> The reason thereof is that Mtb possesses a special cell wall construction which contains a high amount of mycolic acids. This results in a thick, wax-like cell wall with a complex permeability behaviour.<sup>72,73</sup>

The cell wall is composed of two main parts: an inner covalent part and an outer non-covalent part. The inner covalently connected, lipophilic core consists of a layer of peptidoglycan which is placed directly above the membrane. The peptidoglycan layer is connected with the polysaccharide arabinogalactan which itself is connected with mycolic acids.<sup>72</sup> These consist of short  $\alpha$ -chains and longer meromycolic acid chains.<sup>74</sup> The second non-covalent part of the Mtb cell wall consists of free lipids which complement the short and long mycolic acid chains, respectively. These comprise for example sulfolipids and the so-called cord-factor and play a major role in Mtb's pathogenicity and virulence.<sup>75-77</sup> Additionally, this outer cell wall part

contains various components such as proteins, phosphatidyl mannoside, phthiocerol lipids, lipomannan and lipoarabinomannan which all contribute to the overall complexity of the cell wall.<sup>78-82</sup>

As the cell wall contributes essentially to the viability and pathogenicity of Mtb, its formation is an attractive target point for drugs. Indeed, isoniazid, one of the currently used first-line drugs, intervenes in cell wall formation. The effect of isoniazid is based on the inhibition of both the elongation of fatty acids and the synthesis of mycolic acid.<sup>83</sup> Isoniazid itself is a prodrug which is activated through the catalase-peroxidase enzyme KatG. The reactive product subsequently inhibits the target enoyl acyl carrier protein reductase InhA. Resistance to isoniazid is caused by a mutation in the *katG* gene or its deletion.<sup>64,84-86</sup>

A resistance against (at least) the two first-line drugs isoniazid and rifampicin is defined as multiple drug resistance (MDR).<sup>64</sup> Furthermore, increasing occurrence of extensively/totally drug resistant strains (XDR/TDR) was reported in the last years.<sup>87,88</sup>

All these described circumstances, the characteristics of Mtb, the current treatment options, the number of infections and deaths and the rising resistances, stress the need for novel effective drugs against Mtb.

### **1.2.2 Mycobacterial Cytochrome P450s as Potential Targets**

The genome of Mtb was published in 1998 by Cole *et al.* and revealed an overproportioned amount of 20 Cytochrome P450 (CYP) enzymes.<sup>89-91</sup> In contrast, there are some bacteria without any CYP enzymes such as *Escherichia Coli*.<sup>92</sup> In comparison to the genome size, Mtb possesses 240-fold more CYPs than humans.<sup>93</sup>

CYP enzymes are abundant in nature, they occur in bacteria and fungi as well as in animals and humans. Their characteristic is a heme group consisting of an iron ion which is coordinated by a porphyrin scaffold. CYP enzymes belong to the group of monooxygenases which typically transfer an oxygen atom to their substrate.<sup>94</sup> In the catalyzed reaction, one atom of molecular oxygen is transferred while the second oxygen atom is reduced to water. The range of CYP-catalyzed reactions involves hydroxylations, epoxidations, dealkylations of sulfur, nitrogen or oxygen, oxidations of nitrogen or sulfur and others.<sup>95,96</sup> There are several proposals for the catalytic cycle in literature; however, the most probable one involves the following steps:<sup>95,97</sup>

1. The substrate coordinates to the active center, the iron ion, and shifts the coordinated water molecule away.
2. The heme iron is reduced from the oxidation state 3<sup>+</sup> to 2<sup>+</sup> with the help of an electron transport system and molecular oxygen is bound to the iron.

3. One more electron and two protons are transferred to the iron-oxygen complex. By this, one oxygen atom is released in the form of water and a reactive intermediate is formed: the iron-(IV)-oxo-porphyrin-radical-cation  $[\text{Fe}^{\text{IV}}=\text{O}]^{+\bullet}$  (called Compound I).

4. The oxygen atom of Compound I is incorporated into the substrate via a radical mechanism.

There are 57 human genes encoding CYPs which are typically membrane-bound and have diverse functions. They are involved in phase I metabolism of xenobiotics and in the biosynthesis of various compounds such as steroids for example.<sup>98–100</sup> In contrast, bacterial CYPs are mostly soluble and located in the cytosol. They catalyze various reactions and are involved in the processing of carbon sources or in the synthesis of secondary metabolites such as antimycotics or antiparasitics.<sup>101,102</sup>

There are several drugs which target CYP enzymes. Fungal infections are often treated with azoles that act as CYP51A1 inhibitors.<sup>103</sup> Furthermore, there are drugs targeting human CYP enzymes such as abiraterone which is a CYP17A1 inhibitor used in prostate cancer therapy.<sup>104</sup> CYP19A1 (aromatase) inhibitors are used in the treatment of breast cancer.<sup>105</sup> However, there are currently no drugs on the market which target bacterial CYP enzymes.

The 20 CYP enzymes of Mtb have been assigned due to their amino acid sequence. So far, structure or function was elucidated for some of them: Nine enzymes (CYP51, CYP125, CYP121, CYP142, CYP126, CYP130, CYP128, CYP144, CYP124) have been characterized to a certain extent and three of them (CYP121, CYP125 and CYP142) are currently considered as potential drug targets.<sup>93,97,101,106–109</sup>

### 1.2.3 CYP121: Properties and Inhibitors

CYP121 was shown to be expressed in Mtb cells and to be essential for the viability of Mtb.<sup>110</sup> Analysis of amino acid sequence shows that there are relatives present in some *Streptomyces* strains (maximum 66% identity).<sup>111</sup> However, one homologue in *S. venezuelae* (60 % identity) was shown to have different binding site residues which indicates a different substrate specificity.<sup>112</sup> Apart from that CYP121 is unique to a few representatives of mycobacteria.

The atomic structure of CYP121 was determined up to 1.06 Å by Leys *et al.* in 2003 (PDB-ID: 1N40).<sup>113</sup> It revealed a relatively large and rigid binding pocket (1350 Å<sup>3</sup>). The heme is slightly deformed by a proline residue (Pro246) so that it is not totally planar. Interestingly, a helix (helix I) is located near to the heme resulting in the occurrence of a positively charged arginine residue (Arg386) directly above the heme group.<sup>113</sup>

The function of CYP121 was elucidated after its neighboring gene (located in the same operon) was identified as a cyclo(L-Tyr-L-Tyr) (cYY) synthetase.<sup>114</sup> It turned out that CYP121 uses

cYY as substrate and catalyzes an unusual C-C bond formation between two *ortho* hydroxy atoms of the phenol rings resulting in a compound named mycocyclosin (Figure 1.1).<sup>115</sup> The reaction mechanism was evaluated with computer-based simulations by Dumas *et al.* in 2013.<sup>116</sup> They proposed that the oxy-complex is formed after substrate binding followed by the formation of Compound I which generates the first tyrosyl radical. A PCET reaction (proton coupled electron transfer) induced by Arg386 generates the second tyrosyl radical which creates a C-C bond with the formerly generated radical.

The analysis of the substrate specificity revealed that CYP121 is also capable to convert cyclo(L-Tyr-L-Trp) (cYW), but much slower than cYY.<sup>117</sup>

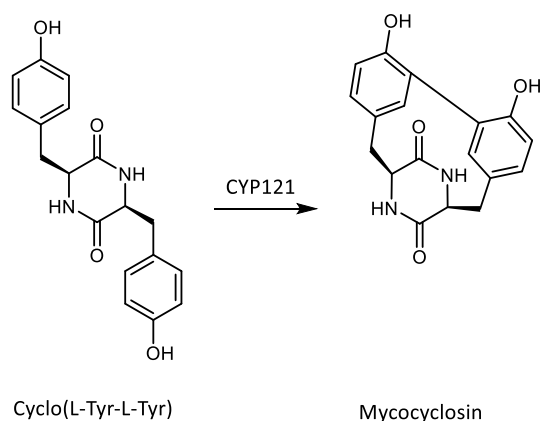


**Figure 1.1:** Schematic representation of the reaction catalyzed by CYP121. cYY is converted to mycocyclosin through a C-C bond formation between the two tyrosyl moieties.

The role of mycocyclosin has so far not been clarified. However, there are eukaryotic and prokaryotic enzymes known which generate analogues of cYY.<sup>118,119</sup> In some cases, these are also placed in gene clusters with enzymes that modify the respective cyclodipeptides.<sup>112,119</sup> Nevertheless, no other modification via C-C-coupling as for CYP121 is reported. Interestingly, the biological function of these cyclodipeptides and their derivatives is also unclear. However, cyclic dipeptides belong to the class of 2-5-diketopiperazines which is relatively abundant in nature and exerts various interesting functions (more discussion in chapter 4.1.1).<sup>120</sup>

As CYP121 belongs to the P450 family it was evaluated whether known CYP inhibitors bind to its catalytic center. Indeed, it was found that theazole antimycotics clotrimazole, econazole and fluconazole bind the heme iron of CYP121.<sup>121,122</sup> The determined  $K_D$  values correlate with the respective MIC values against *M. smegmatis* and Mtb.<sup>110,121</sup> There is a cocrystal structure with fluconazole which was determined by Seward *et al.* in 2006 (PDB-ID: 2IJ7). Interestingly, fluconazole does not directly coordinate to the iron with its triazole ring but coordinates the iron indirectly via a water molecule.<sup>123</sup>

Until now, there were several attempts undertaken to identify potent inhibitors of CYP121. Hudson *et al.* screened a fragment library and merged several fragments resulting in an azole compound with a  $K_D$  value of 28  $\mu\text{M}$  (Figure 1.2, compound 1).<sup>124</sup> Two follow-up studies applied fragment merging strategies which resulted in CYP121 binders with  $K_D$  values of 15  $\mu\text{M}$  (Figure 1.2, compound 3) and 15 nM (Figure 1.2, compound 2).<sup>125,126</sup> A different approach was applied by Fonvielle *et al.* who evaluated substrate modifications and identified cyclo(L-DOPA-L-Tyr) as binder with a  $K_D$  value of 15  $\mu\text{M}$  (Figure 1.2, compound 5).<sup>127</sup> A substrate fragmentation approach by Kavanagh *et al.* resulted in a CYP121 binder with a  $K_D$  value of 16  $\mu\text{M}$  (Figure 1.2, compound 7).<sup>128</sup> However, all of these compounds did either not show any antimycobacterial activity or respective data is missing in the publications. Recently, Abd El-wahab *et al.* designed azole substrate analogues and evaluated not only their affinity to CYP121 but also their antimycobacterial activity.<sup>129</sup> However, the best CYP121 binder ( $K_D = 81 \mu\text{M}$ ) had a  $\text{MIC}_{90} > 100 \mu\text{g/mL}$  (Figure 1.2, compound 6) and the best antimycobacterial compound ( $\text{MIC}_{90} = 12.5 \mu\text{g/mL}$ ) showed an affinity as low as 1435  $\mu\text{M}$  (Figure 1.2, compound 4).

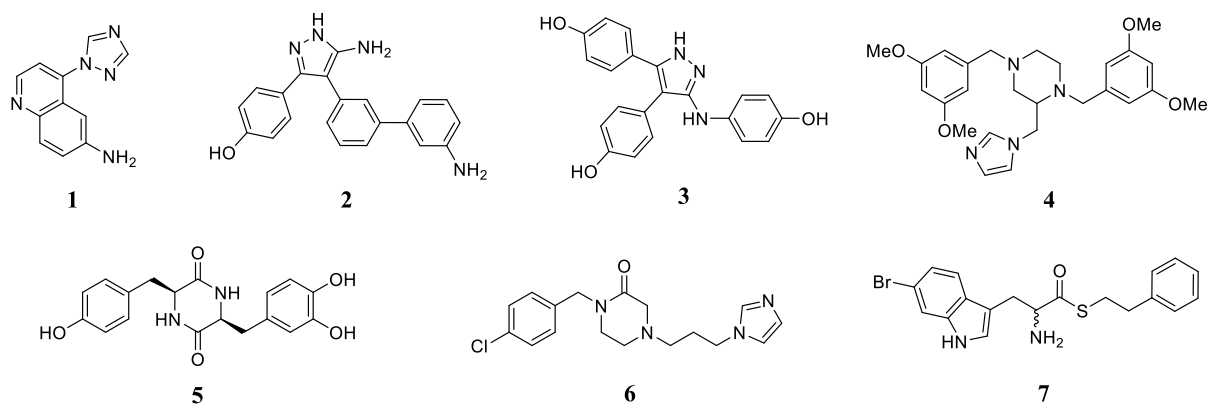


**Figure 1.2:** CYP121 inhibitors described in literature. 1:  $K_D = 28 \mu\text{M}$ <sup>124</sup>; 2:  $K_D = 15 \text{ nM}$ <sup>126</sup>; 3:  $K_D = 15 \mu\text{M}$ <sup>125</sup>; 4:  $K_D = 1435 \mu\text{M}$ <sup>129</sup>; 5:  $K_D = 15 \mu\text{M}$ <sup>117</sup>; 6:  $K_D = 81 \mu\text{M}$ <sup>129</sup>; 7:  $K_D = 16 \mu\text{M}$ <sup>128</sup>.

## **1.3 *Pseudomonas aeruginosa***

### **1.3.1 Characteristics of *Pseudomonas aeruginosa***

*Pseudomonas aeruginosa* is an opportunistic gram-negative bacterium which is omnipresent in moist environments such as water pipes, surface water, sinks, showers *et cetera*. It is the causative agent of around 10-20 % of all hospital acquired infections.<sup>30,130,131</sup> The main focus of infection is the lung which is especially harmful for cystic fibrosis patients.<sup>132-135</sup> Additionally, *P. aeruginosa* can cause infections of the eye, skin, urinary tract, respiratory tract or brain.<sup>37,131,136-139</sup>

The special properties of the bacterium constitute its unique pathogenicity, virulence and resistance.<sup>140</sup> A major part of *P. aeruginosa*'s intrinsic resistance is based on its cell envelope structure which is composed of two cell membranes.<sup>141</sup> The outer cell membrane of *P. aeruginosa* has an especially low permeability compared to other gram-negative bacteria.<sup>142</sup> An additional part of the bacterium's intrinsic resistance is based on its extensive efflux system which efficiently removes drugs from the inside.<sup>143,144</sup> Furthermore, *P. aeruginosa* has the ability to express  $\beta$ -lactamases which causes resistance to many  $\beta$ -lactam antibiotics.<sup>145</sup>

Besides the intrinsic resistance mechanisms, *P. aeruginosa* established various mutational resistances in the last decades.<sup>141</sup> Antibiotics of several classes can be administered in the case of an infection such as penicillins, cephalosporins, carbapenems, aminoglycosides and quinolones. However, resistances have been reported for all classes. In most cases, these are based on expression of  $\beta$ -lactamases, overexpression of efflux systems (caused by mutations) or target site mutations.<sup>140,141,146</sup>

*P. aeruginosa* developed a range of strategies to increase its pathogenicity and ensure its survival inside the host. It can adapt to environments with low oxygen supply or anaerobic conditions.<sup>147</sup> Furthermore, the bacteria have the ability to form biofilms in order to isolate themselves from attacks of the immune system or antibiotics.<sup>148</sup> Another important property is their extensive use of virulence factors, for example toxins and phenazines, which contribute significantly to pathogenicity and *P. aeruginosa*'s survival technique.<sup>149</sup>

### **1.3.2 Virulence Factors as Potential Targets**

The term "virulence factors" can be defined as molecules that are part of the promotion of a disease, host damage or the evasion of the host immune system. These include for example adhesins, toxins and siderophores but also factors that impact immune system modulation or

evasion and factors that affect regulatory systems or promote biofilm formation. These virulence factors are unique to a single species or closely related species.<sup>42,43</sup>

Due to the great impact of virulence factors on some diseases and the current lack of effective antibiotics, there is a strong interest in developing anti-virulence drugs. The principle of the anti-virulence approach is described in chapter 1.1.2.

Up to now there are only a few anti-virulence drugs approved for clinical use. These involve BabyBIG and BAT for *Clostridium botulinum*<sup>150</sup>, Raxibacumab<sup>151</sup> and Obiltoxaximab<sup>152</sup> for *Bacillus anthracis* and Bezlotoxumab<sup>153</sup> for *Clostridium difficile*. All of these agents target bacterial toxins which cause severe damage of the host.<sup>42</sup>

In 2017, there were nine anti-virulence drugs for *P. aeruginosa* in preclinical studies, one drug was in Phase I and II trials and one drug has failed in phase II. Most of them interfere with the four quorum sensing pathways of *P. aeruginosa*.<sup>42</sup> Quorum sensing is a system in which the bacteria regulate gene expression dependent on their population and the production of signal molecules. Due to the involvement of virulence factors in these systems they represent an interesting target.<sup>154</sup> However, one of the preclinical drugs also targets a single virulence factor: PcrV. PcrV is involved in the type III secretion system which can deliver toxins through the cell envelope.<sup>42,155,156</sup> In general, the anti-virulence approach seems to be a promising strategy in the development of drugs against *P. aeruginosa*.

### 1.3.3 LasB: Properties and Inhibitors

The virulence factor elastase (LasB) of *P. aeruginosa* belongs to the class of proteases and cleaves peptide bonds. It is a matrix metalloproteinase (MMP) of the thermolysin family (M4) which contains a zinc ion ( $Zn^{2+}$ ) in its active centre.<sup>157</sup> The zinc ion is tetrahedrally coordinated by two histidines, one glutamate and water as the fourth ligand.<sup>157</sup>

There are two proposed versions of the catalytic mechanism: In the first, the glutamate ligand acts as proton acceptor and in the second version one of the histidine ligands undertakes this role. In both mechanisms the water gets displaced towards the proton acceptor (Glu or His) upon substrate binding. One proton of the water molecule is transferred to the base while the lone pair of its oxygen attacks the peptide carbonyl-C. In the second step a proton is transferred to the peptide nitrogen and the positive charge is stabilized via surrounding amino acid residues. With the transfer of a second proton to the peptide nitrogen (via the base), the peptide bond is cleaved to a carboxylic acid and an amine.<sup>158–161</sup>

The first crystal structure of LasB was published by Thayer *et al* in 1991 (PDB-ID: 1EZM).<sup>162</sup> The first co-crystal structure was determined in 2004 (PDB-ID: 1U4G). The tertiary structure

is divided in two domains, C-terminal and N-terminal domain, which build the substrate binding pocket in their middle. The N-terminal domain contains the zinc binding motif HEXXH (H=His, E=Glu, X=any amino acid), which is conserved in the M4 family.<sup>157</sup> The C-terminal domain contains the zinc coordinating glutamate that is typically located 18-72 amino acids C-terminal to the HEXXH motif. The protein is proposed to undergo a hinge bending motion upon substrate or inhibitor binding.<sup>163,164</sup>

Another interesting feature of LasB or the MMP family in general is that the binding pocket consists of several subsites which determine substrate specificity and recognition. The main subsite is the S1' pocket which generally accommodates large hydrophobic residues. This subsite is surrounded by several subsites in the C-terminal (S1, S2, etc.) and N-terminal (S2', S3', etc.) direction. The differences of the subsites between the individual MMPs are especially important for the design of selective inhibitors.<sup>157,165,166</sup>

LasB is a major virulence factor of *P. aeruginosa* that is involved in host invasion, immunomodulation and biofilm formation.<sup>149,167</sup> It can degrade tissue components such as collagen, fibrin, casein and elastin.<sup>168-170</sup> The latter is an essential part of human lung tissue and blood vessels. LasB is also involved in corneal liquefaction during eye infections and the degradation of human wound fluids and skin proteins associated with chronic ulcers.<sup>171,172</sup> Additionally, LasB interferes with the human immune system: It can destroy human immunoglobulins A and G and is involved in the inactivation of the human cytokines gamma-interferon and tumor necrosis factor alpha.<sup>173-175</sup> Furthermore, it degrades serum alpha1-proteinase inhibitor and human bronchial mucosal proteinase inhibitor which usually protect the respiratory tract from proteolysis.<sup>176,177</sup>

Due to the significant impact of LasB upon *P. aeruginosa* infection several inhibitors have been identified and characterized so far, among which are two natural products: phosphoramidon (Figure 1.3, compound **1**) and *Streptomyces nigrescens* metallo-proteinase inhibitor (SMPI) which is a 102 amino acid protein.<sup>178,179</sup> The synthetic LasB inhibitors can be divided in two classes: peptidic and non-peptidic. The first group contains small peptides modified with zinc chelating groups such as thiol, hydroxamate or phosphoryl (Figure 1.3, compound **2**).<sup>179-182</sup> These compounds show *in vitro* activities up to submicromolar values. The second group consists of small molecules that contain thiol or hydroxamate as chelating motif and tropolones (Figure 1.3, compound **3-6**).<sup>165,183-185</sup> Their  $K_i$  values are typically in the two or single digit micromolar range.

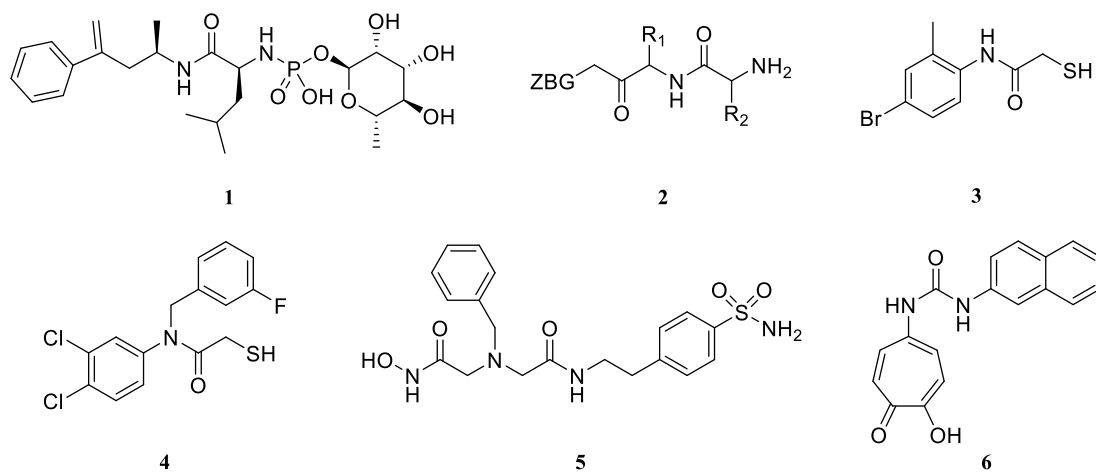


**Figure 1.3:** LasB inhibitors described in literature. **1:**  $IC_{50} = 40 \text{ nM}$ ;<sup>179</sup> **2:** ZBG = SH or NHOH or  $PO_3$ , R<sub>1</sub> and R<sub>2</sub> are amino acid residues;<sup>180,181</sup> **3:**  $IC_{50} = 1.8 \text{ }\mu\text{M}$ ;<sup>184</sup> **4:**  $IC_{50} = 12 \text{ }\mu\text{M}$ ;<sup>185</sup> **5:**  $IC_{50} = 0.4 \text{ }\mu\text{M}$ <sup>165</sup>; **6:**  $IC_{50} = 1.2 \text{ }\mu\text{M}$ <sup>183</sup>.

## 2 Aim of the Thesis

The rise and spread of antibiotic resistances in the last decades force the development of novel drugs against pathogenic bacteria. The two pathogens addressed in this thesis are *Pseudomonas aeruginosa* and *Mycobacterium tuberculosis* (Mtb). Both bacteria can cause severe and life-threatening infections which are difficult to treat due to limited treatment options and the unique characteristics of these pathogens.

For Mtb the classical antibiotic approach was pursued targeting an essential function of the bacteria. In this case, former results revealed that the Cytochrome P450 enzyme CYP121 is essential for viability. As the HIPS-DDOP group has a library of putative CYP inhibitors (which were originally designed to target human CYP enzymes) a screening approach should be initiated in order to identify potent CYP121 inhibitors (chapter 3.1). Upon identification of CYP121 binders these should be characterized by biological and biophysical methods (inhibition of mycobacterial growth, binding to iron-center of the enzyme, cytotoxicity, physicochemical properties) to define frontrunner compounds. As crystallographic data is available for CYP121, docking studies should propose the binding mode.

Upon identification of a hit compound the aim was to elucidate the structure-activity relationship via the evaluation of a second defined library that is created by selection of compounds from the in-house library and synthesis of promising candidates (chapter 3.2). A functional assay to prove the inhibitory activity and further mode of action studies should support the efficacy of the identified hit compounds.

For *P. aeruginosa* the objective was to target virulence instead of bacterial survival in order to reduce the selective pressure for resistance development. The selected anti-virulence target was LasB which plays a major role for pathogenicity, the interaction with the human immune system and biofilm formation.

In a recently published study, the class of N-aryl mercaptoacetamides was identified as potent LasB inhibitors with good selectivity over human MMP's. However, a structure-based optimization approach in which a benzyl group was introduced at the nitrogen failed to maintain activity. In this thesis, the aim was to increase activity via different structure-based approaches based on the former results (chapter 3.3). The existing crystal structure should be used for the design of promising derivatives. After synthesis and determination of activity, the promising candidates should be further evaluated regarding selectivity and cytotoxicity. Ideally, new crystal structures should be generated to elucidate the binding mode.

In a different approach the thiol function of the N-aryl mercaptoacetamides should be replaced through other zinc-coordinating functions (chapter 3.4). The synthesis should be followed by intensive biological characterization including inhibitory activity and interference with resistance mechanisms such as biofilm formation for example.

## 3 Results

### 3.1 Chapter A: Biophysical Screening of a Focused Library for the Discovery of CYP121 Inhibitors as Novel Antimycobacterials<sup>186</sup>

Christian Brengel, Andreas Thomann, Alexander Schiffrin, Giuseppe Allegretta, Ahmed A. M. Kamal, Jörg Haupenthal, Isabell Schnorr, Sang Hyun Cho, Scott G. Franzblau, Martin Empting, Jens Eberhard, Rolf W. Hartmann

Reprinted with permission from *ChemMedChem* **2017** *12* (19), 1616-1626, DOI: 10.1002/cmdc.201700363

Copyright (2017) ChemMedChem

# Biophysical Screening of a Focused Library for the Discovery of CYP121 Inhibitors as Novel Antimycobacterials

Christian Brengel<sup>+, [a]</sup>, Andreas Thomann<sup>+, [a]</sup>, Alexander Schiffrin,<sup>[b]</sup> Giuseppe Allegretta,<sup>[a]</sup> Ahmed A. M. Kamal,<sup>[a]</sup> Jörg Haupenthal,<sup>[a]</sup> Isabell Schnorr,<sup>[a]</sup> Sang Hyun Cho,<sup>[c]</sup> Scott G. Franzblau,<sup>[c]</sup> Martin Empting,<sup>[a]</sup> Jens Eberhard,<sup>[a]</sup> and Rolf W. Hartmann<sup>\*[a, d]</sup>

The development of novel antimycobacterial agents against *Mycobacterium tuberculosis* (Mtb) is urgently required due to the appearance of multidrug resistance (MDR) combined with complicated long-term treatment. CYP121 was shown to be a promising novel target for inhibition of mycobacterial growth. In this study, we describe the rational discovery of new CYP121 inhibitors by a systematic screening based on biophysical and microbiological methods. The best hits originating from only one structural class gave initial information about molecular

motifs required for binding and activity. The initial screening procedure was followed by mode-of-action studies and further biological characterizations. The results demonstrate superior antimycobacterial efficacy and a decreased toxicity profile of our frontrunner compound relative to the reference compound econazole. Due to its low molecular weight, promising biological profile, and physicochemical properties, this compound is an excellent starting point for further rational optimization.

## Introduction

Tuberculosis belongs to the most lethal infectious diseases caused by bacteria. According to the WHO Global Tuberculosis Report,<sup>[1]</sup> 1.5 million people died in 2013 due to infections caused by Mtb. This goes along with an estimated amount of 9 million new cases of Mtb infections arising each year. Despite a broad spectrum of first- and second-line antimycobacterial drugs, there is an antibiotic gap for the treatment of infections with multidrug-resistant (MDR) and extensively drug-resistant (XDR) tuberculosis (TB).<sup>[1]</sup> Additionally, alarming reports have been published describing totally drug-resistant TB (TDR-TB).<sup>[2,3]</sup> Moreover, tuberculosis still requires long-term treatment leading to an increased probability for noncompliance,

which impairs therapeutic outcome.<sup>[4]</sup> Hence, there is an urgent need for new antimycobacterial agents with novel modes of action, which, in the best case, could also lead to shorter treatment periods.

Driven by the elucidation of the Mtb genome in 1998,<sup>[5]</sup> new potential drug targets were identified.<sup>[6]</sup> Interestingly, Mtb exhibits an unusual high number of twenty P450 enzymes in contrast to other bacteria. Further studies have revealed some of them to be essential for viability, survival and/or pathogenicity.<sup>[7]</sup> Out of these, CYP121 was shown to be essential for bacterial growth by an in vitro knock out study.<sup>[8]</sup> Moreover, the deficient strain could be revived by a complementary plasmid.<sup>[8,9]</sup> The first evidence of CYP121 function in Mtb was derived from its gene position which is located in an operon harboring two enzymes involved in the formation of cyclo-di-L-tyrosine (cYY).<sup>[10]</sup> In vitro studies provided proof, that CYP121 catalyzes the reaction of cYY to mycocyclusin with high substrate specificity.<sup>[10,11]</sup> The role of its substrate and product in the cellular setting remains to be elucidated. However, the variety of biological functions of diketopiperazines is well described for example, as quorum sensing signals.<sup>[12]</sup> Thus, besides development of antimycobacterials targeting CYP121, a small selective molecule with in cellulose efficiency may help to understand the precise function of CYP121.

Due to the fact that CYP121 is a potential target for Mtb treatment, some efforts have been undertaken to identify potent inhibitors. Hudson et al.<sup>[13]</sup> and Kavanagh et al.<sup>[14]</sup> published several compounds designed for selective CYP121 binding and inhibition. However, none of them were shown to be effective against Mtb. Fonvielle et al. described a CYP121 inhib-

[a] Dr. C. Brengel,<sup>\*</sup> Dr. A. Thomann,<sup>\*</sup> Dr. G. Allegretta, A. A. M. Kamal, Dr. J. Haupenthal, I. Schnorr, Dr. M. Empting, Dr. J. Eberhard, Prof. Dr. R. W. Hartmann  
Helmholtz Institute for Pharmaceutical Research Saarland, HIPS, Department for Drug Design and Optimization, Campus E8.1, 66123 Saarbrücken (Germany)  
E-mail: rolf.hartmann@helmholtz-hzi.de

[b] Dr. A. Schiffrin  
Department of Biochemistry, Saarland University, Campus B2.2, 66123 Saarbrücken (Germany)

[c] Dr. S. H. Cho, Prof. Dr. S. G. Franzblau  
Institute for Tuberculosis Research, College of Pharmacy, University of Illinois at Chicago, 833 S. Wood Street, Chicago, IL 60612-7231 (USA)

[d] Prof. Dr. R. W. Hartmann  
Department of Pharmacy, Pharmaceutical and Medicinal Chemistry, Saarland University, Campus C2.3, 66123 Saarbrücken (Germany)

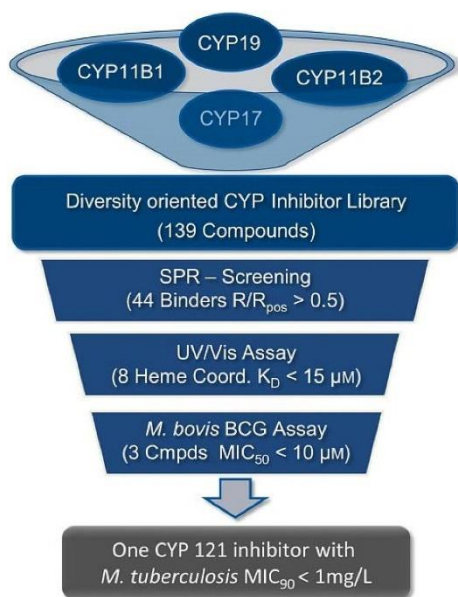
[\*] These authors contributed equally to this work.

Supporting information and the ORCID identification number(s) for the author(s) of this article can be found under:  
<https://doi.org/10.1002/cmdc.201700363>.

itory effect of cYy derivatives without data on bacterial growth.<sup>[11,15]</sup> Kavanagh et al. designed compounds based on substrate fragmentation with micromolar affinity and selectivity over other Mtb P450's without data concerning biological activity.<sup>[16]</sup> Regarding compounds with cellular activity, it was shown that azole antifungals bind tightly to CYP121 and exhibit an in vitro and in vivo activity against Mtb.<sup>[17–22]</sup> Furthermore, the binding to the enzyme was in good correlation with the antimycobacterial effect.<sup>[8,22]</sup> As the azole antifungals are active on Mtb cells and effective in mice infection models they display a valuable reference for antimycobacterial CYP inhibitors.<sup>[17–22]</sup>

The essential role of CYP121 for Mtb survival and our expertise in developing potent and selective human steroidogenic CYP enzyme inhibitors motivated us to identify novel CYP121 inhibitors with increased efficiency and improved properties relative to the azole antifungals.<sup>[23–27]</sup>

Potential antimycobacterial activity could provide further evidence of target validity, drugability and stimulate development of respective inhibitors toward new therapeutic agents bearing the potential to treat MDR and XDR Mtb infections. For these reasons, we established a screening strategy based on in vitro and cell-based assays (Scheme 1). By the use of a



**Scheme 1.** Hit finding progress. The initial library (139 compounds) was built of inhibitors designed for inhibition of human CYP11B1/2, CYP17, and CYP19 with regard to structural diversity. A positive SPR screening hit was defined by the coefficient of its response divided by the response of the positive control (econazole) which had to be above 0.5 ( $R/R_{pos} > 0.5$ ). This resulted in 44 positives. From this preselection, eight compounds coordinated iron-heme with  $K_D < 15 \mu\text{M}$ . These compounds were tested against BCGT and three showed  $\text{MIC}_{\text{BCGT}} < 10 \mu\text{M}$ . Finally, one compound was highly active on Mtb with  $\text{MIC}_{\text{Mtb}} < 1 \text{ mg L}^{-1}$ .

small highly diverse library composed of our CYP-inhibitors, we could identify a CYP121 inhibitor with increased antimycobacterial potency relative to positive control econazole. This compound possesses desirable physicochemical properties, low toxicity toward human cells and high antibacterial selectivity against Mtb, rendering it an appropriate candidate for further optimization.

## Results and Discussion

### Library generation

For hit discovery we selected 139 compounds from our in-house CYP-inhibitor library designed for inhibition of CYP17, CYP19, CYP11B1 and B2 (Supporting Information [SI]). The screening library is composed of six different scaffolds to ensure a broad structural diversity (Figure 1). Additionally,

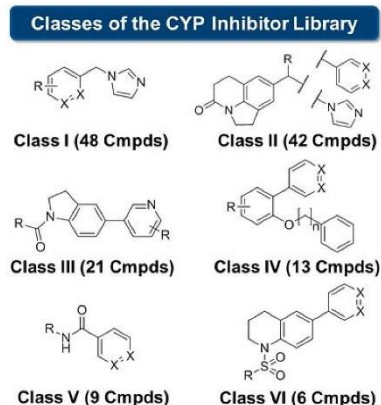


**Figure 1.** Classes of the library used for screening against CYP121 with their respective number of representatives stated in brackets. The structures represent the core scaffold of the compound, where R is a substituent, X represents the position of either nitrogen or CH, and [n] the alkyl chain length of n methylene units.

known pharmacological profiles, drug-likeness, and established synthetic routes of the compounds provide an ideal starting point for future optimization. As a reference compound we chose econazole which was shown to have the highest reported affinity to CYP121 (UV/Vis heme P450 binding assay) and the strongest inhibition of mycobacterial growth in the class of azole antifungals.<sup>[19,22]</sup>

### Enzyme expression, characterization and initial SPR screening

As starting point for SPR screening we expressed CYP121 in a heterologous host (*E. coli* K12 BL21) and purified the protein by ion affinity chromatography (IMAC). Notably, addition of 1% Triton X-100 into the lysis buffer during purification in-

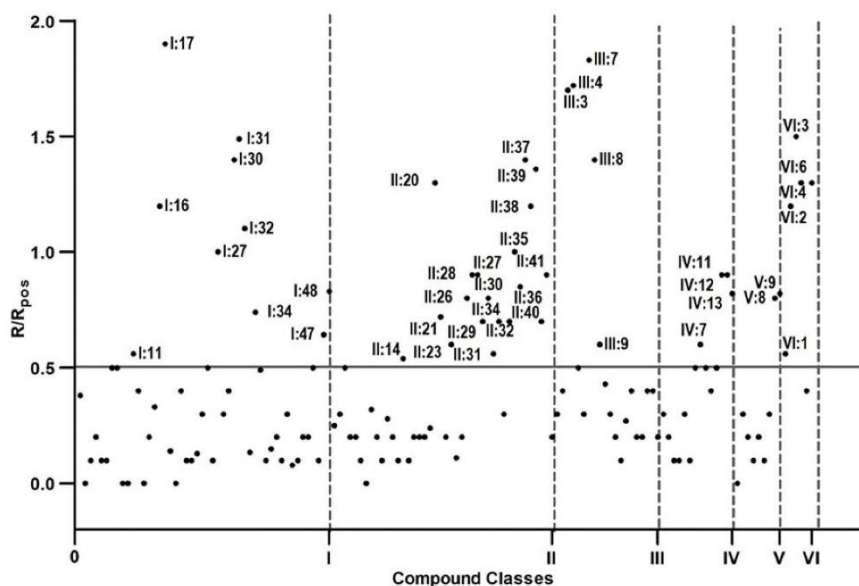


**Figure 2.** SPR screening results: compounds plotted versus their  $R/R_{\text{pos}}$  values. Econazole ( $100\ \mu\text{M}$ ) was used as a positive control and its SPR response was set at 1 ( $R_{\text{pos}}$ ). The compounds were tested at a concentration of  $100\ \mu\text{M}$  and their response ( $R$ ) was divided by the response of the positive control ( $R/R_{\text{pos}}$ ). Hit compounds possess  $R/R_{\text{pos}}$  values  $> 0.5$  (horizontal solid grey line). Vertical dashed lines separate the six classes.

creased the protein yield by about 10-fold.<sup>[28]</sup> The purity of the enzyme was determined by SDS-PAGE (SI, section 2, Figure S1). To ensure active protein conformation we conducted enzymatic in vitro activity tests. A first experiment to gain information about activity of P450 enzymes is the determination of CO-binding spectra.<sup>[29]</sup> 50% of the expressed enzyme showed the typical P450 band of CO-bound heme after dithionite reduction (SI, section 3, Figures S2 and S3). Using the same experimental conditions but replacing sodium dithionite, we were able to identify Etp1fd (516–618) as ferredoxin and Arh1\_A18G as ferredoxin reductase, two proteins of the fungus/fission yeast *Schizosaccharomyces pombe*<sup>[30,31]</sup> as suitable heterologous electron-transfer system for CYP121. Additionally, using the latter system, we could show conversion of cYY to mycocylosin proving enzymatic activity of CYP121 (SI, section 4, Figures S4 and S5).

Surface plasmon resonance spectroscopy (SPR) is a modern yet well-established biophysical methodology that allows the detection of binding events between an immobilized target (e.g., enzyme) and a solvated analyte.<sup>[32]</sup> However, interactions detected by SPR can also occur outside the enzymes active site. Hence, this SPR-based primary screening filter was used to distinguish between binders and non-binders.

For SPR immobilization of the protein we used the biotin-streptavidin interaction.<sup>[33]</sup> Prior to immobilization we conjugated a biotin tag to CYP121. To confirm applicability of the SPR method, we determined a response curve of econazole to the target protein (SI, section 5, Figure S6).<sup>[8]</sup> The SPR signal of eco-

nazole, measured in response units (RU), was set to one ( $R_{\text{pos}}$ ). The binding event of library compounds ( $R$ ) was referenced to the positive control and declared as  $R/R_{\text{pos}}$ . We defined  $R/R_{\text{pos}} > 0.5$  as the threshold for hits from SPR screening procedure. Using this approach, we identified 44 binders out of 139 compounds with representatives from all of the six classes (Figure 2). Notably, we found 17 compounds with higher responses than econazole (SI, section 6, Table S1).

#### Binding mode and affinity characterization by UV/Vis heme binding assay

The 44 SPR binders were investigated for their ability to interact with the iron(II)-heme by monitoring the shift of the characteristic absorbance band at 416 nm of CYP121 (Figure 3).<sup>[8,13]</sup> In addition to the 44 SPR hits, we also took two weak SPR binders into consideration (I:1 and I:33,  $R/R_{\text{pos}} < 0.5$ ) to conduct a retrospective evaluation of the reliability of our SPR screening. McLean et al. reported that econazole has a tight-binding profile to CYP121 with a  $K_D = 0.02\ \mu\text{M}$ .<sup>[8]</sup> However, we observed a  $K_D$  of  $3\ \mu\text{M}$ . This discrepancy could be due to a difference in UV/Vis spectrometric devices used and, thus, limited sensitivity. To provide a higher throughput employing 96-well plates, we were limited to a higher enzyme concentration which impairs measurement in lower nanomolar ranges. Compounds were initially tested at a concentration of  $100\ \mu\text{M}$  to identify iron-heme interactions and distinguish between type I (water-bridged iron interaction) and type II (direct iron interac-

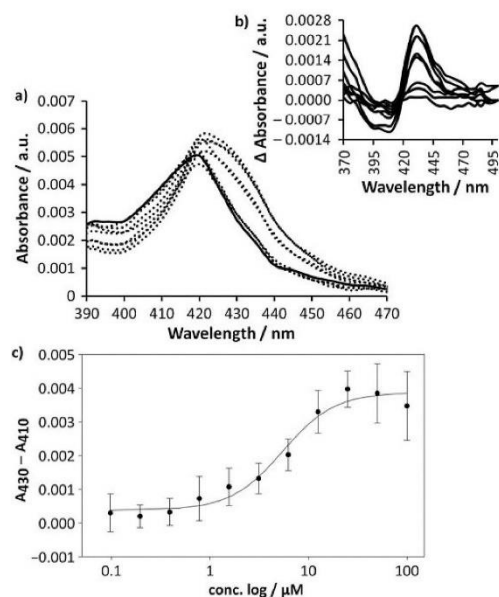


**Figure 3.** Binding of I:47 to CYP121 as determined from heme coordination assay: a) UV/Vis spectra of the enzyme were recorded in the presence of I:47 (100, 50, 25, 12.5, 6.25, 3.13, 1.56, 0.78, 0.39, 0.20, 0.10  $\mu\text{M}$ ; dotted lines) and in the absence of I:47 (solid line). b) Corresponding difference spectra. c) The  $K_D$  value of I:47 was derived by nonlinear fitting of the data using Equation (1) and the difference in absorbance at 430 and 410 nm. Error bars represent the standard deviation of three replicate measurements.

tion) binding. 30 compounds showed a type II shift while none showed type I binding behavior. The latter compounds appear in class I, II, III and IV indicating that the catalytic center accepts imidazolyl and pyridinyl moieties for iron–heme coordination. I:1 and I:33 (weak SPR binders) did not coordinate the heme iron which emphasizes the suitability of our SPR screening procedure. The identified type II binders were further investigated regarding their  $K_D$ . For eight binders an affinity better than 15  $\mu\text{M}$  was observed (SI, section 6, Table S1). Interestingly, this subset of compounds only arose from classes I and II. Pyridinyl (class II) as well as imidazolyl (class I) motifs were tolerated as heme coordinators while the imidazolyl ligands showed higher affinities (SI, section 6, Table S1). With regard to class I the highest affinity could be found for compounds decorated with hydrophobic and space-demanding moieties connected to the benzylimidazole substructure. This is also a structural trend in the class of antimycobacterial azoles (e.g., econazole, clotrimazole).<sup>[8]</sup> The most affine binder I:16 showed threefold improved  $K_D$  relative to econazole ( $K_D = 3 \mu\text{M}$ ; SI, section 6, Table S1). Furthermore, two linearized, *para*-substituted biphenyl compounds of this class (I:47 and I:48) possessed a CYP121 affinity similar to that of econazole. As mentioned before, molecules with linear biphenyl units bearing an *N*-methylenbenzimidazolyl moiety instead of an unsub-

stituted benzylimidazolyl scaffold did not bind to the heme (I:33). Additionally, replacement of the interconnecting phenyl group within this class by pyridinyl resulted in inactive compounds (I:1). Moreover, the analysis of all regioisomers of benzylimidazol scaffolds substituted with phenyl revealed that the *para* (I:32) and *meta* (I:30) position lead to similar affinities. A phenyl group at the *ortho* position (I:15) impairs binding. The *para*-benzodioxine substituent of I:48 and the *para*-benzodioxole substituent of I:47 increase the affinity by about two- to threefold (SI, section 6 Table S1). However, compared with econazole our most active compounds showed similar (e.g., I:47 5  $\mu\text{M}$  and I:48 5  $\mu\text{M}$ ) or slightly better  $K_D$  (I:16 1  $\mu\text{M}$ ; SI, section 7, Figure S7).

#### MIC determination in BCGT and Mtb

For investigating cellular activity we focused on those compounds with a  $K_D$  lower than 15  $\mu\text{M}$ , but also added selected compounds showing low affinity to CYP121 as negative controls (SI, section 6, Table S1). In this setting, econazole was used as described antimycobacterial reference compound.<sup>[34]</sup> For initial screening on mycobacterial growth inhibition we used the bovine strain BCGT. The strain serves as a suitable substitute for Mtb as it carries a copy of CYP121 in its genome with an overall amino acid identity of 100% in comparison with its Mtb congener (SI, section 8, Figure S8).<sup>[35]</sup> Regarding the more complex situation in the cellular context, the six identified classes have to be discussed separately. In case of subset III to VI, we could only detect weak growth inhibition ( $\text{MIC}_{\text{BCGT}} > 10 \text{ mg L}^{-1}$ ; SI, section 6, Table S1). In class II three compounds were found to have a  $K_D$  value below 15  $\mu\text{M}$  but none of them had  $\text{MIC}_{\text{BCGT}}$  below 10  $\text{mg L}^{-1}$  (II:20, see SI, section 6, Table S1). For econazole, we observed a  $\text{MIC}_{\text{BCGT}} = 5.4 \text{ mg L}^{-1}$  which is in good correlation to previous findings.<sup>[34]</sup> Most active compounds were observed in class I (SI, section 9, Figures S9 and S10). The best heme binder to CYP121 (I:16) with a threefold increased affinity relative to econazole showed a  $\text{MIC}_{\text{BCGT}}$  of 1.6  $\text{mg L}^{-1}$ . For I:47 and I:48 we could determine  $\text{MIC}_{\text{BCGT}} = 0.3 \text{ mg L}^{-1}$  and 2  $\text{mg L}^{-1}$  which renders I:47 to be the most potent antimycobacterial compound in this subset. The MIC tests of negative controls out of class I (I:1 and I:33) showed no significant growth inhibition. Within class I results of the MIC assay are in good correlation to the  $K_D$  values on the target enzyme CYP121 (Table 1).

To test the potency of the most effective antimycobacterial compounds against the human pathogen Mtb, we used the MABA assay system. For  $\text{MIC}_{\text{Mtb}}$  determination we chose the common laboratory strain H<sub>37</sub>Rv. In several studies the  $\text{MIC}_{\text{Mtb}}$  value of econazole was determined ranging from 0.12  $\text{mg L}^{-1}$  to 8  $\text{mg L}^{-1}$ .<sup>[8,20]</sup> To facilitate comparability of the  $\text{MIC}_{\text{Mtb}}$  values, we referenced them to results made in our assay system where a  $\text{MIC}_{\text{Mtb}}$  for econazole of 4.2  $\text{mg L}^{-1}$  was determined previously.<sup>[34]</sup> The most effective compounds were I:47 with  $\text{MIC}_{\text{Mtb}} = 0.3 \text{ mg L}^{-1}$  followed by I:16 ( $\text{MIC}_{\text{Mtb}} = 1.9 \text{ mg L}^{-1}$ ) and I:48 ( $\text{MIC}_{\text{Mtb}} = 3.5 \text{ mg L}^{-1}$ , see Table 1). Notably, in terms of cellular efficiency metrics, I:47 has an  $\text{AE} = 0.39$  and hence, a

**Table 1.** Structures, relative SPR responses ( $R/R_{\text{econ}}$ ), binding affinities ( $K_D$ ), and antimycobacterial activities of econazole, most active hits (**I:16**, **I:47**, **I:48**), examples for negatives (**I:1**, **I:33**), and for moderately active hits (**I:15**, **I:30**, **I:32**).

Compd	SPR	Heme $K_D$	$MIC_{\text{BCGT}}$		$MIC_{\text{Mtb}}$	
	[ $R/R_{\text{econ}}$ ]	[ $\mu\text{M}$ ]	[ $\text{mg L}^{-1}$ ]	[ $\mu\text{M}$ ]	[ $\text{mg L}^{-1}$ ]	[ $\mu\text{M}$ ]
Eco <sup>[a]</sup>	1	$2.8 \pm 0.2$	5.4	14	$4.2^{\text{[c]}}$	$11^{\text{[c]}}$
<b>I:1</b>	0.4	>100	>25	>100	–	–
<b>I:15</b>	0.3	$34.3 \pm 5.9$	9.6	41	–	–
<b>I:16</b>	1.2	$1.3 \pm 0.4$	1.6	5	1.9	6
<b>I:30</b>	1.4	$10.6 \pm 2.0$	2.6	11	11.2	48
<b>I:32</b>	1.1	$13.9 \pm 2.1$	7.0	30	9.6	41
<b>I:33</b>	0.1	>100	>25	>100	–	–
<b>I:47</b>	0.6	$5.4 \pm 1.0$	0.3	1	0.3	1
<b>I:48</b>	0.6	$5.3 \pm 0.6$	2.0	7	3.5	12

[a] Econazole. [b] Values are the mean  $\pm$  SD of three replicate measurements. [c]  $MIC_{\text{Mtb}}$  values determined previously.<sup>[34]</sup>

higher AE than econazole (0.24) and rifampicin (0.16) (SI, section 10, Table S2).

#### Toxicity on human cell lines

The azole antifungals are known to attenuate growth of several human cell lines.<sup>[36,37]</sup> To compare cellular toxicity of econazole with our three most promising hits we used HEK293 cells in a MTT-based assay.<sup>[38]</sup>  $6.0 \text{ mg L}^{-1}$  of econazole killed 50% of HEK293 cell population after 48 h. Notably, the toxicity of our most active antimycobacterial compounds was lower than that of the azole antifungal drug (**I:16**  $LD_{50} = 6.1 \text{ mg L}^{-1}$ ; **I:47**  $LD_{50} = 18.6 \text{ mg L}^{-1}$ ; **I:48**  $22.3 \text{ mg L}^{-1}$ ). For comparability reasons, we calculated the toxicity factor for **I:47** ( $MIC_{\text{Mtb}}/LD_{50}$ ), which revealed a 44-fold improvement over econazole (Table 2). One of the most prominent undesirable effects of azole antifungals is their hepatotoxicity observed in mice.<sup>[37,39]</sup> For this reason, we also conducted toxicity experiments employing HepG2 cells.

Table 2. Comparison of human cellular toxicity and anti-Mtb effect.			
Compd	$MIC_{\text{Mtb}}$ [ $\text{mg L}^{-1}$ ]	$LD_{50}$ [ $\text{mg L}^{-1}$ ] <sup>[a]</sup>	TF: $MIC_{\text{Mtb}}/LD_{50}$ <sup>[b]</sup>
Eco	4.2	6.0	1.4
<b>I:16</b>	1.9	6.1	3.2
<b>I:47</b>	0.3	18.6	62.0
<b>I:48</b>	3.5	22.3	6.4

[a] 50% lethal dose toward HEK293 cells. [b] Toxicity factor = ( $MIC_{\text{Mtb}}/LD_{50, \text{HEK293}}$ ); this was used to enhance the comparability of compounds with regard to their antimycobacterial effect.

We could observe an approximate twofold increased toxicity for econazole ( $3.1 \text{ mg L}^{-1}$ ) and **I:16** ( $3.9 \text{ mg L}^{-1}$ ) relative to HEK293 cells. The  $LD_{50}$  of **I:47** was  $17.1 \text{ mg L}^{-1}$  which is close to the toxicity observed in HEK293 cells (see above, SI, section 11, Table S3).

#### In vitro and in cellulo mode-of-action studies

In addition to the binding constant, we determined inhibition of CYP121 enzymatic reaction by **I:47**. The enzyme catalyzes the formation of an intramolecular C–C bond between the carbon atoms at the *ortho* position to the hydroxy group of the phenol moiety of cYY resulting in the production of mycrocyclosin.<sup>[10]</sup> For assessing CYP121 activity we used an artificial redox system from *Schizosaccharomyces pombe* (ferredoxin Etp1fd (516–618) and ferredoxin reductase Arh1\_A18G).<sup>[31]</sup> This redox system is known for its broad applicability as electron donor for CYP enzymatic reactions but firstly described for CYP121 herein. Indeed, we could observe an inhibition of product formation confirming **I:47** to be a potent inhibitor of mycrocyclosin production by interference with CYP121 in vitro (SI, section 4). To gather further evidence for target-based mycobacterial selectivity toward other bacteria, we assessed the activity of our compounds on growth of *E. coli* TolC as a representative for Gram-negative bacteria and *S. aureus* Newmann strain for Gram-positive. The results show no significant growth inhibition of **I:47** and **I:48** against the latter bacteria ( $MIC_{\text{Mtb}} > 100 \mu\text{M}$  or  $> 25 \text{ mg L}^{-1}$ ). In contrast to econazole and **I:16** that showed certain inhibitory effects for *E. coli* and *S. aureus* in higher concentrations (SI, section 12, Figure S11).

### Physicochemical and selectivity profile of I:47

The aforementioned compounds were originally designed as inhibitors of human CYP17, CYP19 and CYP11B1/2 known to be involved in steroid biosynthesis. I:47 was initially synthesized as an inhibitor of CYP17. The compound showed only a low activity on CYP17 relative to other inhibitors with an  $IC_{50}$  = 3.1  $\mu$ M. Additionally, only a 48% inhibition of aromatase at a concentration of 25  $\mu$ M was observed.<sup>[40]</sup> Regarding physicochemical properties suitable for permeation through the cellular membranes, one has to differentiate between biological barriers of human and mycobacterial origin. For humans, a guidepost for appropriate physicochemical properties is the Lipinski's rule of five for oral bioavailability of drugs (< 5 hydrogen bond donors,  $\leq$  10 hydrogen bond acceptors,  $M_r$  < 500 Da,  $\log P \leq 5$ ).<sup>[41]</sup> Our frontrunner compound I:47 fulfils all four criteria (0 hydrogen bond donors, 3 hydrogen bond acceptors,  $M_r$  = 278 Da,  $\log P$  = 3.1; SI, section 13). To the best of our knowledge, similar correlations for physicochemical properties with mycobacterial membrane passage have not yet been established. Thus, a respective guide for compound development is still missing.<sup>[42]</sup>

### Molecular modeling studies on the binding mode of I:47

As a type II binding profile was observed for I:47, we set up a constrained docking protocol to predict its binding mode to the heme center of CYP121. Docking to the active site of CYP121 was restricted by two essential pharmacophore features reflecting the direct interaction between the coordinated iron and I:47 (type II binding). The resulting docking poses were sorted by their predicted binding energies and the best scored docking pose was chosen for further studies (Figure 4). This modeling approach revealed new possibilities for further derivatization or rigidification. For instance, intramolecular linking of the methylene bridge at the imidazolyl unit with the *ortho* position of phenyl using for example, a five-membered ring should be tolerated by CYP121 and increase affinity through a decrease in entropic penalties upon binding. Furthermore, the central hydrophobic aromatic moiety shows van der Waals contacts to flanking hydrophobic amino acids Phe168 and Met62. Regarding steric factors, the ring could easily rotate in this position. This degree of rotatable freedom might be necessary to place the aforementioned phenyl in a suitable position to grant access to a large flat sub-pocket (composed of Met61, Asn84 and the backbone of Asn83) which could then be reached by substituents at its 2-position. The 1,3-benzodioxole moiety was placed in a hydrophilic sub-pocket, formed by Arg72, Asn74 and Thr65, which is in good accordance with the low lipophilicity of this motif ( $cLogP$  = 0.27). Moreover, the 5-position of 1,3-benzodioxole holds great potential for further enlargement of the molecule, as it directly points to another sub-pocket which is decorated with several hydrophobic amino acids, namely Leu73, Phe280, Leu284, and the side chain of Gln385.

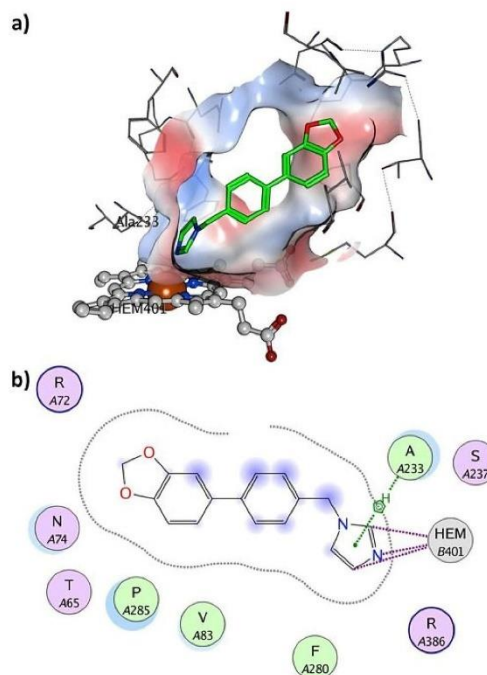


**Figure 4.** Molecular docking of I:47 against the prepared co-crystal structure of CYP121. Heme coordination was a prerequisite for the docking process which was achieved by placing a pharmacophore feature on the interacting metal and ligand position. Resulting docking poses were sorted by score (*E<sub>refine</sub>*), and the highest scored pose is depicted as a) a 3D model and b) a 2D-interaction chart. I:47 shows close van der Waals contacts to surrounding amino acids but also possibilities for compound enlargement (b). The grey surface in panel (a) represents the van der Waals surface of the protein, which is also shown as dotted lines in panel (b).

### Conclusions

Despite the fact that CYP121 had been reported to be a potential target for the treatment of Mtb infections, not many inhibitors with cellular activity had been discovered. Herein we have presented a rational screening approach to address CYP121 by a small library focused on privileged scaffolds for CYP enzyme inhibition. The identified compounds could help to clarify the hitherto unknown role of CYP121 in Mtb metabolism and provide a good starting point for a drug optimization program.

Our search for new inhibitors of CYP121 started with an initial SPR screen of the aforementioned focused library. As the compounds were designed for P450 inhibition we observed a high number of binders (32%). The identified compound classes differed highly with regard to their structures. Clearly, the large pocket of CYP121 (1350  $\text{\AA}^3$ ) which is necessary for the sterically demanding enzyme reaction can accept a large variety of differently shaped molecules.<sup>[8,10,43,44]</sup> However, it has to be noted that the SPR method does not exclude compound attachment outside the enzymes active site.

For rational design approaches it is of high interest to clarify the binding mode and affinity of our hit compounds. A common method for P450 enzymes to address this issue is the heme coordination assay.<sup>[6]</sup> All SPR binders from classes III, IV, V and VI had only weak affinity to the heme iron ( $K_D > 100 \mu\text{M}$ ). **IV:13** is the only compound from this subset that could be titrated and gave a  $K_D$  of  $62 \mu\text{M}$  (SI, section 6, Table 1). Therefore, we conclude that most of the compounds from these classes do not bind directly to heme but address another unknown site. This information could, however, be valuable for fragment-linking approaches at a later stage of drug development. For classes I and II we identified eight compounds with  $K_D$  values below  $15 \mu\text{M}$ . Notably, the best compounds of class II (**II:20** and **II:34**) contained a space-demanding trityl moiety. It was discussed for a crystal structure of CYP121 (PDB ID: 1N40) that Arg386 may restrict access of voluminous moieties to the iron-heme.<sup>[43]</sup> Nevertheless, we observed that the enzyme can accommodate space-demanding molecules at the heme site as shown by our UV/Vis experiments. Binders with the best affinity were found in class I. A comparison of compound structures and binding efficiencies within this class gave first evidence for properties needed to gain affinity toward CYP121. Imidazolyl head group linked by a methylene bridge to a hydrophobic core can be considered as an important basic structure for a good binding efficiency (**I:16**, **I:47** and **I:48**). In case of the linearized compounds, an *N*-methylenbenzimidazolyl head group (**I:33**), *ortho*-substituted biphenyl system (**I:15**), and an interconnecting pyridinyl (**I:1**) ring had unfavorable binding properties. In a hit optimization process these structural characteristics should be avoided. In contrast to this observation, a *para*-benzodioxine substituent (**I:48**) and a *para*-benzodioxole substituent (**I:47**) linked to the biphenyl system increases affinity. This might provide a possible position for further derivatization. Our docking study supports this result as this motif was predicted to be placed in a sub-pocket having a great potential for new interactions.

A straightforward approach for target validation is to correlate on-target potency and cellular activity. Although it has to be noted, that such a correlation can be flawed by the fact that compounds might also be inefficient due to poor membrane penetration, for example. We hypothesized that class II might be a prime example for compounds that poorly permeate the membrane of mycobacteria and, thus, cannot reach their intracellular target. This could be an explanation for the lack of in cellulo activity although a moderate affinity to the target was measured.

Class I is the most remarkable of the six classes showing reasonable affinity toward CYP121 and, more importantly, also high activity in cellulo against Mtb and BCGT. Furthermore, the on-target affinity of class I compounds directly correlates with their activity on mycobacteria which provides further evidence of a CYP121-dependent effect. In detail, on-target inactive compounds like **I:1** and **I:33** had no activity against BCGT, while moderate binders for example, **I:15**, **I:30** and **I:32** had low antimycobacterial effects. Finally, compounds with highest affinity (**I:16**, **I:47**, **I:48**) were the most potent in the cellular setting. Especially, compounds **I:16**, **I:47**, and **I:48** are even

more effective on mycobacteria than the positive control, econazole, although no optimization has been undertaken, yet (Table 1). In terms of antibacterial efficiency (AE), **I:47** is superior to econazole and the first-line drug rifampicin indicating an excellent optimization potential of this novel inhibitor class. Moreover, we could provide data that **I:47** does not only bind to CYP121 but does also inhibit the enzyme reaction (SI, section 4). The correlation between MIC and  $K_D$  bares minor inconsistencies, which might be due to poor penetration through the mycobacterial cell wall of some compounds (see for example, **I:47** and econazole). A highly lipophilic molecule (e.g., econazole  $\text{cLogP} = 5.3$  versus **I:47**  $\text{cLogP} = 3.1$ ) might be trapped in this lipophilic barrier containing mycolic acids and slowly or only partially released into the mycobacterial cytoplasm. This results in lower cellular activity than expected from on-target affinities. A second explanation for the differences in MIC and  $K_D$ , at least for econazole, is its promiscuous behavior in different growth inhibition assays. This suggests that there are additional targets for econazole. An explanation for the antibacterial activity of econazole against *E. coli* and *S. aureus* was already provided before. In these studies econazole was described as an inhibitor of flavohemoglobin.<sup>[45,46]</sup> Further possible target systems of azole antifungals within Mtb metabolism have also been described.<sup>[47-49]</sup> However, evaluation of **I:47** and **I:48** leads to the conclusion that these novel structures are of improved selectivity toward Mtb with a good correlation of CYP121 affinity and antimycobacterial activity. Furthermore, the two compounds possess lower toxicity against human cells than determined for econazole. Although toxicity to hepatocytes was low, it is of high interest to clarify potential inhibition of metabolizing CYP enzymes (e.g., CYP3A4). These results further underline the target-based mycobacterial specificity of our compounds, at least in the subset of bacterial and human cells tested. Taken together the in vitro and cell-based studies conducted herein, CYP121 is most certainly the major target of **I:47** and **I:48**.

In summary, we have reported a biophysical screening procedure employing a focused library of privileged scaffolds, which ultimately lead to the discovery of novel CYP121 inhibitors. From this process, **I:47** turned out to be the most promising hit compound pairing convincing antimycobacterial activity and bacterial selectivity with a good toxicity profile. Furthermore, this compound exhibits a fragment-like molecular weight and preferable physicochemical properties that fulfil the Lipinski rules for oral bioavailability (SI, section 13). Thus, **I:47** is an excellent starting point for rational structure-based drug discovery. Our in silico studies revealed several possible modifications to be investigated in future optimization steps. Additionally, the inhibitor might be a suitable candidate for an in vivo proof-of-concept study toward validation of CYP121 as a drug target.

## Experimental Section

**Bacterial strains and growth conditions:** Bacterial strains used in this study were *Mycobacterium bovis* DSM-43990 (BCGT), *Mycobacterium tuberculosis* H<sub>37</sub>Rv (Mtb), *Escherichia coli* TolC acr A/B defi-

cient, *Staphylococcus aureus* (Newman strain) and *E. coli* K12 BL21. Mammalian cell lines for cytotoxicity evaluation were HEK293 (human embryonic kidney) and Hep2G (human liver carcinoma cells) cells. Mycobacteria were cultured in 7H9GC-Tween<sup>[50]</sup> or Middlebrook 7H9 broth complemented with ADC Enrichment (Middlebrook), *E. coli* TolC and *S. aureus* tests were performed in lysogenic broth (LB) and LB plus ADC Enrichment.

**Chemical synthesis and analytical characterization:** Chemicals were purchased from commercial suppliers and used without further purification. Column flash chromatography was performed on silica gel (40–63  $\mu\text{m}$ ), and reaction progress was monitored by TLC on TLC Silica Gel 60 F<sub>254</sub> plates (Merck, Darmstadt, Germany). All moisture-sensitive reactions were performed under nitrogen atmosphere using anhydrous solvents. <sup>1</sup>H and <sup>13</sup>C NMR spectra were recorded on Bruker Fourier spectrometers (300 MHz) at ambient temperature with the chemical shifts recorded as  $\delta$  values in ppm units by reference to the hydrogenated residues of deuterated solvent as internal standard. Coupling constants (*J*) are given in Hertz (Hz), and signal patterns are indicated as follows: s, singlet; d, doublet; dd, doublet of doublets; t, triplet; m, multiplet, br, broad signal. The purity of the final compounds was >95% measured by HPLC with UV detection at 254 nm. The SpectraSystem LC system consisted of a pump, an autosampler, and a UV/Vis detector (ThermoFisher, Dreieich, Germany). Mass spectrometry was performed on an LC-coupled Surveyor MSQ electrospray mass spectrometer (ThermoFisher, Dreieich, Germany). The system was operated by the Xcalibur software package. An RP C<sub>18</sub> NUCLEODUR ec 100-5 125  $\times$  3 mm 5  $\mu\text{m}$  column (Macherey-Nagel GmbH, Düren, Germany) was used as the stationary phase. All solvents were HPLC grade. In a gradient run, the percentage of acetonitrile (containing 0.1% trifluoroacetic acid) was increased from an initial concentration of 0% at 0 min to 100% at 15 min and kept at 100% for 5 min. The injection volume was 10  $\mu\text{L}$ , and flow rate was set to 800  $\mu\text{L}\cdot\text{min}^{-1}$ . MS analysis was carried out at a spray voltage of 3800 V, a source CID of 10 V and a capillary temperature of 350 °C. Spectra were acquired in positive mode from 100 to 1000 *m/z*. cYY and mycocyclusin were synthesized as described.<sup>[11,51]</sup> Experimental details on modification of cYY and mycocyclusin synthesis and analytical data can be found in the Supporting Information (SI, section 4). The synthesis of library compounds has been described previously: class I,<sup>[40,52–56]</sup> class II,<sup>[57,58]</sup> class III,<sup>[59]</sup> class IV,<sup>[60]</sup> class V,<sup>[61]</sup> and class VI.<sup>[62]</sup>

**Protein expression, purification and biotinylation:** *E. coli* K12 BL21 (DE3) cells were transformed with plasmid harboring *cyp121* gene (pHAT2/*cyp121*).<sup>[13]</sup> The previously described<sup>[28]</sup> enzyme expression and purification method was slightly modified: His<sub>6</sub>-tagged CYP121 (H<sub>6</sub>-CYP121) was expressed in *E. coli* K12 BL21 and purified using a single affinity chromatography step. Briefly, *E. coli* K12 BL21 cells containing the pHAT2/*cyp121* were grown in terrific broth medium containing 100  $\mu\text{g}\cdot\text{mL}^{-1}$  ampicillin at 37 °C until an OD<sub>600</sub> of approximately 0.8 units was reached, followed by induction with 0.5 mM IPTG and 0.5 mM  $\delta$ -aminolevulinic acid for 36 h at 25 °C and 200 rpm. The cells were harvested by centrifugation (5000 rpm, 10 min, 4 °C), and the cell pellet was resuspended in 100 mL of binding buffer containing 1% Triton X-100 (50 mM Tris-HCl, 300 mM NaCl, 20 mM imidazole, 10% glycerol, pH 7.2) and lysed by sonication for a total process time of 2.5 min. Cellular debris was removed by centrifugation (18500 rpm, 38264  $\times$ g, 40 min, 4 °C), and the supernatant was filtered through a syringe filter (0.2  $\mu\text{m}$ ). The clear lysate was immediately applied to a Ni-NTA affinity column, washed with binding buffer, and eluted with a one-step gradient of 500 mM imidazole. The protein containing

fractions were buffer-exchanged into storage buffer (140 mM NaCl, 10 mM Na<sub>2</sub>HPO<sub>4</sub>, 2.7 mM KCl, 1.8 mM KH<sub>2</sub>PO<sub>4</sub> and 10% glycerol (*v/v*), pH 7.2), using a PD10 column (GE Healthcare, Little Chalfont, UK) and judged to be pure by SDS-PAGE analysis. Then protein was stored in aliquots at –80 °C in a final concentration of 50  $\mu\text{M}$ .<sup>[28]</sup>

Before SPR streptavidin immobilization CYP121 was biotinylated. For biotinylation, Sulfo-NHS-LC-LC-Biotin (Thermo Science, Waltham, USA) was dissolved in storage buffer (140 mM NaCl, 10 mM Na<sub>2</sub>HPO<sub>4</sub>, 2.7 mM KCl, 1.8 mM KH<sub>2</sub>PO<sub>4</sub> and 10% glycerol (*v/v*)) with CYP121 in 1:1 molar ratio. The solution was incubated on ice for 2 h and mixed carefully every 30 min. The biotinylated CYP121 was purified by size exclusion chromatography using the storage buffer and subsequently stored at –80 °C at a final concentration of 10  $\mu\text{M}$ .<sup>[63]</sup>

**Spectroscopic characterization of enzyme activity:** Recombinant CYP121 from *Mycobacterium tuberculosis* as well as ferredoxin Etp1fd (516–618) and ferredoxin reductase Arh1\_A18G from the fission yeast *Schizosaccharomyces pombe* were expressed and purified as described previously.<sup>[30,31]</sup> Functionality of CYP121 and electron transfer was assayed by the occurrence of the characteristic absorbance maximum at  $\lambda \approx 450$  nm, related to the reduced, CO-bound heme complex. The assay was conducted following the method of Omura and Sato<sup>[29]</sup> with slight modifications. CYP121 (2  $\mu\text{M}$ ) was reduced through the addition of a few grains of sodium dithionite or incubation with NADPH (100  $\mu\text{M}$ ), ferredoxin Etp1fd (516–618) (40  $\mu\text{M}$ ), and Arh1\_A18G ferredoxin reductase (2  $\mu\text{M}$ ) and divided in two cuvettes to record a baseline. One of the samples was saturated with carbon monoxide for 60 s and difference spectra were recorded until the absorbance at  $\lambda \approx 450$  nm was constant.

**SPR screening:** SPR binding studies were performed using a Reichert SR7500DC instrument optical biosensor (Reichert Technologies, Munich, Germany) and SAD500m sensor chips obtained from Xantec Bioanalytics. CYP121 was immobilized on a SAD500m sensor chip at 12 °C using standard biotin-streptavidin complexation. The surface of both channels was quenched by a 3 min injection of 0.003  $\text{mg}\cdot\text{mL}^{-1}$  biotin. CYP121 was immobilized at densities between 5000 and 6000 RU for binding studies.

**UV/Vis heme P450 binding assay:** Optical titration experiments were performed in 96 well plates (Greiner, Kremsmünster, Austria; transparent round bottom). The data were recorded using Tecan infinite M200Pro Nano Quant (Tecan Gruppe Ltd., Männedorf, Germany). Absorbance of enzyme and enzyme-inhibitor complex was measured between 350 and 500 nm in 1 nm steps with 10 flashes. Compounds were titrated from DMSO stock solutions maintaining a final DMSO concentration of 1%. CYP121 was used in a concentration of 0.25  $\mu\text{M}$ . Data were plotted as optical shift versus ligand concentration. Equation (1) was used for nonlinear regression of the resulting dose-response curves employing the Levenberg-Marquardt algorithm of Sigma Plot 12 (Systat Software GmbH, Erkrath, Germany).

$$f = y_{\min} + \frac{y_{\max} - y_{\min}}{1 + \left(\frac{x}{K_D}\right)^{\text{slope}}} \quad (1)$$

for which *f* is the observed difference in absorbance at wavelengths 410 nm and 430 nm within the difference spectrum (see Figure 3) at ligand concentration *x*. This difference spectrum is obtained by subtracting the pure heme absorption spectrum from those with ligand present. *y*<sub>max</sub> refers to the absorbance change at

ligand saturation,  $y_{\min}$  is the extrapolated minimal difference in absorbance;  $K_D$  refers to the dissociation constant of the CYP121 ligand complex.<sup>[22]</sup>

**Determination of BCGT MIC<sub>BCGT</sub> by OD<sub>600</sub> assay:** A pre-culture of BCGT was grown in 7H9 medium supplemented with ADC Enrichment for 10 days. The assay was performed in 48 well plates (Greiner, Kremsmünster, Austria). Prior to culture addition, compounds were serially diluted in DMSO to fit a final DMSO concentration of 1%. For compound susceptibility the pre-culture was diluted 1:100 with fresh medium (7H9 + ADC enrichment). After 168 h of incubation at 37 °C and 80% air moisture, bacterial growth was measured by determination of OD<sub>600</sub>. Absorption data was recorded on a Polarstar Omega Multidetector Plate Reader (BMG LABTECH, Ortenberg, Germany). Graphs were plotted with GraphPad Prism using OneSite Log IC<sub>50</sub> model provided by the software. MIC<sub>BCGT</sub> was defined as the concentration at which 50 percent of growth was detected in accordance with previous methods used.<sup>[34]</sup> In analogy to ligand efficiency, which relates activity of compounds to their number of heavy atoms, a new metric has been introduced: antibacterial efficiency (AE).<sup>[64,65]</sup> This coefficient was developed for better comparability of antimicrobial compounds differing in molecular weight [Eq. (2)].

$$AE = -\ln\left(\frac{MIC}{NHA}\right) \quad (2)$$

in which AE refers to the antibacterial efficiency, MIC is the minimal inhibitory concentration, and NHA equals the number of heavy atoms in a given compound.

**Cyp121 in vitro enzyme inhibition assay:** The enzyme inhibition assay was performed in 200  $\mu$ L PBS buffer pH 7.2. Compounds were used in a concentration of 100  $\mu$ M and incubated with 1  $\mu$ M CYP121 for 30 minutes at 30 °C. The final DMSO concentration did not exceed 2%. After incubation the electron transfer system Arh1\_A18G (5  $\mu$ M), Etp1fd (15  $\mu$ M) and NADPH + H<sup>+</sup> (200  $\mu$ M) was added. The reaction was started with the addition of cYY (50  $\mu$ M) and stopped after 30 min by addition of 200  $\mu$ L methanol with internal standard estrone (1  $\mu$ M final concentration, addition included). The characterization of CYP121 activity was conducted by a UHPLC-MS/MS analysis carried out on a TSQ Quantum Access Max mass spectrometer equipped with an HESI-II source and a triple quadrupole mass detector (Thermo Scientific, Dreieich, Germany). Compounds were separated on an Accucore RP-MS 150  $\times$  2.1 mm 2.6  $\mu$ m column (Thermo Fisher, Waltham, US) by a methanol/water gradient (from 1.4 min –3.5 min 50% methanol to 3.5 min –5.0 min 90% methanol) with a flow of 550  $\mu$ L min<sup>-1</sup>. Compounds were ionized in negative mode by electrospray ionization. Ionization was assisted by a post-column addition of 2 mM ammonia in methanol with an automated syringe at 1.25  $\mu$ L min<sup>-1</sup>. Monitored ions were (mother ion [m/z], product ion [m/z], scan time [s], scan width [m/z], collision energy [V], tube lens offset [V], polarity): mycrocyclin: 323.101, 111.100, 0.3, 0.7, 28, negative; cYY: 325.129, 113.043, 0.3, 0.7, 29, negative; internal standard (estrone): 269.153, 145.035, 0.3, 0.7, 42, negative. Samples were injected in a volume of 25  $\mu$ L. Xcalibur software was used for data acquisition. For quantification, the ratios of the area under the curve of the educt and the product were used.

**Determination MIC<sub>Mtb</sub> using MABA:** The assay for determination of minimal inhibition concentration against Mtb was performed as previously described.<sup>[50]</sup>

**MIC<sub>Eco</sub> E. coli TolC and MIC<sub>Sa</sub> S. aureus Newman:** MIC<sub>Eco</sub>/MIC<sub>Sa</sub> values were performed for econazole, **1:16**, **1:47**, **1:48** in *E. coli* TolC and *S. aureus* Newman. A start OD<sub>600</sub> of 0.03 was used in a total volume of 200 mL in lysogeny broth (LB) + ACD enrichment containing the compounds predissolved in DMSO. Final compound concentrations were prepared from serial dilutions ranging from 1.56 to 100  $\mu$ M in duplicates. The maximal DMSO concentration in the experiment was 1%. The recorded OD<sub>600</sub> values were determined after addition of the compounds and again after incubation for 18 h at 37 °C and 50 rpm in a 96-well plate (Sarstedt, Nümbrecht, Germany) using a FLUOStar Omega (BMG Labtech, Ortenberg, Germany). Given MIC<sub>Eco</sub>/MIC<sub>Sa</sub> values are means of two independent experiments (two different clones) and are defined as concentrations at which no bacterial growth was detectable.

**Human cytotoxicity assay:** HEK293 cells (2  $\times$  10<sup>5</sup> cells per well) were seeded in 24-well, flat-bottomed plates (Greiner Bioscience, Kremsmünster, Austria). Culturing of cells, incubations and OD measurements were performed as described previously<sup>[38]</sup> with minor modifications. 24 h after seeding of the cells the incubation was started by the addition of the compounds from DMSO stock solutions to a final DMSO concentration of 1%. The living cell mass was determined 48 h after addition of the compounds and was followed by the calculation of LD<sub>50</sub> values. The calculation of the LC<sub>50</sub> values was performed by plotting the percent inhibition versus the concentration of inhibitor on a semi-logarithmic plot. From this, the molar concentration causing 50% reduction of the living cell mass was calculated. At least three independent experiments were performed for each compound.

**In silico binding mode of 1:47:** In silico studies were performed with the X-ray co-crystal structure of a type II inhibitor and CYP121 (PDB ID: 4G44) using MOE software package (Chemical Computing Group).<sup>[66]</sup> Prior to modeling, a pharmacophore model was created, placing a feature for an interacting metal on the heme iron (ML2, R=1) and a second feature for a metal ligand (ML, R=1) on the iron-coordinating nitrogen of the co-crystallized ligand. Both features were set to be essential and constrained (Atoms/Projections). Before energy minimization with LigX the solvent and the ligand was deleted from the structure. For LigX, an AMBER10:EHT force-field with the default parameters were used but the solvation model was changed to R-Field as recommended by the manufacturer. For docking experiments the following parameters were used: Protocols = induced fit, Receptor = Receptor + Solvent, Site = Selected Atoms (these consisted of the heme and the surrounding amino acids in 4.5 Å proximity), Pharmacophore = File (as described above), Ligand = MDB File (Database file with **1:47**, energy minimized with MMFF94x), Placement = Pharmacophore, Rescoring 1 = London dG, Refinement = Forcefield, Rescoring 2 = GBVI/WSA dG. 30 poses were retained within the placement and refinement step. The resulting poses were sorted by their  $E_{refine}$  score and the first (best) pose was selected for further evaluation.

**Physicochemical properties:** Physicochemical properties were calculated using ACD/Percepta version 2012 (Build 2203, January 29, 2013), ACD/Labs.

## Acknowledgements

Many thanks go to Jeannine Jung, Mellissa Meng, and Phil Servatius for their experimental support. We also thank Prof. Munro (University of Manchester) for kindly providing us the plasmid harboring the *cyp121* gene (pHAT2/*cyp121*), and Prof. Bernhardt

(Saarland University) for the kind gift of the purified ferredoxin Etp1fd (516–618) and ferredoxin reductase Arh1\_A18G.

## Conflict of interest

The authors declare no conflict of interest.

**Keywords:** anti-infectives · biophysics · inhibitors · *Mycobacterium tuberculosis* · screening

- [1] Global Tuberculosis Report 2014, World Health Organization (WHO): [http://apps.who.int/iris/bitstream/10665/137094/1/9789241564809\\_eng.pdf](http://apps.who.int/iris/bitstream/10665/137094/1/9789241564809_eng.pdf), ISBN 978-92-4-156480-9.
- [2] Z. F. Udawadia, R. A. Amale, K. K. Ajbani, C. Rodrigues, *Clin. Infect. Dis.* **2012**, *54*, 579–581.
- [3] A. A. Velayati, M. R. Masjedi, P. Farnia, P. Tabarsi, J. Ghanavi, A. H. ZiaZarifi, S. E. Hoffner, *Chest* **2009**, *136*, 420–425.
- [4] L. E. Connolly, P. H. Edelstein, L. Ramakrishnan, *PLoS Med.* **2007**, *4*, 435–442.
- [5] S. T. Cole, R. Brosch, J. Parkhill, T. Garnier, C. Churcher, D. Harris, S. V. Gordon, K. Eiglmeier, S. Gas, C. E. Barry, F. Tekaiia, K. Badcock, D. Basham, D. Brown, T. Chillingworth, R. Connor, R. Davies, K. Devlin, T. Feltwell, S. Gentles, N. Hamlin, S. Holroyd, T. Hornby, K. Jagels, A. Krogh, J. McLean, S. Moule, L. Murphy, K. Oliver, J. Osborne, M. A. Quail, M. A. Rajandream, J. Rogers, S. Rutter, K. Seeger, J. Skelton, R. Squares, S. Squares, J. E. Sulston, K. Taylor, S. Whitehead, B. G. Barrell, *Nature* **1998**, *393*, 537–544.
- [6] K. Duncan, *Curr. Pharm. Des.* **2004**, *10*, 3185–3194.
- [7] K. J. McLean, D. Clift, D. G. Lewis, M. Sabri, P. R. Balding, M. J. Sutcliffe, D. Leys, A. W. Munro, *Trends Microbiol.* **2006**, *14*, 220–228.
- [8] K. J. McLean, P. Carroll, D. G. Lewis, A. J. Dunford, H. E. Seward, R. Neeli, M. R. Cheesman, L. Marsollier, P. Douglas, W. E. Smith, I. Rosenkrands, S. T. Cole, D. Leys, T. Parish, A. W. Munro, *J. Biol. Chem.* **2008**, *283*, 33406–33416.
- [9] A. G. Tsolaki, A. E. Hirsh, K. Deriemer, J. A. Enciso, M. Z. Wong, M. Hannan, Y. L. G. De Salmoniere, K. Aman, M. Kato-maeda, P. M. Small, *Proc. Natl. Acad. Sci. USA* **2004**, *101*, 4865–4870.
- [10] P. Belin, M. H. Le Du, A. Fielding, O. Lequin, M. Jacquet, J.-B. Charbonnier, A. Lecoq, R. Thai, M. Courcon, C. Masson, C. Dugave, R. Genet, J.-L. Pernodet, M. Gondry, *Proc. Natl. Acad. Sci. USA* **2009**, *106*, 7426–7431.
- [11] M. Fonville, M.-H. Le Du, O. Lequin, A. Lecoq, R. Thai, S. Dubois, G. Grach, M. Gondry, P. Belin, *J. Biol. Chem.* **2013**, *288*, 17347–17359.
- [12] M. B. Martins, I. Carvalho, *Tetrahedron* **2007**, *63*, 9923–9932.
- [13] S. A. Hudson, K. J. McLean, S. Surade, Y. Q. Yang, D. Leys, A. Ciulli, A. W. Munro, C. Abell, *Angew. Chem. Int. Ed.* **2012**, *51*, 9311–9316; *Angew. Chem.* **2012**, *124*, 9445–9450.
- [14] M. E. Kavanagh, A. G. Coyne, K. J. McLean, G. G. James, C. W. Levy, L. B. Marino, L. P. S. De Carvalho, D. S. H. Chan, S. A. Hudson, S. Surade, D. Leys, A. W. Munro, C. Abell, *J. Med. Chem.* **2016**, *59*, 3272–3302.
- [15] M.-H. Beaupaire Ledu, P. Belin, M. Gondry, A. Lecoq, J.-L. Pernodet (Commissariat A L'energie Atomique), Eur. Pat. No. EP2088143 A1, **2009**.
- [16] M. E. Kavanagh, J. L. Gray, S. H. Gilbert, A. G. Coyne, K. J. McLean, H. J. Davis, A. W. Munro, C. Abell, *ChemMedChem* **2016**, *11*, 1924–1935.
- [17] Z. Ahmad, S. Sharma, G. K. Khuller, P. Singh, J. Faujdar, V. M. Katoch, *Int. J. Antimicrob. Agents* **2006**, *28*, 543–544.
- [18] Z. Ahmad, S. Sharma, G. K. Khuller, *FEMS Microbiol. Lett.* **2006**, *261*, 181–186.
- [19] Z. Ahmad, S. Sharma, G. K. Khuller, *FEMS Microbiol. Lett.* **2006**, *258*, 200–203.
- [20] Z. Ahmad, S. Sharma, G. K. Khuller, *FEMS Microbiol. Lett.* **2005**, *251*, 19–22.
- [21] S. T. Byrne, S. M. Denkin, P. Gu, E. Nuernberger, Y. Zhang, *J. Med. Microbiol.* **2007**, *56*, 1047–1051.
- [22] K. J. McLean, K. R. Marshall, A. Richmond, I. S. Hunter, K. Fowler, T. Kieser, S. S. Gurcha, G. S. Besra, A. W. Munro, *Microbiology* **2002**, *148*, 2937–2949.
- [23] M.-P. Lézé, M. Le Borgne, P. Pinson, A. Paluszczak, M. Duflos, G. Le Baut, R. W. Hartmann, *Bioorg. Med. Chem. Lett.* **2006**, *16*, 1134–1137.
- [24] H. Bayer, C. Batzl, R. W. Hartmann, A. Mannschreckt, *J. Med. Chem.* **1991**, *34*, 2685–2691.
- [25] F. Leroux, T. U. Hutschenreuter, C. Charriere, R. Scopelliti, R. W. Hartmann, *Helv. Chim. Acta* **2003**, *86*, 2671–2686.
- [26] M. Voets, I. Antes, C. Scherer, U. Mu, K. Biemel, S. Marchais-oberwinkler, *J. Med. Chem.* **2006**, *49*, 2222–2231.
- [27] S. Lucas, R. Heim, C. Ries, K. E. Schewe, B. Birk, R. W. Hartmann, *J. Med. Chem.* **2008**, *51*, 8077–8087.
- [28] K. J. Mclean, M. R. Cheesman, S. L. Rivers, A. Richmond, D. Leys, S. K. Chapman, G. A. Reid, N. C. Price, S. M. Kelly, J. Clarkson, W. E. Smith, A. W. Munro, *J. Inorg. Biochem.* **2002**, *91*, 527–541.
- [29] T. Omura, R. Sato, *J. Biol. Chem.* **1964**, *239*, 2379–2385.
- [30] K. M. Ewen, B. Schiffler, H. Uhlmann-schiffler, R. Bernhardt, F. Hanne-mann, *FEMS Yeast Res.* **2008**, *8*, 432–441.
- [31] J. J. Müller, F. Hannemann, B. Schif, K. M. Ewen, R. Kappl, U. Heinemann, R. Bernhardt, *J. Inorg. Biochem.* **2011**, *105*, 957–965.
- [32] J. Homola, *Anal. Bioanal. Chem.* **2003**, *377*, 528–539.
- [33] H. Morgan, D. M. Taylor, *Biosens. Bioelectron.* **1992**, *7*, 405–410.
- [34] S. G. Franzblau, M. A. Degroote, S. H. Cho, K. Andries, E. Nuernberger, I. M. Orme, K. Mdluli, I. Angulo-Barturen, T. Dick, V. Dartois, A. J. Lenaerts, *Tuberculosis* **2012**, *92*, 453–488.
- [35] M. Altaf, C. H. Miller, D. S. Bellows, R. O'Toole, *Tuberculosis* **2010**, *90*, 333–337.
- [36] I. Benkoo, F. Hernadi, A. Megyeri, A. Kiss, G. Somogyi, Z. Tegye, F. Kraicsovits, P. Kovács, *J. Antimicrob. Chemother.* **1999**, *43*, 675–681.
- [37] H. M. Korashy, A. Shayeganpour, D. R. Brocks, A. O. S. El-Kadi, *Toxicol. Sci.* **2007**, *97*, 32–43.
- [38] J. Hauptenthal, C. Baehr, S. Zeuzem, A. Piiper, *Int. J. Cancer* **2007**, *121*, 206–210.
- [39] C. Liu, C. Lin, C. Lin, Y. Lin, C. Chen, C. Lin, S. Lin, *Toxicology* **2004**, *196*, 87–93.
- [40] B. G. Wachall, M. Hector, Y. Zhuang, R. W. Hartmann, *Bioorg. Med. Chem.* **1999**, *7*, 1913–1924.
- [41] C. A. Lipinski, F. Lombardo, B. W. Dominy, P. J. Feeney, *Adv. Drug Delivery Rev.* **2001**, *46*, 3–26.
- [42] A. Koul, E. Arnoult, N. Lounis, J. Guillemont, K. Andries, *Nature* **2011**, *469*, 483–490.
- [43] D. Leys, C. G. Mowat, K. J. McLean, A. Richmond, S. K. Chapman, M. D. Walkinshaw, A. W. Munro, *J. Biol. Chem.* **2003**, *278*, 5141–5147.
- [44] C. Tanford, *Science* **1978**, *200*, 1012–1018.
- [45] L. S. Nobre, S. Todorovic, A. F. N. Tavares, E. Oldfield, P. Hildebrandt, M. Teixeira, L. M. Saraiva, *J. Bacteriol.* **2010**, *192*, 1527–1533.
- [46] R. A. Helmick, A. E. Fletcher, A. M. Gardner, C. R. Gessner, A. N. Hvitved, M. C. Gustin, P. R. Gardner, *Antimicrob. Agents Chemother.* **2005**, *49*, 1837–1843.
- [47] H. M. Guardiola-Diaz, L. Foster, D. Mushrush, A. D. N. Vaz, *Biochem. Pharmacol.* **2001**, *61*, 1463–1470.
- [48] H. I. M. Boshoff, T. G. Myers, B. R. Copp, M. R. Mcneil, M. A. Wilson, C. E. Barry, *J. Biol. Chem.* **2004**, *279*, 40174–40184.
- [49] A. Milano, M. R. Pasca, R. Proveddi, A. P. Lucarelli, G. Manina, A. L. D. J. L. Ribeiro, R. Manganelli, G. Riccardi, *Tuberculosis* **2009**, *89*, 84–90.
- [50] L. A. Collins, S. G. Franzblau, *Antimicrob. Agents Chemother.* **1997**, *41*, 1004–1009.
- [51] J. R. Cochrane, J. M. White, U. Wille, C. A. Hutton, *Org. Lett.* **2012**, *14*, 2402–2405.
- [52] U. E. Hille, C. Zimmer, C. A. Vock, R. W. Hartmann, *ACS Med. Chem. Lett.* **2011**, *2*, 2–6.
- [53] C. Jagusch, M. Negri, U. E. Hille, Q. Hu, M. Bartels, K. Jahn-Hoffmann, M. A. E. P.-B. Mendieta, B. Rodenwaldt, U. Müller-Vieira, D. Schmidt, T. Lauterbach, M. Recanatini, A. Cavalli, R. W. Hartmann, *Bioorg. Med. Chem.* **2008**, *16*, 1992–2010.
- [54] M. A. E. Pinto-Bazurco Mendieta, M. Negri, Q. Hu, U. E. Hille, C. Jagusch, K. Jahn-Hoffmann, U. Müller-Vieira, D. Schmidt, T. Lauterbach, R. W. Hartmann, *Arch. Pharm.* **2008**, *341*, 597–609.
- [55] U. E. Hille, Q. Hu, C. Vock, M. Negri, M. Bartels, U. Müller-Vieira, T. Lauterbach, R. W. Hartmann, *Eur. J. Med. Chem.* **2009**, *44*, 2765–2775.
- [56] U. E. Hille, C. Zimmer, J. Hauptenthal, R. W. Hartmann, *ACS Med. Chem. Lett.* **2011**, *2*, 559–564.

- [57] L. Yin, S. Lucas, F. Maurer, U. Kazmaier, Q. Hu, R. W. Hartmann, *J. Med. Chem.* **2012**, *55*, 6629–6633.
- [58] L. Yin, Q. Hu, R. W. Hartmann, *J. Med. Chem.* **2013**, *56*, 460–470.
- [59] L. Yin, Q. Hu, J. Emmerich, M. M. C. Lo, E. Metzger, A. Ali, R. W. Hartmann, *J. Med. Chem.* **2014**, *57*, 5179–5189.
- [60] Q. Hu, J. Kunde, N. Hanke, R. W. Hartmann, *Eur. J. Med. Chem.* **2015**, *96*, 139–150.
- [61] C. Zimmer, M. Hafner, M. Zender, D. Ammann, R. W. Hartmann, C. A. Vock, *Bioorg. Med. Chem. Lett.* **2011**, *21*, 186–190.
- [62] W. Zhu, Q. Hu, N. Hanke, C. J. Van Koppen, R. W. Hartmann, *J. Med. Chem.* **2014**, *57*, 7811–7817.
- [63] K. Hüsecken, S. Hinsberger, W. A. Elgaher, J. Hauptenthal, R. W. Hartmann, *Future Med. Chem.* **2014**, *6*, 1529–1543.
- [64] A. L. Hopkins, C. R. Groom, A. Alex, *Drug Discovery Today* **2004**, *9*, 430–431.
- [65] L. G. Czaplewski, I. Collins, E. A. Boyd, D. Brown, S. P. East, M. Gardiner, R. Fletcher, D. J. Haydon, V. Henstock, P. Ingram, C. Jones, C. Noula, L. Kennison, C. Rockley, V. Rose, H. B. Thomaidis-Brears, R. Ure, M. Whittaker, N. R. Stokes, *Bioorg. Med. Chem. Lett.* **2009**, *19*, 524–527.
- [66] Molecular Operating Environment (MOE) version 2013.08, Chemical Computing Group Inc., Montréal, QC, H3A 2R7 (Canada), **2015**.

---

Manuscript received: June 20, 2017

Revised manuscript received: August 4, 2017

Accepted manuscript online: August 16, 2017

Version of record online: September 26, 2017

**3.2 Chapter B: Structure-Activity Relationship and Mode of Action Studies**  
**Highlight 1-(4-Biphenylmethyl)-1H-imidazole Derived Small Molecules as**  
**Potent *Mycobacterium tuberculosis* CYP121 Inhibitors**

The following person contributed experimentally to this chapter:

Maria Virginia Gentilini: performed cytotoxicity and intracellular replication experiments with macrophages.

## Introduction

Tuberculosis is still one of the leading infectious diseases worldwide with around 10 million new infections and 1.6 million cases of deaths every year.<sup>31</sup> The disease gained more and more attention in the last years due to arising resistances of its pathogen *Mycobacterium tuberculosis* (Mtb) against currently applied first-line drugs and its high prevalence in immune deprived patients such as those infected with HIV.<sup>31,63,64</sup> With the sequence of the genome deciphered in 1998 there were a lot of new possible targets identified.<sup>89</sup> However, the cell wall of Mtb is highly complex and forms a wax-like barrier with partly unknown permeability behavior. This exceptional property impedes the discovery of new inhibitors as they could possibly fail to reach their target and thus appear biologically inactive.<sup>72</sup> One of these identified targets is the Cytochrome-P450 enzyme 121 (CYP121) which was shown to be essential for the viability of Mtb.<sup>110</sup> The gene encoding CYP121 is besides the *Mycobacterium tuberculosis* complex only found in some *Streptomyces* strains with maximum 64 % identity.<sup>111</sup> The elucidation of its function was encouraged by the identification of the role of its neighboring gene in Mtb which encodes a cyclodityrosin (cYY) synthetase.<sup>114</sup> CYP121 was subsequently identified to utilize cYY as substrate and to catalyze its conversion to mycocyclosin via a c-c coupling reaction.<sup>115</sup> However, the biological role of substrate and product remain unknown up to now.

McLean *et al.* identified known antifungal azoles such as econazole or ketoconazole as the first inhibitors of CYP121.<sup>122</sup> Interestingly, the compounds also showed biological activity against Mtb correlating with their respective affinities to CYP121.<sup>110</sup> Furthermore, econazole exhibited activity against multi-drug resistant Mtb, murine TB *in vivo* as well as latent TB *in vitro* and *in vivo*.<sup>187-189</sup>

In several subsequent studies fragment-based approaches were employed and small molecules binding to CYP121 were identified.<sup>124-126,128</sup> Additionally, some substrate analogues were discovered to inhibit CYP121.<sup>127,190</sup> However, none of these compounds was shown to exhibit any *in vitro* activity toward Mtb (or *M. bovis* BCG). Recently, we described a screening approach based on a CYP-inhibitor library which resulted in the identification of the first potent inhibitors of CYP121 with activity against *M. bovis* BCG and Mtb.<sup>186</sup>

Based on this breakthrough in the search for potent CYP121 inhibitors we herein employed a screening of a similarity-oriented library in order to evaluate the possible structural diversity of the hit scaffold and to identify favorable features for affinity and/or activity. Furthermore, we investigated the ability of our compounds to inhibit the enzymatic conversion *in vitro* and their inhibitory effect on *M. bovis* BCG. Mode of action studies after addition of the substrate cYY demonstrated the importance of CYP121 inhibition for the antimycobacterial effect of our compounds. Additionally, the influence of several CYP121 and CYP125 inhibitors on the intracellular replication of *M. bovis* BCG in macrophages was evaluated.

## Results and Discussion

### Library generation and screening results

As a starting point for our screening approach we chose the hit compound **I:47** which was recently identified in a screening of a diversity oriented CYP-inhibitor library (described in chapter 3.1).<sup>186</sup> With its high affinity to CYP121, biological activity against *M. bovis* BCG and Mtb as well as its structure, which offers various optimization possibilities, it serves as an ideal basis for further exploration of the binding and activity properties of this structural class. The created screening library was composed of 94 compounds which all can be assigned to a general structure scheme derived from **I:47** (Figure 3.2.1). The imidazole moiety appeared to be essential for the binding to the heme iron of the enzyme and thus was conserved.<sup>186</sup> Additionally the template consists of a substituted methylene bridge (Figure 3.2.1, motif C) or a propylene linker which connects the imidazole ring with the middle aromatic moiety

(Figure 3.2.1, motif B) and a Western part aromatic moiety (Figure 3.2.1, motif A) which is directly linked to the aforementioned one. The library covered various structural motifs for each of the different parts ensuring a broad analysis of structure-activity-relationships and offering the possibility to discover highly potent hits. The structures of all library compounds (**L1** to **L94**) are displayed in the respective supporting information (chapter 7.1.2, table S1).

The screening library was examined in a UV/Vis heme binding assay regarding affinity toward CYP121 as previously described.<sup>186</sup> The compounds were screened at concentrations of 100  $\mu\text{M}$  and 20  $\mu\text{M}$ . For 79 compounds which showed a visible shift of the absorption maximum at concentrations of 20  $\mu\text{M}$  the binding constant  $K_D$  was determined by concentration dependent titration of the enzyme (respective  $K_D$  values are listed in chapter 7.1.2, table S1). All of these binders showed a type-II binding behavior (direct iron interaction) identical to **I:47** as expected because of the structural similarity. 38 of the approved binders (hit rate 40 %) exhibited a binding constant below or equal to **I:47** ( $K_D = 5 \mu\text{M}$ ). The highest affinity was shown by compounds **L89**, **L16**, **L78** with  $K_D$  values of 0.3, 0.5, 0.6  $\mu\text{M}$ , respectively. Interestingly, these compounds have the methoxynaphthalene moiety in position A in common which seems to be particularly favorable for binding.

In parallel to affinity determination the library was analyzed regarding biological activity against *M. bovis* BCG *in vitro*. The compounds were initially tested at a concentration of 100  $\mu\text{M}$  and inhibitors showing inhibition higher than or equal to 80 % were further examined at 10  $\mu\text{M}$ . For 29 compounds with inhibition higher than or equal to 60 % at 10  $\mu\text{M}$   $\text{MIC}_{50}$  values were determined as described previously.<sup>186</sup> **I:47** ( $\text{MIC}_{50} = 4.0 \mu\text{M}$ ) was used as a reference. Ten compounds (hit rate 11 %) showed better activity than **I:47**. Interestingly, the two compounds with a propylene linker (**L15** and **L21**) exhibited the highest activity ( $\text{MIC}_{50} = 1.8 \mu\text{M}$  and 1.5  $\mu\text{M}$ ).

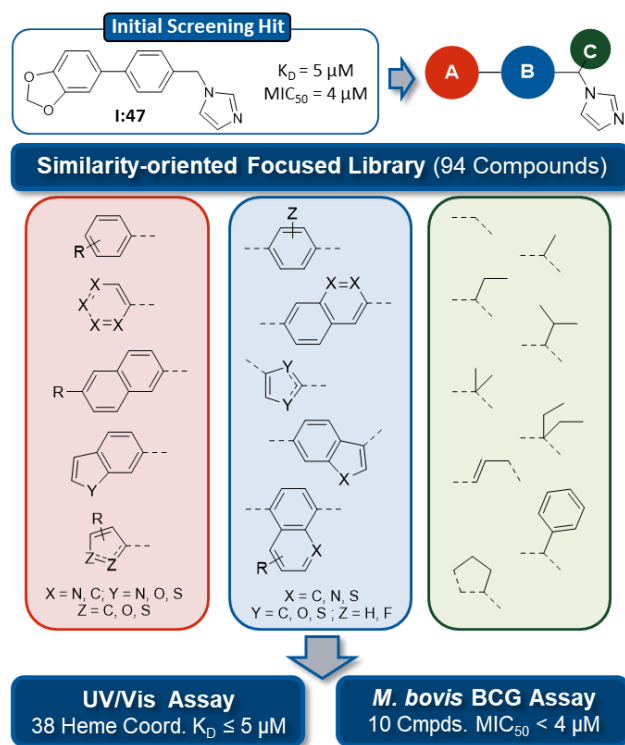
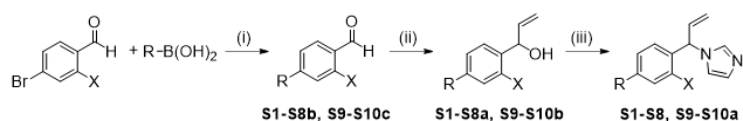


**Figure 3.2.1:** Similarity-guided screening of a focused library. Compounds were selected based on the former screening hit **I:47** with variations in the three displayed structure motifs.  $K_D$  values were determined for 79 positive hits showing visible shift of absorbance maximum at concentrations  $\leq 20 \mu\text{M}$ .  $\text{MIC}_{50}$  values were determined for 29 compounds which showed inhibition  $\geq 60\%$  at 10  $\mu\text{M}$ .

## Chemical Synthesis

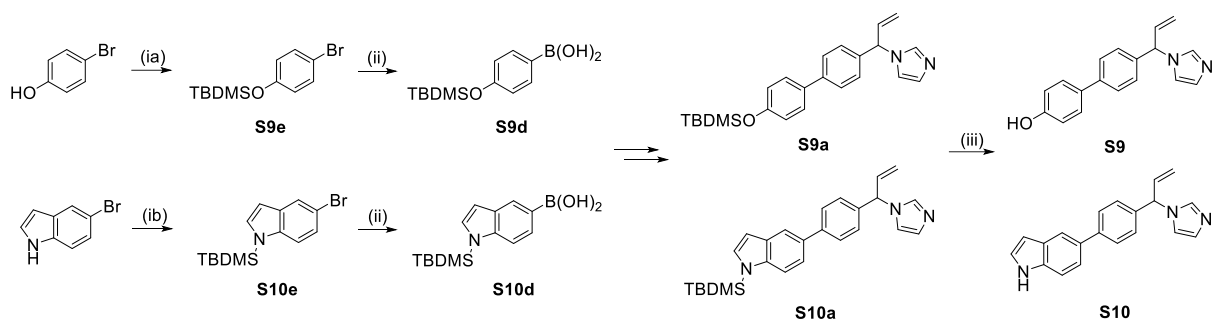
Based on the two most potent inhibitors identified in the screening, **L15** and **L21**, compounds with a novel substituent at the methylene linker were designed. As the ethyl substitution was a promising motif regarding affinity, it was combined with the double bond feature of the propylene linker resulting in an ethenyl substituted methylene bridge.

Compounds **S1-S10** were prepared according to Scheme 3.2.1 starting with a Suzuki coupling of the corresponding boronic acid and 4-bromobenzaldehyde or 4-bromo-2-fluorobenzaldehyde, respectively. For compounds **S9** and **S10** the protected boronic acids were synthesized beginning with a tert-butyldimethylsilyl (TBDMS) protection of the hydroxyl function of 4-bromophenol or the amino group of 5-bromo-1*H*-indole. The boronic acid function was subsequently introduced by a substitution reaction with *n*-butyllithium and triisopropylborate (Scheme 3.2.2). The coupled aldehydes were reduced in a Grignard reaction with vinyl magnesium bromide to the corresponding alcohols with simultaneous introduction of the ethenyl substituent. Consequently, the resulting alcohols were converted to the respective imidazoles through a  $S_N1$  reaction with carbonyldiimidazole (CDI). The compounds were obtained as racemates and principally no separation of the enantiomers was performed. For the protected compounds, the final step was the cleavage of the TBDMS group with tetrabutylammonium fluoride. In contrast, compound **S11**, a fluorinated derivative of hit **I:47**, was synthesized as described in scheme 3.2.3. The first step, a  $S_N1$  reaction of 4-bromo-2-fluorobenzylbromide with imidazole, was followed by a Suzuki coupling of the intermediate with 3,4-methylenedioxyphenylboronic acid resulting in the desired compound. The respective  $K_D$  values of the synthesized derivatives **S1-S11** are listed in the table S3 in chapter 7.1.2.

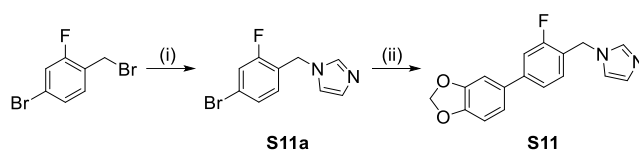


Compound	R	X	Compound	R	X
<b>S1</b>		H	<b>S6</b>		H
<b>S2</b>		H	<b>S7</b>		H
<b>S3</b>		H	<b>S8</b>		F
<b>S4</b>		H	<b>S9a</b>		H
<b>S5</b>		H	<b>S10a</b>		H

**Scheme 3.2.1:** Reagents and conditions: (i) method A: Pd(PPh<sub>3</sub>)<sub>4</sub>, Na<sub>2</sub>CO<sub>3</sub>, toluene:EtO:H<sub>2</sub>O = 5:3:2, 100 °C, 1-4 h; (ii) method B: VinylMgBr, THF abs., -15 °C → rt, 1-2 h; (iii) method C: CDI, MeCN, 110 °C, 1-4 h.



**Scheme 3.2.2:** Reagents and conditions: (ia) method D a): TBDMSCl, imidazole, CH<sub>2</sub>Cl<sub>2</sub>, rt, 16 h; (ib) method D b): TBDMSCl, NaH, CH<sub>2</sub>Cl<sub>2</sub>, 0 °C → rt, 16 h; (ii) method E: nBuLi, B(OiPr)<sub>3</sub>, THF, -78 °C → rt, 3 h; (iii) method F: TBAF, K<sub>2</sub>HPO<sub>4</sub>, THF, rt, 16 h.



**Scheme 3.2.3:** Reagents and conditions: (i) imidazole, NaH, 60 °C, 1.5 h; (ii) method A: 3,4-methylene-dioxyphenylboronic acid, Pd(PPh<sub>3</sub>)<sub>4</sub>, Na<sub>2</sub>CO<sub>3</sub>, toluene:EtOH:H<sub>2</sub>O = 5:3:2, 110 °C, 2.5 h.

### Structure-affinity-relationship

Based on the determined binding constants the compounds were analyzed regarding their structural features in order to identify favorable motifs that contribute positively to affinity. The different parts of the binding compounds were, as far as possible, considered separately to avoid interference of the influence of several features.

First of all, the methylene bridge between imidazole ring and aromatic moiety B tolerated various substituents such as methyl, ethyl, i-propyl, n-butyl, ethenyl or phenyl (**L75**, **L80**, **L92**, **L93**, **S7**, **L1**). Additionally, a decoration with two methyl (**L27**) or ethyl (**L35**) substituents or the exchange with a propylene linker (**L15**) was accepted as well. Moreover, the rigidification we recently addressed in our docking study of **I:47**,<sup>186</sup> performed by connecting the methylene bridge to the adjacent phenyl moiety via an ethylene linker, was also possible without loss of affinity (**L90**). The affinity increased slightly (around twofold compared to ethyl) for space filling substituents such i-propyl, n-butyl, phenyl or two ethyl substituents indicating the involvement of hydrophobic interactions. In contrast, a hydroxyethyl substituent (**L13**) led to weaker binding compared to its ethyl analogue (**L80**) which supports the aforementioned hypothesis.

Compounds with a substituted methylene bridge were evaluated as racemic mixtures. It is known that very often the two enantiomers show strong differences in binding affinity or activity. However, as seen in the docking study of **I:47** the binding pocket of CYP121 principally offers space to harbor both orientations of substituents.<sup>186</sup> To confirm this hypothesis the enantiomers were separated for three exemplarily chosen ethenyl derivatives (chapter 7.1.2, table S4). As expected, only minor differences could be observed between the two enantiomers of a racemate.

The used library contained compounds with various aromatic ring systems in the middle part (Figure 3.2.1, motif B). According to previous findings compounds with a pyridine ring in this position show only weak binding.<sup>186</sup> A furan ring (**L70**, K<sub>D</sub> = 34 μM) was rather unfavorable compared to an unsubstituted benzene whereas a thiophene (2,4- or 2,5 connected) led in some cases to similar affinities (**L42**, **L60**), in other cases, however, to weaker affinities (**L62**, **L64**). Furthermore, other motives such as fluorinated benzene, indole, benzothiophene, naphthalene or quinolone (**L47**, **L48**, **L86**, **L79**, **L82**) were tolerated as well with increased affinities (> twofold) for the latter two scaffolds.

Additionally, a range of motifs for the Western part aromatic ring (Figure 3.2.1, motif A) was evaluated including differently substituted phenyls, thiophene and furan rings and bicyclic ring systems such as benzofuran, benzothiophen, indole and naphthalene. Nearly all of those were tolerated with the exception of nitrogen containing 6-membered rings (**L43**, **L59**). However, some appeared to be particularly favorable such as the bicyclic moieties with 6-methoxynaphthalene leading to the highest affinity (**L16**:  $K_D = 0.5 \mu\text{M}$ , **L78**:  $K_D = 0.6 \mu\text{M}$ ). Further motifs with increased affinities ( $K_D \leq 6 \mu\text{M}$ ) were electron deprived phenyls such as a meta- and para-difluorinated phenyl (**L34**) and para-trifluoromethyl (**L44**) or para-trifluoromethoxy phenyls (**L22**). Additionally, motifs with substituents capable of hydrogen bond formation such as methylthio decorated phenyl or thiophene (**L23**, **L37**) as well as phenyls with a hydroxyl (**L87**) or a N-acetamide group (**L7**) in para position also led to increased affinities.

### Structure-activity-relationship

A good correlation between affinity and activity against *M. bovis* BCG cannot necessarily be expected as the antimycobacterial activity is influenced by additional cellular factors such as permeability, efflux and metabolism. The features of compounds exhibiting high or weak activity were therefore regarded in detail to identify those which impair biological activity.

It is striking that, apart from the propylene linked structures (**L15** and **L21**), the highly active compounds are either not substituted at the methylene bridge (**L10**, **L44**) or possess a methyl substituent (**L73**) or a rigid 5-membered ring structure (**L94**). Other substituents such as ethyl (**L9**), ethenyl (**S10**) or i-propyl (**L92**) led only to weak activity. Interestingly, the attempt to combine the properties of the propylene linker with the ethyl substituent of the methylene bridge via the introduction of an ethenyl substituent did not lead to the desired highly biologically active compound. In comparison with their non-substituted analogues, the ethenyl derivatives show a loss in activity while their affinity is similar (compare **I:47** and **S11** with **S5** and **S8**).

Concerning the middle aromatic moieties (Figure 3.2.1, motif B), benzene, fluorinated benzene, thiophene and indole were able to maintain biological activity (**L44**, **L14**, **L66**, **L48**). Rather unfavorable were bulky center parts such as naphthalene (**L79**) and quinolone (**L81**). Concerning the Western part aromatic moiety (Figure 3.2.1, motif A) trifluoromethylphenyl (**L44**) as well as fluorinated phenyls (**L14**, **L45**) were accepted as well as various bicyclic moieties, para-methoxyphenyl (**L94**) and 2-methylthio(thiophene) (**L76**). In contrast, hydroxyl groups significantly impaired activity (**L2**, **S9**). Furthermore, it has to be mentioned that some motifs of the Western part aromatic moiety (naphthalene, benzothiophene, trifluoromethoxyphenyl, thiomethylphenyl, acetanilide) could not be definitely classified regarding biological activity as the respective evaluated compounds bear substituents at the methylene bridge which already impair activity.

Figure 3.2.2 highlights the structural features identified as favorable for affinity and/or activity. In total, **L15** and **L21** were the most active compounds identified in this study with  $\text{MIC}_{50}$  values of 0.7 and 0.5  $\mu\text{g/mL}$ , respectively (Table 3.2.1). The other eight compounds with superior activity to **I:47** (Table 3.2.1) were similarly active with  $\text{MIC}_{50}$  values between 0.8 or 1.2  $\mu\text{g/mL}$ . Noticeably, all these compounds are not substituted at the methylene bridge except **L94** which contains a 5-membered ring structure. The respective ethyl analogues of **L46**, **L14** and **L76** (compounds **L18**, **L20** and **L37**) showed similar affinities as their parent compounds but failed to significantly inhibit mycobacterial growth.

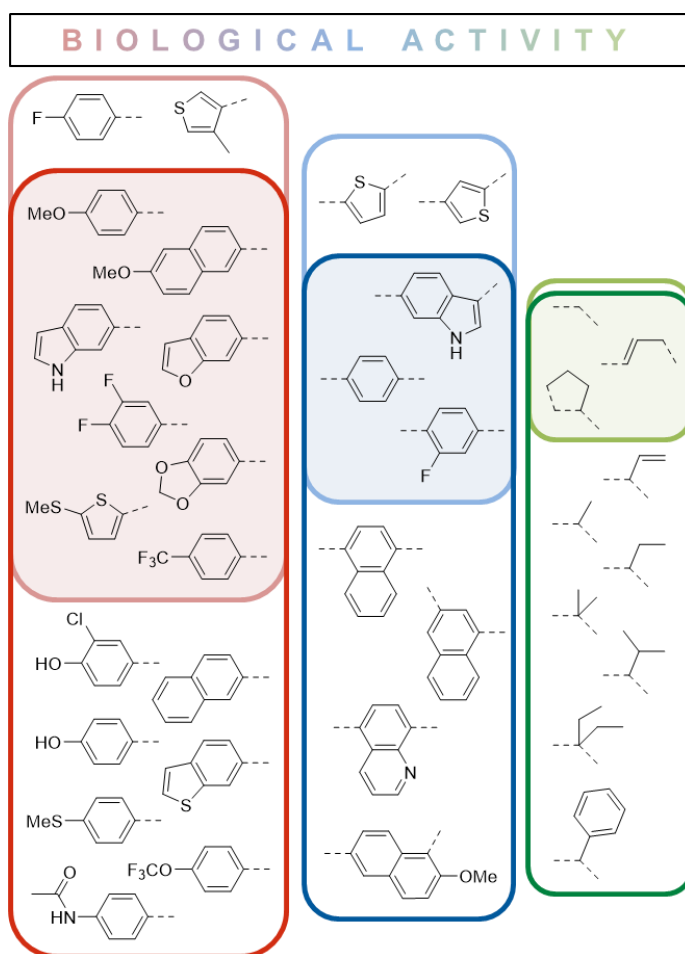


**Figure 3.2.2:** Structure-affinity/activity-relationships. Favorable features for affinity ( $K_D$ ) and activity ( $MIC_{50}$ ) were identified through comparison of similar compounds. Features leading to good affinity are framed in dark green, blue or red respectively to the structure template and oriented to the bottom. In contrast, features related to good biological activity are framed in light green, blue or red and are oriented to the top. The overlap of these favorable features is shaded in the respective color.

In contrast, the ethyl analogue of **L78**, namely **L16**, was relatively active with a  $MIC_{50}$  value of  $7.4 \mu M$  ( $K_D = 0.5 \mu M$ ) similar to the ethenyl analogue **S1** ( $K_D = 0.8 \mu M$ ,  $MIC_{50} = 9.7 \mu M$ ). For these compounds the discrepancy between  $K_D$  and  $MIC_{50}$  was high and can be associated to the methoxynaphthalene motif which led to high affinities that were not translated into the expected biological activity. For the ethyl analogue **L16** the activity was probably further reduced by the substituent as observed for similar compound pairs.

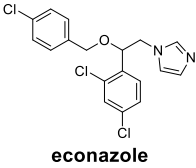
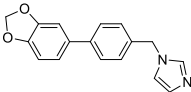
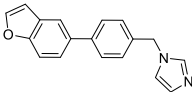
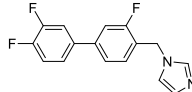
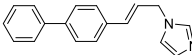
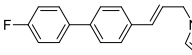
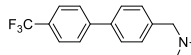
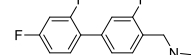
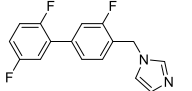
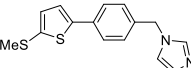
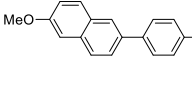
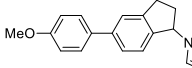
One of the most active compounds was the benzofuran analogue (**L10**) of compound **I:47** (Table 3.2.1). **L10** showed a slightly higher affinity and activity. Compound **L78** resembles the latter two compounds with thiophene as a bioisosteric substitute for phenyl and its methylthio group replacing a part of the attached furan motif. The same applies to the methoxyphenyl motif of compound **L94**. Their affinities and activities are likewise similar to those of their analogues.

In contrast, the potent compounds **L14**, **L44**, **L45** and **L46** share an electron deprived phenyl ring at the Western part aromatic motif (Table 3.2.1). Furthermore, **L14**, **L45** and **L46** contain a fluorinated benzene ring at their middle aromatic position. Although the affinities of **L45** and **L46** are slightly lower compared to **L14** and **L44**, the activities within this group are similar amongst each other and comparable to the aforementioned group of compounds.

Overall, a good a correlation between affinity and activity was observed for twelve compounds (**S7**, **S11**, **L10**, **L47**, **L48**, **L49**, **L60**, **L66**, **L75**, **L90**, **L91**, **L94**). For 13 compounds a bad correlation was explained by unfavorable structural features (**L8**, **L9**, **L16**, **L19**, **L41**, **L77**, **L78**, **L79**, **L84**, **L89**, **S1**, **S2**, **S9**). For further seven compounds (**S3**, **S4**, **S5**, **S6**, **S8**, **S10**, **L12**) a correlation was not observed ( $MIC_{50} > 2 \times K_D$ ) probably due to structural drawbacks that were not identified so far. Further compounds have to be evaluated to confirm this hypothesis.

Interestingly, eight compounds (**L14**, **L15**, **L21**, **L44**, **L45**, **L46**, **L73**, **L76**) showed higher activity than expected based on their affinities ( $K_D \approx 2-3 \times MIC_{50}$ ). One explanation for this discrepancy is that the  $K_D$  values might be actually lower than determined with our method. For econazole we determined a  $K_D$  value of 2.8  $\mu M$ , although the  $K_D$  value was previously reported to be 0.02  $\mu M$ .<sup>110</sup> Apart from that, the inhibition of other targets cannot be excluded. In this context it is of interest that it was shown that antifungal azoles bind to others of the 20 CYP enzymes of Mtb.<sup>191</sup>

**Table 3.2.1:**  $K_D$  and  $MIC_{50}$  values of compounds showing better activity than **I:47**.

Compound	$K_D \pm STD$ [ $\mu M$ ]	$MIC_{50}$ [mg/L]	$MIC_{50}$ [ $\mu M$ ]
 econazole	$2.8 \pm 0.2^{[a]}$	2.6	12.7
 <b>I:47</b>	$5.4 \pm 1.0^{[a]}$	1.4	4.0
 <b>L10</b>	$2.9 \pm 0.4$	0.9	2.6
 <b>L14</b>	$6.4 \pm 0.9$	0.9	2.7
 <b>L15</b>	$4.3 \pm 0.8$	0.7	1.8
 <b>L21</b>	$5.9 \pm 0.6$	0.5	1.5
 <b>L44</b>	$5.6 \pm 0.9$	0.8	2.4
 <b>L45</b>	$12.6 \pm 2.0$	1.2	3.4
 <b>L46</b>	$9.2 \pm 2.0$	1.0	2.9
 <b>L76</b>	$6.6 \pm 1.0$	1.1	3.2
 <b>L78</b>	$0.6 \pm 0.2$	0.8	2.4
 <b>L94</b>	$4.7 \pm 0.8$	1.1	3.3

<sup>[a]</sup> determined previously.<sup>186</sup>

### Inhibition of cYY conversion *in vitro*

In order to evaluate the influence of the identified heme binders on the inhibition of CYP121 we used our *in vitro* assay consisting of CYP121, two electron transfer proteins (etp1<sub>fd</sub> and Arh1\_A18G), NADPH as electron donor and an electron regenerating system.<sup>186</sup> Under the defined conditions the substrate cYY was converted to mycocyclusin within approximately 10 minutes (Figure 3.2.3). The presence of a heme binder is expected to inhibit this enzymatic conversion in a concentration dependent manner. Indeed, we could observe the anticipated behavior for four exemplarily chosen compounds (**I:47**, **L10**, **L15**, **L21**) and the reference econazole. The  $IC_{50}$  values ranged between 19 and 36  $\mu M$  in the presence of 20  $\mu M$  substrate (chapter 7.1.2, table S5). The  $IC_{50}$  values were determined for both,

substrate depletion and product formation and resulted in similar values (chapter 7.1.2, figure S5). Compared to the determined binding constants the  $IC_{50}$  values are significantly higher. This is probably caused by the high substrate concentration which was necessary for LC-MS/MS analysis.<sup>192,193</sup> As expected, there is a correlation between binding affinities of the compounds and their  $IC_{50}$  values. In contrast, the reference compound econazole has a twofold lower  $IC_{50}$  value despite of having a similar binding constant. An explanation for this finding could be the described inhibitory effect of econazole on NADPH-dependent reductases and G6P dehydrogenase which are present in the assay.<sup>194,195</sup>

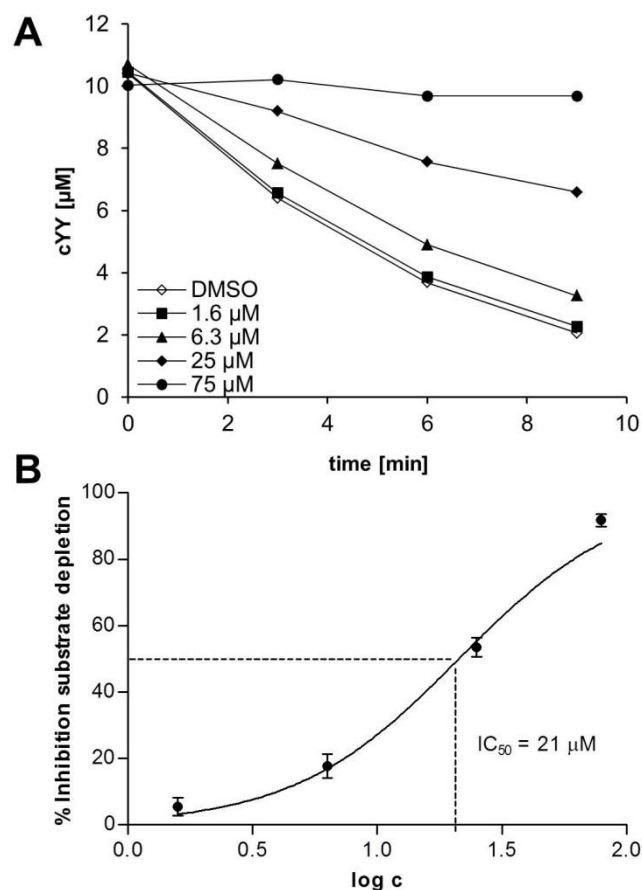


**Figure 3.2.3:** Influence of **L21** on the conversion of cYY to mycocyclusin by CYP121. CYP121 was incubated with **L21**, electron transfer system (Arh1, etp1fd), regenerative system (G6P-DH, G6P, MgCl<sub>2</sub>) and substrate cYY. The conversion was stopped by the addition of MeOH with ISTD and analyzed via LC-MS/MS. DMSO was used as control. A: time-dependent concentration of cYY for different inhibitor concentrations. The relative inhibition was calculated via determination of the respective reaction velocity.  $IC_{50}$  values were determined through non-linear regression of inhibition vs.  $\log c$  (B). The error bars represent the standard deviation of at least 2 replicate measurements.

### Effect of cYY on *M. bovis* BCG growth and CYP121 inhibition

To investigate whether the reduced growth of *M. bovis* BCG in presence of our compounds was indeed caused by inhibition of CYP121, we evaluated the growth inhibition effect of **I:47** in presence of cYY. In the control without inhibitor the growth was significantly accelerated (Figure 3.2.4A). CYP121 was previously shown to be essential for viability, however, the reason for this was not yet elucidated.<sup>110</sup> Our observation suggests that a potential toxic effect of accumulated cYY is rather unlikely and the reaction product mycocyclusin may be essential for growth. In presence of **I:47** the growth enhancing effect of cYY was completely blocked at inhibitor concentrations higher than 0.6  $\mu\text{M}$ , whereas at lower concentration the stimulating effect of cYY was partly reduced (Figure 3.2.4B). These findings support the hypothesis that the binding of our compounds to the heme iron of CYP121 blocking the formation of mycocyclusin is the main reason for the antimycobacterial activity.

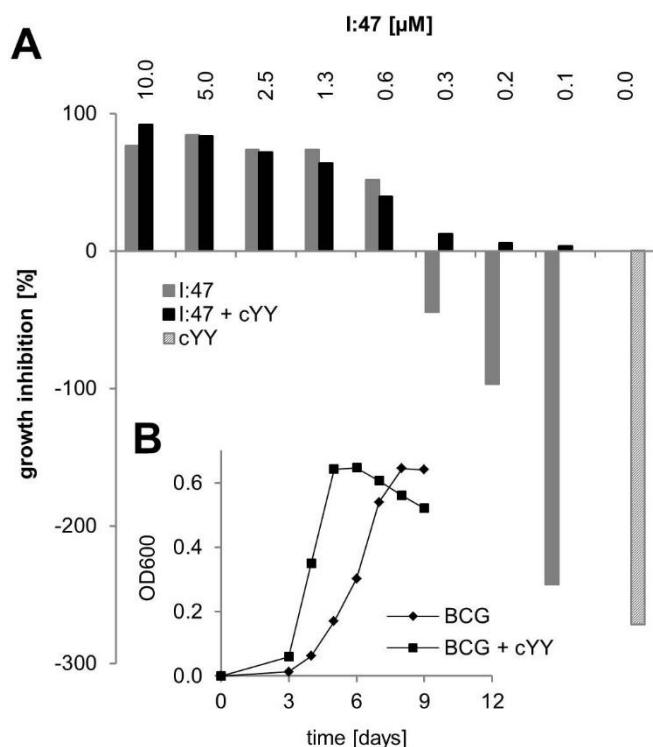


**Figure 3.2.4:** Effect of CYP121 substrate cYY on the growth of *M. bovis* BCG and its inhibition by **I:47**. The addition of 50 μM cYY accelerated the growth of *M. bovis* BCG (B). The resulting growth enhancement of cYY (A, grey striped bar) can be reversed through the CYP121 inhibitor **I:47** in a concentration-dependent manner (grey bars) in accordance to its growth inhibiting effect (black bars).

### Inhibition of intracellular replication of macrophages

*Mtb* has the ability to survive and replicate within the macrophages of the host.<sup>61,196</sup> Therefore, we determined whether our compounds can influence the intracellular replication of *M. bovis* BCG in macrophages. The effects of three recently identified CYP121 inhibitors (**I:16**, **I:48**, **I:47**)<sup>186</sup>, two previously described inhibitors of CYP125 (**C36**, **C23**)<sup>197</sup> and one dual inhibitor of CYP121 and CYP125 (**C43**)<sup>197</sup> were evaluated (chapter 7.1.2, table S7). CYP125 is part of the *igr* operon which was identified as a key player for intracellular survival of mycobacteria in macrophages.<sup>198</sup> It catalyses the oxidation of cholest-4-en-3-one as part of the cholesterol detoxification and is in addition to CYP121 a further promising target for TB treatment.<sup>199</sup>

First of all, the compounds were evaluated regarding their cytotoxicity toward macrophages. None of them showed any significant reduction of viability (chapter 7.1.2, figure S6). Regarding antimycobacterial activity, among the two evaluated CYP125 inhibitors only **C23** showed a strong reduction of intracellular replication (Figure 3.2.5). In contrast, **C36** showed only little efficacy. This marked difference in antimycobacterial activity could be due to impaired permeability of **C36**. The compounds have to cross the macrophage cell membrane as well as the mycobacterial cell envelope to reach their target and the structure differences of the two compounds could cause different permeability. Furthermore, **C23** also binds to CYP121, the selectivity towards CYP125, however, is more than 6-fold higher.<sup>197</sup>

The treatment with CYP121 inhibitors **I:47** and **I:48** significantly reduced the replication of *M. bovis* BCG inside macrophages. However, the effect of **I:16** was more pronounced. This finding can be explained by an additional inhibition of another CYP enzyme present in the mycobacteria. As the imidazole moiety of the compounds is known to be a typical interaction partner for CYP enzymes, inhibition of another CYP cannot be excluded.<sup>89,91</sup>

Interestingly, compound **C43** could block the intracellular replication comparable to the penicillin-streptomycin control. **C43** binds to CYP121 and CYP125 with similar affinities and its strong effect is

probably caused by these two activities. Thus, the dual inhibition of the two CYP enzymes shown to play an important role in viability and persistence is a successful strategy to prevent the proliferation of the mycobacteria in macrophages.<sup>101,110,198</sup>

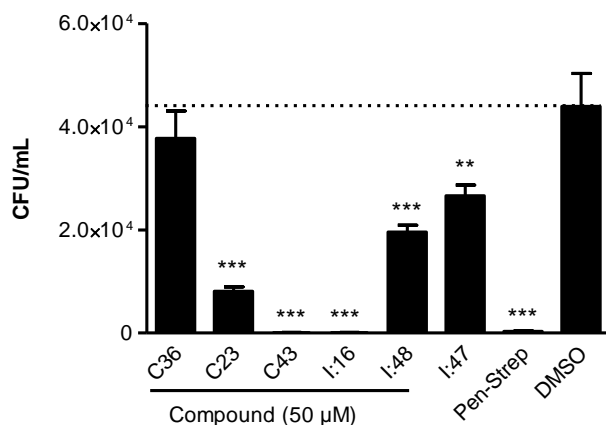


**Figure 3.2.5:** Effect on intracellular replication in macrophages. Macrophages were infected with *M. bovis* BCG and maintained in the presence of selected CYP125 inhibitors **C36** and **C23**, CYP121 inhibitors **I:16**, **I:47** and **I:48** or dual inhibitor **C43**. At 72 h post infection macrophages were plated on agar to determine intracellular CFU. Penicillin-Streptomycin and DMSO were used as positive and negative controls, respectively. Significance of results for treated versus untreated cells (DMSO). \*\* $p < 0.001$ ; \*\*\* $p < 0.0001$ .

## Conclusion

The recently published screening of a CYP-inhibitor library which led to the identification of hit compound **I:47** with micromolar affinity toward CYP121 and activity against Mtb highlighted CYP121 as a possible target for treatment of Mtb infections.<sup>186</sup> We herein presented a continuation of the former study by the screening of a similarity-oriented library based on the frontrunner compound **I:47**.

The screening approach comprised the evaluation of the respective compound class regarding affinity toward CYP121 and biological activity against *M. bovis* BCG. 38 compounds (hit rate 40 %) showed binding constants lower than or equal to **I:47** ( $K_D = 5 \mu\text{M}$ ) with the same type-II binding mode determined in a UV-Vis heme coordination assay. In contrast, the hit rate regarding activity, which was measured by means of growth inhibition of *M. bovis* BCG *in vitro*, was comparatively low (11 %) emphasizing that further criteria like permeability or stability toward mycobacterial metabolism and efflux must be met.

Based on the analysis of the structural features for biological activity we enlarged our library by synthesis of further promising compounds to ensure a comprehensive SAR study. Ten compounds with an ethenyl substituted methylene linker that differ in their Western part aromatic motifs were synthesized accompanied by a fluorine analogue of the former hit **I:47**.

The quantity of determined binding affinities enabled a broad analysis of structure-affinity-relationships. This analysis revealed the tolerance of various substituents at the methylene bridge with increased affinities for hydrophobic space-filling groups. As the library compounds were principally screened as racemates the enantiomers were separated for three exemplarily chosen ethenyl derivatives. The binding constants revealed only minor differences between the enantiomers and thus a separation was of less importance. Concerning the middle aromatic motif, a negative influence on affinity could be observed for pyridine and furan and partly for thiophene. In contrast, benzene, fluorinated phenyl, indole, benzothiophene, naphthalene or quinolone were accepted with the tendency of increasing affinity for large moieties indicating that hydrophobic interactions might be involved. For the Western part aromatic motif, a wide range of different aromatic ring systems was tolerated with highest affinities for compounds with a 6-methoxynaphthalene motif.

Besides the elucidation of the binding mode, we were also interested in the correlation between affinity and antimycobacterial activity. A direct correlation between these two properties would be a straightforward way to validate our target. However, there are several limitations that impair this approach such as the mycobacterial cell wall which has special permeability properties. There are some models for permeability described in literature though principal rules for the design of compounds with good penetration properties do not exist.<sup>200,201</sup> Additionally, other factors such as the mycobacterial metabolism of the compound or the involvement of efflux pumps could also impede the correlation. Notably, it was reported that Mtb and *M. bovis* BCG possess efflux systems which are able to reduce the intracellular level of econazole in resistant mutants and could possibly also transport other azoles.<sup>202</sup> Based on the results of our screening we were able to identify structural features that impair the correlation between affinity and activity. First of all, the substituent at the methylene linker has strong influence on antimycobacterial activity. Only compounds with either no substituent or a methyl or ethenyl substituent as well as compounds with an interconnecting five-membered ring between linker and adjacent phenyl ring showed an inhibitory effect on growth. Other substituted compounds did not show appropriate growth inhibition despite their high affinities. Similar negative effects had bulky middle parts such as naphthalene or quinolone which is in accordance to previously described permeability simulation results.<sup>200</sup> The Western part aromatic motif tolerated diverse functions with the exception of hydroxyl groups which also impair a good correlation. Interestingly, some combinations of “accepted” motifs for the linker substituent and the Western part aromatic motif inexplicably failed to achieve the expected activity. However, in general there is a correlation for compounds without any of the identified features that impair the translation of binding potency into antimycobacterial efficacy. The hit compounds of this screening, which exhibited superior (maximum 2.7-fold) activity to the former hit **I:47**, can be structurally divided into three groups: Firstly, the two most active compounds (**L15** and **L21**) possess a propylene linker and a rather simple structure with two phenyl rings connected to each other (the Western part phenyl being fluorinated for **L21**). The second group (**L10**, **L76**, **L78**, **L94**) has a methylene linker, a benzene ring in the middle part and a Western part aromatic ring with an electron donor function similar to **I:47**. Finally, the third group of compounds (**L45**, **L46**, **L14**, **L44**) has a non-substituted methylene bridge and an electron deprived Western part aromatic ring caused by fluorine or fluorine-containing substituents. Overall, the compounds offer the possibility for further optimization based on the gained insights into structure-activity-relationships.

In order to validate CYP121 as the main target of the described compound class further mode of action studies were performed. First of all, four exemplarily chosen hit compounds were shown to inhibit the enzymatic conversion of cYY to mycocyclosin *in vitro*. Furthermore, we evaluated the effect of a potent CYP121 inhibitor (**I:47**) on the growth of *M. bovis* BCG in the presence of cYY. In absence of inhibitor cYY caused a significant growth enhancement of the mycobacteria. However, in presence of **I:47** this effect was only observed at very low inhibitor concentrations indicating that the conversion to mycocyclosin is essential for the intensified growth. These results strengthen the hypothesis that inhibition of CYP121 is the main reason for the antimycobacterial effect of our compounds.

Finally, we were also able to show that compounds targeting CYP121 and/or CYP125 can reduce the intracellular replication of *M. bovis* BCG in macrophages. Most promising herein appeared the dual inhibitor **C43** and the CYP121 inhibitor **I:16**. Both could block the intracellular proliferation of mycobacteria although the results indicate a possible involvement of an additional target for the latter compound. The inhibition of other CYP enzymes cannot be excluded especially since the genome of Mtb encodes 20 of them which are in general prone to inhibition by azoles.<sup>89,108</sup> Noticeably, the dual inhibition of two of these CYP enzymes seems to be a successful strategy to address Mtb infections.

In summary, we described a screening approach for the discovery of CYP121 inhibitors which led to a deeper understanding of the binding properties of the respective compound class and revealed possibilities for optimization. Furthermore, we gained insights into structure-activity-relationships,

highlighted CYP121 inhibition as the main reason for the antimycobacterial activity of our compounds and introduced the concept of dual CYP inhibition as a promising strategy for the treatment of TB. The results of this study lay the foundation for the development and optimization of CYP121 inhibitors as potent drugs against Mtb infections.

## Experimental Section

**Bacterial strains and growth conditions:** Bacterial strains used in this study were *Mycobacterium bovis* DSM-43990 (BCGT) and *E. coli* K12 BL21. Mycobacteria were cultured in Middlebrook 7H9 broth complemented with ADC Enrichment (Middlebrook).

**Protein expression and purification:** *E. coli* K12 BL21 (DE3) cells were transformed with plasmid harboring *cyp121* gene (pHAT2/*cyp121*).<sup>124</sup> The enzymes were expressed and purified as described previously.<sup>186,203</sup>

**UV/Vis heme P450 binding assay:** Optical titration experiments were performed and analyzed as described previously.<sup>121,186</sup>

**Determination of BCG MIC<sub>50</sub> by OD<sub>600</sub> assay:** A pre-culture of *M. bovis* BCG was grown in 7H9 medium supplemented with ADC Enrichment until OD<sub>600</sub> reached a value of 0.7 and was then used for susceptibility testing in the following 72 h. The assay was performed in 48 well plates (Greiner, Kremsmünster, AT). Prior to culture addition, compounds were serially diluted in DMSO to fit a final DMSO concentration of 1%. For compound susceptibility testing the pre-culture was diluted with fresh medium (7H9 + ADC enrichment) to a concentration of  $1-5 \times 10^5$  cfu/mL. After 4 to 6 days of incubation (until OD<sub>600</sub> of positive control approached its maximum) at 37 °C and 80 % air moisture, bacterial growth was measured by determination of OD<sub>600</sub>. Absorption data was recorded on a Fluostar Omega Multidetector Plate Reader (BMG LABTECH, Ortenberg, DE). The relative inhibition compared to the positive control was plotted against concentration with GraphPad Prism and MIC<sub>50</sub> values were fitted using OneSite Log IC<sub>50</sub> model provided by the software with the following constraints: bottom=0 and top=100. MIC<sub>50</sub> was defined as the concentration at which 50 percent of growth was detected in accordance with previous methods used.<sup>204</sup>

**Determination of influence of cYY on growth and inhibition of I:47:** The assay was performed as described above with the following adjustments: The final DMSO concentration was set to 2 % as I:47 was serially diluted in DMSO and eventually supplied with cYY. The readout time point for cultures supplemented with cYY occurred after 3 to 5 days as the addition of cYY induced an earlier onset of exponential growth phase.

**CYP121 in vitro enzyme inhibition assay:** The enzyme inhibition assay was performed in 200 µL PBS buffer pH 7.2. Compounds were used in concentrations of 1.6, 6.3, 25 and 50, 75 or 100 µM dependent on the respective solubility. The final DMSO concentration was set to 7.5 %. The compounds were incubated with 0.5 µM CYP121 for 10 minutes at 30 °C. After incubation the electron transfer system consisting of Arh1\_A18G (2.5 µM), Etp1fd (7.5 µM) and NADPH+H<sup>+</sup> (200 µM) as well as a regeneration system consisting of glucose-6-phosphate (2 mM), glucose-6-phosphate dehydrogenase (1 unit/200 µL) and MgCl<sub>2</sub> (1 mM) were added. The reaction was started with the addition of cYY (20 µM) and stopped after 0, 3, 6 and 9 min by addition of 200 µL methanol with internal standard dichloro-cYY (4 µM final concentration, addition included).

The characterization of CYP121 activity was conducted by a UHPLC-MS/MS analysis carried out on a TSQ Quantum Access Max mass spectrometer equipped with an ESI-II source and a triple quadrupole mass detector (Thermo Scientific, Dreieich, Germany). Compounds were separated on an Accucore RP-MS 150×2.1 mm 2.6 µm column (Thermo Fisher, Waltham, US) by a methanol/water gradient (from 1.4 min - 3.5 min 50% methanol to 3.5 min - 5.0 min 90% methanol) with a flow of 400 µL/min. Compounds were ionized in negative mode by electrospray ionization. Ionization was assisted by a post-column addition of 2 mM ammonia in methanol with an automated syringe at 1.25 µL/min. Monitored ions were (mother ion [m/z], product ion [m/z], scan time [s], scan width [m/z], collision energy [V], tube lens offset [V], polarity): mycocyclosin: 323.101, 111.100, 0.30, 0.01, 28, 95, negative; cYY:

325.129, 113.043, 0.3, 0.01. 29, 85, negative; internal standard (diiodo-cYY): 576.878, 126.930, 0.3, 0.01, 43, 77, negative. Samples were injected in a volume of 20  $\mu$ L. Xcalibur software was used for data acquisition.

For quantification, the ratios of the area under the curve of the educt and the product were converted to respective concentrations on the basis of determined calibration curves of mycocyclosin and cYY which were synthesized as previously described.<sup>186,205</sup> The initial velocity  $v_0$  of the cYY conversion was determined by linear fit of the respective concentrations of mycocyclosin or cYY over time (0-9 min) with Microsoft Excel software. The IC<sub>50</sub> values were calculated using GraphPad Prism by fitting the relative inhibition of  $v_0$  versus concentration with the OneSite Log IC<sub>50</sub> model provided by the software with the following constraints: bottom=0 and top=100.

**Chemical synthesis:** Chemical synthesis and analytical characterization: Chemicals were purchased from commercial suppliers and used without further purification. Column flash chromatography was performed on silica gel (40–63  $\mu$ m), and reaction progress was monitored by TLC on TLC Silica Gel 60 F<sub>254</sub> plates (Merck, Darmstadt, Germany). All moisture-sensitive reactions were performed under nitrogen atmosphere using anhydrous solvents. <sup>1</sup>H and <sup>13</sup>C NMR spectra were recorded on Bruker Fourier spectrometers (300 MHz) at ambient temperature with the chemical shifts recorded as  $\delta$  values in ppm units by reference to the hydrogenated residues of deuterated solvent as internal standard. Coupling constants (J) are given in Hertz (Hz), and signal patterns are indicated as follows: s, singlet; d, doublet; dd, doublet of doublets; t, triplet; m, multiplet, br, broad signal. The purity of the final compounds was >95% measured by HPLC with UV detection at 254 nm. The SpectraSystem LC system consisted of a pump, an autosampler, and a UV/Vis detector (ThermoFisher, Dreieich, Germany). Mass spectrometry was performed on an LC-coupled Surveyor MSQ electrospray mass spectrometer (ThermoFisher, Dreieich, Germany). The system was operated by the Xcalibur software. A RP C18 NUCLEODUR ec 100-5 125  $\times$  3 mm 5  $\mu$ m column (Macherey-Nagel GmbH, Düren, Germany) was used as the stationary phase. All solvents were HPLC grade. In a gradient run, the percentage of acetonitrile (containing 0.1 % trifluoroacetic acid) was initially kept constant for 2 min at 30 % and was consequently increased from 30 % at 2 min to 100 % at 8 min, kept at 100 % for 2 min and finally at 30% for 2 min. The injection volume was 10  $\mu$ L, and flow rate was set to 700  $\mu$ L/min. MS analysis was carried out in ESI ionization mode at a spray voltage of 3800 V, a cone voltage of 55 V and a probe temperature of 350 °C. Spectra were acquired in positive mode from 100 to 600 m/z.

### 1. Method A: Suzuki coupling

The aldehyde (1 eq.) and the boronic acid (1.3 eq.) were dissolved in toluene (7.5 mL/mmol) and ethanol (4.5 mL/mmol). After addition of 2 M Na<sub>2</sub>CO<sub>3</sub> solution (3 mL/mmol) the mixture was flushed with N<sub>2</sub> for 10 min. Subsequently, Pd(PPh<sub>3</sub>)<sub>4</sub> (0.05 eq.) was added and the mixture flushed for further 5 min with N<sub>2</sub>. The mixture was heated to 100 °C for 1 to 4h until TLC control showed complete conversion. The reaction was quenched with water (20 mL) and extracted with ethyl acetate (3  $\times$  20 mL). The combined organic phases were washed with brine and dried over MgSO<sub>4</sub>. The solvent was evaporated under reduced pressure and the crude product was purified by chromatography on silica gel.

#### 1.1: 4-(6-methoxynaphthalen-2-yl)benzaldehyde (**S1b**):

Synthesized according to method A using 4-bromobenzaldehyde (1.35 mmol; 250 mg) and 6-Methoxy-2-naphthaleneboronic acid (1.73 mmol; 350 mg). **S1b** was obtained as a white solid (330 mg, 93 %): R<sub>f</sub>=0.58 (hexane/EtOAc 8:2); <sup>1</sup>H NMR (300 MHz, CDCl<sub>3</sub>):  $\delta$ =3.97 (s, 3H), 7.17-7.25 (m, 2H), 7.75 (dd, J=8.1, 2.2 Hz, 1H), 7.80-7.92 (m, 4H), 7.99 (d, J=8.4 Hz, 2H), 8.05 (d, J=1.5 Hz, 1H), 10.08 ppm (s, 1H); <sup>13</sup>C NMR (75 MHz, CDCl<sub>3</sub>):  $\delta$ =55.4, 105.6, 119.5, 125.6, 126.4, 127.6, 127.6, 129.0, 129.9, 130.3, 147.2, 158.3, 191.9 ppm; LC-MS (ESI): R<sub>t</sub>=9.54 min, m/z: 263.01 [M+H]<sup>+</sup>.

#### 1.2: 3'-chloro-4'-hydroxy-[1,1'-biphenyl]-4-carbaldehyde (**S2b**):

Synthesized according to method A using 4-bromobenzaldehyde (1.35 mmol; 250 mg) and 3-Chloro-4-hydroxyphenylboronic acid (1.45 mmol; 250 mg). **S2b** was obtained as a white solid (112 mg, 36 %): R<sub>f</sub>=0.27 (hexane/EtOAc 8:2); <sup>1</sup>H NMR (300 MHz, CDCl<sub>3</sub>):  $\delta$ =5.71 (br. s., 1H), 7.14 (d, J=8.5 Hz, 1H), 7.49 (dd, J=8.5, 2.1 Hz, 1H), 7.64 (d, J=2.1 Hz, 1H), 7.70 (d, J=8.3 Hz, 2H), 7.95 (d, J=8.2 Hz, 2H), 10.06 ppm (s, 1H); <sup>13</sup>C NMR (75 MHz, CDCl<sub>3</sub>):  $\delta$ =117.2, 121.0, 127.6, 127.9, 128.2, 130.8, 133.7, 135.5, 145.8, 152.2, 192.2 ppm; LC-MS (ESI): R<sub>t</sub>=7.22 min, m/z: 232.99 [M+H]<sup>+</sup>.

1.3: 3',4'-dimethoxy-[1,1'-biphenyl]-4-carbaldehyde (**S3b**):

Synthesized according to method A using 4-bromobenzaldehyde (1.35 mmol; 250 mg) and 3,4-Dimethoxyphenylboronic acid (1.76 mmol; 320 mg). **S3b** was obtained as a white solid (342 mg, 100 %):  $R_f=0.48$  (hexane/EtOAc 7:3);  $^1\text{H NMR}$  (300 MHz,  $\text{CDCl}_3$ ):  $\delta=3.86\text{--}4.02$  (m, 6H), 6.98 (d,  $J=8.3$  Hz, 1H), 7.15 (d,  $J=1.9$  Hz, 1H), 7.18-7.29 (m, 1H), 7.73 (d,  $J=8.1$  Hz, 2H), 7.90-7.97 (m, 2H), 10.04 ppm (s, 1H);  $^{13}\text{C NMR}$  (75 MHz,  $\text{CDCl}_3$ ):  $\delta=56.4, 110.8, 111.9, 120.4, 127.6, 130.7, 132.9, 135.2, 147.4, 149.8, 150.1, 192.2$  ppm; LC-MS (ESI):  $R_t=7.08$  min;  $m/z$ : 242.99  $[\text{M}+\text{H}]^+$ .

1.4: 4'-methoxy-3'-methyl-[1,1'-biphenyl]-4-carbaldehyde (**S4b**):

Synthesized according to method A using 4-bromobenzaldehyde (1.35 mmol; 250 mg) and 4-Methoxy-3-methylphenylboronic acid (1.75 mmol; 291 mg). **S4b** was obtained as a white solid (317 mg, 100 %):  $R_f=0.54$  (hexane/EtOAc 9:1);  $^1\text{H NMR}$  (300 MHz,  $\text{CDCl}_3$ ):  $\delta=2.31$  (s, 3H), 3.90 (d,  $J=1.2$  Hz, 3H), 6.94 (d,  $J=8.1$  Hz, 1H), 7.41-7.52 (m, 2H), 7.65-7.77 (m, 2H), 7.87-7.97 (m, 2H), 10.04 ppm (s, 1H);  $^{13}\text{C NMR}$  (75 MHz,  $\text{CDCl}_3$ ):  $\delta=16.4, 55.4, 110.3, 125.8, 127.0, 127.3, 129.6, 130.3, 131.6, 134.6, 147.0, 158.4, 191.9$  ppm; LC-MS (ESI):  $R_t=9.04$  min,  $m/z$ : 227.04  $[\text{M}+\text{H}]^+$ .

1.5: 4-(benzo[d][1,3]dioxol-5-yl)benzaldehyde (**S5b**):

Synthesized according to method A using 4-bromobenzaldehyde (1.35 mmol; 250 mg) and 3,4-methylenedioxyphenylboronic acid (1.75 mmol; 290 mg). **S5b** was obtained as a white solid (322 mg, 100 %):  $R_f=0.66$  (hexane/EtOAc 8:2);  $^1\text{H NMR}$  (300 MHz,  $\text{CDCl}_3$ ):  $\delta=6.04$  (s, 2H), 6.92 (dd,  $J=7.7, 0.7$  Hz, 1H), 7.10-7.17 (m, 2H), 7.64-7.71 (m, 2H), 7.88-7.97 (m, 2H), 10.04 ppm (s, 1H);  $^{13}\text{C NMR}$  (75 MHz,  $\text{CDCl}_3$ ):  $\delta=101.4, 107.6, 108.8, 121.3, 127.3, 130.3, 133.9, 134.9, 146.8, 148.1, 148.4, 191.8$  ppm; LC-MS (ESI):  $R_t=8.20$  min,  $m/z$ : 227.01  $[\text{M}+\text{H}]^+$ .

1.6: 3'-fluoro-4'-methoxy-[1,1'-biphenyl]-4-carbaldehyde (**S6b**):

Synthesized according to method A using 4-bromobenzaldehyde (1.35 mmol; 250 mg) and 3-Fluoro-4-methoxybenzeneboronic acid (1.75 mmol; 297 mg). **S6b** was obtained as a white solid (289 mg, 93 %):  $R_f=0.46$  (hexane/EtOAc 8:2);  $^1\text{H NMR}$  (300 MHz,  $\text{CDCl}_3$ ):  $\delta=3.96$  (s, 3H), 7.01-7.13 (m, 1H), 7.34-7.45 (m, 2H), 7.70 (d,  $J=8.5$  Hz, 2H), 7.91-7.99 (m, 2H), 10.05 (s, 1H);  $^{13}\text{C NMR}$  (75 MHz,  $\text{CDCl}_3$ ):  $\delta=56.4$  (s), 113.7 (d,  $J=2.2$  Hz), 115.0 (d,  $J=18.6$  Hz), 123.1 (d,  $J=3.7$  Hz), 127.1 (s), 130.3 (s), 132.7 (d,  $J=6.7$  Hz), 135.1 (s), 145.6 (d,  $J=1.5$  Hz), 148.1 (d,  $J=10.4$  Hz), 152.6 (d,  $J=246.6$  Hz), 191.8 ppm (s); LC-MS (ESI):  $R_t=8.50$  min,  $m/z$ : 231.05  $[\text{M}+\text{H}]^+$ .

## 2. Method B: Grignard reaction

The aldehyde (1.0 eq.) was dissolved in a heat dried flask in dry THF (2 mL/mmol) and cooled to  $-15$  °C in an ice/acetone bath. Vinylmagnesium bromide (1.2 eq., 0.7 M in THF) was added dropwise and the reaction was stirred for 5 min before letting it warm to room temperature for 1-2 h and TLC showed complete conversion. The reaction mixture was quenched with saturated  $\text{NH}_4\text{Cl}$  solution (15 mL) and extracted with ethyl acetate ( $3 \times 20$  mL). The combined organic phases were washed with brine and dried over  $\text{MgSO}_4$ . The solvent was evaporated under reduced pressure and the crude product was purified by chromatography on silica gel.

2.1: 1-(4-(6-methoxynaphthalen-2-yl)phenyl)prop-2-en-1-ol (**S1a**):

Synthesized according to method B using 1b (1.14 mmol; 300 mg) and vinylmagnesium bromide (0.7 M in THF; 1.37 mmol; 2.0 mL). **S1a** was obtained as a yellow solid (201 mg, 61 %):  $R_f=0.33$  (hexane/EtOAc 8:2);  $^1\text{H NMR}$  (300 MHz,  $\text{CDCl}_3$ ):  $\delta=3.96$  (s, 3H), 5.21-5.32 (m, 2H), 5.43 (dd,  $J=17.1, 1.3$  Hz, 1H), 6.13 (ddd,  $J=16.9, 10.6, 6.1$  Hz, 1H), 7.14-7.22 (m, 2H), 7.50 (d,  $J=8.1$  Hz, 2H), 7.71 (d,  $J=8.1$  Hz, 3H), 7.77-7.85 (m, 2H), 7.98 ppm (s, 1H);  $^{13}\text{C NMR}$  (75 MHz,  $\text{CDCl}_3$ ):  $\delta=55.8, 75.6, 106.0, 115.7, 119.6, 126.0, 126.4, 127.3, 127.7, 127.8, 130.1, 134.2, 136.4, 140.6, 141.2, 141.8, 158.2$  ppm; LC-MS (ESI):  $R_t=8.94$  min,  $m/z$ : 274.08  $[\text{M}-\text{OH}]^+$ .

2.2: 3-chloro-4'-(1-hydroxyallyl)-[1,1'-biphenyl]-4-ol (**S2a**):

Synthesized according to method B using 2b (0.25 mmol; 60 mg) and vinylmagnesium bromide (0.7 M in THF; 0.49 mmol; 0.7 mL). **S2a** was obtained as a yellow solid (44 mg, 67 %):  $R_f=0.44$  (hexane/EtOAc 7:3);  $^1\text{H NMR}$  (300 MHz,  $\text{CDCl}_3$ ):  $\delta=5.20\text{--}5.29$  (m, 2H), 5.35-5.44 (m, 1H), 5.60 (br. s., 1H), 6.09 (ddd,  $J=16.9, 10.5, 6.1$  Hz, 1H), 7.09 (d,  $J=8.5$  Hz, 1H), 7.38-7.47 (m, 3H), 7.49-7.54 (m, 2H), 7.56 ppm (d,  $J=2.2$  Hz, 1H).

2.3: 1-(3',4'-dimethoxy-[1,1'-biphenyl]-4-yl)prop-2-en-1-ol (**S3a**):

Synthesized according to method B using 3b (1.24 mmol; 300 mg) and vinylmagnesium bromide (0.7 M in THF; 1.48 mmol; 2.1 mL). **S3a** was obtained as a yellow solid (230 mg, 69 %):  $R_f=0.37$  (hexane/EtOAc 7:3);  $^1\text{H NMR}$  (300 MHz,  $\text{CDCl}_3$ ):  $\delta=3.93$  (s, 3H), 3.95 (s, 3H), 5.21-5.29 (m, 2H), 5.40 (d,  $J=17.1$  Hz, 1H), 6.10 (ddd,  $J=16.9, 10.5, 6.0$  Hz, 1H), 6.95 (d,  $J=8.3$  Hz, 1H), 7.09-7.18 (m, 2H), 7.42-7.46 (m, 2H), 7.53-7.59 ppm (m, 2H);  $^{13}\text{C NMR}$  (75 MHz,  $\text{CDCl}_3$ ):  $\delta=55.9, 56.0, 75.1, 110.4, 111.5, 115.2, 119.4, 126.7, 127.0, 133.8, 140.2, 140.6, 141.2, 148.7, 149.2$  ppm; LC-MS (ESI):  $R_t=6.48$  min,  $m/z$ : 254.04  $[\text{M-OH}]^+$ .

2.4: 1-(4'-methoxy-3'-methyl-[1,1'-biphenyl]-4-yl)prop-2-en-1-ol (**S4a**):

Synthesized according to method B using 4b (1.10 mmol; 250 mg) and vinylmagnesium bromide (0.7 M in THF; 1.40 mmol; 2.0 mL). **S4a** was obtained as a yellow solid (96 mg, 34 %):  $R_f=0.26$  (hexane/EtOAc 9:1);  $^1\text{H NMR}$  (300 MHz,  $\text{CDCl}_3$ ):  $\delta=2.29$  (s, 3H), 3.88 (s, 3H), 5.20-5.29 (m, 2H), 5.40 (d,  $J=17.0$  Hz, 1H), 6.11 (ddd,  $J=16.8, 10.4, 6.0$  Hz, 1H), 6.90 (d,  $J=8.9$  Hz, 1H), 7.37-7.45 (m, 4H), 7.53-7.58 ppm (m, 2H);  $^{13}\text{C NMR}$  (75 MHz,  $\text{CDCl}_3$ ):  $\delta=15.9, 55.0, 74.8, 109.8, 114.7, 124.9, 126.3, 126.5, 126.5, 129.0, 132.5, 139.8, 140.2, 140.4, 157.0$  ppm; LC-MS (ESI):  $R_t=8.66$  min,  $m/z$ : 238.09  $[\text{M-OH}]^+$ .

2.5: 1-(4-(benzo[d][1,3]dioxol-5-yl)phenyl)prop-2-en-1-ol (**S5a**):

Synthesized according to method B using 5b (1.24 mmol; 280 mg) and vinylmagnesium bromide (0.7 M in THF; 1.49 mmol; 2.1 mL). **S5a** was obtained as a yellow solid (209 mg, 66 %):  $R_f=0.48$  (hexane/EtOAc 8:2);  $^1\text{H NMR}$  (300 MHz,  $\text{CDCl}_3$ ):  $\delta=5.18$ -5.29 (m, 2H), 5.40 (dd,  $J=17.1, 1.1$  Hz, 1H), 6.10 (ddd,  $J=16.9, 10.5, 6.1$  Hz, 1H), 6.85-6.92 (m, 1H), 7.03-7.10 (m, 2H), 7.43 (d,  $J=8.1$  Hz, 2H), 7.52 ppm (d,  $J=8.5$  Hz, 2H);  $^{13}\text{C NMR}$  (75 MHz,  $\text{CDCl}_3$ ):  $\delta=75.1, 101.1, 107.6, 108.6, 115.2, 120.6, 126.7, 127.0, 135.2, 140.1, 140.4, 141.3, 147.1, 148.1$  ppm; LC-MS (ESI):  $R_t=7.65$  min,  $m/z$ : 238.04  $[\text{M-OH}]^+$ .

### 3. Method C: CDI reaction

The alcohol (1.0 eq.) and 1,1'-carbonyldiimidazole (3.0 eq.) were dissolved in acetonitrile (15 mL/mmol) and heated to reflux for 1-4 h until TLC control showed complete conversion. The reaction was quenched with water (15 mL) and extracted with ethyl acetate ( $3 \times 20$  mL). The combined organic phases were washed with brine and dried over  $\text{MgSO}_4$ . The solvent was evaporated under reduced pressure and the crude product was purified by chromatography on silica gel.

3.1 1-(1-(4-(6-methoxynaphthalen-2-yl)phenyl)allyl)-1H-imidazole (**S1**):

Synthesized according to method C using 1a (100 mg, 0.34 mmol) and CDI (162 mg, 1.0 mmol). **S1** was obtained as a light yellow solid (39 mg, 34 %):  $R_f=0.19$  (EtOAc);  $^1\text{H NMR}$  (300 MHz,  $\text{CDCl}_3$ ):  $\delta=3.95$  (s, 3H), 5.20 (d,  $J=17.0$  Hz, 1H), 5.47 (d,  $J=10.3$  Hz, 1H), 5.85 (d,  $J=6.3$  Hz, 1H), 6.33 (ddd,  $J=17.0$  Hz, 10.2 Hz, 6.3 Hz, 1H), 6.94 (s, 1H), 7.18 (m, 3H), 7.29 (m, 2H), 7.58 (s, 1H), 7.70 (m, 3H), 7.81 (m, 2H), 7.97 ppm (s, 1H);  $^{13}\text{C NMR}$  (75 MHz,  $\text{CDCl}_3$ ):  $\delta=55.8, 63.7, 106.0, 119.0, 119.7, 119.8, 126.1, 126.2, 127.8, 128.1, 128.4, 129.5, 129.9, 130.1, 134.4, 135.8, 136.2, 137.1, 137.3, 141.9, 158.4$  ppm; LC-MS (ESI):  $R_t=6.77$  min,  $m/z$ : 341.18  $[\text{M+H}]^+$ , 237.04  $[\text{M-Imidazole}]^+$ .

3.2 4'-(1-(1H-imidazol-1-yl)allyl)-3-chloro-[1,1'-biphenyl]-4-ol (**S2**):

Synthesized according to method C using 2a (64mg, 0.25 mmol) and CDI (121 mg, 0.75 mmol). **S2** was obtained as a yellow oil (24 mg, 31 %):  $R_f=0.27$  (EtOAc);  $^1\text{H NMR}$  (300 MHz,  $\text{CDCl}_3$ ):  $\delta=5.18$  (d,  $J=17.0$  Hz, 1H), 5.47 (d,  $J=10.2$  Hz, 1H), 5.82 (d,  $J=6.2$  Hz, 1H), 6.30 (ddd,  $J=16.9$  Hz, 10.4 Hz, 6.3 Hz, 1H), 6.94 (s, 1H), 7.08 (d,  $J=8.4$  Hz, 1H), 7.15 (s, 1H), 7.25 (m, 2H), 7.34 (dd,  $J=8.4$  Hz, 2.2 Hz, 1H), 7.54 (m, 3H), 7.60 ppm (s, 1H);  $^{13}\text{C NMR}$  (75 MHz,  $\text{CDCl}_3$ ):  $\delta=63.4, 116.9, 118.7, 119.6, 121.0, 126.6, 127.2, 127.9, 128.6, 132.9, 135.4, 136.4, 136.5, 140.2, 152.5$  ppm; LC-MS (ESI):  $R_t=2.46$  min,  $m/z$ : 311.15  $[\text{M+H}]^+$ , 243.09  $[\text{M-Imidazole}]^+$ .

3.3 1-(1-(3',4'-dimethoxy-[1,1'-biphenyl]-4-yl)allyl)-1H-imidazole (**S3**):

Synthesized according to method C using 3a (200 mg, 0.74 mmol) and CDI (360 mg, 2.22 mmol). **S3** was obtained as a yellow oil (70 mg, 30 %):  $R_f=0.27$  (EtOAc);  $^1\text{H NMR}$  (300 MHz,  $\text{CDCl}_3$ ):  $\delta=3.93$  (d,  $J=6.89$  Hz, 6H), 5.17 (d,  $J=17.04$  Hz, 1H), 5.44 (d,  $J=10.24$  Hz, 1H), 5.81 (d,  $J=6.24$  Hz, 1H), 6.30 (ddd,  $J=16.88, 10.36, 6.29$  Hz, 1H), 6.90-6.98 (m, 2H), 7.07-7.16 (m, 3H), 7.21-7.28 (m, 2H), 7.53-7.59 ppm (m, 3H);  $^{13}\text{C NMR}$  (75 MHz,  $\text{CDCl}_3$ ):  $\delta=55.9, 63.2, 110.3, 111.5, 118.5, 119.2, 119.4, 127.2, 127.8,$

129.3, 133.1, 135.7, 136.6, 141.2, 148.8, 149.2 ppm; LC-MS (ESI):  $R_t=2.04$  min,  $m/z$ : 253.13 [M-Imidazole]<sup>+</sup>.

#### 3.4 1-(1-(4'-methoxy-3'-methyl-[1,1'-biphenyl]-4-yl)allyl)-1H-imidazole (**S4**):

Synthesized according to method C using 4a (95 mg, 0.37 mmol) and CDI (182 mg, 1.1 mmol). **S4** was obtained as a yellow oil (51 mg, 45 %):  $R_f=0.33$  (EtOAc); <sup>1</sup>H NMR (300 MHz, CDCl<sub>3</sub>):  $\delta=2.29$  (s, 3H), 3.87 (s, 3H), 5.17 (d,  $J=17.04$  Hz, 1H), 5.44 (d,  $J=10.24$  Hz, 1H), 5.81 (d,  $J=6.33$  Hz, 1H), 6.30 (ddd,  $J=16.86, 10.34, 6.33$  Hz, 1H), 6.86-6.95 (m, 2H), 7.11 (s, 1H), 7.20-7.29 (m, 2H), 7.35-7.43 (m, 2H), 7.53-7.61 ppm (m, 3H); <sup>13</sup>C NMR (75 MHz, CDCl<sub>3</sub>):  $\delta=16.3, 55.3, 63.2, 110.2, 118.5, 119.1, 125.3, 126.9, 127.1, 127.8, 129.2, 129.3, 132.2, 135.8, 136.2, 136.6, 141.2, 157.6$  ppm. LC-MS (ESI):  $R_t=4.40$  min,  $m/z$ : 237.18 [M-Imidazole]<sup>+</sup>.

#### 3.5 1-(1-(4-(benzo[d][1,3]dioxol-5-yl)phenyl)allyl)-1H-imidazole (**S5**):

Synthesized according to method C using 5a (200 mg, 0.79 mmol) and CDI (382 mg, 2.35 mmol). **S5** was obtained as a colorless oil (65 mg, 27 %):  $R_f=0.26$  (EtOAc/MeOH 98:2); <sup>1</sup>H NMR (300 MHz, CDCl<sub>3</sub>):  $\delta=5.17$  (d,  $J=17.23$  Hz, 1H), 5.44 (d,  $J=10.24$  Hz, 1H), 5.80 (d,  $J=6.15$  Hz, 1H), 6.00 (s, 2H), 6.29 (ddd,  $J=16.86, 10.34, 6.33$  Hz, 1H), 6.84-6.94 (m, 2H), 7.01-7.13 (m, 3H), 7.22 (d,  $J=8.10$  Hz, 2H), 7.47-7.58 ppm (m, 3H); <sup>13</sup>C NMR (75 MHz, CDCl<sub>3</sub>):  $\delta=63.2, 101.2, 107.5, 108.6, 118.5, 119.3, 120.7, 127.3, 127.9, 129.4, 134.6, 135.7, 136.7, 136.8, 141.2, 147.4, 148.2$  ppm. LC-MS (ESI):  $R_t=4.32$  min,  $m/z$ : 305.14 [M+H]<sup>+</sup>, 237.09 [M-Imidazole]<sup>+</sup>.

### 4. Method D: TBDMS protection

a) 4-Bromophenol (1.0 eq.) and imidazole (1.1 eq.) were dissolved in dry CH<sub>2</sub>Cl<sub>2</sub> (3 mL/mmol) before TBDMS chloride (1.1 eq.) was added. The reaction was stirred at room temperature overnight and quenched with water (30 mL) and 1M HCl (3 mL). The aqueous phase was extracted with CH<sub>2</sub>Cl<sub>2</sub> (2 × 30 mL) and the combined organic phases were washed with brine and dried over MgSO<sub>4</sub>. The solvent was evaporated under reduced pressure and the crude product was purified by chromatography on silica gel.

#### 4.1: (4-bromophenoxy)(tert-butyl)dimethylsilane (**S9e**):

Synthesized according to method D a) using 4-Bromophenol (2.89 mmol; 500 mg), imidazole (3.18 mmol; 216 mg) and TBDMSCl (3.18 mmol; 479 mg). **S9e** was obtained as a colorless oil (810 mg, 98 %):  $R_f=0.89$  (hexane/EtOAc 8:2); <sup>1</sup>H NMR (300 MHz, CDCl<sub>3</sub>):  $\delta=0.19$  (s, 6H), 0.99 (s, 9H), 6.70-6.75 (m, 2H), 7.30-7.35 ppm (m, 2H); <sup>13</sup>C NMR (75 MHz, CDCl<sub>3</sub>):  $\delta=-4.5, 18.2, 25.6, 113.6, 121.9, 132.3, 154.9$  ppm; LC-MS (ESI):  $R_t=11.59$  min.

b) NaH (1.2 eq.) was dissolved in acetonitrile (1 mL/mmol) and cooled to 0 °C. 5-Bromo-1H-indole was dissolved in acetonitrile (1 mL/mmol) and slowly added to the NaH suspension. After stirring for 15 min TBDMS chloride (1.25 eq.) was added and the suspension was let warm to room temperature and stirred overnight. The reaction was quenched with saturated NH<sub>4</sub>Cl (10 mL) solution and extracted with CH<sub>2</sub>Cl<sub>2</sub> (3 × 20 mL). The combined organic phases were washed with brine and dried over MgSO<sub>4</sub>. The solvent was evaporated under reduced pressure and the crude product was purified by chromatography on silica gel.

#### 4.2: 5-bromo-1-(tert-butyl)dimethylsilyl-1H-indole (**S10e**):

Synthesized according to method D b) using 5-Bromo-1H-indole (2.55 mmol; 500 mg), NaH (3.06 mmol; 73.4 mg) and TBDMSCl (3.19 mmol; 480 mg). **S10e** was obtained as a colorless oil (267 mg, 34 %):  $R_f=0.95$  (hexane/EtOAc 9:1); <sup>1</sup>H NMR (300 MHz, CDCl<sub>3</sub>):  $\delta=0.60$  (s, 6H), 0.92 (s, 9H), 6.56 (d,  $J=3.2$  Hz, 1H), 7.18 (d,  $J=3.2$  Hz, 1H), 7.23 (dd,  $J=8.8, 2.0$  Hz, 1H), 7.38 (d,  $J=8.8$  Hz, 1H), 7.75 ppm (d,  $J=2.0$  Hz, 1H); <sup>13</sup>C NMR (75 MHz, CDCl<sub>3</sub>):  $\delta=-4.0, 19.4, 26.2, 104.3, 113.1, 115.1, 123.1, 124.1, 132.2, 133.2, 139.6$  ppm; LC-MS (ESI):  $R_t=11.40$  min,  $m/z$ : 312.11 [M+H]<sup>+</sup>.

### 5. Method E: Boronic acid preparation

The TBDMS protected alcohol or amine (1.0 eq.) was dissolved in dry THF (1 mL/mmol) and cooled to -78 °C. nBuLi (1.25 eq., 2.5 M in THF) was added dropwise and the solution was stirred for 30 min. Triisopropylborate (2.5 eq.) was added slowly and the mixture was stirred for further 45 min at -78 °C. After letting the mixture warm to room temperature for 3 h it was quenched with ethyl acetate : 1 M

HCl = 1 : 1 (10 mL). The organic layer was separated, washed with brine (2 × 10 mL) and dried over MgSO<sub>4</sub>. The solvent was evaporated under reduced pressure and the crude product was washed with cold hexane followed by warm water and dried under reduced pressure.

#### 5.1: (4-((tert-butyldimethylsilyl)oxy)phenyl)boronic acid (**S9d**):

Synthesized according to method E using 9e (2.78 mmol; 800 mg), nBuLi (2.5 M in THF; 3.48 mmol; 1.4 mL) and B(OiPr)<sub>3</sub> (5.56 mmol; 970 mg). **S9d** was obtained as an orange solid (400 mg, 57 %): <sup>1</sup>H NMR (300 MHz, CDCl<sub>3</sub>): δ=0.27 (s, 6H), 1.03 (s, 9H), 6.96 (d, *J*=8.5 Hz, 2H), 8.12 ppm (d, *J*=8.5 Hz, 2H); LC-MS (ESI): R<sub>t</sub>=9.03 min.

#### 5.2: (1-(tert-butyldimethylsilyl)-1H-indol-5-yl)boronic acid (**S10d**):

Synthesized according to method E using 10e (2.58 mmol; 800 mg), nBuLi (2.5 M in THF; 3.23 mmol; 1.3 mL) and B(OiPr)<sub>3</sub> (5.16 mmol; 1.05 g). **S10d** was obtained as a white solid (487 mg, 69 %): R<sub>t</sub>=0.93 (hexane/EtOAc 9:1), <sup>1</sup>H NMR (300 MHz, CDCl<sub>3</sub>): δ=0.69 (s, 5H), 1.00 (s, 8H), 6.81 (d, *J*=2.9 Hz, 1H), 7.26-7.30 (m, 1H), 7.69 (d, *J*=8.4 Hz, 1H), 8.16 (d, *J*=8.4 Hz, 1H), 8.69 ppm (s, 1H); <sup>13</sup>C NMR (75 MHz, CDCl<sub>3</sub>): δ=-3.9, 19.6, 26.3, 105.6, 113.4, 128.4, 129.6, 131.2, 131.3, 144.0 ppm; LC-MS (ESI): R<sub>t</sub>=8.84 min, *m/z*: 276.18 [M+H]<sup>+</sup>.

### 6. Method F: TBDMS deprotection

The aldehyde (1.0 eq.) was dissolved in dry THF (9 mL/mmol), tetrabutylammonium fluoride solution (0.5 eq., 1 M in THF) and 0.1 M K<sub>2</sub>HPO<sub>4</sub> solution (100 μL/mmol, pH 7) were added and the reaction mixture was stirred overnight. The solvent was evaporated under reduced pressure and the crude product was purified by chromatography on silica gel.

#### 6.1 5-(4-(1-(1H-imidazol-1-yl)allyl)phenyl)-1H-indole (**S10**):

Synthesized according to method F using 10a (106 mg, 0.25 mmol) and TBAF (0.13 mL 1M sol., 0.13 mmol). **S10** was obtained as a light brown solid (57 mg, 76 %): R<sub>t</sub>=0.20 (EtOAc/MeOH 98:2); <sup>1</sup>H NMR (300 MHz, CDCl<sub>3</sub>): δ=5.20 (dt, *J*=17.0, 1.1 Hz, 1H), 5.46 (dt, *J*=10.2, 1.0 Hz, 1H), 5.83 (d, *J*=6.2 Hz, 15H), 6.33 (ddd, *J*=16.9, 10.4, 6.3 Hz, 1H), 6.61-6.64 (m, 1H), 6.94-6.97 (m, 1H), 7.13 (s, 1H), 7.24-7.30 (m, 3H), 7.41-7.49 (m, 2H), 7.58 (s, 1H), 7.64-7.69 (m, 2H), 7.86 (d, *J*=0.8 Hz, 1H), 8.38 ppm (br s, 1H); <sup>13</sup>C NMR (75 MHz, CDCl<sub>3</sub>): δ=63.5, 102.9, 111.4, 118.7, 119.2, 119.2, 121.6, 125.1, 127.8, 128.4, 128.9, 132.2, 135.5, 135.8, 135.8, 136.6, 142.9 ppm. LC-MS (ESI): R<sub>t</sub>=3.02 min, *m/z*: 300.19 [M+H]<sup>+</sup>, 232.18 [M-Imidazole]<sup>+</sup>.

#### 6.2 4'-(1-(1H-imidazol-1-yl)allyl)-[1,1'-biphenyl]-4-ol (**S9**):

Synthesized according to method F using 9a (55 mg, 0.14 mmol) and TBAF (0.07 mL 1M sol., 0.07 mmol). **S9** was obtained as a white solid (7.8 mg, 20 %): R<sub>t</sub>=0.19 (EtOAc); <sup>1</sup>H NMR (300 MHz, CD<sub>3</sub>OD): δ=4.59 (s, 1H), 5.18 (dt, *J*=16.9, 1.3 Hz, 1H), 5.44 (dt, *J*=10.2, 1.1 Hz, 1H), 6.04 (d, *J*=6.4 Hz, 1H), 6.42 (ddd, *J*=16.9, 10.3, 6.4 Hz, 1H), 6.82-6.88 (m, 2H), 7.01 (t, *J*=1.1 Hz, 1H), 7.10 (t, *J*=1.3 Hz, 1H), 7.29 (d, *J*=8.1 Hz, 2H), 7.43-7.49 (m, 2H), 7.55-7.62 (m, 2H), 7.70 ppm (s, 1H); <sup>13</sup>C NMR (75 MHz, CD<sub>3</sub>OD): δ=64.7, 116.9, 119.5, 120.2, 128.0, 129.2, 129.2, 133.0, 137.7, 138.0, 138.2, 142.8, 158.7 ppm; LC-MS (ESI): R<sub>t</sub>=1.47 min, *m/z*: 277.09 [M+H]<sup>+</sup>, 209.09 [M-Imidazole]<sup>+</sup>.

#### 7. 1-(4-Bromobenzyl)-1H-imidazole (**S11a**):

NaH (19.5 mmol, 800 mg, 60 % in paraffin oil) was suspended in 3 mL dry DMF. After cooling to 4 °C a solution of imidazole (15.0 mmol, 1.02 g) in DMF (3 mL) was added dropwise. The solution was stirred at 4 °C for 1 h. 1-Bromo-4-(bromomethyl)benzene (15.0 mmol, 3.75 g) was dissolved in 5 mL DMF added dropwise to the reaction mixture which was subsequently warmed to room temperature and then to 60 °C for 1.5 h. The reaction was quenched with H<sub>2</sub>O (5 mL) and extracted with ethyl acetate (3 × 15 mL). The combined organic phases were washed with brine, dried over MgSO<sub>4</sub> and the solvent was evaporated under reduced pressure. Remaining DMF was removed by repeated addition of n-heptane and evaporation under reduced pressure. The crude product was purified by chromatography on silica gel (EtOAc : petrol ether = 9 : 1). The product was obtained as white solid (2.10 g, 59 %): R<sub>t</sub>=0.21 (EtOAc); <sup>1</sup>H NMR (500 MHz, DMSO-*d*<sub>6</sub>): δ=5.19 (s, 2H), 6.92 (m, 1H), 7.20 (m, 2H), 7.56 (m, 3H), 7.75 ppm (m, 1H); <sup>13</sup>C NMR (125 MHz, DMSO-*d*<sub>6</sub>): δ=86.2, 157.0, 158.3, 166.3, 167.1, 169.0, 174.8, 174.9 ppm; LC-MS (ESI): R<sub>t</sub>=4.99 min, *m/z*: 236.9 [M+H]<sup>+</sup>.

**Enantiomer separation and analysis:** The enantiomers were separated using a Daicel ChiralPak® IE column (5 µm, 10 × 250 mm) with a preparative HPLC (Thermo Scientific Ultimate 3000, consisting of Dionex Ultimate 3000 pump, diode array detector and automated fraction collector) monitoring the absorbance at 254 nm. An isocratic flow of 5 mL/min was applied with the following solvent composition: Compound **S1** and **S4**: methyl-tert-butyl ether (MtBE):(EtOH + 0.5% ethylenediamine) = 98:2, Compound **S5**: MtBE:(EtOH + 0.5% ethylenediamine) = 96:4.

**Macrophage cytotoxicity and intracellular macrophage replication:** *Strain and growth conditions:* *M. bovis* BCG Pasteur strain was grown at 37°C in Middlebrook 7H9 broth (BD Biosciences) supplemented with 10% Middlebrook OADC enrichment medium (BD Biosciences), 0.002% glycerol (Roth), and 0.05% Tween 80 (Roth). Midlog phase cultures were harvested, aliquoted, and frozen at -80°C. Bacteria were prepared from frozen stocks by thawing at 37°C, resuspension in PBS and passage through a 27G needle. Determination of optical density at 580 nm was done to adjust the amount of the bacteria required in cell culture medium without antibiotics.

*Cells and media:* Bone marrow derived macrophages were prepared from femurs and tibiae remove from C57BL/6 mice using a standard protocol. Briefly, bone marrow cells were cultured for 7 days in complete RPMI (RPMI 1640 plus Glutamax (Gibco), fetal calf serum 10% (HyClone), 100 U/mL penicillin and 100 µg/mL streptomycin (Biochrom) and 50 µM β-Mercaptoethanol (Gibco)) supplemented with 10% L929 cell-conditioned medium as a source of murine M-CSF. On day 7, fully differentiated macrophages were transferred to 96-well plates. Antibiotics were omitted from cell culture medium 24 hours prior to and during the experiments.

*Mycobacteria infection:* Macrophages at 200,000 cells/well were seeded on 96 flat well plates (100 µL) 24 hours previous infection in DMEM 10% L929 CM. After 2.5 hours of infection with *M. bovis* BCG Pasteur at multiplicity of infection (MOI) 10:1, cells were extensively washed with RPMI to remove extracellular mycobacteria. Infected macrophages were maintained in cell culture medium at 37°C and 5% CO<sub>2</sub> in the presence or absence of the compounds at the indicated concentrations. Penicillin-Streptomycin and DMSO were used as control at the indicated concentrations.

To monitor the bacterial intracellular survival, cells were lysed with a sterile solution of 0.1% (vol/vol) Triton X-100 in H<sub>2</sub>O, and serial dilutions of lysates were rapidly plated on 7H9 agar plates to enumerate CFU. This procedure was done at 72 hours after compound incubation. Experiments were carried out in triplicate. Each assay was repeated in at least three independent experiments.

*Statistical analysis:* Statistical analysis was performed with one-way analysis of variance, followed by a post hoc Tukey test, using Graph- Pad Prism 5.0 software. The data are represented as means ± standard errors of the means (SEM).

*In vitro cytotoxicity assay:* *In vitro* cytotoxicity assays were performed with murine macrophages generated as mentioned before. Microtiter plates (96 wells) were loaded with at 200,000 cells/well suspended in 100 µL of RPMI 1640 plus Glutamax (GIBCO) supplemented with 10% heat inactivated fetal calf serum 10% (HyClone) and 50 µM β-Mercaptoethanol (Gibco) in presence or absence of the compounds at the indicated concentrations. Isoniazid, rifampicin and DMSO were used as control at the indicated concentrations. The plates were incubated for 48 h at 37 °C in 5% CO<sub>2</sub>. Cell viability was assessed by measuring using LIVE/DEAD Fixable Aqua Dead Cell Stain Kit by FACS. The data were analyzed using FlowJo (Treestar). Experiments were carried out in triplicate. Each assay was repeated in at least three independent experiments.

### **3.3 Chapter C: Fragment-based Design of $\alpha$ -substituted Mercaptoacetamides as Inhibitors of the Virulence Factor LasB from *Pseudomonas aeruginosa***

The following persons contributed experimentally to this chapter:

Asfandyar Sikandar: purified LasB, performed LasB crystallization experiments and structure determination.

Katrin Voos: synthesized  $\alpha$ -alkylated thiols.

Andreas M. Kany: expressed LasB.

## Introduction

*Pseudomonas aeruginosa* is a gram-negative bacterium which is ranked by the WHO amongst the most critical pathogens today.<sup>29</sup> The opportunistic bacterium causes around 10 % of hospital acquired infections and has a high occurrence among immunocompromised and cystic fibrosis patients.<sup>30,131,132,134</sup> The development of potent antibiotics is urgently needed due to the lack of efficient therapeutics on the market.<sup>16,140</sup>

This task is complicated by the high intrinsic resistance of the pathogen.<sup>141,206</sup> *P. aeruginosa* has an especially low permeability of the outer membrane preventing the entrance of antibiotics into the cell.<sup>142</sup> Additionally, its efflux pumps efficiently move undesired antimicrobials out of the cell and its inducible chromosomal  $\beta$ -lactamases are able to inactivate respective  $\beta$ -lactam antibiotics.<sup>143–145,207</sup> An additional difficulty is the rising mutational resistance rate of *P. aeruginosa* strains.<sup>141,146</sup> Fluoroquinolone and aminoglycoside resistance range up to 30 % now.<sup>208,209</sup> Furthermore, resistances against almost all drugs used for *P. aeruginosa* infection treatment (for example cephalosporins and carbapenems) as well as multidrug resistances are described.<sup>135,140,210</sup> These facts emphasize the need for new therapeutic options. Besides the common strategy to target the bacterial viability a different approach gained more and more attention lately which is anti-virulence.<sup>42,43</sup> Virulence factors are common among pathogenic bacteria and are acting by damaging their host or evading its immune response.<sup>149</sup> Virulence factor inhibitors reduce the bacterial virulence and in this way enable the clearance of the pathogen by either the host immune system or with the help of antibiotics.<sup>44,45</sup> Although only a few compounds have reached clinical application yet, many *in vitro* and *in vivo* studies support the efficacy of this strategy.<sup>42,154</sup> Its main advantage is the reduced selective pressure on the bacteria and thus lower risk for resistance development.<sup>42</sup>

A possible anti-virulence target of *P. aeruginosa* is the elastase LasB. The extracellular zinc-containing protease plays a role in the pathogenic invasion of tissues and is thought to be predominantly relevant during acute infections.<sup>149,167</sup> It has the ability to destroy elastin which is an important component of lung tissue and blood vessels.<sup>169</sup> Additionally, LasB can degrade fibrin, collagen and surfactant proteins in the lung and is also involved in the inactivation of human immunoglobulins A and G, cytokines gamma-interferon and tumor necrosis factor alpha.<sup>168,170,173–175,211</sup> All these properties contribute to a severe reduction of the host immunity.

As LasB is an interesting anti-virulence target, there are quite a few LasB inhibitors described in literature up to now: Natural products such as streptomycetes metalloproteinase inhibitor from *Streptomyces nigrescens* TK-23 (SMPI) and Phosphoramidon,<sup>178,179</sup> small peptides containing metal-chelating motifs such as thiol or hydroxamate groups<sup>179–182</sup> and small synthetic molecules with hydroxamate, thiol or mercaptoacetamide groups<sup>165,185,212</sup> as well as compounds based on tropolone.<sup>183</sup> We recently described a group of mercaptoacetamides as potent LasB inhibitors.<sup>185</sup> The crystal structure of the most promising compound **R36** showed that there are two molecules present in the binding pocket (Figure 3.3.1). Therefore, these molecules were combined into one benzylamide compound. However, this approach failed to maintain the potency of the single molecule.<sup>185</sup> As the SAR study did not reveal a promising way to overcome this issue we now applied three different approaches to create potent LasB inhibitors based on the previous crystallographic data of compound **R36**.

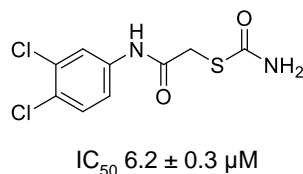
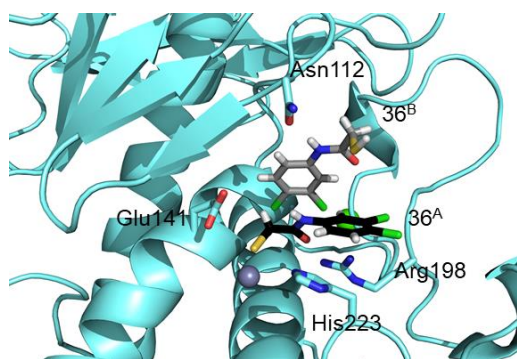


**Figure 3.3.1:** Binding mode and structure of compound **R36**.<sup>185</sup> The crystal structure revealed the presence of two molecules inside the binding pocket.

## Results and Discussion

### Approach 1: N-benzyl mercaptoacetamide class

The first approach of our study was based on the N-benzyl mercaptoacetamide class described recently.<sup>185</sup> As there is no crystal structure available for this compound class the orientation of the two aromatic moieties is unknown. Based on molecular modelling starting with **R36** the benzyl moiety is proposed to reach into the lipophilic inner region of the binding pocket. In this case, the dichloro-phenyl ring would be located near the rather hydrophilic entrance of the pocket and somehow lingering on the surface of the protein (Figure 3.3.2).

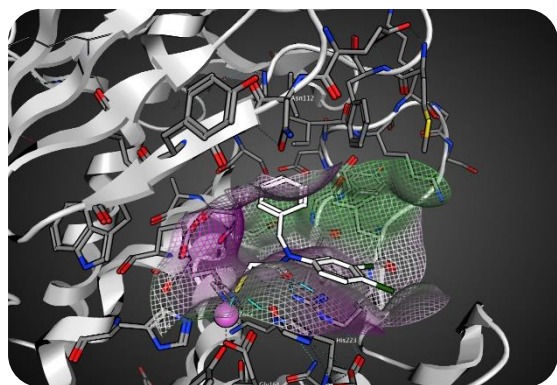
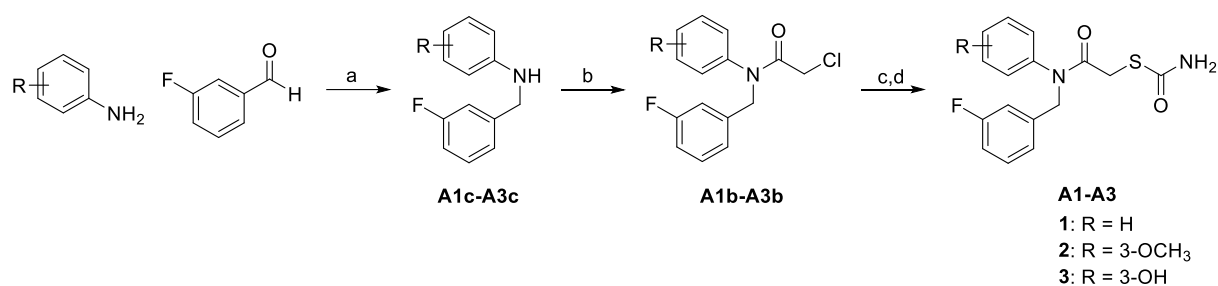


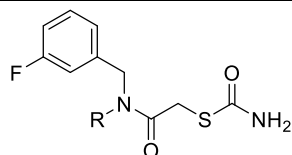
**Figure 3.3.2:** Molecular modelling of N-benzylamide compound **R64** into the binding pocket of LasB. The surface map represents lipophilic (green) and hydrophilic (magenta) areas of the binding pocket.

As optimization was formerly only performed at the benzyl moiety, we now synthesized three compounds with variations at the dichloro-phenyl ring. Therefore, we chose the 3-fluorophenyl motif for the benzylic part as it was part of the most potent compound **R64** ( $IC_{50} 12.6 \mu M$ ).<sup>185</sup> The derivatives were synthesized as described previously (Scheme 3.3.1).<sup>185</sup>



**Scheme 3.3.1:** Synthesis scheme for N-benzyl mercaptoacetamide compounds. (a) sodium triacetoxyborohydride, DCM, RT, 20 h; (b) chloroacetyl chloride, acetone, 0°C – r.t., 1.5 h; (c) ammonium thiocyanate, ethanol, 80°C, 2 h; (d) sulfuric acid, acetic acid, 0°C, 30 min.

**Table 3.3.1:** Synthesized compounds of the benzylamide class and determined IC<sub>50</sub> values.



Cp.	R	IC <sub>50</sub> [μM]
<b>A1</b>	Ph	24.6 ± 1.4
<b>A2</b>	3-OCH <sub>3</sub> -Ph	13.9 ± 0.8
<b>A3</b>	3-OH-Ph	28.1 ± 1.4

The removal of the two chloro substituents resulted in a loss of activity by a factor of 2 (**A1**, IC<sub>50</sub> 24.6 ± 1.4 μM, Table 3.3.1). The same loss of activity was observed for the substitution of the two chloro substituents with a hydroxyl group in *meta* position (**A3**, IC<sub>50</sub> 28.1 ± 1.4 μM). However, the substitution with a methoxy group in the same position (**A2**, IC<sub>50</sub> 13.9 ± 0.8 μM) led to an activity similar to compound **R64** (IC<sub>50</sub> 12.6 ± 0.4 μM).

In total, the loss of the lipophilic character of the phenyl motif causes a decrease in activity. These results complete the formerly described SAR study and indicate that a further improvement of potency can probably not be achieved in this compound class. This effect may be caused by the substitution of the amide hydrogen, which seems to contribute significantly to the activity through beneficial interactions with amino acid residues in the binding pocket.

## Approach 2: $\alpha$ -Aminomethyl thiol

In the second approach we tried to establish an interaction with a glutamic acid residue (Glu141) that is located near the catalytic center inside the binding pocket. In order to target this function, we introduced an amine group which is connected to the  $\alpha$ -carbon via a methylene linker (Figure 3.3.3).

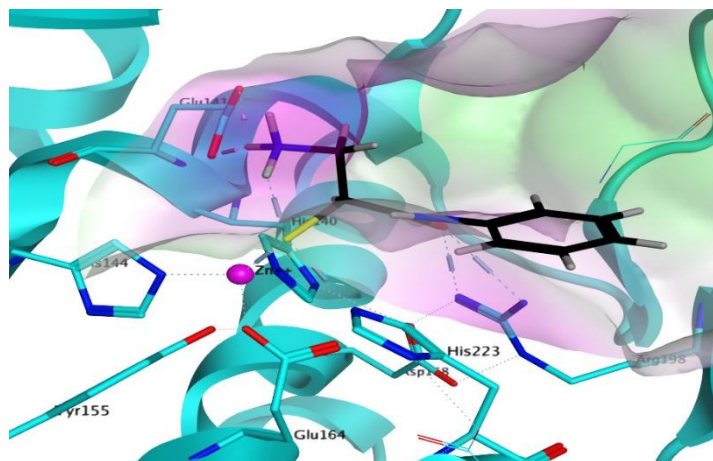
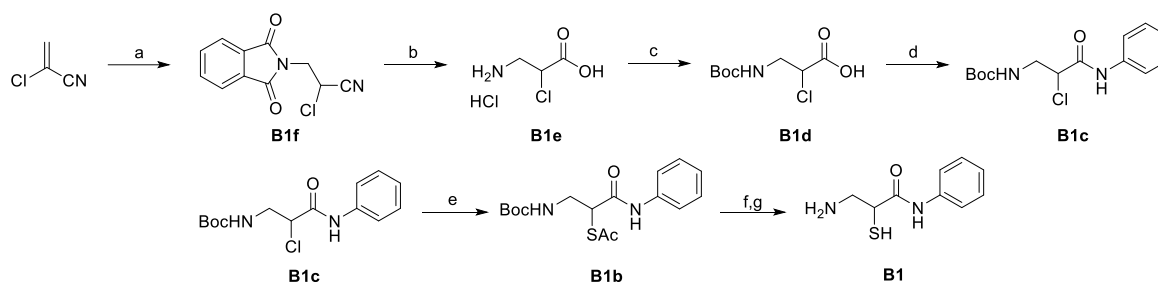


**Figure 3.3.3:** Compound **B1** (R-enantiomer) modeled into the binding pocket based on the crystal structure of compound **R36**. The surface map represents lipophilic (green) and hydrophilic (magenta) areas of the binding pocket.

The synthesis started with the addition of phthalimide to 2-chloroacrylonitrile followed by hydrolysis in concentrated hydrochloric acid (Scheme 3.3.2). The amine function of the product, 2-chloro-3-aminopropionic acid (racemic mixture) as hydrochloric acid salt, was protected with a BOC group to enable the following peptide coupling with aniline. A  $S_N2$  reaction with potassium thioacetate gave the thioacetate derivative (racemic mixture) which was deacetylated and deprotected in a final step with sodium hydroxide in methanol.



**Scheme 3.3.2:** Synthesis scheme of compound **B1**. (a) phthalimide, triethylamine, methanol, reflux, 16 h; (b) conc. HCl, 80°C, 15 h; (c) di-tert-butyl dicarbonate, sodium hydroxide, tert-butanol, 0°C – r.t., 16 h; (d) 1-Ethyl-3-(3-dimethylaminopropyl)carbodiimide, dimethylaminopyridine, aniline, 0°C – r.t., 16 h; (e) potassium thioacetate, acetone, r.t., 5 h; (f) sodium hydroxide, H<sub>2</sub>O, r.t., 30 min; (g) trifluoroacetic acid, r.t. 1 h.

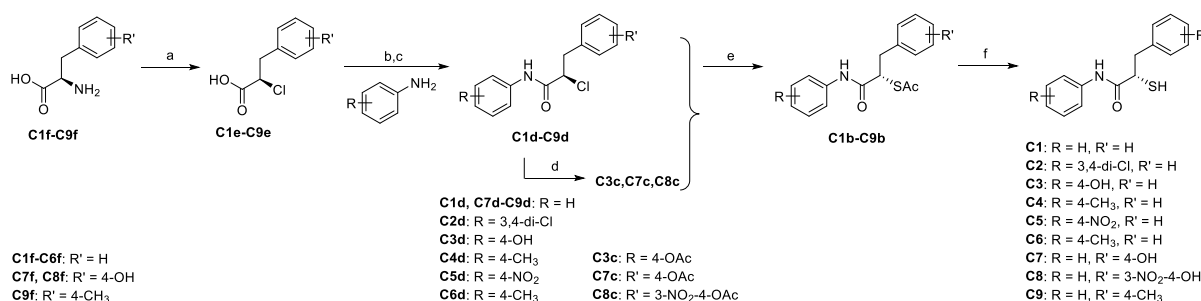
The activity determination for compound **B1** revealed an  $IC_{50}$  value of  $82 \pm 4 \mu M$ . The relatively poor potency provokes the assumption that the proposed interaction with Glu141 did not establish. The added amine function could cause a binding mode that differs from the proposed position in the pocket and thus prevents this interaction.

### Approach 3: $\alpha$ -Benzylmercaptoacetamide class

As both described approaches did not lead to the desired increase in potency, we started a new attempt to combine the two molecules of **R36** present in the binding pocket.<sup>185</sup> The introduction of the benzyl function did in this case not occur at the amide nitrogen but at the  $\alpha$ -carbon next to the thiol motif (Scheme 3.3.3).

#### Synthesis

The synthesis began with the substitution of the amine function of enantiopure phenylalanine (or derivatives) with chlorine. The reaction proceeds via diazotization and subsequent chlorination resulting in a retained conformation as a double inversion occurs.<sup>213</sup> The  $\alpha$ -chloro carboxylic acid was then coupled with the respective aniline to give the desired amide function. Intermediates containing hydroxyl groups were protected via reaction with acetic anhydride and the thioacetate function was introduced via a  $S_N2$  reaction that should result in an inversed conformation. Final deprotection of the thioacetate under basic conditions yielded the free thiol.



**Scheme 3.3.3:** Synthesis scheme of  $\alpha$ -benzyl compound class. (a) Sodium nitrite, 6N HCl, 0°C – r.t., 16 h; (b) thionyl chloride, DMF, 70°C, 1h; (c) aniline derivative, DMF, 0°C – r.t., 16 h; (d) triethylamine, dimethylaminopyridine, dichloromethane, acetic anhydride, 0°C – r.t., 30 min; (e) potassium thioacetate, acetone, r.t., 5 h; (f) sodium hydroxide, H<sub>2</sub>O, r.t., 1.5 h.

Although the synthesis route should in principle result in enantiopure compounds (if started with the respective enantiopure material), we found that our final products were racemic mixtures (chapter 7.1.3, section 2). An explanation could be that racemization occurs during reaction, work-up or storage of intermediates or final products. Differences in activity of the enantiomers will be discussed in the following paragraphs.

#### Activity against LasB

The introduction of the benzyl moiety at the  $\alpha$ -carbon of the dichloro compound resulted in a two-fold increase in activity (**C2**) compared to compound **R64** (Table 3.3.2). Interestingly, the removal of the chloro substituents (**C1**) increased the activity to 1.2  $\mu$ M. This is the opposite effect as observed for the N-benzylated compound class. Thus, we expect that the binding modes of these classes differ in the orientation of the aromatic moieties.

Different substituents were introduced in *para* position of the phenyl moiety. A nitro group (**C5**) maintained the activity similar to the naked phenyl (**C1**). A slight improvement could be achieved through a methoxy substitution (**C6**, IC<sub>50</sub> 0.73  $\mu$ M). The most potent compounds have either a hydroxyl (**C3**, IC<sub>50</sub> 0.59  $\mu$ M) or a methyl substituent (**C4**, IC<sub>50</sub> 0.48  $\mu$ M) in *para* position.

In contrast, the introduction of a hydroxyl substituent in *para* position of the benzyl group led to a decrease of activity by a factor of 6. However, an additional nitro substituent in *meta* position (**C8**) increased the activity again to 2.5  $\mu$ M.

Furthermore, the introduction of a lipophilic methyl group in the benzyl part decreased the activity by a factor of 2.5 (**C9**, IC<sub>50</sub> 2.8 μM) compared to the naked reference **C1**. In total, the three different modifications in this part of the molecule were all unfavorable.

As the introduction of substituents in the benzyl part is not easy to synthesize, it was not further pursued in this work. However, an improvement in potency may be achieved through other modifications.

**Table 3.3.2:** Activities of α-benzylmercaptoacetamides against LasB.

<b>Cp.</b>	<b>R<sub>1</sub></b>	<b>R<sub>2</sub></b>	<b>IC<sub>50</sub> [μM]</b>
<b>C1</b>	Ph	Ph	1.2 ± 0.1
<b>C2</b>	3,4-di-Cl-Ph	Ph	2.7 ± 0.3
<b>C3</b>	4-OH-Ph	Ph	0.59 ± 0.04
<b>C4</b>	4-CH <sub>3</sub> -Ph	Ph	0.48 ± 0.04
<b>C5</b>	4-NO <sub>2</sub> -Ph	Ph	0.97 ± 0.1
<b>C6</b>	4-OCH <sub>3</sub> -Ph	Ph	0.73 ± 0.03
<b>C7</b>	Ph	4'-OH-Ph	7.3 ± 0.5
<b>C8</b>	Ph	3'-NO <sub>2</sub> -4'-OH-Ph	2.5 ± 0.1
<b>C9</b>	Ph	4'-CH <sub>3</sub> -Ph	2.8 ± 0.3

The differences in activity are not easily explicable but it seems that they are based on a combination of the electronic effect on the phenyl ring, the size of the substituent and possible interactions of the substituent itself.

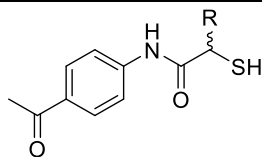
For the phenyl part electron-donating substituents have a positive effect irrespective of their hydrophilicity (**C3**, **C4**, **C6**). In contrast, electron-withdrawing and simultaneously lipophilic substituents are unfavorable (**C2**). However, an electron-withdrawing but polar substituent is neutral (**C5**).

For the benzylic part electron-donating substituents (both lipophilic and hydrophilic) are unfavorable (**C7**, **C9**). As the introduction of a nitro substituent (**C8**) improved the activity compared to **C7**, the introduction of electron-withdrawing substituents might be beneficial but has to be further elucidated.

### Comparison with α-alkylated derivatives

We also tested compounds with different alkyl substituents at the α-carbon for their activity against LasB. These compounds bear an acetyl substituent in *para* position of the phenyl moiety which was less favorable in the non-substituted mercaptoacetamide series (Compound **R1**, IC<sub>50</sub> = 73.1 ± 2.5 μM<sup>185</sup>). However, as described above the effect of aromatic substituents can change upon the introduction of a substituent at the α-carbon. Thus, we will neglect the influence of the acetyl group in the following discussion (Table 3.3.3).

The substitution with two methyl groups at the α-position led to a poorly active compound (**C10**). In contrast, the activity increased from *i*-propyl (**C11**) to ethyl (**C12**) to propyl (**C13**) (31 > 21 > 4.5 μM). These results suggest that a linear growth in α-position increases potency. This is in accordance with the results of the α-benzylated mercaptoacetamides which can be regarded as an extension of these α-alkylated derivatives.

**Table 3.3.3:** IC<sub>50</sub> values of  $\alpha$ -alkylated thiol compounds.

Cp.	R	IC <sub>50</sub> [ $\mu$ M]
<b>C10</b>	2 x CH <sub>3</sub>	> 500 $\mu$ M
<b>C11</b>	<i>i</i> -propyl	31 $\pm$ 3 $\mu$ M
<b>C12</b>	ethyl	21 $\pm$ 2 $\mu$ M
<b>C13</b>	propyl	4.5 $\pm$ 0.4 $\mu$ M

### Activity of enantiomers

To elucidate whether the configuration of the stereocenter has an influence on activity we separated the enantiomers (E1 and E2, labelled respective to their elution order from the chiral column) for compounds **C1** and **C2** and examined them independently. Indeed, we observed a difference in activity between the configurations (Table 3.3.4). For both, the E2 enantiomer was more active (by factor 4 or 2 respectively). In order to ensure that no racemization occurs during our assays we examined the enantiomer stability in methanol and aqueous buffer. The CD spectra were stable within one hour indicating that racemization does not occur during this period. (chapter 7.1.3, section 3).

**Table 3.3.4:** Activity of the pure enantiomers for **C1** and **C2**.

Cp.		IC <sub>50</sub> [ $\mu$ M]
<b>C1</b>	E1	4.8 $\pm$ 0.7
	E2	1.0 $\pm$ 0.1
	Rac	1.2 $\pm$ 0.1
<b>C2</b>	E1	5.2 $\pm$ 0.6
	E2	2.0 $\pm$ 0.4
	Rac	2.7 $\pm$ 0.3

### Crystal structure

Compound **C1** was cocrystallized with LasB in order to evaluate the binding mode of this novel class of inhibitors. The crystal structure of the complex was solved in a resolution of 1.7 Å in the P1211 space group (Figure 3.3.4A) using the LasB apo structure (PDB-ID 1EZM) as a search model. Interestingly, the orientation of **C1** is very similar to the one proposed by molecular modelling based on the crystal structure of **R36** (Figure 3.3.4B). Detailed crystallographic data are given in chapter 7.1.3 part 4.

As described for other thiol inhibitors, the sulfur atom displaces the water molecule as the fourth zinc ligand (sulfur-zinc distance 2.4 Å) in addition to His140, His 144 and Glu 164, which typically coordinate the zinc ion of LasB. The carbonyl oxygen of **C1** forms a bond with Arg198 while the benzyl side chain occupies the S2' binding pocket.

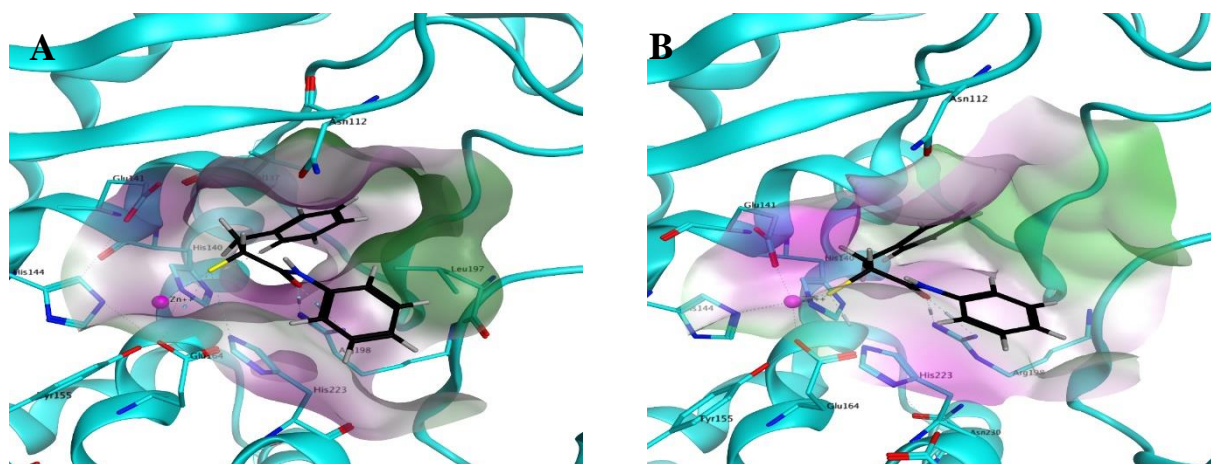


**Figure 3.3.4:** **A:** Crystal structure of **C1** with LasB. **B:** Proposed binding mode of **C1** (R-enantiomer), derived through molecular modelling based on crystal structure of **R36**. The surface map represents lipophilic (green) and hydrophilic (magenta) areas of the binding pocket.

The phenyl part of **C1** is placed near the entrance of the binding pocket, next to the protein surface but without any specific interaction. The differences in activity that we observed for substitutions at this part of the molecule (Table 3.3.2) are possibly caused by different affinities of the aromatic ring or the substituents to the protein surface.

On the other hand, the benzyl part of **C1** is orientated inside the inner region of the binding pocket and is surrounded more closely by amino acid residues and the protein backbone. Thus, the introduction of substituents should in principle lead to more significant changes in activity.

Indeed, the introduction of a hydroxyl group in *para* position of the benzyl part (**C3**) instead of the phenyl part (**C7**) caused a more than 10-fold decrease of activity (Table 3.3.2). Unfortunately, none of our derivatizations at the benzyl part led to an increase in activity. However, the introduction of different substituents at the benzyl part may lead to the establishment of a beneficial interaction and is thus a promising strategy to create more active inhibitors.

Interestingly, we only found the (R)-conformation of **C1** in the crystal structure although the racemic mixture was used for cocrystallisation. This indicates that the (R)-enantiomer is probably the more affine and thus more active one and represents the E2 enantiomer in Table 3.3.4. However, it can be seen in the binding mode of **C1** that the benzyl group could in principle also be orientated in the (S)-configuration without causing great deviations in the overall orientation of the molecule explaining the similar activities of the enantiomers.

Additionally, it is described that for some inhibitors the protein undergoes hinge bending upon binding for example with phosphoramidon.<sup>164</sup> However, for the N-aryl mercaptoacetamide **R36**, which was the starting point of this study, an open conformation (similar to the one without inhibitor) was observed.<sup>185</sup> Interestingly, the crystal structure of LasB with **C1** is neither completely open nor closed but can be described as half-closed.

## Selectivity

The inhibition of other zinc-containing enzymes is described frequently for LasB inhibitors and poses a serious difficulty in the development of selective compounds. Especially the inhibition of human targets such as metalloproteases should be avoided. We tested three derivatives (**C1**, **C3** and **C4**) for their selectivity against MMPs and the off-target ADAM17 (Table 3.3.5).

The selectivity of the compounds is high regarding the MMPs but relatively low for ADAM17 with IC<sub>50</sub> values of 2.2 and 2.3 μM for **C1** and **C3** respectively. However, optimization strategies in order to increase selectivity are still necessary to create a drug which is closer to a possible application in humans.

**Table 3.3.5:** Selectivity of **C1** and **C3** against off-targets. (n.d. = not determined)

	conc. [ $\mu\text{M}$ ]	Residual activity [%]		
		<b>C1</b>	<b>C3</b>	<b>C4</b>
MMP-1	100	91 $\pm$ 2	92 $\pm$ 6	97 $\pm$ 2
MMP-2	100	91 $\pm$ 9	99 $\pm$ 6	No inh.
MMP-3	100	No inh.	No inh.	n.d.
MMP-7	100	99 $\pm$ 2	No inh.	96 $\pm$ 1
MMP-8	100	66 $\pm$ 14	81 $\pm$ 4	96 $\pm$ 10
MMP-14	100	92 $\pm$ 1	No inh.	No inh.
		<b>IC50</b>		
ADAM17		2.2 $\pm$ 0.1 $\mu\text{M}$	2.3 $\pm$ 1.4 $\mu\text{M}$	n.d.

### Cytotoxicity

**C1** and **C3** were not cytotoxic against the cell lines HepG2, HEK293 and A549 (Table 3.3.6). Additionally, the inhibitory effect against *P. aeruginosa* PA14 was evaluated in order to exclude an antibacterial effect of our compounds. This is important as we aim to target virulence and not viability of the bacteria. LD<sub>50</sub> values on PA14 were greater than 100  $\mu\text{M}$  for both compounds.

**Table 3.3.6:** Cytotoxicity data and PA14 inhibition of **C1** and **C3**.

	<b>C1</b>	<b>C3</b>
HepG2 LD <sub>50</sub>	> 100 $\mu\text{M}$	> 100 $\mu\text{M}$
HEK293 LD <sub>50</sub>	> 100 $\mu\text{M}$	> 100 $\mu\text{M}$
A549 LD <sub>50</sub>	> 100 $\mu\text{M}$	> 100 $\mu\text{M}$
MIC PA14	> 100 $\mu\text{M}$	> 100 $\mu\text{M}$

### Conclusion

In this study we applied three different ligand-based approaches based on the formerly discovered thiol inhibitor **R36**. In the first approach three further derivatives of the N-benzyl mercaptoacetamides class were synthesized. In contrast to the study of Kany *et al.* the derivations were focused on the phenyl part of the structure instead of the benzyl part.<sup>185</sup> However, the IC<sub>50</sub> values did not show any improvement in activity compared to formerly evaluated derivatives.

In the second approach an  $\alpha$ -aminomethyl substituent was introduced next to the thiol motif of **R36** in order to achieve a beneficial interaction with the Glu141 residue inside the binding pocket. However, compound **B1** only showed an IC<sub>50</sub> value of 82  $\mu\text{M}$  suggesting that the desired interaction could not be established with this motif.

In the third approach the benzyl substituent was not introduced at the nitrogen atom as for the N-benzyl mercaptoacetamide class (as for **R64**) but in  $\alpha$ -position to the thiol.

As compound **C1** did show an increased activity of 1.2  $\mu\text{M}$  a small library was generated to evaluate the SAR of this novel class. In total 9 compounds were synthesized and the best compound **C4** showed an activity of 0.48  $\mu\text{M}$  which reflects a 13-fold improvement compared to compound **R36**. The SAR was extended with the evaluation of some  $\alpha$ -alkyl substituted derivatives which showed increasing activities the more their structure resembled the benzyl motif.

The separation and evaluation of the enantiomers of the  $\alpha$ -benzylated mercaptoacetamides revealed a slightly higher activity for one enantiomer. As the determination of the crystal structure of **C1** showed only the (R)-configuration we propose that this is the more active enantiomer. The crystal structure did additionally reveal a half-closed conformation of the protein.

Interestingly, the orientation of **C1** in the binding pocket is in accordance with the model generated based on the crystal structure of compound **R36**. With the help of the new crystal structure and the conclusions of the SAR, it may now be possible to introduce favorable substitution patterns for the benzyl part in order to further increase activity.

Together with their good selectivity against human off-targets the compounds of the  $\alpha$ -benzyl mercaptoacetamide class represent a promising starting point for the development of an effective drug against *Pseudomonas aeruginosa*.

## Experimental

**General Chemistry:** All reagents were used from commercial suppliers without further purification. Procedures were not optimized regarding yield. NMR spectra were recorded on a Bruker Fourier 500 (500 MHz) spectrometer. Chemical shifts are given in parts per million (ppm) and referenced against the residual proton, <sup>1</sup>H, or carbon, <sup>13</sup>C, resonances of the >99% deuterated solvents as internal reference. Coupling constants (*J*) are given in Hertz. Data are reported as follows: chemical shift, multiplicity (s = singlet, d = doublet, t = triplet, m = multiplet, br = broad and combinations of these) coupling constants and integration. Mass spectrometry was performed on a SpectraSystems-MSQ LCMS system (Thermo Fisher, Dreieich, Germany). Flash chromatography was performed using the automated flash chromatography system CombiFlash Rf+ (Teledyne Isco, Lincoln, NE, USA) equipped with RediSepRf silica columns (Axel Semrau, Sprockhövel Germany) or Chromabond Flash C18 columns (Macherey-Nagel, Düren, Germany). Purity of synthesized compounds was determined by LCMS using the area percentage method on the UV trace recorded at a wavelength of 254 nm and found to be >95%.

## Synthesis

**N-benzylmercaptoacetamides** were synthesized as described previously.<sup>185</sup>

**A1c** was prepared according to literature using aniline (250 mg, 2.68 mmol), 3-fluorobenzaldehyde (399 mg, 3.22mmol), acetic acid (17  $\mu$ L, 0.27 mmol) and sodium triacetoxy borhydride (966 mg, 4.56 mmol). The obtained yellow oil (721 mg) was used without further purification. MS (ESI<sup>+</sup>) *m/z* 202.19 (M+H)<sup>+</sup>.

**A1b** was prepared according to literature using **A1c** (720 mg), chloroacetyl chloride (301  $\mu$ L, 3.80 mmol). The crude product was purified using automated flash chromatography (petroleum ether:ethyl acetate = 100:0 to 0:100). The product was obtained as yellow oil (440 mg). MS (ESI<sup>+</sup>) *m/z* 278.11 (M+H)<sup>+</sup>.

**A1** was prepared according to literature using **A1b** (440mg, 1.58 mmol) and ammonium thiocyanate (133 mg, 1.74 mmol). The crude product was purified using automated flash chromatography in reversed phase mode (water:acetonitrile (each with 0.1% formic acid) = 30:70 to 0:100). The product was obtained as light yellow solid (278 mg, 32 % over 3 steps). <sup>1</sup>H NMR (500 MHz, DMSO-d<sub>6</sub>)  $\delta$  = 3.51 (br. s., 2 H), 4.88 (s, 2 H), 7.00 - 7.08 (m, 3 H), 7.26 (d, *J*=7.3 Hz, 2 H), 7.29 - 7.36 (m, 2 H), 7.37 - 7.43 (m, 2 H), 7.44 - 7.77 (m, 2 H). <sup>13</sup>C NMR (126 MHz, DMSO-d<sub>6</sub>)  $\delta$  = 32.8, 52.1, 113.9 (d, *J*=21 Hz), 114.4 (d, *J*=21 Hz), 123.8, 128.0, 128.1, 129.6, 130.2, 130.3, 140.3 (d, *J*=6 Hz), 141.7, 162.1 (d, *J*=244 Hz), 166.1, 168.0. MS (ESI<sup>+</sup>) *m/z* 319.18 (M+H)<sup>+</sup>.

**A2c** was prepared according to literature using m-anisidine (250 mg, 2.03 mmol), 3-fluorobenzaldehyde (302 mg, 2.44 mmol), acetic acid (12.5  $\mu$ L, 0.2 mmol) and sodium triacetoxy borhydride (731 mg, 3.45 mmol). The obtained brown oil (680 mg) was used without further purification. MS (ESI<sup>+</sup>) *m/z* 232.14 (M+H)<sup>+</sup>.

**A2b** was prepared according to literature using **A2c** (680 mg), chloroacetyl chloride (226  $\mu$ L, 2.8 mmol). The crude product was purified using automated flash chromatography (petroleum ether:ethyl acetate = 100:0 to 0:100). The product was obtained as yellow oil (680 mg). MS (ESI<sup>+</sup>) *m/z* 308.15 (M+H)<sup>+</sup>.

**A2** was prepared according to literature using **A2b** (680 mg, 2.21 mmol) and ammonium thiocyanate (185 mg, 2.43 mmol). The crude product was purified using automated flash chromatography in reversed phase mode (water:acetonitrile (each with 0.1% formic acid) = 30:70 to 0:100). The product was obtained as yellow solid (1.37 mg, 67 % over 3 steps). <sup>1</sup>H NMR (500 MHz, DMSO-d<sub>6</sub>) δ = 3.33 (s, 3 H), 3.55 (br. s., 2 H), 4.87 (s, 2 H), 6.78 - 6.94 (m, 3 H), 7.01 - 7.08 (m, 3 H), 7.25 - 7.37 (m, 2 H), 7.40 - 7.80 (m, 2 H). <sup>13</sup>C NMR (126 MHz, DMSO-d<sub>6</sub>) δ = 32.8, 51.9, 55.2, 113.5, 113.9 (d, J=20 Hz), 114.0, 114.4 (d, J=21 Hz), 120.1, 123.8, 130.2, 130.2, 140.4 (d, J=6 Hz), 142.8, 159.8, 162.1 (d, J=240 Hz), 166.1, 167.9. MS (ESI<sup>+</sup>) *m/z* 349.21 (M+H)<sup>+</sup>.

**A3c** was prepared according to literature using 3-aminophenol (250 mg, 2.30 mmol), 3-fluorobenzaldehyde (342 mg, 2.76 mmol), acetic acid (14 μL, 0.23 mmol) and sodium triacetoxy borohydride (829 mg, 3.91 mmol). The obtained orange-brown oil (549 mg) was used without further purification. MS (ESI<sup>+</sup>) *m/z* 218.15 (M+H)<sup>+</sup>.

**A3b** was prepared according to literature using **A3c** (549 mg, 2.53 mmol), chloroacetyl chloride (281 μL, 3.54 mmol). The crude product was purified using automated flash chromatography (petroleum ether:ethyl acetate = 100:0 to 0:100). The product was obtained as orange-brown oil (615 mg). MS (ESI<sup>+</sup>) *m/z* 294.11 (M+H)<sup>+</sup>.

**A3** was prepared according to literature using **A3b** (615 mg, 2.10 mmol) and ammonium thiocyanate (175 mg, 2.30 mmol). The crude product was purified using automated flash chromatography in reversed phase mode (water:acetonitrile (each with 0.1% formic acid) = 30:70 to 100:0). The product was obtained as white solid (193 mg, 25 % over 3 steps). <sup>1</sup>H NMR (500 MHz, DMSO-d<sub>6</sub>) δ = 3.54 (s, 2 H), 4.82 (s, 2 H), 6.62 (t, J=2.1 Hz, 1 H), 6.67 (d, J=7.8 Hz, 1 H), 6.73 (d, J=8.1 Hz, 1 H), 7.01 - 7.09 (m, 3 H), 7.18 (t, J=8.0 Hz, 1 H), 7.33 (q, J=7.5 Hz, 1 H), 7.37 - 7.81 (m, 2 H), 9.72 (s, 1 H). <sup>13</sup>C NMR (126 MHz, DMSO-d<sub>6</sub>) δ = 32.7, 52.0 (br. s.), 113.8 (d, J=22 Hz), 114.3 (d, J=23 Hz), 114.8, 115.1, 118.5, 123.7, 130.2, 130.2, 140.5 (d, J=7 Hz), 142.8, 158.1, 162.1 (d, J=238 Hz), 166.1, 167.9. MS (ESI<sup>+</sup>) *m/z* 335.19 (M+H)<sup>+</sup>.

**B1f**: Phthalimide (1.0 g, 6.8 mmol, 1.0 eq) and triethylamine (0.5 mL, 3.4 mmol, 0.5 eq) were dissolved in methanol (8 mL) under nitrogen atmosphere. Chloroacrylonitrile (1.08 mL, 13.6 mmol, 2.0 eq) was added and the mixture was heated to reflux for 16 hours. The solvent was removed under reduced pressure and the crude was purified via automated flash chromatography (hexane:ethyl acetate = 100:0 to 0:100). The product was obtained as white solid (737 mg, 46 %). <sup>1</sup>H NMR (500 MHz, DMSO-*d*<sub>6</sub>) δ = 4.17 (dd, *J*=14.5, 6.4 Hz, 1 H), 4.24 (dd, *J*=14.8, 6.6 Hz, 1 H), 5.51 (t, *J*=6.5 Hz, 1 H), 7.90 (dd, *J*=5.6, 3.4 Hz, 2 H), 7.96 (dd, *J*=5.5, 3.1 Hz, 2 H).

**B1e**: **B1f** (300 mg, 1.28 mmol, 1.0 eq) was dissolved in 10 mL concentrated hydrochloric acid and heated to reflux for 15 h. The mixture was cooled to room temperature and the precipitate was removed by filtration. The solvent of the filtrate was removed under reduced pressure and a yellow solid was obtained. The crude was washed with acetone and dried to obtain a white solid (200 mg, 100 %) which was used without further purification. <sup>1</sup>H NMR (500 MHz, METHANOL-*d*<sub>4</sub>) δ = 3.44 (dd, *J*=13.9, 7.5 Hz, 1 H), 3.55 (dd, *J*=13.7, 4.7 Hz, 1 H), 4.75 (dd, *J*=7.3, 4.6 Hz, 1 H).

**B1d**: **B1e** (100 mg, 0.63 mmol, 1.0 eq) was dissolved in 4 mL *tert*-butanol and 2 mL 1M aqueous sodium hydroxide solution and cooled to 0°C. Di-*tert*-butyl dicarbonate was added and the mixture was stirred at room temperature overnight. *Tert*-butanol was removed under reduced pressure and the remaining suspension was diluted with 1M hydrochloric acid to pH < 3. The mixture was extracted three times with ethyl acetate. The combined organic extracts was washed with brine and dried over sodium sulfate. The crude product was obtained as colorless oil (124 mg, 88 %) and used without further purification.

**B1c**: **B1d** (58 mg, 0.26 mmol, 1.0 eq) and aniline (32 μL, 0.35 mmol, 1.35 eq) were dissolved in dry dichloromethane (5 mL) and cooled to 0°C. Dimethylamino pyridine (6.4 mg, 0.05 mmol, 0.2 eq) was added and the mixture was stirred for 15 min. 1-Ethyl-3-(3-dimethylaminopropyl)carbodiimid (75 mg, 0.39 mmol, 1.5 eq) was suspended in dichloromethane and added slowly. The mixture was stirred at

room temperature for 16 h and then washed three times with 1M hydrochloric acid and once with brine. The solution was dried over sodium sulfate and the solvent was removed under reduced pressure. The product was obtained as light brown solid (123 mg) and used without further purification.  $^1\text{H NMR}$  (500 MHz, CHLOROFORM-*d*)  $\delta$  = 1.44 (s, 9 H), 1.47 (s, 9 H), 3.76 - 3.81 (m, 2 H), 4.55 (t,  $J$ =5.9 Hz, 1 H), 7.18 (t,  $J$ =7.8 Hz, 1 H), 7.36 (t,  $J$ =7.9 Hz, 2 H), 7.55 (d,  $J$ =8.1 Hz, 2 H), 8.15 (br. s., 1 H). MS (ESI<sup>+</sup>)  $m/z$  299.17 (M+H)<sup>+</sup>.

**B1b:** **B1c** (222 mg, 0.74 mmol, 1.0 eq) was dissolved in 5 mL acetone under argon atmosphere. Potassium thioacetate (127 mg, 1.10 mmol, 1.5 eq) was added and the mixture was stirred for 6 h. The reaction was quenched with water and extracted 3 times with ethyl acetate. The combined organic extracts were washed with brine and dried over sodium sulfate. The solvent was removed under reduced pressure to obtain the crude product as yellow oil. Purification was done via automated flash chromatography (hexane:ethyl acetate = 100:0 to 0:100). The product was obtained as white solid (152 mg, 60 %).  $^1\text{H NMR}$  (500 MHz, CHLOROFORM-*d*)  $\delta$  = 1.45 (s, 9 H), 2.45 (s, 3 H), 3.61 - 3.67 (m, 1 H), 4.34 (dd,  $J$ =7.2, 4.9 Hz, 1 H), 5.26 - 5.34 (m, 1 H), 7.13 (t,  $J$ =7.4 Hz, 1 H), 7.33 (t,  $J$ =7.9 Hz, 2 H), 7.51 (d,  $J$ =8.1 Hz, 2 H), 8.30 (br. s., 1 H). MS (ESI<sup>+</sup>)  $m/z$  339.23 (M+H)<sup>+</sup>.

**B1:** **B1b** (152 mg, 0.45 mmol, 1.0 eq) was dissolved in 9 mL methanol under nitrogen atmosphere. 1M aqueous sodium hydroxide solution (500  $\mu\text{L}$ , 0.50 mmol, 1.11 eq) was added dropwise and the solution was stirred for 30 min at room temperature. Trifluoroacetic acid (173  $\mu\text{L}$ , 2.25 mmol, 5.0 eq) was added and the mixture was stirred for 10 min. Methanol was removed under reduced pressure. The residue was dissolved in 2.5 mL dichloromethane and trifluoroacetic acid (693  $\mu\text{L}$ , 9.0 mmol, 20.0 eq) was added. After 40 min the reagents were removed under a nitrogen stream and the residue was dried under reduced pressure. Purification was done via automated flash chromatography (hexane:ethyl acetate = 100:0 to 0:100). The product was obtained as white solid (30 mg, 34 %).  $^1\text{H NMR}$  (500 MHz, Acetone-*d*<sub>6</sub>)  $\delta$  = 3.88 (dd,  $J$ =12.4, 6.6 Hz, 1 H), 4.12 (dd,  $J$ =12.5, 4.0 Hz, 1 H), 4.55 (dd,  $J$ =6.3, 4.2 Hz, 1 H), 5.73 (br. s., 4 H), 7.10 (t,  $J$ =7.4 Hz, 1 H), 7.32 (t,  $J$ =7.8 Hz, 2 H), 7.65 (d,  $J$ =8.1 Hz, 2 H), 9.56 (br. s., 1 H).  $^{13}\text{C NMR}$  (126 MHz, Acetone-*d*<sub>6</sub>)  $\delta$  = 50.3, 51.62, 120.4, 124.9, 129.8, 139.7, 170.6.

#### General procedure A:

Amino acid (1.0 eq) was dissolved in 6N hydrochloric acid (2 mL/mmol or until mostly dissolved) under nitrogen atmosphere and cooled to  $-5^\circ\text{C}$ . Sodium nitrite (1.5 to 2.5 eq) was dissolved in water (0.3 mL/mmol amino acid) and added slowly dropwise. The mixture was stirred overnight while warming to room temperature. The reaction mixture was extracted three times with dichloromethane. The combined organic extracts were washed with brine and dried over sodium sulfate. The solvent was removed under reduced pressure to obtain the crude product.

**C1e** was prepared according to general procedure A using L-phenylalanine (1000 mg, 6.0 mmol) and sodium nitrite (1460 mg, 21.2 mmol). The crude product was obtained as light yellow oil (1050 mg) and used without further purification.  $^1\text{H NMR}$  (CHLOROFORM-*d*)  $\delta$  = 3.21 (dd,  $J$ =14.1, 7.9 Hz, 1 H), 3.42 (dd,  $J$ =14.0, 6.7 Hz, 1 H), 4.51 (dd,  $J$ =7.8, 6.9 Hz, 1 H), 7.24 - 7.37 (m, 5 H). MS (ESI<sup>-</sup>)  $m/z$  183.25 (M-H)<sup>-</sup>, 147.23 (M-H-HCl)<sup>-</sup>.

**C7e** was prepared according to general procedure A using L-tyrosine (500 mg, 2.76 mmol) and sodium nitrite (286 mg, 4.10 mmol). The crude product was purified using automated flash chromatography (petroleum ether:ethyl acetate = 100:0 to 0:100). The product was obtained in a mixture as light yellow oil (385 mg) and used without further purification.  $^1\text{H NMR}$  (CHLOROFORM-*d*)  $\delta$  = 3.14 (dd,  $J$ =14.1, 7.2 Hz, 1 H), 3.27 - 3.35 (m, 1 H), 4.44 (t,  $J$ =7.3 Hz, 1 H), 6.77 (m, 2 H), 7.10 (m, 2 H). MS (ESI<sup>-</sup>)  $m/z$  199.22 (M-H)<sup>-</sup>, 163.20 (M-H-HCl)<sup>-</sup>.

**C8e** was prepared according to general procedure A using L-tyrosine (500 mg, 2.76 mmol) and sodium nitrite (665 mg, 3.5 mmol). The crude product was purified using automated flash chromatography (petroleum ether:ethyl acetate = 100:0 to 0:100). The product was obtained in a mixture as brown oil (344 mg) and used without further purification.  $^1\text{H NMR}$  (CHLOROFORM-*d*)  $\delta$  = 3.22 (dd,  $J$ =14.4, 7.9 Hz, 1 H), 3.39 (dd,  $J$ =14.4, 6.2 Hz, 1 H), 4.49 (dd,  $J$ =7.5, 6.4 Hz, 1 H), 7.14 (d,  $J$ =8.7 Hz, 1 H), 7.50

(dd,  $J=8.5, 2.1$  Hz, 1 H), 8.02 (d,  $J=2.0$  Hz, 1 H), 10.53 (br s, 1 H). MS (ESI<sup>-</sup>)  $m/z$  244.19 (M-H)<sup>-</sup>, 208.22 (M-H-HCl)<sup>-</sup>.

**C9e** was prepared according to general procedure A using 4-methyl-DL-phenylalanine (200 mg, 1.12 mmol) and sodium nitrite (192 mg, 2.79 mmol). The crude product was obtained as yellow oil (206 mg) and used without further purification. MS (ESI<sup>-</sup>)  $m/z$  197.15 (M-H)<sup>-</sup>, 161.15 (M-H-HCl)<sup>-</sup>.

#### General procedure B:

The acid (1.0 eq), thionyl chloride (2.0 eq) and a few drops of dimethylformamide were heated to 70 °C for 1h. The cooled mixture was added dropwise to a cooled solution (0°C) of aniline (1.1 eq) in dimethylformamide (1mL/mmol). The mixture was stirred over night at room temperature. The reaction was quenched with water and extracted three times with ethyl acetate. Combined organic extracts were washed with brine and dried over sodium sulfate. The solvent was removed under reduced pressure to obtain the crude product.

**C1d** was prepared according to general procedure B using **C1e** (934 mg), thionyl chloride (734  $\mu$ L, 10.1 mmol) and aniline (507  $\mu$ L, 5.56 mmol). Purification was done via automated flash chromatography (hexane:ethyl acetate = 100:0 to 0:100). The product was obtained as white solid (404 mg). <sup>1</sup>H NMR (DMSO-*d*<sub>6</sub>)  $\delta$  = 3.13 (dd,  $J=13.9, 7.8$  Hz, 1 H), 3.41 (dd,  $J=13.8, 7.2$  Hz, 1 H), 4.76 (t,  $J=7.5$  Hz, 1 H), 7.04 - 7.11 (m, 1 H), 7.19 - 7.27 (m, 1 H), 7.28 - 7.38 (m, 6 H), 7.52 - 7.60 (m, 2 H), 7.95 (s, 1 H). MS (ESI<sup>+</sup>)  $m/z$  260.08 (M+H)<sup>+</sup>.

**C2d** was prepared according to general procedure B using **C1e** (350 mg, 1.90 mmol), thionyl chloride (275  $\mu$ L, 3.8 mmol) and 3,4-dichloroaniline (339 mg, 2.1 mmol). Purification was done via automated flash chromatography (hexane:ethyl acetate = 100:0 to 0:100). The product was obtained as white solid (388 mg). MS (ESI<sup>+</sup>)  $m/z$  330.09 (M+H)<sup>+</sup>.

**C3d** was prepared according to general procedure B using **C1e** (300 mg, 1.62 mmol), thionyl chloride (239  $\mu$ L, 3.25 mmol) and 4-aminophenol (195 mg, 1.79 mmol). Purification was done via automated flash chromatography (hexane:ethyl acetate = 100:0 to 0:100). The product was obtained as yellow solid (264 mg). <sup>1</sup>H NMR (acetone)  $\delta$  = 3.16 (dd,  $J=13.8, 7.2$  Hz, 1 H), 3.47 (dd,  $J=13.7, 7.3$  Hz, 1 H), 4.65 (t,  $J=7.3$  Hz, 1 H), 6.76 (d,  $J=8.8$  Hz, 2 H), 7.20 - 7.24 (m, 1 H), 7.26 - 7.33 (m, 4 H), 7.41 (d,  $J=8.8$  Hz, 2 H), 8.24 (s, 1 H), 9.19 (br s, 1 H). MS (ESI<sup>+</sup>)  $m/z$  276.00 (M+H)<sup>+</sup>.

**C4d** was prepared according to general procedure B using **C1e** (200 mg, 1.08 mmol), thionyl chloride (157  $\mu$ L, 2.17 mmol) and p-toluidine (128 mg, 1.19 mmol). Purification was done via automated flash chromatography (hexane:ethyl acetate = 100:0 to 0:100). The product was obtained as yellow solid (198 mg). <sup>1</sup>H NMR (CHLOROFORM-*d*)  $\delta$  = 2.34 (s, 3 H), 3.31 (dd,  $J=14.3, 7.8$  Hz, 1 H), 3.54 (dd,  $J=14.3, 4.4$  Hz, 1 H), 4.68 (dd,  $J=7.8, 4.4$  Hz, 1 H), 7.15 (d,  $J=8.2$  Hz, 2 H), 7.26 - 7.37 (m, 7 H), 8.02 (br s, 1 H).

**C5d** was prepared according to general procedure B using **C1e** (200 mg, 1.08 mmol), thionyl chloride (157  $\mu$ L, 2.17 mmol) and 4-nitroaniline (164 mg, 1.19 mmol). Purification was done via automated flash chromatography (hexane:ethyl acetate = 100:0 to 0:100). The product was obtained in a 6:4 mixture with educt as yellow oil (198 mg). <sup>1</sup>H NMR (CHLOROFORM-*d*)  $\delta$  = 3.34 (dd,  $J=14.3, 7.5$  Hz, 1 H), 3.53 (dd,  $J=14.3, 4.6$  Hz, 1 H), 4.73 (dd,  $J=7.5, 4.6$  Hz, 1 H), 7.24 - 7.36 (m, 5 H), 7.65 - 7.70 (m, 2 H), 8.21 - 8.26 (m, 2 H), 8.33 (br s, 1 H). MS (ESI<sup>+</sup>)  $m/z$  305.11 (M+H)<sup>+</sup>.

**C6d** was prepared according to general procedure B using **C1e** (200 mg, 1.08 mmol), thionyl chloride (157  $\mu$ L, 2.17 mmol) and p-anisidine (147 mg, 1.19 mmol). Purification was done via automated flash chromatography (hexane:ethyl acetate = 100:0 to 0:100). The product was obtained in a 6:4 mixture with educt as green solid (234 mg). <sup>1</sup>H NMR (CHLOROFORM-*d*)  $\delta$  = 3.32 (dd,  $J=14.3, 7.6$  Hz, 1 H), 3.52 (dd,  $J=14.3, 4.4$  Hz, 1 H), 3.81 (s, 3 H), 4.71 (dd,  $J=7.8, 4.4$  Hz, 1 H), 6.86 - 6.90 (m, 2 H), 7.24 - 7.38 (m, 7 H), 8.01 (br s, 1 H). MS (ESI<sup>+</sup>)  $m/z$  290.04 (M+H)<sup>+</sup>.

**C7d** was prepared according to general procedure B using **C7e** (283 mg, 1.4 mmol), thionyl chloride (205  $\mu$ L, 2.8 mmol) and aniline (142  $\mu$ L, 1.55 mmol). Purification was done via automated flash chromatography (hexane:ethyl acetate = 100:0 to 0:100). The product was obtained as yellow oil (194 mg, 50 %).  $^1\text{H}$  NMR (acetone)  $\delta$  = 3.08 (dd,  $J$ =13.9, 6.9 Hz, 1 H), 3.39 (dd,  $J$ =13.9, 7.8 Hz, 1 H), 4.61 (t,  $J$ =7.3 Hz, 1 H), 6.75 (d,  $J$ =8.4 Hz, 2 H), 7.09 (t,  $J$ =7.0 Hz, 1 H), 7.14 (d,  $J$ =8.4 Hz, 2 H), 7.30 (t,  $J$ =7.8 Hz, 2 H), 7.62 (d,  $J$ =8.1 Hz, 2 H), 8.22 (s, 1 H), 9.36 (br s, 1 H).  $^{13}\text{C}$  NMR (acetone)  $\delta$  = 40.9, 60.9, 116.2, 120.6, 125.0, 128.4, 129.7, 131.5, 139.5, 157.4, 167.4. MS (ESI<sup>+</sup>)  $m/z$  276.08 (M+H)<sup>+</sup>.

**C8d** was prepared according to general procedure B using **C8e** (300 mg, 1.22 mmol), thionyl chloride (218  $\mu$ L, 3.0 mmol) and aniline (150  $\mu$ L, 1.65 mmol). Purification was done via automated flash chromatography (hexane:ethyl acetate = 100:0 to 0:100). The product was obtained as yellow solid (189 mg, 48 %).  $^1\text{H}$  NMR (CHLOROFORM-*d*)  $\delta$  = 3.39 (dd,  $J$ =14.6, 7.5 Hz, 1 H), 3.50 (dd,  $J$ =14.6, 4.7 Hz, 1 H), 4.69 (dd,  $J$ =7.4, 4.3 Hz, 1 H), 7.12 (d,  $J$ =8.7 Hz, 1 H), 7.19 (t,  $J$ =7.9 Hz, 1 H), 7.37 (t,  $J$ =7.9 Hz, 2 H), 7.49 (d,  $J$ =7.8 Hz, 2 H), 7.52 (dd,  $J$ =8.5, 2.1 Hz, 1 H), 8.07 (d,  $J$ =2.1 Hz, 1 H), 8.15 (br s, 1H), 10.54 (s, 1 H).  $^{13}\text{C}$  NMR (CHLOROFORM-*d*)  $\delta$  = 39.6, 60.8, 119.9, 120.0, 125.2, 125.7, 127.9, 128.9, 133.1, 136.2, 138.8, 154.0, 165.1. MS (ESI<sup>+</sup>)  $m/z$  321.16 (M+H)<sup>+</sup>.

**C9d** was prepared according to general procedure B using **C8e** (335 mg, 1.68 mmol), thionyl chloride (244  $\mu$ L, 3.36 mmol) and aniline (196  $\mu$ L, 1.85 mmol). Purification was done via automated flash chromatography (hexane:ethyl acetate = 100:0 to 0:100). The product was obtained as yellow solid (169 mg, 37 %).  $^1\text{H}$  NMR (CHLOROFORM-*d*)  $\delta$  = 2.34 (s, 3 H), 3.28 (dd,  $J$ =14.3, 7.8 Hz, 1 H), 3.50 (dd,  $J$ =14.3, 4.4 Hz, 1 H), 4.67 (dd,  $J$ =7.8, 4.4 Hz, 1 H), 7.11 - 7.20 (m, 6 H), 7.36 (t,  $J$ =7.8 Hz, 2 H), 7.49 (br d,  $J$ =8.2 Hz, 2 H), 8.07 (br s, 1 H).  $^{13}\text{C}$  NMR (CHLOROFORM-*d*)  $\delta$  = 20.8, 40.8, 61.8, 120.0, 124.9, 128.8, 128.9, 129.3, 132.5, 136.5, 136.7, 166.0. MS (ESI<sup>+</sup>)  $m/z$  274.04 (M+H)<sup>+</sup>.

### General procedure C:

The amide (1.0 eq), triethylamine (2.0 eq) and dimethylaminopyridine (0.03 eq) were dissolved in dichloromethane (5mL/mmol) and cooled to 0°C. Acetic anhydride (2.0 eq) was added dropwise. The solution was warmed to room temperature and stirred for 30 min. The reaction was quenched with dichloromethane, washed with brine and dried over sodium sulfate. The solvent was removed under reduced pressure to obtain the crude product.

**C3c** was prepared according to general procedure C using **C3d** (264 mg, 0.96 mmol), trimethylamine (266  $\mu$ L, 1.92 mmol), dimethylaminopyridine (3.5 mg, 0.03 mmol) and acetic anhydride (181  $\mu$ L, 1.92 mmol). Purification of the crude was done via automated flash chromatography (hexane:ethyl acetate = 100:0 to 0:100). The product was obtained as yellow solid (300 mg, 94 %).  $^1\text{H}$  NMR (acetone)  $\delta$  = 2.23 (s, 7 H), 3.19 (dd,  $J$ =13.8, 7.2 Hz, 2 H), 3.50 (dd,  $J$ =13.9, 7.5 Hz, 3 H), 4.70 (t,  $J$ =7.3 Hz, 2 H), 7.07 (d,  $J$ =8.9 Hz, 5 H), 7.23 (s, 2 H), 7.28 (br d,  $J$ =5.3 Hz, 2 H), 7.30 (s, 2 H), 7.31 (br d,  $J$ =2.1 Hz, 5 H), 7.64 (d,  $J$ =8.9 Hz, 4 H), 9.48 (br s, 1 H).  $^{13}\text{C}$  NMR (acetone)  $\delta$  = 21.0, 41.5, 60.6, 121.4, 123.0, 123.9, 127.9, 129.4, 130.4, 131.0, 136.9, 137.8, 148.2, 167.3, 169.8. MS (ESI<sup>+</sup>)  $m/z$  318.07 (M+H)<sup>+</sup>.

**C7c** was prepared according to general procedure C using **C7d** (180 mg, 0.65 mmol), trimethylamine (180  $\mu$ L, 1.30 mmol), dimethylaminopyridine (2.4 mg, 0.02 mmol) and acetic anhydride (123  $\mu$ L, 1.30 mmol). Purification of the crude was done via automated flash chromatography (hexane:ethyl acetate = 100:0 to 0:100). The product was obtained as white solid (114 mg, 55 %).  $^1\text{H}$  NMR (acetone)  $\delta$  = 2.23 (s, 10 H), 3.20 (dd,  $J$ =13.9, 7.3 Hz, 4 H), 3.50 (dd,  $J$ =13.9, 7.3 Hz, 4 H), 4.71 (t,  $J$ =7.3 Hz, 4 H), 7.05 (d,  $J$ =8.4 Hz, 8 H), 7.08 - 7.13 (m, 5 H), 7.31 (t,  $J$ =7.9 Hz, 8 H), 7.35 (d,  $J$ =8.4 Hz, 8 H), 7.62 (br d,  $J$ =7.9 Hz, 7 H), 9.44 (br s, 1 H).  $^{13}\text{C}$  NMR (acetone)  $\delta$  = 21.0, 40.8, 60.6, 120.7, 122.7, 125.1, 129.7, 131.4, 135.2, 139.5, 151.1, 167.3, 169.7. MS (ESI<sup>+</sup>)  $m/z$  318.07 (M+H)<sup>+</sup>.

**C8c** was prepared according to general procedure C using **C8d** (189 mg, 0.59 mmol), trimethylamine (164  $\mu$ L, 1.18 mmol), dimethylaminopyridine (2.0 mg, 0.02 mmol) and acetic anhydride (112  $\mu$ L, 1.18 mmol). Purification of the crude was done via automated flash chromatography (hexane:ethyl acetate = 100:0 to 0:100). The product was obtained as yellow solid (200 mg, 93 %).  $^1\text{H}$  NMR (acetone)  $\delta$  = 2.31 (s, 3 H), 3.37 (dd,  $J$ =14.1, 7.9 Hz, 1 H), 3.63 (dd,  $J$ =14.1, 6.6 Hz, 1 H), 4.84 (t,  $J$ =7.2 Hz, 1 H), 7.11 (t,  $J$ =7.4 Hz, 1 H), 7.32 (t,  $J$ =7.9 Hz, 2 H), 7.36 (d,  $J$ =8.2 Hz, 1 H), 7.62 (d,  $J$ =8.2 Hz, 2 H), 7.77 (dd,  $J$ =8.4,

2.0 Hz, 1 H), 8.15 (d,  $J=2.0$  Hz, 1 H), 9.50 (br s, 1 H).  $^{13}\text{C}$  NMR (acetone)  $\delta = 20.8, 40.2, 60.1, 120.7, 125.2, 126.2, 127.3, 129.8, 130.6, 137.3, 139.3, 142.7, 143.8, 166.9, 169.1$ .

#### General Procedure D:

The amide (1.0eq) was dissolved under argon atmosphere in acetone (5mL/mmol). 1.5 eq of potassium thioacetate was added and the reaction was stirred for 2-6 h (TLC control) at room temperature. The reaction was quenched with water and extracted 3 times with ethyl acetate. Combined organic extracts were washed with brine and dried over sodium sulfate. The solvent was removed under reduced pressure to obtain the crude product.

**C1b** was prepared according to general procedure D using **C1d** (242 mg, 0.93 mmol) and potassium thioacetate (118 mg, 1.12 mmol). Purification was done via automated flash chromatography (hexane:ethyl acetate = 100:0 to 0:100). The product was obtained as colorless oil (127 mg, 46 %).  $^1\text{H}$  NMR (CHLOROFORM-*d*)  $\delta = 1.59$  (s, 3 H), 2.38 (s, 3 H), 3.01 (dd,  $J=14.1, 7.1$  Hz, 1 H), 3.46 (dd,  $J=14.1, 8.5$  Hz, 1 H), 4.30 (t,  $J=7.7$  Hz, 1 H), 7.07 - 7.12 (m, 1 H), 7.22 - 7.33 (m, 6H), 7.46 (d,  $J=8.2$  Hz, 2 H), 7.96 (br s, 1 H).  $^{13}\text{C}$  NMR (CHLOROFORM-*d*)  $\delta = 30.4, 35.7, 48.5, 119.8, 124.4, 127.0, 128.6, 128.9, 129.2, 137.6, 137.6, 168.3, 197.3$ . MS (ESI<sup>+</sup>)  $m/z$  300.17 (M+H)<sup>+</sup>, 258.10 (M-Ac+2H)<sup>+</sup>.

**C2b** was prepared according to general procedure D using **C2d** (388 mg, 1.18 mmol) and potassium thioacetate (202 mg, 1.77 mmol). Purification was done via automated flash chromatography (hexane:ethyl acetate = 100:0 to 0:100). The product was obtained as colorless oil (361 mg, 83 %). MS (ESI<sup>+</sup>)  $m/z$  369.11 (M+H)<sup>+</sup>, 327.11 (M-Ac+2H)<sup>+</sup>.

**C3b** was prepared according to general procedure D using **C3c** (280 mg, 0.88 mmol) and potassium thioacetate (151 mg, 1.32 mmol). Purification was done via automated flash chromatography (hexane:ethyl acetate = 100:0 to 0:100). The product was obtained as yellow solid (244 mg, 77 %).  $^1\text{H}$  NMR (acetone)  $\delta = 2.22$  (s, 3 H), 2.34 (s, 3 H), 2.95 (dd,  $J=13.6, 6.0$  Hz, 1 H), 3.35 (dd,  $J=13.6, 9.3$  Hz, 1 H), 4.41 (dd,  $J=9.3, 6.0$  Hz, 1 H), 7.03 (d,  $J=8.9$  Hz, 2 H), 7.18 - 7.22 (m, 1 H), 7.24 - 7.30 (m, 3 H), 7.58 (d,  $J=8.8$  Hz, 2 H), 9.32 (br s, 1 H). MS (ESI<sup>+</sup>)  $m/z$  358.13 (M+H)<sup>+</sup>, 282.03 (M-HSAc+H)<sup>+</sup>.

**C4b** was prepared according to general procedure D using **C4d** (190 mg, 0.69 mmol) and potassium thioacetate (119 mg, 1.04 mmol). Purification was done via automated flash chromatography (hexane:ethyl acetate = 100:0 to 0:100). The product was obtained as yellow solid (156 mg, 72 %).  $^1\text{H}$  NMR (500 MHz, CHLOROFORM-*d*)  $\delta = 2.31$  (s, 3 H), 2.37 (s, 3 H), 3.01 (dd,  $J=14.0, 7.0$  Hz, 1 H), 3.45 (dd,  $J=14.2, 8.4$  Hz, 1 H), 4.26 - 4.32 (m, 1 H), 7.10 (d,  $J=8.2$  Hz, 2 H), 7.22 - 7.36 (m, 8 H), 7.87 (d,  $J=11.9$  Hz, 1 H).  $^{13}\text{C}$  NMR (CHLOROFORM-*d*)  $\delta = 20.8, 30.4, 35.8, 48.5, 119.8, 127.0, 128.6, 129.2, 129.4, 134.1, 135.0, 137.6, 168.1, 197.2$ . MS (ESI<sup>+</sup>)  $m/z$  314.10 (M+H)<sup>+</sup>, 272.04 (M-Ac+2H)<sup>+</sup>.

**C5b** was prepared according to general procedure D using **C5d** (190 mg, 0.78 mmol) and potassium thioacetate (134 mg, 1.17 mmol). Purification was done via automated flash chromatography (hexane:ethyl acetate = 100:0 to 0:100). The product was obtained as yellow oil (127 mg, 47 %).  $^1\text{H}$  NMR (500 MHz, CHLOROFORM-*d*)  $\delta = 2.41$  (s, 3 H), 3.01 (dd,  $J=14.2, 7.0$  Hz, 1 H), 3.46 (dd,  $J=14.2, 8.5$  Hz, 1 H), 4.31 (dd,  $J=8.5, 7.1$  Hz, 1 H), 7.23 - 7.28 (m, 4 H), 7.29 - 7.33 (m, 2 H), 7.61 - 7.66 (m, 2 H), 8.15 - 8.21 (m, 2 H), 8.45 (br. s., 1 H).  $^{13}\text{C}$  NMR (CHLOROFORM-*d*)  $\delta = 30.2, 35.0, 48.1, 119.0, 124.8, 126.9, 128.4, 128.9, 136.8, 143.1, 143.4, 168.6, 197.9$ . MS (ESI<sup>+</sup>)  $m/z$  345.11 (M+H)<sup>+</sup>, 303.03 (M-Ac+2H)<sup>+</sup>.

**C6b** was prepared according to general procedure D using **C6d** (230mg, 0.95 mmol) and potassium thioacetate (162 mg, 1.42 mmol). Purification was done via automated flash chromatography (hexane:ethyl acetate = 100:0 to 0:100). The product was obtained as yellow solid (126 mg, 40 %).  $^1\text{H}$  NMR (500 MHz, CHLOROFORM-*d*)  $\delta = 2.38$  (s, 3 H), 3.01 (dd,  $J=14.1, 7.1$  Hz, 1 H), 3.44 (dd,  $J=14.0, 8.4$  Hz, 1 H), 3.79 (s, 3 H), 4.28 (dd,  $J=8.4, 7.2$  Hz, 1 H), 6.81 - 6.86 (m, 2 H), 7.23 - 7.33 (m, 8 H), 7.34 - 7.37 (m, 2 H), 7.81 (br. s., 1 H).  $^{13}\text{C}$  NMR (CHLOROFORM-*d*)  $\delta = 30.7, 36.1, 48.7, 55.7, 114.3, 121.8, 127.2, 128.8, 129.5, 130.9, 137.9, 156.7, 168.3, 197.4$ . MS (ESI<sup>+</sup>)  $m/z$  330.08 (M+H)<sup>+</sup>, 288.08 (M-Ac+2H)<sup>+</sup>.

**C7b** was prepared according to general procedure D using **C7c** (130 mg, 0.41 mmol) and potassium thioacetate (70 mg, 0.61 mmol). Purification was done via automated flash chromatography (hexane:ethyl acetate = 100:0 to 0:100). The product was obtained as yellow oil (125 mg, 87 %). <sup>1</sup>H NMR (CHLOROFORM-*d*)  $\delta$  = 2.29 (s, 3 H), 2.39 (s, 3 H), 2.99 (dd, *J*=14.2, 7.0 Hz, 1 H), 3.45 (dd, *J*=14.2, 8.5 Hz, 1 H), 4.25 - 4.29 (m, 1 H), 7.02 (d, *J*=8.4 Hz, 2 H), 7.11 (br d, *J*=7.3 Hz, 1 H), 7.26 - 7.33 (m, 5 H), 7.46 (d, *J*=7.9 Hz, 2 H), 7.97 (s, 1 H). MS (ESI<sup>+</sup>) *m/z* 358.10.08 (M+H)<sup>+</sup>, 316.10 (M-Ac+2H)<sup>+</sup>.

**C8b** was prepared according to general procedure D using **C8c** (185 mg, 0.51 mmol) and potassium thioacetate (87 mg, 0.76 mmol). Purification was done via automated flash chromatography (hexane:ethyl acetate = 100:0 to 0:100). The product was obtained as yellow oil (166 mg, 81 %). <sup>1</sup>H NMR (acetone)  $\delta$  = 2.30 (s, 3 H), 2.35 (s, 3 H), 3.12 (dd, *J*=13.7, 6.4 Hz, 1 H), 3.50 (dd, *J*=13.8, 8.8 Hz, 1 H), 4.51 (dd, *J*=8.7, 6.6 Hz, 1 H), 7.07 (t, *J*=7.4 Hz, 1 H), 7.28 (t, *J*=7.9 Hz, 2 H), 7.32 (d, *J*=8.4 Hz, 1 H), 7.56 (d, *J*=8.2 Hz, 2 H), 7.71 (dd, *J*=8.2, 1.8 Hz, 1 H), 8.09 (d, *J*=1.7 Hz, 1 H), 9.36 (br s, 1 H). <sup>13</sup>C NMR (acetone)  $\delta$  = 20.7, 38.0, 49.8, 120.5, 124.9, 126.1, 127.1, 129.7, 137.0, 138.5, 139.6, 142.6, 143.6, 168.5, 169.1, 194.8.

**C9b** was prepared according to general procedure D using **C9d** (169 mg, 0.62 mmol) and potassium thioacetate (106 mg, 0.93 mmol). Purification was done via automated flash chromatography (hexane:ethyl acetate = 100:0 to 0:100). The product was obtained as yellow oil (122 mg, 63 %). <sup>1</sup>H NMR (CHLOROFORM-*d*)  $\delta$  = 2.32 (s, 3 H), 2.38 (s, 3 H), 2.97 (dd, *J*=14.2, 7.2 Hz, 1 H), 3.41 (dd, *J*=14.1, 8.3 Hz, 1 H), 4.28 (dd, *J*=8.3, 7.2 Hz, 1 H), 7.09 - 7.13 (m, 3 H), 7.14 - 7.18 (m, 2 H), 7.28 - 7.32 (m, 2 H), 7.44 - 7.48 (m, 2 H), 7.96 (br s, 1 H). <sup>13</sup>C NMR (CHLOROFORM-*d*)  $\delta$  = 21.1, 30.4, 35.3, 48.6, 119.8, 124.4, 129.0, 129.1, 129.3, 134.5, 136.6, 137.7, 168.4, 197.4. MS (ESI<sup>+</sup>) *m/z* 314.10 (M+H)<sup>+</sup>, 272.03 (M-Ac+2H)<sup>+</sup>.

#### General procedure E:

The thioacetate (1.0 eq) was dissolved in methanol (5 mL/mmol) under argon atmosphere and 2M aqueous solution of sodium hydroxide (2.0 eq) was added. The reaction was stirred 1h at room temperature before quenching with 1M hydrochloric acid. Reaction was extracted 3 times ethyl acetate. Combined organic extracts were washed with brine and dried over sodium sulfate. The solvent was removed under reduced pressure to obtain the crude product.

**C1** was prepared according to general procedure E using **C1b** (127 mg, 0.42 mmol) and 2M sodium hydroxide solution (420  $\mu$ L, 0.84 mmol). Purification was done via automated flash chromatography (hexane:ethyl acetate = 100:0 to 0:100). The product was obtained as white solid (46 mg, 43 %). <sup>1</sup>H NMR (500 MHz, CHLOROFORM-*d*)  $\delta$  = 2.11 (d, *J*=8.9 Hz, 1 H), 3.24 (dd, *J*=13.8, 6.8 Hz, 1 H), 3.38 (dd, *J*=13.8, 6.5 Hz, 1 H), 3.72 (dd, *J*=14.8, 6.6 Hz, 1 H), 7.14 (t, *J*=7.6 Hz, 1 H), 7.23 - 7.29 (m, 4 H), 7.29 - 7.36 (m, 4 H), 7.46 (d, *J*=8.1 Hz, 2 H), 8.02 (br. s., 1 H). <sup>13</sup>C NMR (126 MHz, CHLOROFORM-*d*)  $\delta$  = 41.5, 45.9, 120.0, 124.8, 127.1, 128.6, 129.0, 129.4, 137.2, 137.3, 169.5. MS (ESI<sup>+</sup>) *m/z* 258.09 (M+H)<sup>+</sup>.

**C2** was prepared according to general procedure E using **C2b** (361 mg, 0.98 mmol) and 2M sodium hydroxide solution (980  $\mu$ L, 1.96 mmol). Purification was done via automated flash chromatography (hexane:ethyl acetate = 100:0 to 0:100). The product was obtained as white solid (138 mg, 43 %). <sup>1</sup>H NMR (500 MHz, CHLOROFORM-*d*)  $\delta$  = 2.11 (d, *J*=9.0 Hz, 1 H), 3.25 (dd, *J*=13.9, 6.7 Hz, 1 H), 3.34 (dd, *J*=14.3, 6.6 Hz, 1 H), 3.72 (dd, *J*=15.3, 6.9 Hz, 1 H), 7.22 (d, *J*=7.2 Hz, 2 H), 7.25 - 7.28 (m, 1 H), 7.31 (dd, *J*=14.6, 6.9 Hz, 3 H), 7.37 (d, *J*=8.7 Hz, 1 H), 7.71 (d, *J*=2.0 Hz, 1 H), 8.06 (br. s., 1 H). <sup>13</sup>C NMR (126 MHz, CHLOROFORM-*d*)  $\delta$  = 41.3, 45.7, 119.1, 121.6, 127.3, 128.0, 128.7, 129.4, 130.5, 132.9, 136.6, 137.0, 169.7. MS (ESI<sup>+</sup>) *m/z* 326.24 & 328.02 (M+H)<sup>+</sup> (Cl isotopes).

**C3** was prepared according to general procedure E using **C3b** (240 mg, 0.67 mmol) and 2M sodium hydroxide solution (1050  $\mu$ L, 2.1 mmol). Purification was done via automated flash chromatography (hexane:ethyl acetate = 100:0 to 0:100). The product was obtained as white solid (68 mg, 37 %). <sup>1</sup>H NMR (500 MHz, Acetone-*d*<sub>6</sub>)  $\delta$  = 2.50 (d, *J*=9.5 Hz, 1 H), 2.99 (dd, *J*=13.6, 6.3 Hz, 1 H), 3.32 (dd, *J*=13.5, 8.8 Hz, 1 H), 3.70 (td, *J*=8.9, 6.5 Hz, 1 H), 6.75 (d, *J*=9.3 Hz, 2 H), 7.19 (dt, *J*=5.8, 2.8 Hz, 1 H),

7.26 (d,  $J=2.3$  Hz, 2 H), 7.27 (s, 2 H), 7.38 (d,  $J=8.8$  Hz, 2 H), 8.22 (s, 1 H), 9.05 (br. s., 1 H).  $^{13}\text{C}$  NMR (126 MHz, Acetone- $d_6$ )  $\delta = 43.3, 45.2, 116.0, 122.1, 127.5, 129.2, 130.1, 132.1, 139.9, 154.8, 170.7$ . MS (ESI $^+$ )  $m/z$  274.01 (M+H) $^+$ .

**C4** was prepared according to general procedure E using **C4b** (100 mg, 0.32 mmol) and 2M sodium hydroxide solution (320  $\mu\text{L}$ , 0.64 mmol). Purification was done via automated flash chromatography (hexane:ethyl acetate = 100:0 to 0:100). The product was obtained as white solid (58 mg, 67 %).  $^1\text{H}$  NMR (500 MHz, CHLOROFORM- $d$ )  $\delta = 2.10$  (d,  $J=8.9$  Hz, 1 H), 2.33 (s, 3 H), 3.24 (dd,  $J=13.0, 6.4$  Hz, 1 H), 3.37 (dd,  $J=14.0, 6.4$  Hz, 1 H), 3.70 (dt,  $J=8.8, 6.7$  Hz, 1 H), 7.13 (d,  $J=8.4$  Hz, 2 H), 7.23 - 7.28 (m, 5 H), 7.29 - 7.36 (m, 4 H), 7.94 (br. s., 1 H).  $^{13}\text{C}$  NMR (126 MHz, CHLOROFORM- $d$ )  $\delta = 20.9, 41.5, 45.8, 120.1, 127.1, 128.6, 129.5, 129.5, 134.5, 134.7, 137.4, 169.4$ . MS (ESI $^+$ )  $m/z$  272.03 (M+H) $^+$ .

**C5** was prepared according to general procedure E using **C5b** (95 mg, 0.28 mmol) and 2M sodium hydroxide solution (280  $\mu\text{L}$ , 0.56 mmol). Purification was done via automated flash chromatography (hexane:ethyl acetate = 100:0 to 0:100). The product was obtained as colorless oil (52 mg, 61 %).  $^1\text{H}$  NMR (500 MHz, CHLOROFORM- $d$ )  $\delta = 2.15$  (d,  $J=9.0$  Hz, 1 H), 3.28 (dd,  $J=13.9, 6.9$  Hz, 1 H), 3.37 (dd,  $J=13.9, 6.4$  Hz, 1 H), 3.77 (dt,  $J=9.1, 6.6$  Hz, 1 H), 7.22 - 7.25 (m, 2 H), 7.27 - 7.34 (m, 3 H), 7.64 - 7.69 (m, 2 H), 8.20 - 8.24 (m, 2 H), 8.35 (br. s., 1 H).  $^{13}\text{C}$  NMR (126 MHz, CHLOROFORM- $d$ )  $\delta = 41.5, 46.1, 119.5, 125.3, 127.6, 129.0, 129.6, 137.1, 143.2, 144.2, 170.3$ . MS (ESI $^+$ )  $m/z$  303.06 (M+H) $^+$ .

**C6** was prepared according to general procedure E using **C6b** (95 mg, 0.29 mmol) and 2M sodium hydroxide solution (290  $\mu\text{L}$ , 0.58 mmol). Purification was done via automated flash chromatography (hexane:ethyl acetate = 100:0 to 0:100). The product was obtained as white solid (45 mg, 54 %).  $^1\text{H}$  NMR (500 MHz, CHLOROFORM- $d$ )  $\delta = 2.10$  (d,  $J=8.9$  Hz, 1 H), 3.24 (dd,  $J=14.0, 6.4$  Hz, 1 H), 3.36 (dd,  $J=13.7, 6.7$  Hz, 1 H), 3.70 (dt,  $J=8.9, 6.6$  Hz, 1 H), 3.80 (s, 3 H), 6.84 - 6.89 (m, 2 H), 7.23 - 7.28 (m, 4 H), 7.31 (d,  $J=7.5$  Hz, 2 H), 7.33 - 7.37 (m, 2 H), 7.90 (br. s., 1 H).  $^{13}\text{C}$  NMR (126 MHz, CHLOROFORM- $d$ )  $\delta = 41.8, 46.0, 55.7, 114.4, 122.2, 127.4, 128.8, 129.7, 130.5, 137.6, 157.0, 169.6$ . MS (ESI $^+$ )  $m/z$  288.05 (M+H) $^+$ .

**C7** was prepared according to general procedure E using **C7b** (120 mg, 0.34 mmol) and 2M sodium hydroxide solution (340  $\mu\text{L}$ , 0.68 mmol). Purification was done via automated flash chromatography (hexane:ethyl acetate = 100:0 to 0:100). The product was obtained as white solid (41 mg, 44 %).  $^1\text{H}$  NMR (500 MHz, Acetone- $d_6$ )  $\delta = 2.48$  (br. s., 1 H), 2.91 (dd,  $J=13.7, 6.1$  Hz, 1 H), 3.24 (dd,  $J=13.7, 8.9$  Hz, 1 H), 3.67 (dd,  $J=8.7, 6.1$  Hz, 1 H), 6.72 (d,  $J=8.4$  Hz, 2 H), 7.05 (t,  $J=7.3$  Hz, 1 H), 7.09 (d,  $J=8.4$  Hz, 2 H), 7.27 (t,  $J=7.9$  Hz, 2 H), 7.59 (d,  $J=8.2$  Hz, 2 H), 8.16 (br. s., 1 H), 9.21 (br. s., 1 H).  $^{13}\text{C}$  NMR (126 MHz, Acetone- $d_6$ )  $\delta = 42.5, 45.6, 116.0, 120.3, 124.5, 129.6, 130.4, 131.1, 140.1, 157.1, 171.5$ . MS (ESI $^+$ )  $m/z$  274.01 (M+H) $^+$ .

**C8** was prepared according to general procedure E using **C8b** (160 mg, 0.40 mmol) and 2M sodium hydroxide solution (600  $\mu\text{L}$ , 1.2 mmol). Purification was done via automated flash chromatography (hexane:ethyl acetate = 100:0 to 0:100). The product was obtained as light green solid (70 mg, 50 %).  $^1\text{H}$  NMR (500 MHz, Acetone- $d_6$ )  $\delta = 2.60$  (d,  $J=9.8$  Hz, 1 H), 3.07 (dd,  $J=13.8, 6.6$  Hz, 1 H), 3.36 (dd,  $J=13.7, 8.4$  Hz, 1 H), 3.79 (ddd,  $J=8.9, 7.0$  Hz, 1 H), 7.06 (t,  $J=7.3$  Hz, 1 H), 7.12 (d,  $J=8.5$  Hz, 1 H), 7.28 (t,  $J=7.9$  Hz, 2 H), 7.58 (d,  $J=8.1$  Hz, 2 H), 7.63 (dd,  $J=8.5, 2.1$  Hz, 1 H), 8.06 (d,  $J=2.0$  Hz, 1 H), 9.33 (br. s., 1 H), 10.33 (s, 1 H).  $^{13}\text{C}$  NMR (126 MHz, Acetone- $d_6$ )  $\delta = 41.5, 45.0, 120.4, 120.6, 124.7, 126.2, 129.7, 132.2, 134.8, 139.7, 139.9, 154.3, 171.0$ . MS (ESI $^+$ )  $m/z$  319.04 (M+H) $^+$ .

**C9** was prepared according to general procedure E using **C9b** (90 mg, 0.29 mmol) and 2M sodium hydroxide solution (290  $\mu\text{L}$ , 0.58 mmol). Purification was done via automated flash chromatography (hexane:ethyl acetate = 100:0 to 0:100). The product was obtained as white solid (55 mg, 70 %).  $^1\text{H}$  NMR (500 MHz, CHLOROFORM- $d$ )  $\delta = 2.09$  (d,  $J=8.9$  Hz, 1 H), 2.33 (s, 3 H), 3.21 (dd,  $J=13.8, 6.8$  Hz, 1 H), 3.33 (dd,  $J=13.9, 6.7$  Hz, 1 H), 3.70 (dt,  $J=8.6, 6.7$  Hz, 1 H), 7.09 - 7.17 (m, 5 H), 7.34 (t,  $J=7.9$  Hz, 2 H), 7.48 (br d,  $J=7.8$  Hz, 2 H), 8.03 (br s, 1 H).  $^{13}\text{C}$  NMR (CHLOROFORM- $d$ )  $\delta = 21.1, 41.0, 46.0, 120.0, 124.7, 129.0, 129.3, 129.3, 134.1, 136.8, 137.3, 169.6$ . MS (ESI $^+$ )  $m/z$  272.02 (M+H) $^+$ .

**Enantiomer separation:** The enantiomers were separated using a Daicel ChiralPak® IE column (5 µm, 10 × 250 mm) with a preparative HPLC (Thermo Scientific Ultimate 3000, consisting of Dionex Ultimate 3000 pump, diode array detector and automated fraction collector) monitoring the absorbance at 254 nm. An isocratic flow of 5 mL/min was applied with the following solvent composition: Compound C1: hexane:methyl-tert-butyl ether (MtBE) = 55:45, Compound C2: hexane:MtBE = 65:35.

**Characterization of Enantiomers:** A JASCO J-1500 CD spectrometer was used for sample analysis, employing a 1 cm quartz cuvette. Instrument conditions were as follows: temperature 25°C, bandwidth of 2 nm, wavelength range of 280-210 or 280-230 nm (dependent on compound absorbance), data pitch of 1 nm, scanning speed of 50 nm/min, and two-scan accumulation (averaged at end).

**LC-MS Based Stability Assay:** The stability assay was performed as described previously with slight modifications<sup>214</sup>: The UV254 chromatogram of 20 µM thiol compound in buffer (50 mM Tris pH 7.2, 2.5 mM CaCl<sub>2</sub>) in presence of 20 µM caffeine as internal standard was measured. Injections were performed every 6.5 minutes during 120 minutes in total. Compounds and ISTD were dissolved in MeOH and diluted in assay buffer, giving a final volume of 2000 µL with a methanol concentration of 10% (v/v). The solution of internal standard in assay buffer was incubated at 22.5°C for at least 10 min before adding thiols. Measurements were started directly after compound addition.

**Expression and Purification of LasB** was done as described previously.<sup>185</sup>

**In vitro Inhibition Assay** was performed as described previously.<sup>185</sup>

**Human MMP Inhibition Assay** was performed as described previously.<sup>214</sup>

**ADAM17 Inhibition Assay** was performed as described previously.<sup>215</sup>

**Cytotoxicity Assay** was performed as described previously for HepG2 and HEK293.<sup>185,216</sup>

**X-Ray Crystallography:** LasB was expressed and purified as described previously.<sup>185</sup> The protein was concentrated to 12 mg/ml and mixed with inhibitor C1 at a final concentration of 1 mM. Complex crystals were obtained in 0.1 M sodium acetate pH 4.6, and 15 % (w/v) PEG 20,000. Crystals were cryoprotected in glycerol, and diffraction data was collected from single crystals at 100 K at beamline ID30A-3 (ESRF) at a wavelength of 0.967 Å. Data was processed using Xia2<sup>217</sup> or XDS<sup>218</sup> and the structure solved using PHASER<sup>219</sup> Molecular Replacement with *Pseudomonas aeruginosa* elastase (PDB ID 1EZM) as a search model. The models were manually rebuilt with COOT<sup>220</sup> and refined using PHENIX<sup>221</sup> and Refmac5<sup>222</sup>.

**Molecular Modelling** was performed as described previously.<sup>185</sup>

### **3.4 Chapter D: Tackling *Pseudomonas aeruginosa* Virulence by a Hydroxamic Acid-Based LasB Inhibitor**<sup>215</sup>

Andreas M. Kany, Asfandyar Sikandar, Samir Yahiaoui, Jörg Haupenthal, Isabell Walter, Martin Empting, Jesko Köhnke, and Rolf W. Hartmann

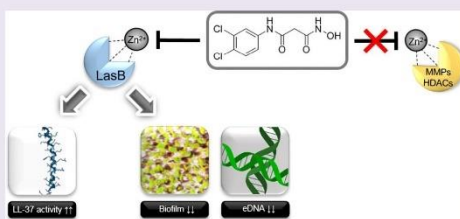
Reprinted with permission from *ACS Chemical Biology* **2018** 13 (9), 2449-2455, DOI: 10.1021/acscchembio.8b00257

Copyright (2018) American Chemical Society

Tackling *Pseudomonas aeruginosa* Virulence by a Hydroxamic Acid-Based LasB InhibitorAndreas M. Kany,<sup>†</sup> Asfandyar Sikandar,<sup>‡</sup> Samir Yahiaoui,<sup>†</sup> Jörg Hauptenthal,<sup>†</sup> Isabell Walter,<sup>†</sup> Martin Empting,<sup>†</sup> Jesko Köhnke,<sup>‡</sup> and Rolf W. Hartmann<sup>\*,†,§</sup><sup>†</sup>Department of Drug Design and Optimization, Helmholtz Institute for Pharmaceutical Research Saarland (HIPS), Campus E8.1, 66123 Saarbrücken, Germany<sup>‡</sup>Workgroup Structural Biology of Biosynthetic Enzymes, Helmholtz Institute for Pharmaceutical Research Saarland (HIPS), Campus E8.1, 66123 Saarbrücken, Germany<sup>§</sup>Department of Pharmacy, Pharmaceutical and Medicinal Chemistry, Saarland University, Campus E8.1, 66123 Saarbrücken, Germany

## Supporting Information

**ABSTRACT:** In search of novel antibiotics to combat the challenging spread of resistant pathogens, bacterial proteases represent promising targets for pathoblocker development. A common motif for protease inhibitors is the hydroxamic acid function, yet this group has often been related to unspecific inhibition of various metalloproteases. In this work, the inhibition of LasB, a harmful zinc metalloprotease secreted by *Pseudomonas aeruginosa*, through a hydroxamate derivative is described. The present inhibitor was developed based on a recently reported, highly selective thiol scaffold. Using X-ray crystallography, the lack of inhibition of a range of human matrix metalloproteases could be attributed to a distinct binding mode sparing the S1' pocket. The inhibitor was shown to restore the effect of the antimicrobial peptide LL-37, decrease the formation of *P. aeruginosa* biofilm and, for the first time for a LasB inhibitor, reduce the release of extracellular DNA. Hence, it is capable of disrupting several important bacterial resistance mechanisms. These results highlight the potential of protease inhibitors to fight bacterial infections and point out the possibility to achieve selective inhibition even with a strong zinc anchor.



Proteases have proven to be attractive targets for the treatment of various diseases, including infections.<sup>1</sup> While antiviral protease inhibitors are in clinical use for the treatment of e.g. HIV or HCV, no bacterial protease inhibitors have been approved as anti-infective drugs yet.<sup>2,3</sup> However, to combat the spread of antibiotic resistance, new antibacterial agents with novel modes of action are urgently needed.<sup>4–6</sup> This applies especially for Gram-negative pathogens which are challenging to treat as their cell wall is difficult to permeate.<sup>7</sup> The development of pathoblockers which target bacterial virulence rather than killing bacteria is of growing interest in anti-infective drug discovery due to the reduced selection pressure such a strategy is supposed to have.<sup>8–12</sup> In this context, bacterial proteases represent attractive targets.<sup>2,3,13</sup> Notably, the only FDA-approved antivirulence drugs are immunoglobulins that target secreted virulence factors, highlighting the potential of extracellular targets to circumvent cell wall permeation problems.<sup>8</sup> The highly problematic Gram-negative pathogen *Pseudomonas aeruginosa* has been assigned critical priority by the WHO<sup>14</sup> and urgently requires novel treatment options because of increasing resistance.<sup>15,16</sup> *P. aeruginosa* is responsible for fatal lung infections in cystic fibrosis patients.<sup>17</sup> Among its numerous virulence factors representing potential

drug targets,<sup>12,16,18–20</sup> the zinc–metalloprotease elastase (LasB) is of specific interest, given its extracellular location.<sup>21</sup> LasB substantially contributes to disease progression in *P. aeruginosa* infected individuals by facilitating host invasion and immune evasion.<sup>22</sup> It was for example found to degrade and thereby inactivate the endogenous antimicrobial peptide (AMP) LL-37.<sup>23</sup> Furthermore, LasB was reported to be involved in the formation of *P. aeruginosa* biofilms either by periplasmic activation of nucleoside diphosphate kinase (NDK) required for alginate synthesis<sup>24</sup> or by upregulation of rhamnolipids.<sup>25</sup> The aggregation of bacteria in the biofilm matrix seriously impedes successful antibiotic treatment and blocks host defense mechanisms.<sup>26,27</sup>

Several thiol-based inhibitors with promising activity on LasB have been described.<sup>28–32</sup> A class of *N*-aryl mercaptoacetamides turned out to be particularly attractive because these thiols display high selectivity against a range of human matrix metalloproteinases (MMPs).<sup>32,33</sup> Thiol-containing compounds

Received: March 19, 2018

Accepted: August 8, 2018

Published: August 8, 2018

are in clinical use for the treatment of various diseases.<sup>34–36</sup> However, a disadvantage of this class compared to other zinc-chelating inhibitors is the possible oxidation to the respective disulfides, resulting in inactivation of the compounds.<sup>37</sup>

In this study, we describe the synthetic replacement of the sulfhydryl function of LasB inhibitor **1**<sup>32</sup> ( $IC_{50}$ :  $6.6 \pm 0.3 \mu\text{M}$ ) by zinc-binding groups insensitive to oxidation (Figure 1).

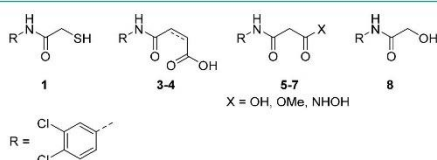


**Figure 1.** Structures of lead LasB inhibitor **1** and compounds **3–8** synthesized in this article.

Among the compounds tested, a hydroxamic acid derivative was found to inhibit LasB in the low micromolar range as well. Hydroxamates have been reported as LasB inhibitors, but the described compounds lack selectivity against human MMPs.<sup>38,39</sup> In contrast, the inhibitor described in this work maintained the remarkable selectivity of thiol **1** against human MMPs, despite a binding mode equivalent to described hydroxamate–MMP complexes. The new compound was further able to reduce biofilm formation and eDNA release by *P. aeruginosa* and to restore the antimicrobial effect of LL-37.

## RESULTS AND DISCUSSION

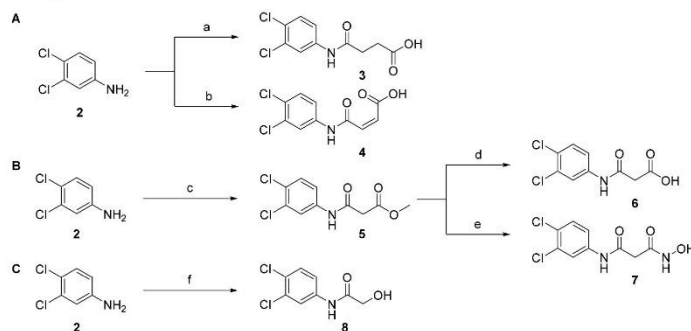
**Synthesis of Novel Compounds 3–8.** Among the variety of chemically diverse zinc binding groups in literature,<sup>40</sup> we focused on hydroxyl, carboxyl, and hydroxamate functions. By introduction of these relatively small zinc chelating groups, drastic changes in the size of the thiol function of **1** were avoided to allow the inhibitor backbone to preserve the previously observed binding mode.<sup>32</sup> Carboxylic acid derivatives **3**, **4**, and **6** were obtained either by reacting aniline **2** with succinic/maleic anhydride or via hydrolysis of methyl ester intermediate **5**. Similarly, **7** was synthesized by reacting **5** with

hydroxylamine (Schemes 1A and B). As an isosteric modification we further synthesized the alcohol derivative of **1**, compound **8**, using glycolic acid in a neat reaction (Scheme 1C).

**Identification of Compound 7 as a Promising LasB Inhibitor.** Using a FRET-based inhibition assay,<sup>41</sup> it turned out that replacement of the thiol function of **1** by a hydroxy group led to a complete loss of activity when tested at  $600 \mu\text{M}$  (**8**). Compounds bearing a carboxylic acid in  $\gamma$ - (**3**, **4**) or in  $\beta$ -position (**6**) to the carbonyl group were also inactive. Contrary to that, the activity was maintained for the  $\beta$ -hydroxamic acid derivative **7**, displaying an  $IC_{50}$  of  $17.4 \pm 0.8 \mu\text{M}$  and a  $K_{i,app}$  of  $12.3 \pm 0.6 \mu\text{M}$ . This is slightly less active compared to the free thiol analogue **1**; however, the oxidation issue was resolved by replacing the thiol by a hydroxamic acid function.

**Binding Mode of 7 to LasB.** To rationalize whether the minor difference in activity compared to **1** was due to a different binding mode, the X-ray cocrystal structure of the LasB–**7** complex was solved. The complex crystallized in space group  $P2_12_12_1$  and crystals diffracted to 2.1 Å resolution (Figure 2A). The structure was solved by molecular replacement using the published LasB structure (PDB ID 1EZM) as a search model. Full details of the data collection and refinement statistics can be found in Supplementary Table 1. Hydroxamate **7** was found to be orientated toward the primed binding site of the protease. As expected, the active site zinc atom is coordinated by both the carbonyl oxygen and the hydroxamate oxygen of **7**, leading to a distorted trigonal-bipyramidal geometry. The carbonyl oxygen further undergoes a weaker interaction with His223 (3.5 Å). Additionally, the hydroxamate oxygen forms a hydrogen bond with the adjacent Glu141 (2.5 Å), while the amide nitrogen interacts with the carbonyl group of Ala113 (3.0 Å). These observations are in excellent accordance with the reported binding of hydroxamate functions to MMP-7,<sup>42</sup> MMP-3<sup>43</sup> or to thermolysin.<sup>44</sup> Inhibitor binding to thermolysin-like proteases like LasB was described to lead to a closure of the binding pocket due to hinge-bending motion.<sup>45</sup> Intriguingly, thiol **1** has recently been discovered by us to keep the active site cleft in an open conformation due to the unexpected binding of two molecules to the primed binding site (Supplementary Figure S1).<sup>32</sup> In contrast, only one molecule of the hydroxamate binds to the

**Scheme 1.** Synthesis of 3–8<sup>44</sup>



<sup>44</sup>Reagents and conditions: (a) succinic anhydride, dioxane, 70 °C, 6 h; (b) maleic anhydride, dioxane, 70 °C, 6 h; (c) methyl malonyl chloride, Et<sub>3</sub>N, DCM, RT, 4 h; (d) NaOH, THF, RT, 24 h; (e) H<sub>2</sub>NOH, DIPEA, MeOH, 8 h reflux, 16 h RT; (f) glycolic acid, 130 °C, 24 h.

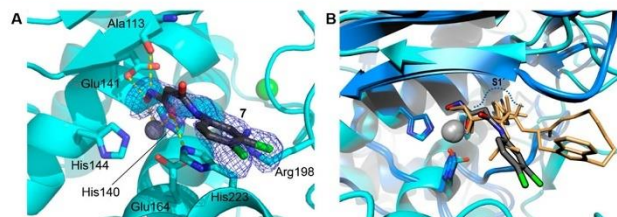


**Figure 2.** (A) Structure of LasB in complex with 7. Cartoon representations of LasB (cyan) in complex with 7 (black). The difference electron density ( $F_o - F_c$ ) contoured to  $3\sigma$  with phases calculated from a model that was refined in the absence of 7 is shown as a blue isomesh. The active-site zinc ion is shown as gray, and the calcium ion is shown as a green sphere. Residues involved in binding of 7 are shown as sticks, and their interactions depicted as yellow dashed lines. Zinc-liganding distances are 2.1 Å (OH) and 2.4 Å (NH). (B) Overlay of LasB (cyan) in complex with 7 (gray) and MMP-3/-7 (green) occupied by hydroxamate inhibitors 9 and 10 (brown, PDB codes 4G9L/1MMQ). Zinc ligands are highlighted.

protease, which undergoes the characteristic hinge-bending. Unlike the zinc-chelating thiol, the hydroxamate directly interacts with the edge strand via a hydrogen bond with the main chain oxygen of Ala113. This interaction presumably promotes closure of the active site cleft, which is hampered in case of thiol 1 by the second molecule interacting with Asn112. Due to the twisted orientation of the aromatic core of 7 compared to 1, a previously observed bidentate hydrogen bond with Arg198 in the S1' binding site is not possible. This observation could explain the slightly weaker activity of the hydroxamate compared to the thiol.

**Selectivity against Six MMPs and ADAM-17.** Strong zinc chelating groups such as hydroxamic acids can be the reason for poor selectivity against further metalloproteases, when compound binding is driven more by the chelating moiety than by the rest of the molecule.<sup>46</sup> In fact, the lack of selectivity against MMP antitargets has been one reason for the failure of various hydroxamate-based MMP inhibitors in clinical trials.<sup>47,48</sup> Considering the high similarity in zinc chelation by 7 and the hydroxamates in MMP-3 or MMP-7, it was investigated whether the previously demonstrated selectivity of *N*-aryl mercaptoacetamides toward six human MMPs<sup>32,33</sup> could be maintained. Fortunately, 7 did not inhibit these MMPs comprising members with differing depth of the S1' binding site,<sup>49</sup> including MMP-3 and -7 (Table 1). By contrast, the unselective inhibitor Batimastat<sup>50</sup> (Supplementary Figure S2) inhibited all tested enzymes in the low nanomolar range.

This of course prompted the question why, despite comparable interactions of the hydroxamate function, LasB was inhibited but MMP-7 was not. Logically, the selectivity

might be related to differences in the positioning of the inhibitor backbone in the pocket. To investigate this, published X-ray structures of MMPs in complex with hydroxamates were overlaid with the LasB-7 complex. The shallow S1' pocket of MMP-7 is occupied by an isobutyl moiety of inhibitor 9<sup>32</sup> and the deep S1' pocket of MMP-3 by an aromatic core of inhibitor 10<sup>43</sup> (for inhibitor structures, see Supplementary Figure S3). In contrast, the core of 7 does not bind to the respective pocket of LasB (Figure 2B). The ability to bind the S1' pocket of the respective MMP is a common feature of reported hydroxamate-based MMP inhibitors, which can also be the cause for a lack of selectivity.<sup>46,51</sup> Consequently, the high selectivity against various MMPs with differing depth of the S1' binding pocket might be explained by an inability of 7 to bind to this site of the protease. ADAMs (A disintegrin and metalloproteinase), a class of zinc-dependent proteases playing essential roles in muscle development, cell migration, or shedding, display additional antitargets for the presented LasB inhibitor. In this context, an *in vitro* inhibition assay toward ADAM-17 revealed that 7 exerted moderate inhibitory effects (Table 1). Consequently, further optimization regarding selectivity toward this antitarget is needed. Still, the promising selectivity toward a range of MMPs makes 7 an attractive starting point for LasB inhibitor development.

**Cytotoxicity Assays.** In addition to selectivity, it was also investigated whether the cytotoxicity of 7 toward human cell lines was as low as described for thiol 1.<sup>32</sup> This was of specific interest because cytotoxic properties are a known drawback of hydroxamates.<sup>52</sup> Notably, 7 had only low effects on the viability of HEP G2 cells, comparable to thiol 1 and rifampicin (Figure 3). The effect on HEK293 cells was more pronounced at the tested concentrations, which might be related to the inhibition of antitargets such as ADAM-17. For comparison, residual enzyme activities in the LasB *in vitro* assay are listed for each inhibitor concentration in Supplementary Table S2.

**Selectivity against HDACs.** Considering the cytotoxic effects of 7 against HEP G2 cells, it was investigated whether this observation could furthermore be related to inhibition of histone deacetylases (HDACs).<sup>53</sup> These zinc-dependent enzymes are involved in the epigenetic regulation of cell proliferation and differentiation.<sup>54</sup> Given that HDACs are known to be inhibited by hydroxamic acids such as vorinostat or trichostatin A,<sup>55</sup> assessing a potential inhibitory effect of hydroxamate 7 was of special interest. Figure 4 shows that 7 does not exert any inhibitory effect on HDAC3 and HDAC8, while these enzymes are efficiently inhibited by the positive

**Table 1. Residual Activity of Six MMPs and ADAM-17 in the Presence of 100  $\mu$ M 7 and IC<sub>50</sub> Values of Batimastat<sup>33,49</sup>**

	7 residual activity at 100 $\mu$ M (%)	Batimastat IC <sub>50</sub> (nM)
MMP-1	91 $\pm$ 9	2.2 $\pm$ 0.1
MMP-2	87 $\pm$ 3	1.8 $\pm$ 0.1
MMP-3	84 $\pm$ 5	5.6 $\pm$ 0.9
MMP-7	98 $\pm$ 3	7.0 $\pm$ 0.2
MMP-8	73 $\pm$ 6	0.7 $\pm$ 0.2
MMP-14	98 $\pm$ 4	2.8 $\pm$ 0.2
ADAM-17	38 $\pm$ 12	ND
ADAM-17	61 $\pm$ 23*	ND

\*Means and SD of at least two independent measurements are displayed. \*: test at 25  $\mu$ M. ND: not determined.

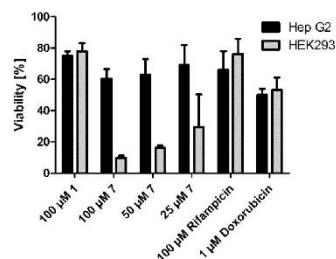


**Figure 3.** Cytotoxicity of 1, 7, and two reference compounds toward HEP G2 and HEK293 cells (values for 1 are taken from ref 32).

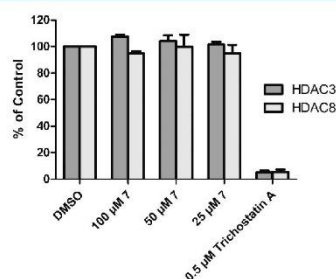


**Figure 4.** Residual activity of selected HDAC enzymes in the presence of 100 μM 7.

control trichostatin A (Supplementary Figure S2). The observed selectivity against these additional antitargets could be explained by the absence of a long linker separating the zinc chelating function from the aromatic core, as it is typical for hydroxamate-based HDAC inhibitors.<sup>52,56</sup>

**Restoration of LL-37 Antibacterial Activity against *P. aeruginosa* PA14.** LL-37 is an  $\alpha$ -helical human cathelicidin peptide which shows increased prevalence in cystic fibrosis patients.<sup>57</sup> Its effectiveness against *P. aeruginosa* is considerably reduced as it is susceptible toward cleavage by LasB.<sup>23</sup> To assess a potential restoration effect of 7 on the activity of LL-37, a bacterial growth assay with PA14 and LL-37 in presence/absence of 7 was performed (Figure 5). The antibacterial effect of LL-37 alone was only minor at 25 μg/mL ( $p = 0.0211$ ). However, when combined with the LasB inhibitor, it recovered its ability to reduce bacterial growth in a dose-dependent way. Significant reduction of the OD<sub>600</sub> was observed starting from a hydroxamate concentration of 62.5 μM ( $p = 0.0047$ ). At high concentrations, 7 itself slightly inhibited PA14 growth, yet to a much lower extent than in combination with LL-37 ( $p = 0.0255$  at 250 μM 7). These findings highlight the potential of LasB inhibitor 7 to restore a host defense mechanism which is otherwise hampered by LasB.

**Biofilm Volume and eDNA Reduction.** The biofilm matrix, a key element of *P. aeruginosa* resistance,<sup>26</sup> is composed of extracellular polysaccharides, lipids, proteins and, importantly, extracellular DNA (eDNA).<sup>58,59</sup> Inhibition of LasB was shown to inhibit biofilm formation.<sup>28</sup> Therefore, it was of great interest to investigate whether treatment of PA14 cultures with 7 would result in reduced biofilm formation as well. Indeed, the hydroxamate caused a concentration-dependent reduction

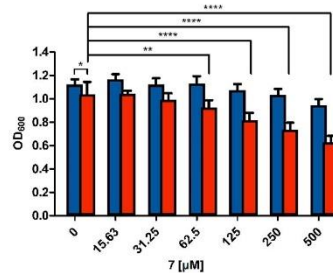


**Figure 5.** Growth of PA14 cultures incubated with 7 in absence (blue) and presence (red) of 25 μg/mL LL-37. Means and SD of three independent measurements are depicted. \* =  $p < 0.05$ , \*\* =  $p < 0.01$ , \*\*\* =  $p < 0.0001$ .

of eDNA release (Figure 6A) and of the overall biofilm volume (Figure 6B). Because significant inhibition was observed at concentrations lower than 250 μM, these effects can be attributed to the on-target activity of the compound and are not due to a reduction of bacterial growth or lysis of cells. Hence, LasB inhibitor 7 has demonstrated important pathoblocker activity. It is able to interfere with crucial factors leading to bacterial resistance of *P. aeruginosa* toward antibiotics and host defense molecules.<sup>27,60</sup> To the best of our knowledge, no direct correlation between LasB inhibition and a reduction of eDNA release has been reported to date. Regarding the two mechanisms discussed in literature, the reduced biofilm formation is either due to a reduced NDK-mediated alginate synthesis<sup>24</sup> or rhamolipid-mediated synthesis.<sup>25</sup> Which of these mechanisms inhibitor 7 interferes with cannot be concluded. Yet, these findings could hint at the capacity of 7 to permeate at least the outer membrane of the Gram-negative cell wall, as far as an inhibition of periplasmic NDK<sup>24</sup> is concerned.

## CONCLUSION

Based on our recent findings that *N*-aryl mercaptoacetamides are promising highly selective inhibitors of the virulence factor LasB from *P. aeruginosa*, the lead inhibitor was modified by changing the zinc-chelating moiety to a hydroxamate. Using X-ray crystallography, it was shown that similar to the thiol analogue 1, hydroxamate 7 occupied the primed binding site. Contrary to our recent observations for 1, only one inhibitor molecule was bound to the protease, which could undergo the characteristic hinge-bending motion resulting in a closed conformation of the enzyme. This was attributed to the ability of the inhibitor to interact with catalytic zinc and the edge strand alike. Despite the high similarity of zinc binding to hydroxamates inhibiting MMP-7, inhibitor 7 was unexpectedly able to maintain the remarkable selectivity of 1 toward a range of MMPs. This could be rationalized by the fact that the S1' pocket was not occupied by 7, unlike that observed for MMP inhibitors. These findings show that despite the selectivity issues related to hydroxamic acids, selectivity can indeed be achieved by sparing the S1' pocket. Because cytotoxic effects toward mammalian cell lines were observed, the activity of 7 was investigated regarding other antitargets, revealing a moderate inhibition of ADAM-17 and high selectivity against HDAC3 and 8. Consequently, there will be a special focus on selectivity and cytotoxicity during future compound optimization.

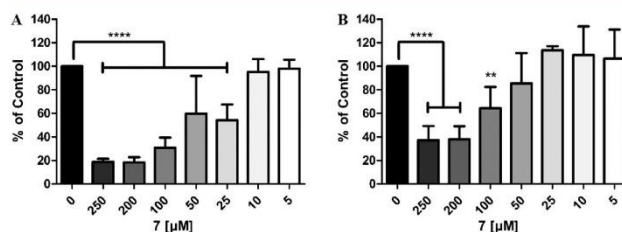


**Figure 6.** Reduction of eDNA release by treatment of PA14 cultures with 7. (A) Reduction of overall PA14 biofilm volume by 7. (B) Columns represent mean and SD of at least four independent measurements. \*\* =  $p < 0.01$ , \*\*\*\* =  $p < 0.0001$ .

tion. Below an antibacterial concentration of 250  $\mu\text{M}$ , LasB was efficiently inhibited *in vitro*. This inhibition could be translated into more complex, cellular assays, highlighting this compound as a promising antivirulence agent. After reduction of their pathogenicity by such an agent, bacteria are supposed to be cleared by host defense mechanisms or with the help of conventional antibiotics.<sup>10,11</sup> In this context, our results highlight a direct restoration effect of the antibacterial activity of the host defense peptide AMP LL-37 *in vitro*. Indirectly, the activity of host defense mechanisms might be further improved by the inhibition of biofilm formation and eDNA release also observed for 7. The same holds true for the effectiveness of conventional antibiotics, which is seriously hampered by bacterial biofilms. Overall, these findings show hydroxamate 7 to be an interesting lead, which could pave the way for the rational development of selective protease inhibitors as potential new antibiotics.

## METHODS

**Chemistry.** All reagents were used from commercial suppliers without further purification. Procedures were not optimized regarding yield. NMR spectra were recorded on a Bruker Fourier 300 (300 MHz) spectrometer. Chemical shifts are given in parts per million (ppm) and referenced against the residual proton,  $^1\text{H}$ , or carbon,  $^{13}\text{C}$ , resonances of the >99% deuterated solvents as internal reference. Coupling constants ( $J$ ) are given in Hertz. Data are reported as follows: chemical shift, multiplicity ( $s$  = singlet,  $d$  = doublet,  $t$  = triplet,  $m$  = multiplet,  $br$  = broad and combinations of these) coupling constants and integration. Mass spectrometry was performed on a SpectraSystems-MSQ LCMS system (Thermo Fisher). Flash chromatography was performed on silica gel 60 M, 0.04–0.063 mm (Machery-Nagel) or using the automated flash chromatography system CombiFlash Rf+ (Teledyne Isco) equipped with RediSepRf silica columns (Axel Semrau) or Chromabond Flash C18 columns (Machery-Nagel). Purity of compounds synthesized by us was determined by LCMS using the area percentage method on the UV trace recorded at a wavelength of 254 nm and found to be >95%.

**Expression and Purification of LasB.** LasB was expressed and purified as described previously.<sup>32</sup>

***In vitro* Inhibition Assays.** The LasB *in vitro* inhibition assay and the MMP assay were performed as described previously.<sup>32</sup> The LasB concentration that was used in the assay was 0.3 nM. The  $K_m$  value for LasB was determined to be 363.0  $\mu\text{M}$ .

**ADAM Inhibition Assay.** ADAM-17 (TACE) Inhibitor Screening Assay Kit was purchased from Sigma-Aldrich. The assay was performed according to the guidelines of the manufacturer. Fluorescence signals were measured in a CLARIOstar plate reader (BMG Labtech).

**HDAC Inhibition Assay.** HDAC3 and HDAC8 inhibitor screening kits were purchased from Sigma-Aldrich. The assay was performed according to the guidelines of the manufacturer.

Fluorescence signals were measured in a CLARIOstar plate reader (BMG Labtech).

**Cytotoxicity Assays.** Hep G2 or HEK293 cells ( $2 \times 10^5$  cells per well) were seeded in 24-well, flat-bottomed plates. Culturing of cells, incubations, and OD measurements were performed as described previously<sup>61</sup> with small modifications. Twenty-four hours after seeding the cells, the incubation was started by the addition of compounds in a final DMSO concentration of 1%. The living cell mass was determined after 48 h. At least three independent measurements were performed for each compound.

**X-ray Crystallography and Image Preparation.** LasB was concentrated to 10–12 mg  $\text{mL}^{-1}$  and mixed with inhibitor 7 at a final concentration of 1 mM. Complex crystals were grown by the sitting drop method using a reservoir solution containing 1.8 M  $\text{AMSO}_4$  and 0.1 M Tris-Cl, pH 8.8. Crystals were cryoprotected in glycerol, and diffraction data was collected from single crystals at 100 K at beamline ID29 (ESRF) at a wavelength of 1.738 Å. Data was processed using Xia2,<sup>62</sup> and the structure was solved using PHASER<sup>63</sup> molecular replacement with *Pseudomonas aeruginosa* LasB (PAE, PDB ID 1EZM) as a search model. The solution was manually rebuilt with COOT<sup>64</sup> and refined using PHENIX<sup>65</sup> and Refmac5.<sup>66</sup> The final refined structure of LasB in complex with compound 7 was deposited in the Protein Data Bank (PDB) as entry 6FZX. Structural superimposition of complex structures of human MMPs (1MMQ and 4G9L) and LasB (6FZX) was achieved through alignment of residues 201–205 of 4G9L (corresponds to residues 140–144 of 1MMQ) using the align atoms algorithm of YASARA structure (YASARA Biosciences GmbH).<sup>67</sup> Image was rendered using PovRay (<http://www.povray.org/>).

**Bacterial Growth Assay.** The assay was performed in 96 well plates (Greiner) with a final volume of 200  $\mu\text{L}$ . LL-37 was purchased from AnaSpec (Fremont) and diluted to a final concentration of 25  $\mu\text{g mL}^{-1}$  from 125  $\mu\text{g mL}^{-1}$  stocks in 18M $\Omega$   $\text{H}_2\text{O}$ . Prior to culture addition 7 was serially diluted in DMSO. A preculture of PA14 was adjusted to the final start  $\text{OD}_{600}$  0.02 in lysogeny broth medium. All samples contained 1% DMSO and 40% of 18M $\Omega$   $\text{H}_2\text{O}$ .  $\text{OD}_{600}$  was measured using a FLUOstar Omega (BMG Labtech) after inoculation and after incubation for 16.5 h at 37  $^\circ\text{C}$  with 200 rpm. Given  $\text{OD}_{600}$  values were obtained after subtraction of the respective start  $\text{OD}_{600}$  and represent three independent measurements with at least two replicates each. One-way ANOVA was performed using GraphPad Prism 6 software.

**Biofilm and eDNA Assays.** The assays were performed as described previously.<sup>68</sup>

## ASSOCIATED CONTENT

### Supporting Information

The Supporting Information is available free of charge on the ACS Publications website at DOI: 10.1021/acchembio.8b00257.

Supplementary Table 1, X-ray data collection and refinement statistics; Supplementary Table T2, residual activities of LasB in the *in vitro* assay; Supplementary

Figures 1–3, comparison of the LasB-I complex to LasB-7 and structures of hydroxamate-based MMP inhibitors **9**, **10**, Batimastat, and HDAC inhibitor Trichostatin A; synthetic procedures; and spectral data for compounds **3–8** (PDF)

## AUTHOR INFORMATION

### Corresponding Author

\*E-mail: Rolf.Hartmann@helmholtz-hzi.de.

### ORCID

Andreas M. Kany: 0000-0001-7580-3658

Samir Yahiaoui: 0000-0001-5134-5007

Jörg Hauptenthal: 0000-0003-3991-2800

Martin Empting: 0000-0002-0503-5830

Jesko Köhnke: 0000-0002-7153-1365

Rolf W. Hartmann: 0000-0002-5871-5231

### Notes

The authors declare no competing financial interest.

## ACKNOWLEDGMENTS

J.K. acknowledges the DFG for an Emmy–Noether Fellowship (KO 4116/3-1). We thank J. Jung, S. Amann, and D. Jener for technical support and T. Röhrig for help with statistical analysis. The image of LL-37 used in the TOC graphic was created using PDB entry 2K6O.

## REFERENCES

- (1) Turk, B. (2006) Targeting proteases. Successes, failures and future prospects. *Nat. Rev. Drug Discovery* **5**, 785–799.
- (2) Agbowuro, A. A., Huston, W. M., Gamble, A. B., and Tyndall, J. D. A. (2018) Proteases and protease inhibitors in infectious diseases. *Med. Res. Rev.* **38**, 1295.
- (3) Culp, E., and Wright, G. D. (2017) Bacterial proteases, untapped antimicrobial drug targets. *J. Antibiot.* **70**, 366–377.
- (4) Cooper, M. A., and Shlaes, D. (2011) Fix the antibiotics pipeline. *Nature* **472**, 32.
- (5) Taubes, G. (2008) The bacteria fight back. *Science* **321**, 356–361.
- (6) Coates, A. R. M., Halls, G., and Hu, Y. (2011) Novel classes of antibiotics or more of the same? *Br. J. Pharmacol.* **163**, 184–194.
- (7) Payne, D. J., Gwynn, M. N., Holmes, D. J., and Pompliano, D. L. (2007) Drugs for bad bugs. Confronting the challenges of antibacterial discovery. *Nat. Rev. Drug Discovery* **6**, 29–40.
- (8) Dickey, S. W., Cheung, G. Y. C., and Otto, M. (2017) Different drugs for bad bugs. Antivirulence strategies in the age of antibiotic resistance. *Nat. Rev. Drug Discovery* **16**, 457–471.
- (9) Heras, B., Scanlon, M. J., and Martin, J. L. (2015) Targeting virulence not viability in the search for future antibacterials. *Br. J. Clin. Pharmacol.* **79**, 208–215.
- (10) Rasko, D. A., and Sperandio, V. (2010) Anti-virulence strategies to combat bacteria-mediated disease. *Nat. Rev. Drug Discovery* **9**, 117–128.
- (11) Clatworthy, A. E., Pierson, E., and Hung, D. T. (2007) Targeting virulence. A new paradigm for antimicrobial therapy. *Nat. Chem. Biol.* **3**, 541–548.
- (12) Kamal, A. A. M., Maurer, C. K., Allegretta, G., Hauptenthal, J., Empting, M., and Hartmann, R. W. (2017) Quorum Sensing Inhibitors as Pathoblockers for Pseudomonas aeruginosa Infections: A New Concept in Anti-Infective Drug Discovery. In *Topics in Medicinal Chemistry*, pp 1–26, Springer, Berlin, Heidelberg.
- (13) Travis, J., and Potempa, J. (2000) Bacterial proteinases as targets for the development of second-generation antibiotics. *Biochim. Biophys. Acta, Protein Struct. Mol. Enzymol.* **1477**, 35–50.
- (14) World Health Organization (2017) Antibacterial Agents in Clinical Development. *An Analysis of the Antibacterial Clinical Development Pipeline, Including Tuberculosis*, World Health Organization, Geneva.
- (15) Aloush, V., Navon-Venezia, S., Seigman-Igra, Y., Cabili, S., and Carmeli, Y. (2006) Multidrug-resistant Pseudomonas aeruginosa. Risk factors and clinical impact. *Antimicrob. Agents Chemother.* **50**, 43–48.
- (16) Wagner, S., Sommer, R., Hinsberger, S., Lu, C., Hartmann, R. W., Empting, M., and Titz, A. (2016) Novel Strategies for the Treatment of Pseudomonas aeruginosa Infections. *J. Med. Chem.* **59**, 5929–5969.
- (17) Sordé, R., Pahissa, A., and Rello, J. (2011) Management of refractory Pseudomonas aeruginosa infection in cystic fibrosis. *Infect. Drug Resist.* **4**, 31–41.
- (18) Storz, M. P., Maurer, C. K., Zimmer, C., Wagner, N., Brengel, C., de Jong, J. C., Lucas, S., Müsken, M., Häußler, S., Steinbach, A., and Hartmann, R. W. (2012) Validation of PqsD as an anti-biofilm target in Pseudomonas aeruginosa by development of small-molecule inhibitors. *J. Am. Chem. Soc.* **134**, 16143–16146.
- (19) Strateva, T., and Mitov, I. (2011) Contribution of an arsenal of virulence factors to pathogenesis of Pseudomonas aeruginosa infections. *Ann. Microbiol.* **61**, 717–732.
- (20) Lu, C., Maurer, C. K., Kirsch, B., Steinbach, A., and Hartmann, R. W. (2014) Overcoming the unexpected functional inversion of a PqsR antagonist in Pseudomonas aeruginosa. An in vivo potent antivirulence agent targeting pqs quorum sensing. *Angew. Chem., Int. Ed.* **53**, 1109–1112.
- (21) Morihara, K., Tsuzuki, H., Oka, T., Inoue, H., and Ebata, M. (1965) Pseudomonas aeruginosa elastase: isolation, crystallization, and preliminary characterization. *J. Biol. Chem.* **240**, 3295–3304.
- (22) Wretling, B., and Pavlovskis, O. R. (1983) Pseudomonas aeruginosa elastase and its role in Pseudomonas infections. *Clin. Infect. Dis.* **5**, S998–1004.
- (23) Schmidtchen, A., Frick, I.-M., Andersson, E., Tapper, H., and Björck, L. (2002) Proteinases of common pathogenic bacteria degrade and inactivate the antibacterial peptide LL-37. *Mol. Microbiol.* **46**, 157–168.
- (24) Kamath, S., Kapatral, V., and Chakrabarty, A. M. (1998) Cellular function of elastase in Pseudomonas aeruginosa. Role in the cleavage of nucleoside diphosphate kinase and in alginate synthesis. *Mol. Microbiol.* **30**, 933–941.
- (25) Yu, H., He, X., Xie, W., Xiong, J., Sheng, H., Guo, S., Huang, C., and Di Zhang, K. (2014) Elastase LasB of Pseudomonas aeruginosa promotes biofilm formation partly through rhamnolipid-mediated regulation. *Can. J. Microbiol.* **60**, 227–235.
- (26) Høiby, N., Bjarnsholt, T., Givskov, M., Molin, S., and Ciofu, O. (2010) Antibiotic resistance of bacterial biofilms. *Int. J. Antimicrob. Agents* **35**, 322–332.
- (27) Lambert, P. A. (2002) Mechanisms of antibiotic resistance in Pseudomonas aeruginosa. *J. R. Soc. Med.* **95 Suppl** **41**, 22–26.
- (28) Cathcart, G. R. A., Quinn, D., Greer, B., Harriott, P., Lynas, J. F., Gilmore, B. F., and Walker, B. (2011) Novel inhibitors of the Pseudomonas aeruginosa virulence factor LasB. A potential therapeutic approach for the attenuation of virulence mechanisms in pseudomonal infection. *Antimicrob. Agents Chemother.* **55**, 2670–2678.
- (29) Zhu, J., Cai, X., Harris, T. L., Gooyit, M., Wood, M., Lardy, M., and Janda, K. D. (2015) Disarming Pseudomonas aeruginosa virulence factor LasB by leveraging a Caenorhabditis elegans infection model. *Chem. Biol.* **22**, 483–491.
- (30) Burns, F. R., Paterson, C. A., Gray, R. D., and Wells, J. T. (1990) Inhibition of Pseudomonas aeruginosa elastase and Pseudomonas keratitis using a thiol-based peptide. *Antimicrob. Agents Chemother.* **34**, 2065–2069.
- (31) Kessler, E., Israel, M., Landshman, N., Checkick, A., and Blumberg, S. (1982) In vitro inhibition of Pseudomonas aeruginosa elastase by metal-chelating peptide derivatives. *Infect. Immun.* **38**, 716–723.
- (32) Kany, A. M., Sikandar, A., Hauptenthal, J., Yahiaoui, S., Maurer, C. K., Proschak, E., Köhnke, J., and Hartmann, R. W. (2018) Binding Mode Characterization and Early in Vivo Evaluation of Fragment-

- Like Thiols as Inhibitors of the Virulence Factor LasB from *Pseudomonas aeruginosa*. *ACS Infect. Dis.* 4, 988–997.
- (33) Schönauer, E., Kany, A. M., Hauptenthal, J., Hüsecken, K., Hoppe, I. J., Voos, K., Yahiaoui, S., Elsässer, B., Ducho, C., Brandstetter, H., and Hartmann, R. W. (2017) Discovery of a Potent Inhibitor Class with High Selectivity toward Clostridial Collagenases. *J. Am. Chem. Soc.* 139, 12696–12703.
- (34) Pereillo, J.-M., Maftouh, M., Andrieu, A., Uzabiaga, M.-F., Fedeli, O., Savi, P., Pascal, M., Herbert, J.-M., Maffrand, J.-P., and Picard, C. (2002) Structure and stereochemistry of the active metabolite of clopidogrel. *Drug Metab. Dispos.* 30, 1288–1295.
- (35) Primi, M. P., Bueno, L., Baumer, P., Berard, H., and Lecomte, J. M. (1999) Racecadotril demonstrates intestinal antisecretory activity in vivo. *Aliment. Pharmacol. Ther.* 13, 3–7.
- (36) Cushman, D. W., and Ondetti, M. A. (1991) History of the design of captopril and related inhibitors of angiotensin converting enzyme. *Hypertension* 17, 589–592.
- (37) Pramari, Y., Das Gupta, V., and Bethea, C. (1992) Stability of captopril in some aqueous systems. *J. Clin. Pharm. Ther.* 17, 185–189.
- (38) Adekoya, O. A., Sjöli, S., Wuxiuer, Y., Bילו, I., Marques, S. M., Santos, M. A., Nuti, E., Cercignani, G., Rossello, A., Winberg, J.-O., and Sylte, I. (2015) Inhibition of pseudolysin and thermolysin by hydroxamate-based MMP inhibitors. *Eur. J. Med. Chem.* 89, 340–348.
- (39) Sjöli, S., Nuti, E., Camodeca, C., Bילו, I., Rossello, A., Winberg, J.-O., Sylte, I., and Adekoya, O. A. (2016) Synthesis, experimental evaluation and molecular modelling of hydroxamate derivatives as zinc metalloproteinase inhibitors. *Eur. J. Med. Chem.* 108, 141–153.
- (40) Jacobsen, J. A., Major Jourden, J. L., Miller, M. T., and Cohen, S. M. (2010) To bind zinc or not to bind zinc. An examination of innovative approaches to improved metalloproteinase inhibition. *Biochim. Biophys. Acta, Mol. Cell Res.* 1803, 72–94.
- (41) Nishino, N., and Powers, J. C. (1980) *Pseudomonas aeruginosa* elastase. Development of a new substrate, inhibitors, and an affinity ligand. *J. Biol. Chem.* 255, 3482–3486.
- (42) Browner, M. F., Smith, W. W., and Castelhana, A. L. (1995) Matrilysin-inhibitor complexes. Common themes among metalloproteinases. *Biochemistry* 34, 6602–6610.
- (43) Belviso, B. D., Caliendo, R., Siliqi, D., Calderone, V., Arnesano, F., and Natle, G. (2013) Structure of matrix metalloproteinase-3 with a platinum-based inhibitor. *Chem. Commun. (Cambridge, U. K.)* 49, 5492–5494.
- (44) Holmes, M. A., and Matthews, B. W. (1981) Binding of hydroxamic acid inhibitors to crystalline thermolysin suggests a pentacoordinate zinc intermediate in catalysis. *Biochemistry* 20, 6912–6920.
- (45) Holland, D. R., Tronrud, D. E., Pley, H. W., Flaherty, K. M., Stark, W., Jansonius, J. N., McKay, D. B., and Matthews, B. W. (1992) Structural comparison suggests that thermolysin and related neutral proteases undergo hinge-bending motion during catalysis. *Biochemistry* 31, 11310–11316.
- (46) Overall, C. M., and Kleifeld, O. (2006) Towards third generation matrix metalloproteinase inhibitors for cancer therapy. *Br. J. Cancer* 94, 941–946.
- (47) Fisher, J. F., and Mobashery, S. (2006) Recent advances in MMP inhibitor design. *Cancer Metastasis Rev.* 25, 115–136.
- (48) Vandenbroucke, R. E., and Libert, C. (2014) Is there new hope for therapeutic matrix metalloproteinase inhibition? *Nat. Rev. Drug Discovery* 13, 904–927.
- (49) Park, H. I., Jin, Y., Hurst, D. R., Monroe, C. A., Lee, S., Schwartz, M. A., and Sang, Q.-X. A. (2003) The intermediate S1' pocket of the endometase/matrilysin-2 active site revealed by enzyme inhibition kinetic studies, protein sequence analyses, and homology modeling. *J. Biol. Chem.* 278, 51646–51653.
- (50) Rasmussen, H. S., and McCann, P. P. (1997) Matrix metalloproteinase inhibition as a novel anticancer strategy. A review with special focus on batimastat and marimastat. *Pharmacol. Ther.* 75, 69–75.
- (51) Overall, C. M., and Kleifeld, O. (2006) Tumour microenvironment - opinion. Validating matrix metalloproteinases as drug targets and anti-targets for cancer therapy. *Nat. Rev. Cancer* 6, 227–239.
- (52) Shen, S., and Kozikowski, A. P. (2016) Why Hydroxamates May Not Be the Best Histone Deacetylase Inhibitors—What Some May Have Forgotten or Would Rather Forget? *ChemMedChem* 11, 15–21.
- (53) Schrupp, D. S. (2009) Cytotoxicity mediated by histone deacetylase inhibitors in cancer cells. Mechanisms and potential clinical implications. *Clin. Cancer Res.* 15, 3947–3957.
- (54) de Ruijter, A. J. M., van Gennip, A. H., Caron, H. N., Kemp, S., and van Kuilenburg, A. B. P. (2003) Histone deacetylases (HDACs). Characterization of the classical HDAC family. *Biochem. J.* 370, 737–749.
- (55) West, A. C., and Johnstone, R. W. (2014) New and emerging HDAC inhibitors for cancer treatment. *J. Clin. Invest.* 124, 30–39.
- (56) Drummond, D. C., Noble, C. O., Kirpotin, D. B., Guo, Z., Scott, G. K., and Benz, C. C. (2005) Clinical development of histone deacetylase inhibitors as anticancer agents. *Annu. Rev. Pharmacol. Toxicol.* 45, 495–528.
- (57) Chen, C. I.-U., Schaller-Bals, S., Paul, K. P., Wahn, U., and Bals, R. (2004) Beta-defensins and LL-37 in bronchoalveolar lavage fluid of patients with cystic fibrosis. *J. Cystic Fibrosis* 3, 45–50.
- (58) Flemming, H.-C., and Wingender, J. (2010) The biofilm matrix. *Nat. Rev. Microbiol.* 8, 623–633.
- (59) Whitchurch, C. B., Tolker-Nielsen, T., Ragas, P. C., and Mattick, J. S. (2002) Extracellular DNA required for bacterial biofilm formation. *Science* 295, 1487.
- (60) Lewenza, S. (2013) Extracellular DNA-induced antimicrobial peptide resistance mechanisms in *Pseudomonas aeruginosa*. *Front. Microbiol.* 4, 21.
- (61) Hauptenthal, J., Baehr, C., Zeuzem, S., and Piiper, A. (2007) RNase A-like enzymes in serum inhibit the anti-neoplastic activity of siRNA targeting polo-like kinase 1. *Int. J. Cancer* 121, 206–210.
- (62) Winter, G. (2010) xia2. An expert system for macromolecular crystallography data reduction. *J. Appl. Crystallogr.* 43, 186–190.
- (63) McCoy, A. J., Grosse-Kunstleve, R. W., Adams, P. D., Winn, M. D., Storoni, L. C., and Read, R. J. (2007) Phaser crystallographic software. *J. Appl. Crystallogr.* 40, 658–674.
- (64) Emsley, P., Lohkamp, B., Scott, W. G., and Cowtan, K. (2010) Features and development of Coot. *Acta Crystallogr., Sect. D: Biol. Crystallogr.* 66, 486–501.
- (65) Adams, P. D., Afonine, P. V., Bunkóczi, G., Chen, V. B., Davis, I. W., Echols, N., Headd, J. J., Hung, L.-W., Kapral, G. J., Grosse-Kunstleve, R. W., McCoy, A. J., Moriarty, N. W., Oeffner, R., Read, R. J., Richardson, D. C., Richardson, J. S., Terwilliger, T. C., and Zwart, P. H. (2010) PHENIX: A comprehensive Python-based system for macromolecular structure solution. *Acta Crystallogr., Sect. D: Biol. Crystallogr.* 66, 213–221.
- (66) Skubák, P., Murshudov, G. N., and Pannu, N. S. (2004) Direct incorporation of experimental phase information in model refinement. *Acta Crystallogr., Sect. D: Biol. Crystallogr.* 60, 2196–2201.
- (67) Krieger, E., Koraimann, G., and Vriend, G. (2002) Increasing the precision of comparative models with YASARA NOVA—a self-parameterizing force field. *Proteins: Struct., Funct., Genet.* 47, 393–402.
- (68) Thomann, A., de Mello Martins, A. G. G., Brengel, C., Empting, M., and Hartmann, R. W. (2016) Application of Dual Inhibition Concept within Looped Autoregulatory Systems toward Antivirulence Agents against *Pseudomonas aeruginosa* Infections. *ACS Chem. Biol.* 11, 1279–1286.

## 4 Final Discussion

The targets addressed in this thesis are *Mycobacterium tuberculosis* (Mtb) and *Pseudomonas aeruginosa*. Both pathogens can cause severe infections which may lead to death. They additionally share the main focus of infection which is the lung.

Mtb causes tuberculosis which is among the top 10 causes of death worldwide. The disease is spread during the active form of pulmonary tuberculosis and its incidence is especially high among HIV patients. Unfortunately, the pathogen possesses a range of characteristics that hamper treatment such as its unique, barely permeable cell envelope or its propensity for the formation of persister cells. The bacteria can survive in this dormant state for years or decades inside the host and eventually reactivate the infection.

*P. aeruginosa* is a gram-negative nosocomial pathogen that is responsible for around 10 % of all hospital acquired infections. It is especially common and threatful for cystic fibrosis patients. Similar to *Mtb* it has developed mechanisms to evade the human immune response and drug treatment such as the formation of biofilms.

For both pathogens, resistances are on the rise and the occurrence of MDR and XDR strains is increasing. Thus, the need for new anti-infective drugs is high and urgent. Due to the existing resistances it is especially promising to exploit novel targets or utilize different strategies such as anti-virulence approaches.

### 4.1 CYP121

This thesis contains two chapters related to the identification of new CYP121 inhibitors. In the first part (chapter 3.1), a CYP inhibitor library was screened via SPR in order to identify CYP121 binders. The specific heme binding of the identified hits was confirmed with an UV-Vis based assay. The confirmed heme binders were evaluated regarding inhibition of mycobacterial growth on *M. bovis* BCG and Mtb. The frontrunner compound was further evaluated regarding cytotoxicity against human cell lines, antibacterial activity and selectivity towards human CYPs. An *in vitro* assay was set up to prove the inhibition of the reaction catalyzed by CYP121. Additionally, molecular modelling studies revealed a possible binding mode.

The second part of the CYP121 project (chapter 3.2) comprised the screening of a library which was based on the former identified hit compound of chapter 3.1. The simultaneous evaluation of affinity towards CYP121 and activity against *M. bovis* BCG revealed an interesting SAR and structural requirements for antimycobacterial activity. Additionally, the *in vitro* assay was optimized in order to quantify the enzymatic inhibition. Furthermore, the effect of substrate

addition on growth inhibition as well as the inhibition of intracellular replication in macrophages was evaluated.

Several aspects of both chapters will be discussed in the following paragraphs.

#### 4.1.1 Biological Function

CYP121 is one of the 20 CYP enzymes of Mtb and was shown to be essential for viability. Cytochrome P450 enzymes are typical anti-fungal targets and are additionally targeted in diseases that are related to the human steroidogenic pathway. However, as the number of CYPs in Mtb is relatively high and most of them are unique, they appear to be an attractive drug target. CYP121 was shown to catalyse the reaction of cyclo-(L-Tyr-L-Tyr) to mycocyclosin which involves the C-C coupling of two aromatic carbon atoms.<sup>115</sup> The role of both, substrate and product are so far unknown.

The substrate cYY is produced by a cyclodipeptide synthase (CDPS) whose gene is located in an operon with the one encoding CYP121.<sup>114,115</sup> The CDPSs use aminoacyl-tRNAs as substrates to form the diketopiperazines. Besides the cYY synthase from Mtb there are 10 other CDPSs characterized so far, however, with different substrate specificities. These are from the species *Streptomyces noursei*, *Bacillus subtilis*, *Bacillus licheniformis*, *Bacillus thuringiensis*, *Photorhabdus luminescens*, *Staphylococcus haemolyticus*, *Corynebacterium jeikeium*, *Actinosynnema mirum*, *Nocardiopsis dassonvillei* and *Nematostella vectensis*. The resulting products are cLL, cFL, cFY, cWW and cWX (X representing L, F, Y or M).<sup>114,119</sup> For some of these CDPs a modifying enzyme has been identified which catalyzes  $\alpha,\beta$ -dehydrogenation, oxidation of the diketopiperazine ring or N-methylation.<sup>112,119</sup>

Biological properties have been described for three natural products resulting from this pathway: albonoursin has antibacterial activity, pulcherriminic acid chelates iron and nocazines are antibacterial and cytotoxic (Figure 4.1.1, compounds **4**, **1** and **3**).<sup>223–225</sup>

However, most of the known diketopiperazines are not synthesized via the CDPS pathway but by nonribosomal peptide synthetases (NRPS) which use free amino acids as substrates.<sup>226</sup> The variety of synthesized DKPs is massive and for some of them biological functions have been assigned such as antifungal, antibacterial, antiviral or antitumor properties.<sup>120</sup> One representative, which resembles the CDPS derived DKPs, is thaxtomin A, a bacterial phytotoxin produced by *Streptomyces scabies* (Figure 4.1.1, compound **2**).<sup>227</sup>

However, besides mycocyclosin there has been no other DKP described that contains a C-C aryl bond. But similar biaryl scaffolds are part of several natural products such as vancomycin (and related glycopeptides), arylomycin, flaviolin or HPQ melanin. Interestingly, all these biaryl bonds are formed by CYP enzymes.<sup>228,229</sup> Similar to mycocyclosin, the C-C bond of the

antibacterial compound arylomycin is formed in *ortho* position to hydroxyl substituents (Figure 4.1.1, compound 5).<sup>230</sup>

Despite all this knowledge and similarities, the biological function of cYY and mycocyclosin as well as the meaning of cYY synthase and CYP121 remain unknown so far. Until now, it can only be speculated whether mycocyclosin is further modified to a final product or whether it is itself biologically active.

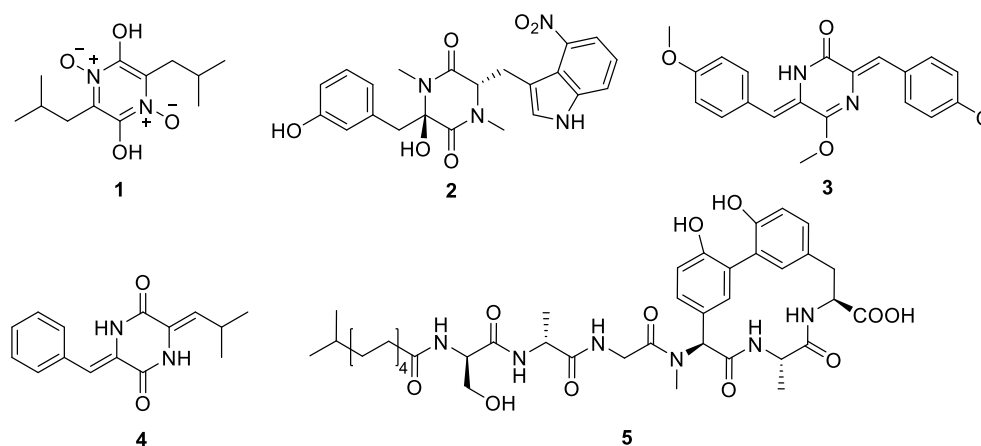


**Figure 4.1.1:** 1: Pulcherriminic acid, 2: Thaxtomin A, 3: Nocazine A, 4: Albonoursin, 5: Arylomycin A2.

#### 4.1.2 Library Screening

Based on the finding that antifungal azoles such as econazole, miconazole and fluconazole bind to CYP121, a screening of compounds from our in-house library against CYP121 was started. The library for the first screening was composed of 139 compounds that were originally designed as inhibitors for CYP17, CYP19, CYP11B1 and CYP11B2. The advantage of this approach is that synthetic availability and drug likeness are ensured. Obviously, the activity against the original targets should be low to ensure good selectivity. The library compounds were selected in order to achieve a great diversity despite their given similarities. All compounds contained a heme coordinating motif such as imidazole, pyridine or pyridazine.

The screening method used was SPR which detects the binding of a compound to the protein. However, the binding event does not necessarily take place in the binding pocket. The hit rate was quite high (44 compounds, 32 %) which is reasonable concerning the selection of compounds. A hit compound was defined according to its response in relation to econazole ( $R/R_{\text{econazole}} > 0.5$ ). The hits were further evaluated in a more specific UV-Vis heme binding assay designed for CYP enzymes.

The screening described in chapter 3.2 was based on the results of chapter 3.1. The structure of the identified frontrunner compound (**I:47**) was used as a template for the compilation of the second similarity-oriented library. The in-house library was scanned for compounds which fit

to this motif and 94 compounds were selected. This time SPR was not applied as we expected almost all compounds to bind to CYP121. In order to compare the affinity, we used the UV-Vis heme binding assay and tested our compounds at concentrations of 100 and 20  $\mu\text{M}$ . For compounds that showed a visible shift at 20  $\mu\text{M}$  the affinity was quantified by determination of the  $K_D$  value. Compounds which showed the same or higher affinity as **I:47** ( $K_D = 5 \mu\text{M}$ ) were defined as hits resulting in a hit rate of 38 %. This rate is again relatively high which was expected due to the high similarity to **I:47**.

Besides determination of affinity, this screening approach (chapter 3.2) compiled the evaluation of antimycobacterial activity. The compounds were tested against *M. bovis* BCG at a concentration of 100  $\mu\text{M}$  and compounds with inhibition greater 80 % were tested at a concentration of 10  $\mu\text{M}$ . The  $\text{MIC}_{50}$  was determined for compounds that showed inhibition of 60 % or higher at 10  $\mu\text{M}$ . Ten compounds showed the same or higher activity than **I:47** resulting in a hit rate of 11 %. The lower hit rate achieved with this screening method is reasonable due to the complex environment in the cellular assay. Several factors may prevent the access of the compounds to their target such as permeability, efflux or metabolism.

#### 4.1.3 Binding Mode

The binding mode of compounds interacting with CYP enzymes can be determined via the analysis of the UV-Vis spectra of inhibitor-enzyme complex in comparison to pure enzyme. The spectrum of CYP121 showed an absorption maximum at 417 nm. This indicates that the iron of the enzyme is predominantly in low-spin state. If the enzyme is completely in high-spin state the absorption maximum appears at 390 nm. In contrast, the maximum appears at 420 nm if the enzyme is completely in low-spin state.<sup>122</sup>

A type I binder is defined as a compound that shifts the absorption maximum to lower wavelengths. The difference spectrum will show a peak at 385-390 nm and a trough at 420 nm.<sup>233</sup> This shift is based on the electronic transition of the heme iron to the high-spin state and is typically caused by compounds that form a bond to the iron via a water-bridge.

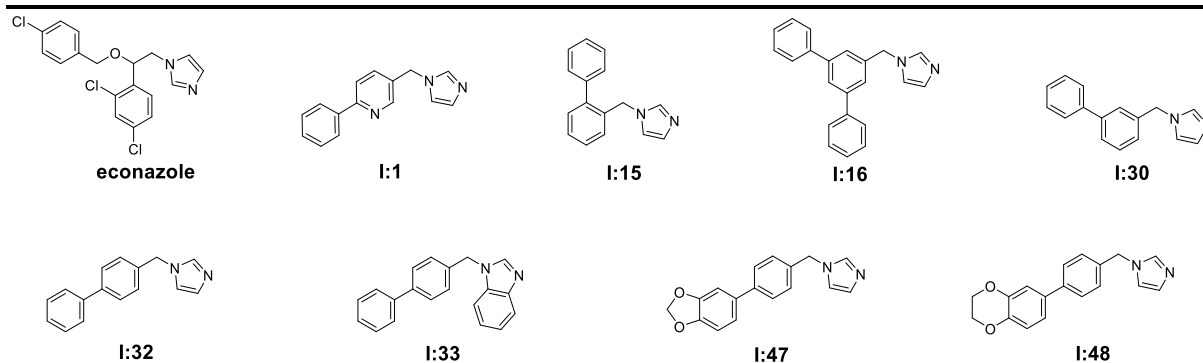
On the other hand, type II binders cause a shift of the absorption maximum to higher wavelength resulting in a difference spectrum with a trough at 390 nm and a peak at 430 nm.<sup>233</sup> This is typically caused by a direct coordination of the heme-iron and its transition to the low-spin state.

The titration of CYP121 with its substrate cYY resulted in a typical substrate like type I behaviour.<sup>115</sup> In contrast, the hits identified in both CYP121 studies (chapter 3.1 and 3.2) showed all a type II binding behavior. Thus, the binding is proposed to involve a coordination of the imidazole nitrogen to the heme-iron.

Interestingly, Seward *et al.* have shown (by co-crystallization and other experiments) that fluconazole, which causes a type II shift in the UV-Vis spectrum, coordinates to the CYP121 heme iron via a water molecule.<sup>123</sup> However, they observed a direct imidazole-iron coordination in a small proportion of their crystals. This direct interaction involves a slight displacement of the helix I which is located above the heme (see chapter 1.2.3). Due to this structural feature the indirect coordination via a water molecule seems to be energetically more favorable. In preliminary crystallization experiments with some of our hit compounds we have also seen this type of indirect coordination for our CYP121 inhibitors.

#### **4.1.4 Affinity vs. Activity**

The first CYP121 screening (chapter 3.1) revealed that among the selected library only imidazole containing compounds were good CYP121 binders. Additionally, the best binders all contained a biaryl motif (Table 4.1.1).

**Table 4.1.1:** Selected compounds from chapter 3.1.

Cmpd.	SPR [R/R <sub>pos</sub> ]	Haem K <sub>D</sub> [μM]	MIC <sub>BCGT</sub> [μM]	MIC <sub>Mtb</sub> [μM]
Eco	1	3	14	11 <sup>b</sup>
I:1	0.4	>100	>100	-
I:15	0.3	34	41	-
I:16	1.2	1	5	6
I:30	1.4	11	11	48
I:32	1.1	14	30	41
I:33	0.1	>100	>100	-
I:47	0.6	5	1	1
I:48	0.6	5	7	12

Interestingly, the substitution of imidazole with benzimidazole (**I:33**) resulted in an inactive compound. A similar effect was observed upon the substitution of the of phenyl with pyridine in the middle part of the molecule (**I:1**). However, the subset of compounds was too small to analyze correlations between affinity and activity.

In the second chapter concerning CYP121 (chapter 3.2) the applied screening approach enabled the analysis of structure-affinity and structure-activity relationships. A range of structural features that contribute beneficially to affinity were identified. For example, bulky substituent at the methylene linker were favorable as well as naphthalene moieties in the middle or outer aromatic part.

Interestingly, a lot of compounds showed high affinity to the enzyme but failed to translate this into *in vitro* activity. Through a detailed analysis several features were identified that seem to hinder a transfer of affinity into activity. For example, a bulky middle part, hydroxy substituents at the western part aromatic motif or bulky substituents at the methylene linker seemed to impair *in vitro* activity.

Due to the complexity of the cellular system there exist several possible reasons for this poor affinity-activity relationship. First of all, the special cell envelope of Mtb (and *M. bovis* BCG respectively) could hinder the access of the compounds to their target. There are some simulated permeability models but overall the required parameters for penetration of the mycobacterial cell wall are unknown.<sup>200,201</sup> Additionally, it was described that there is an efflux system which

is strongly upregulated upon exposure to azole drugs.<sup>202</sup> A third component is the mycobacterial metabolism that could inactivate the CYP121 inhibitors.

Furthermore, an additional factor that has to be taken in account is the high number of CYP enzymes present in Mtb. As imidazole is a common heme-coordinating motif, it is in principal possible that other CYP enzymes are additionally inhibited. Thus, the growth inhibiting effect may be caused by the simultaneous inhibition of several CYP enzymes. However, as CYP121 is essential for viability and we have proven that our compounds effectively inhibit its enzymatic function, the inhibition of CYP121 is probably the main reason for the biological activity.

#### 4.1.5 Mode of action studies

To underline the significance of CYP121 inhibition regarding antimycobacterial activity the activity of **I:47** against *E. coli* and *S. aureus* was assessed. In contrast to econazole which showed inhibition at higher concentrations, no inhibition was observed for **I:47**.

Additionally, the prove that the compounds do not only bind to the heme iron but also significantly inhibit the reaction catalyzed by CYP121 would be a strong indication for the relation of affinity and antimycobacterial activity. Hence, a functional assay was set up with the help of an artificial electron transfer system which consisted of a ferredoxin and a ferredoxin reductase from *Schizosaccharomyces pombe*. Furthermore, mycocyclosin and cYY were synthesized and a LS-MS/MS method for detection of the analytes was established. Through optimization of assay composition and procedure it was possible to quantify the inhibition (chapter 3.2).

The determined IC<sub>50</sub> values were in good correlation with the affinity, however, they were higher (~ factor 4) than the respective K<sub>D</sub> values. As the IC<sub>50</sub> value is strongly dependent on the relation of substrate to inhibitor concentration, this discrepancy is caused by the assay composition.<sup>192</sup> Due to the detection limit it was not possible to further optimize the individual concentrations in order to approximate the 'true' IC<sub>50</sub> value. Despite this limitation, we could prove that our compounds significantly inhibit the conversion of cYY to mycocyclosin.

In order to further underline the significance of CYP121 inhibition for *in vitro* activity, the influence of cYY on growth inhibition was determined (chapter 3.2). Interestingly, cYY accelerated the growth of *M. bovis* BCG significantly. This growth promoting effect did not occur in presence of the CYP121 inhibitor **I:47**. Only at low inhibitor concentrations the effect was visible in a (inhibitor) concentration-dependent manner. This is an additional indication that CYP121 inhibition is the main cause for the antimycobacterial activity of our compounds.

#### **4.1.6 Intracellular Replication in Macrophages**

A characteristic of Mtb is that upon infection the mycobacteria can survive and replicate inside macrophages. To achieve this, the bacteria have developed special mechanisms to avoid their destruction by macrophages. They reside inside phagosomes (inside macrophages) and prevent the fusion of these phagosomes with lysosomes which would be necessary for their elimination.<sup>62,196</sup> The uptake of mycobacteria into the macrophages has been linked to the presence of cholesterol.<sup>66,234</sup> Furthermore, the survival of mycobacteria inside macrophages has been linked to an operon that contains the CYP enzyme CYP125 which catalyzes an essential step in the detoxification of cholesterol.<sup>198,199</sup>

Similar to the CYP121 screening approach, our group has evaluated a CYP library regarding binding to CYP125 and could identify some hit compounds.<sup>197</sup> Interestingly, there were some compounds among these hits that did also bind to CYP121.

As an additional prove for the efficacy of our compounds, we decided to evaluate whether the inhibition of CYP125 or CYP121 or both enzymes has an effect on the intracellular survival inside macrophages (chapter 3.2). Two CYP125 inhibitors, three CYP121 inhibitor and one dual inhibitor were tested. The strongest effects had one of the CYP121 inhibitors and the dual inhibitor. The effective reduction of intracellular replication indicates that the inhibition of mycobacterial CYP enzymes is a promising and effective treatment strategy.

## 4.2 LasB

Chapter 3.3. and 3.4 are devoted to the development of new inhibitors targeting LasB from *Pseudomonas aeruginosa*. In a recently published study of our group, a screening approach led to the identification of N-aryl mercaptoacetamides as potent LasB inhibitors.<sup>185</sup>

Chapter 3.3 describes three optimization approaches beginning with the hits of this former study. Based on molecular modelling, possible inhibitors were designed, synthesized and evaluated regarding activity against LasB. An  $\alpha$ -benzyl mercaptoacetamide compound showed increased activity compared to the original N-aryl mercaptoacetamides. The synthesis and evaluation of a small library resulted in a hit compound with activity in the nanomolar range and good selectivity against other metallo proteases. Additionally, co-crystallization with LasB led to the elucidation of the binding mode.

Chapter 3.4 describes an optimization approach based on the exchange of the zinc coordinating thiol group. Several possible zinc binding groups were introduced into the N-aryl mercaptoacetamide hit compound. The respective hydroxamic acid was identified as potent LasB inhibitor and showed good selectivity over human MMPs. The binding mode was determined via co-crystallization and several cellular experiments proved the efficacy of LasB inhibition.

### 4.2.1 Structure-based Approaches

The approaches described in chapter 3.3 and 3.4 are based on the recently determined co-crystal structure of LasB with compound **R36** ( $IC_{50} = 6.6 \mu M$ ).<sup>185</sup> Surprisingly, the crystal structure revealed the presence of two molecules inside the binding pocket. Based on this finding, Kany *et al.* developed the idea to combine both molecules into one novel inhibitor scaffold. However, the synthesized N-benzyl mercaptoacetamides (**R64** ( $IC_{50} = 12.6 \mu M$ ) and derivatives) were less active than the original N-aryl mercaptoacetamides (**R36** and derivatives).

Chapter 3.3 describes three new structure-based approaches for the optimization of these fragment-like thiols. The first approach was based on the results of the N-benzylated mercaptoacetamide class of **R64**.<sup>185</sup> The molecular modelling of this compound suggested that the di-chloro phenyl ring is placed on the rather hydrophilic entrance region of the binding pocket. Hence, we evaluated whether the removal of the chloro substituents or the substitution with more polar groups (3-OH or 3-OCH<sub>3</sub>) would increase activity. However, the activities were similar to the formerly evaluated derivatives and the approach was not further pursued.

In the second approach, the idea was to initiate the formation of a further interaction between inhibitor and protein. The amino acid residue of Glu141 was chosen as possible interaction

partner. According to molecular modelling based on **R36<sup>A</sup>**, the substitution of the  $\alpha$ -position with an aminomethyl group seemed to enable an interaction with Glu141. However, the synthesized compound **B1** did show only moderate activity ( $IC_{50} = 82 \mu M$ ) towards LasB suggesting that the proposed interaction did not take place.

In the third approach, the starting point was the combination of both molecules of compound **R36** which are present in the co-crystal structure. As Kany *et al.* proposed that the free amide nitrogen is important for binding to LasB and should not be blocked by a substituent, this time the benzyl group was not introduced at the nitrogen but instead in  $\alpha$ -position to the thiol group. According to the proposed binding mode of this new class of compounds, the introduction of substituents at the benzyl ring could lead to additional interactions with the protein (Figure 4.2.1). The synthesis and evaluation of the first compound **C1** ( $IC_{50} = 1.2 \mu M$ ) revealed a significant increase in activity compared to thiol **R36** and thus provoked the synthesis of a small library of  $\alpha$ -benzylated mercaptoacetamides.

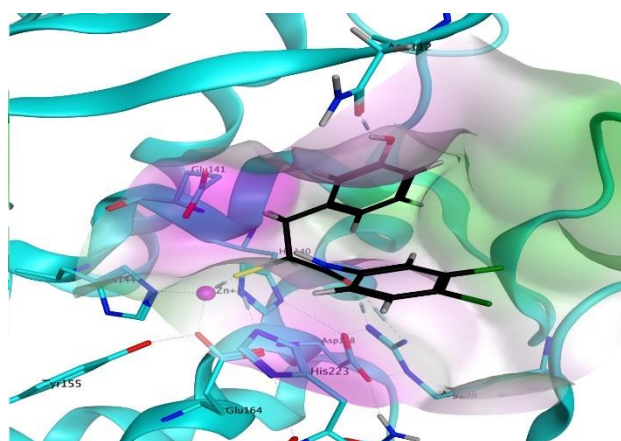


**Figure 4.2.1:** Molecular modelling: Possible interaction of 3-OH-substituted (S)- $\alpha$ -benzyl mercaptoacetamide with LasB. The surface map represents lipophilic (green) and hydrophilic (magenta) areas of the binding pocket.

#### 4.2.2 Binding Mode

As mentioned before, two molecules of **R36** ( $IC_{50} = 6.6 \mu M$ ) were present in the co-crystal, one coordinating the zinc ion (**R36<sup>A</sup>**), the other one occupying the lipophilic S1' pocket (**R36<sup>B</sup>**).<sup>185</sup> The former (**R36<sup>A</sup>**) was used for molecular modelling and will also be utilized for the following comparisons.

Approach 3 resulted in a novel class of LasB inhibitors (**C1-C9**) with increased activity compared to the N-aryl mercaptoacetamide class of **R36**. The co-crystallization of **C1** ( $IC_{50} = 1.2 \mu M$ ) with LasB was successful and revealed that **C1** did indeed bind as proposed by molecular modelling. There were only minor deviations from the binding mode of **R36<sup>A</sup>** (Figure 4.2.2A). The binding mode of hydroxamate compound **7** ( $IC_{50} = 17.4 \mu M$ ) is also similar to

**R36<sup>A</sup>** and **C1** with minor deviations due to the bidentate ligation of the zinc ion (Figure 4.2.2B). Additionally, upon inhibition by compound **7**, the protein undergoes hinge bending resulting in a closed conformation of the binding pocket. For **R36<sup>A</sup>** this closure of the binding pocket was not observed and is probably impaired due to the binding of a second molecule (**R36<sup>B</sup>**). In contrast, we observed a partly closed binding pocket in the cocrystal structure of **C1**.

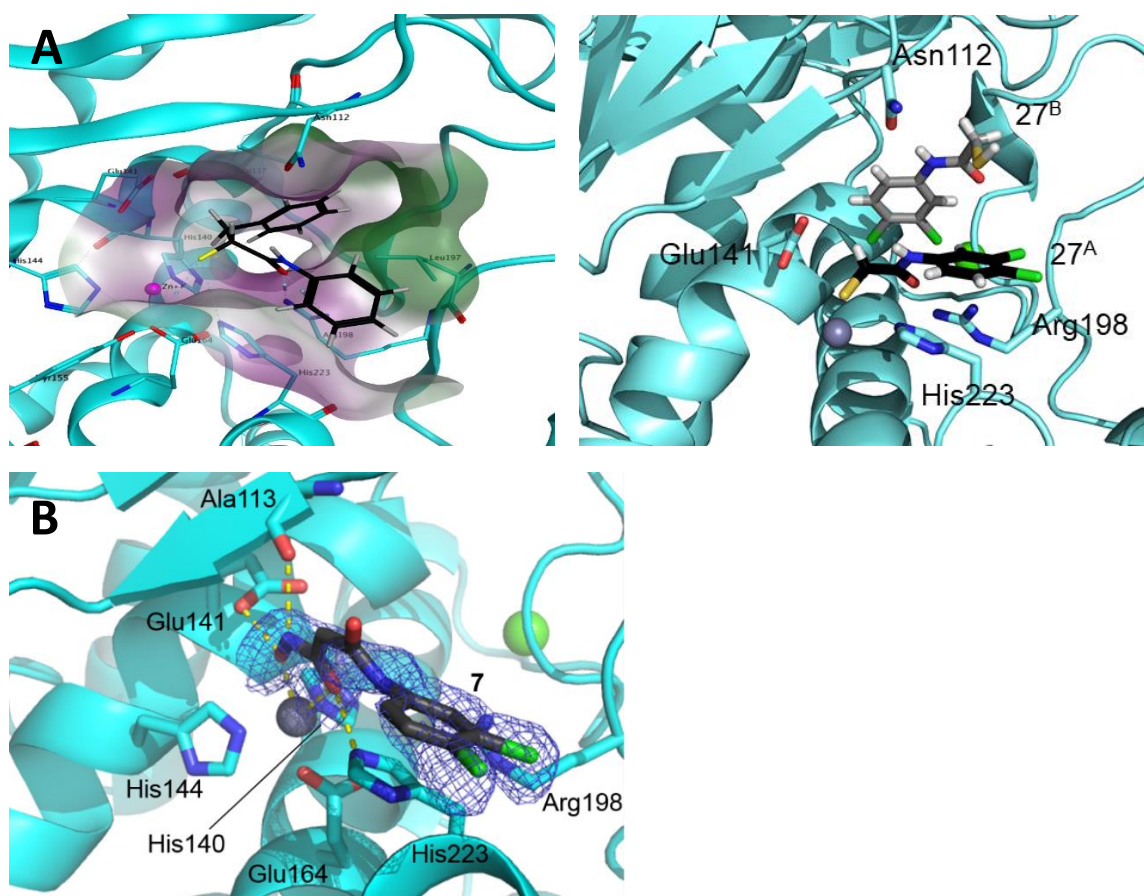


**Figure 4.2.2:** A: Binding Mode of **C1** and **R36<sup>A</sup>**. B: Binding Mode of Hydroxamate **7**. The surface map represents lipophilic (green) and hydrophilic (magenta) areas of the binding pocket.

### 4.2.3 SAR

In the study of Kany *et al.* compound **R36** ( $IC_{50} = 6.6 \mu M$ ) was the most active derivative of the N-aryl mercaptoacetamide series (Figure 4.2.3, compound class **1**). 29 derivatives (thiols and thioacetates) were analyzed in total: 3 showed activities of 5 – 10  $\mu M$ , 11 compounds of 10 – 20  $\mu M$ , 7 compounds of 20 – 50  $\mu M$ , 8 compounds of 50 – 130  $\mu M$ . The SAR was not very sharp but showed a preference for nonpolar substituents especially for halogens. In contrast, polar, hydrogen bond accepting substituents were less favorable.<sup>185</sup>

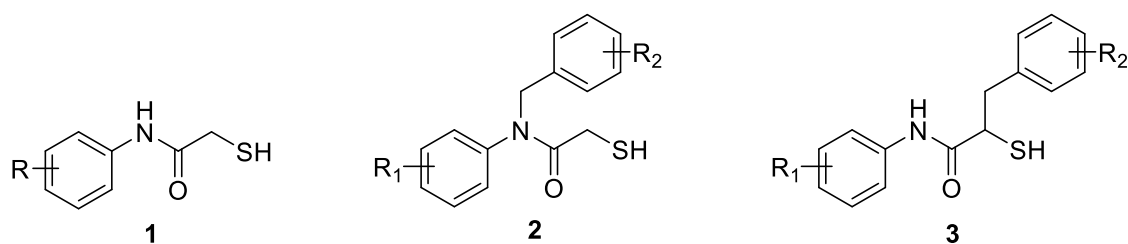


**Figure 4.2.3:** 1: N-aryl mercaptoacetamide, 2: N-benzyl mercaptoacetamide, 3: α-benzyl mercaptoacetamide

The study also described the evaluation of 12 derivatives of the N-benzyl mercaptoacetamide class (Figure 4.2.3, compound class 2). All of these shared the di-chloro motif for the N-aryl part and differed in the substitution pattern of the N-benzyl part. The IC<sub>50</sub> values ranged between 12.6 and 27.4 μM except for one derivative which was less active (IC<sub>50</sub> of 54.5 μM). The results indicate that the true binding mode of this compound class probably differs from the one proposed via molecular modelling.

For the three derivatives synthesized in chapter 3.3 the di-chloro N-aryl motif was exchanged to phenyl (A1), 3-OCH<sub>3</sub>-phenyl (A2) or 3-OH-phenyl (A3). However, activities were similar to the di-chloro derivatives (IC<sub>50</sub> = 13.9 μM, 24.6 μM, 28.1 μM) supporting the hypothesis of a different binding mode.

The α-benzylated mercaptoacetamides described in chapter 3.3 (C1-C9) showed that a shift of the benzyl group from the amide nitrogen to the α-carbon significantly increases activity (Figure 4.2.3, compound class 3). Additionally, the difference in activity between the derivatives supported the proposed binding mode which was confirmed via co-crystallization of C1 with LasB.

Interestingly, the SAR of this class differs from the one observed for the N-aryl mercaptoacetamide series. The 3,4-di-chloro substitution was less favorable (IC<sub>50</sub> = 2.7 μM) compared to the plain phenyl (IC<sub>50</sub> = 1.2 μM). In contrast, the introduction of polar substituents in *para* position (OH, OCH<sub>3</sub>, NO<sub>2</sub>) increased activity (IC<sub>50</sub> = 0.59 μM, 0.73 μM, 0.97 μM, respectively). Interestingly, a methyl substituent in *para* position led to the most active compound (IC<sub>50</sub> = 0.48 μM). Eventually, the SAR of the N-aryl mercaptoacetamides was biased through the binding of two molecules.

#### 4.2.4 Selectivity & Cytotoxicity

Selectivity is a crucial part in the development of potential drugs. In the case of protease inhibitors, multiple off-targets are known to be present in the human body.<sup>235-237</sup> Lacking selectivity has been reported for various MMP inhibitors.<sup>238-240</sup> To evaluate the selectivity of our inhibitors they have been tested for inhibition of several human MMPs that differ in the

depth of their S1' subpockets: MMP1 and MMP7 (shallow), MMP3 and MMP 14 (deep), MMP2 and MMP8 (intermediate).<sup>241</sup>

The N-benzyl mercaptoacetamides (compounds **C1**, **C3** and **C4**, chapter 3.3) and the hydroxamic acid based LasB inhibitor (compound **7**, chapter 3.4) showed high selectivity over all tested MMPs similar to their related N-aryl mercaptoacetamides.<sup>185</sup> The high selectivity of compound **7** over MMPs was proposed to be related to its inability to occupy the S1' subpocket (chapter 3.4). However, the N-benzyl mercaptoacetamides do occupy this subpocket and still show high selectivity. Thus, the selectivity may be caused by other properties.

Unfortunately, the N-benzyl mercaptoacetamide **C1** showed strong inhibition of the anti-target ADAM17. The hydroxamic acid **7** showed intermediate inhibition of ADAM17. Hence, further optimization strategies have to be applied to increase selectivity in order to enable a possible future application as a drug.

The cytotoxicity was evaluated toward human cell lines Hep G2 and HEK293. Compound **7** showed a significant reduction of viability for HEK293 (chapter 3.4). This was proposed to be related to the inhibition of anti-targets such as ADAM17. However, for **C1** & **C3** no cytotoxicity could be observed ( $LD_{50} > 100 \mu M$ ) although they did show strong inhibition of ADAM17. The cytotoxicity of compound **7** is probably caused by other properties of the hydroxamic acid derivative.

#### 4.2.5 Cellular Activity

To underline the relevance of LasB inhibition, the effect of hydroxamic acid based inhibitor **7** (chapter 3.4) on two significant cellular processes of *P. aeruginosa* PA14 was evaluated. First, compound **7** could restore the antibacterial activity of LL37 against PA14. LL37 is an  $\alpha$ -helical human cathelicidin peptide which has antibacterial properties. This protein is produced as a host defense mechanism against bacteria and was shown to be degraded by LasB.<sup>231,232</sup> Additionally, we showed that compound **7** reduced the eDNA release and biofilm formation of PA14.

Furthermore, in the formerly mentioned study of Kany *et al.* compound **R36** significantly increased the survival of PA14 infected *Galleria mellonella*.<sup>185</sup> The effect of the structurally related  $\alpha$ -benzyl mercaptoacetamides (chapter 3.3) on *G. mellonella* is currently under investigation.

Overall, these findings prove that our compounds do not only inhibit LasB but have significant *in vitro* and *in vivo* effects on *P. aeruginosa*.

### 4.3 Conclusion and Outlook

The aim of this thesis was the identification of potent inhibitors targeting CYP121 from Mtb and LasB from *P. aeruginosa*. Indeed, effective inhibitors were identified for both targets through different approaches.

For CYP121, novel inhibitors with significant antimycobacterial activity were found through a screening approach. Mode of action and cellular studies confirmed the efficacy of the identified hit compounds and highlighted CYP121 as an important target for the development of new drugs against TB.

As mentioned in the discussion (chapter 4.1.3), the group was working on co-crystal structures of CYP121 with some hit compounds in order to provide information for further optimization strategies. In the meantime, the cocrystal structures were solved for three hit compounds with different linker scaffolds. All three derivatives show a similar binding mode with a water-mediated coordination of the heme iron by the imidazole nitrogen.

For LasB various structure-based approaches were used to design novel inhibitors. The best synthesized compounds showed *in vitro* activity up to the nanomolar range and significant cellular effects on *P. aeruginosa*'s virulence.

The SAR and co-crystal structure of the  $\alpha$ -benzyl mercaptoacetamide class yielded promising information for further optimization. Additionally, the compounds are currently under evaluation in a *Galleria mellonella in vivo* infection model.

In total, this thesis yielded promising results for two anti-infective targets and will hopefully pave the way for the development of new drugs against Mtb and *P. aeruginosa*.

## 5 References

- (1) Pace, N. R. A Molecular View of Microbial Diversity and the Biosphere. *Science* (80-. ). **1997**, 276, 734–740. <https://doi.org/10.1126/science.276.5313.734>.
- (2) Man, W. H.; De Steenhuijsen Pipers, W. A. A.; Bogaert, D. The Microbiota of the Respiratory Tract: Gatekeeper to Respiratory Health. *Nat. Rev. Microbiol.* **2017**, 15 (5), 259–270. <https://doi.org/10.1038/nrmicro.2017.14>.
- (3) Grice, E. A.; Segre, J. A. The Skin Microbiome. *Nat. Rev. Microbiol.* **2015**, 9 (4), 244–253. <https://doi.org/10.1038/nrmicro2537>.The.
- (4) Gensollen, T.; Iyer, S. S.; Kasper, D. L.; Blumberg, R. S. How Colonization by Microbiota in Early Life Shapes the Immune System. *Science* (80-. ). **2016**, 352 (6285), 539–544. <https://doi.org/10.1126/science.aad9378>.
- (5) Hooper, L. V; Gordon, J. I. Commensal Relationships in the Gut. *Ecol. Evol. Infect.* **2009**, 292 (5519), 1115–1118.
- (6) Hooper, L. V; Littman, D. R.; Macpherson, A. J. Interactions Between the Microbiota and the Immune System. *Science* (80-. ). **2012**, 336 (June), 1268–1274.
- (7) Nugent, R.; Back, E.; Beith, A. *The Race against Drug Resistance*; 2010.
- (8) Davies, M.; Adams, C.; Newell, C. The True Cost of Antibiotic Resistance in Britain and around the World. *The Telegraph*. 2018.
- (9) Baumgaertner, E. We're out of Options: Doctors Battle Drug-Resistant Typhoid Outbreak. *The New York Times*. 2018.
- (10) Bever, L. Our Greatest Fear: Highly Drug-Resistant Gonorrhea Confirmed by Health Officials. *Washington Post*. 2018.
- (11) World Health Organization. Ebola virus disease outbreak news <https://www.who.int/csr/don/archive/disease/ebola/en/>.
- (12) World Health Organization. Cholera disease outbreak news <https://www.who.int/csr/don/archive/disease/cholera/en/>.
- (13) Davies, J. Where Have All the Antibiotics Gone? *Can J Infect Dis Med Microbiol* **2006**, 17 (5), 287–290.
- (14) Aminov, R. I. A Brief History of the Antibiotic Era: Lessons Learned and Challenges for the Future. *Front. Microbiol.* **2010**, 1, 1–7. <https://doi.org/10.3389/fmicb.2010.00134>.
- (15) Domagk, G. Ein Beitrag zur Chemotherapie der bakteriellen Infektionen. *Dtsch med Wochenschr* **1935**, 61 (07), 250–253. <https://doi.org/10.1055/s-0028-1129486>.
- (16) Gary Taubes. The Bacteria Fight Back. *Science* (80-. ). **2008**, 321 (5887), 356–361. <https://doi.org/10.1126/science.321.5887.356>.
- (17) Fleming, A. On the Antibacterial Action of Cultures of a Penicillium, with Special Reference to Their Use in the Isolation of B. Influenzae. *Br. J. experimental Pathol.* **1929**, 10 (3), 226–236. <https://doi.org/10.1093/clinids/2.1.129>.
- (18) Chain, E.; Florey, H. W.; Gardner, A. D.; Heatley, N. G.; Jennings, M. A.; Orr-Ewing, J.; Sanders, A. G. Penicillin as a Chemotherapeutic Agent. *Lancet* **1940**, 236 (6104), 226–228. <https://doi.org/10.1097/01.blo.0000183429.83168.07>.
- (19) Nathan, C. Cooperative Development of Antimicrobials: Looking Back to Look Ahead. *Nat. Rev. Microbiol.* **2015**, 13 (10), 651–657. <https://doi.org/10.1038/nrmicro3523>.
- (20) Hubschwerlen, C.  *$\beta$ -Lactam Antibiotics*; Elsevier, 2007; pp 479–518. <https://doi.org/10.1016/B0-08-045044-X/00218-2>.
- (21) Spratt, B. G. Distinct Penicillin Binding Proteins Involved in the Division, Elongation, and Shape of Escherichia Coli K12. *Proc. Natl. Acad. Sci. U. S. A.* **1975**, 72 (8), 2999–3003. <https://doi.org/10.1073/PNAS.72.8.2999>.

- (22) Bush, K.; Jacoby, G. A.; Medeiros, A. A. A Functional Classification Scheme for Beta-Lactamases and Its Correlation with Molecular Structure. *Antimicrob. Agents Chemother.* **1995**, *39* (6), 1211–1211. <https://doi.org/10.1128/AAC.39.6.1211>.
- (23) Essack, S. Y. The Development of  $\beta$ -Lactam Antibiotics in Response to the Evolution of  $\beta$ -Lactamases. *Pharm. Res.* **2001**, *18* (10), 1391–1399. <https://doi.org/10.1023/A:1012272403776>.
- (24) Spratt, B. G. Resistance to Antibiotics Mediated by Target Alterations. *Science (80-. )*. **1994**, *264* (5157), 388–393. <https://doi.org/10.1126/science.8153626>.
- (25) Mazel, D.; Davies, J. Antibiotic Resistance in Microbes. *Cell. Mol. Life Sci.* **1999**, *56* (9–10), 742–754. <https://doi.org/10.1007/s000180050021>.
- (26) Henriques Normark, B.; Normark, S. Evolution and Spread of Antibiotic Resistance. *J. Intern. Med.* **2002**, *252* (2), 91–106. <https://doi.org/10.1046/j.1365-2796.2002.01026.x>.
- (27) Bennett, P. M. Plasmid Encoded Antibiotic Resistance: Acquisition and Transfer of Antibiotic Resistance Genes in Bacteria. *Br. J. Pharmacol.* **2008**, *153*, S347–S357. <https://doi.org/10.1038/sj.bjp.0707607>.
- (28) World Health Organization. Antimicrobial Resistance: Global Report on Surveillance. *WHO* **2014**. <https://doi.org/10.1017/CBO9781107415324.004>.
- (29) World Health Organization. Global Priority List of Antibiotic-Resistant Bacteria to Guide Research, Discovery, and Development of New Antibiotics. *WHO* **2017**.
- (30) Magill, S. S.; Edwards, J. R.; Bamberg, W.; Beldavs, Z. G.; Dumyati, G.; Kainer, M. A.; Lynfield, R.; Maloney, M.; McAllister-Hollod, L.; Nadle, J.; et al. Multistate Point-Prevalence Survey of Health Care–Associated Infections. *N. Engl. J. Med.* **2014**, *370* (13), 1198–1208. <https://doi.org/10.1056/NEJMoa1306801>.
- (31) WHO. *Global Tuberculosis Report 2017*; 2017; pp 1–262. <https://doi.org/WHO/HTM/TB/2017.23>.
- (32) Besra, G. S.; Kremer, L. Re-Emergence of Tuberculosis: Strategies and Treatment. *Expert Opin. Investig. Drugs* **2002**, *11* (2), 153–157. <https://doi.org/10.1517/13543784.11.2.153>.
- (33) Sacchettini, J. C.; Rubin, E. J.; Freundlich, J. S. Drugs versus Bugs: In Pursuit of the Persistent Predator Mycobacterium Tuberculosis. *Nat. Rev. Microbiol.* **2008**, *6* (1), 41–52. <https://doi.org/10.1038/nrmicro1816>.
- (34) Janeway, C. J.; Travers, P.; Walport, M.; et al. *Immunobiology: The Immune System in Health and Disease*, 5th ed.; Garland Science: New York, 2001.
- (35) Rippke, F.; Schreiner, V.; Schwanitz, H. J. The Acidic Milieu of the Horny Layer: New Findings on the Physiology and Pathophysiology of Skin PH. *Am. J. Clin. Dermatol.* **2002**, *3* (4), 261–272. <https://doi.org/10.2165/00128071-200203040-00004>.
- (36) Madison, K. C. Barrier Function of the Skin: “La Raison d’Être” of the Epidermis. *J. Invest. Dermatol.* **2003**, *121* (2), 231–241. <https://doi.org/10.1046/j.1523-1747.2003.12359.x>.
- (37) Chiller, K.; Selkin, B. A.; Murakawa, G. J. Skin Microflora and Bacterial Infections of the Skin. *J. Investig. Dermatology Symp. Proc.* **2001**, *6* (3), 170–174. <https://doi.org/10.1046/j.0022-202x.2001.00043.x>.
- (38) Cone, R. A. Barrier Properties of Mucus. *Adv. Drug Deliv. Rev.* **2009**, *61* (2), 75–85. <https://doi.org/10.1016/j.addr.2008.09.008>.
- (39) Mahon, J. L.; Stiller, C. R. The Immunocompromised Patient. *Can Fam Physician* **1987**, *33*, 349–359. <https://doi.org/10.1016/B978-0-7234-3496-2.00011-7>.
- (40) Kohanski, M. A.; Dwyer, D. J.; Collins, J. J. How Antibiotics Kill Bacteria: From Targets to Networks. *Nat. Rev. Microbiol.* **2010**, *8* (6), 423–435. <https://doi.org/10.1038/nrmicro2333>.
- (41) Francino, M. P. Antibiotics and the Human Gut Microbiome: Dysbioses and Accumulation of Resistances. *Front. Microbiol.* **2016**, *6* (1543).

- <https://doi.org/10.3389/fmicb.2015.01543>.
- (42) Dickey, S. W.; Cheung, G. Y. C.; Otto, M. Different Drugs for Bad Bugs: Antivirulence Strategies in the Age of Antibiotic Resistance. *Nat. Rev. Drug Discov.* **2017**, *16* (7), 457–471. <https://doi.org/10.1038/nrd.2017.23>.
  - (43) Rasko, D. A.; Sperandio, V. Anti-Virulence Strategies to Combat Bacteria-Mediated Disease. *Nat. Rev. Drug Discov.* **2010**, *9* (2), 117–128. <https://doi.org/10.1038/nrd3013>.
  - (44) Heras, B.; Scanlon, M. J.; Martin, J. L. Targeting Virulence Not Viability in the Search for Future Antibacterials. *Br. J. Clin. Pharmacol.* **2015**, *79* (2), 208–215. <https://doi.org/10.1111/bcp.12356>.
  - (45) Clatworthy, A. E.; Pierson, E.; Hung, D. T. Targeting Virulence: A New Paradigm for Antimicrobial Therapy. *Nat. Chem. Biol.* **2007**, *3* (9), 541–548. <https://doi.org/10.1038/nchembio.2007.24>.
  - (46) Gohlke, H.; Klebe, G. Approaches to the Description and Prediction of the Binding Affinity of Small-Molecule Ligands to Macromolecular Receptors. *Angew. Chemie - Int. Ed.* **2002**, *41* (15), 2644–2676. [https://doi.org/10.1002/1521-3773\(20020802\)41:15<2644::AID-ANIE2644>3.0.CO;2-O](https://doi.org/10.1002/1521-3773(20020802)41:15<2644::AID-ANIE2644>3.0.CO;2-O).
  - (47) Klebe, G. Recent Developments in Structure-Based Drug Design. *J. Mol. Med.* **2000**, *78* (5), 269–281. <https://doi.org/10.1007/s001090000084>.
  - (48) Ginalski, K. Comparative Modeling for Protein Structure Prediction. *Curr. Opin. Struct. Biol.* **2006**, *16*, 172–177. <https://doi.org/10.1016/j.sbi.2006.02.003>.
  - (49) Hillisch, A.; Pineda, L. F.; Hilgenfeld, R. Utility of Homology Models in the Drug Discovery Process. *Drug Discov. Today* **2004**, *9* (15), 659–669. [https://doi.org/10.1016/S1359-6446\(04\)03196-4](https://doi.org/10.1016/S1359-6446(04)03196-4).
  - (50) Kitchen, D. B.; Decornez, H.; Furr, J. R.; Bajorath, J. Docking and Scoring in Virtual Screening for Drug Discovery: Methods and Applications. *Nat. Rev. Drug Discov.* **2004**, *3* (11), 935–949. <https://doi.org/10.1038/nrd1549>.
  - (51) Jorgensen WL. The Many Roles of Computation in Drug Discovery. *Science (80-. )*. **2004**, *303* (19 March), 1813–1817.
  - (52) Schneider, G.; Fechner, U. Computer-Based de Novo Design of Drug-like Molecules. *Nat. Rev. Drug Discov.* **2005**, *4* (8), 649–663. <https://doi.org/10.1038/nrd1799>.
  - (53) Babine, R. E.; Bender, S. L. Molecular Recognition of Protein–Ligand Complexes: Applications to Drug Design. *Chem. Rev.* **1997**, *97* (5), 1359–1472. <https://doi.org/10.1021/cr960370z>.
  - (54) Abad-Zapatero, C. Ligand Efficiency Indices for Effective Drug Discovery. *Expert Opin. Drug Discov.* **2007**, *2* (4), 469–488. <https://doi.org/10.1517/17460441.2.4.469>.
  - (55) Stumpfe, D.; Bajorath, J. Similarity Searching. *Wiley Interdiscip. Rev. Comput. Mol. Sci.* **2011**, *1* (2), 260–282. <https://doi.org/10.1002/wcms.23>.
  - (56) Sheridan, R. P. Chemical Similarity Searches: When Is Complexity Justified? *Expert Opin. Drug Discov.* **2007**, *2* (4), 423–430. <https://doi.org/10.1517/17460441.2.4.423>.
  - (57) Yang, S. Y. Pharmacophore Modeling and Applications in Drug Discovery: Challenges and Recent Advances. *Drug Discov. Today* **2010**, *15* (11–12), 444–450. <https://doi.org/10.1016/j.drudis.2010.03.013>.
  - (58) Lemmen, C.; Lengauer, T. Computational Methods for the Structural Alignment of Molecules. *J. Comput. Aided. Mol. Des.* **2000**, *14* (3), 215–232. <https://doi.org/10.1023/A:1008194019144>.
  - (59) World Health Organization. *Global Tuberculosis Report 2018*; 2018. <https://doi.org/10.1016/j.pharep.2017.02.021>.
  - (60) Fenton, M. J.; Vermeulen, M. W. Immunopathology of Tuberculosis: Roles of Macrophages and Monocytes. *Infect. Immun.* **1996**, *64* (3), 683–690.
  - (61) Russell, D. G. Mycobacterium Tuberculosis: Here Today, and Here Tomorrow. *Nat.*

- Rev. Mol. Cell Biol.* **2001**, 2 (8), 569–577. <https://doi.org/10.1038/35085034>.
- (62) Armstrong, J. A.; Hart, P. D. A. Response of Cultured Macrophages to Mycobacterium Tuberculosis with Observations on Fusion of Lysosomes with Phagosomes. *J. Exp. Med.* **1971**, 134 (3), 713–740.
- (63) Corbett, E. L.; Watt, C. J.; Walker, N.; Maher, D.; Williams, B. G.; Raviglione, M. C.; Dye, C. The Growing Burden of Tuberculosis. *Arch. Intern. Med.* **2003**, 163, 1009–1021. <https://doi.org/10.1001/archinte.163.9.1009>.
- (64) Zhang, Y.; Yew, W. W. Mechanisms of Drug Resistance in Mycobacterium Tuberculosis. *Int J Tuberc Lung Dis* **2009**, 13 (11), 1320–1330.
- (65) Connolly, L. E.; Edelstein, P. H.; Ramakrishnan, L. Why Is Long-Term Therapy Required to Cure Tuberculosis? *PLoS Med.* **2007**, 4 (3), 435–442. <https://doi.org/10.1371/journal.pmed.0040120>.
- (66) Pieters, J.; Gatfield, J. Hijacking the Host: Survival of Pathogenic Mycobacteria inside Macrophages. *Trends Microbiol.* **2002**, 10 (3), 142–146. [https://doi.org/10.1016/S0966-842X\(02\)02305-3](https://doi.org/10.1016/S0966-842X(02)02305-3).
- (67) Zhang, Y.; Yew, W. W.; Barer, M. R. Targeting Persisters for Tuberculosis Control. *Antimicrob. Agents Chemother.* **2012**, 56 (5), 2223–2230. <https://doi.org/10.1128/AAC.06288-11>.
- (68) Telenti, a. Genetics and Pulmonary Medicine. 5. Genetics of Drug Resistant Tuberculosis. *Thorax* **1998**, 53 (9), 793–797. <https://doi.org/10.1136/thx.53.9.793>.
- (69) Hinson, J. M.; Bradsher, R. W.; Bodner, S. J. Gram-Stain Neutrality of Mycobacterium Tuberculosis. *Am. Rev. Respir. Dis.* **1981**, 123 (4), 365–366. <https://doi.org/10.1164/arrd.1981.123.4.365>.
- (70) Fu, L. M.; Fu-Liu, C. S. Is Mycobacterium Tuberculosis a Closer Relative to Gram-Positive or Gram-Negative Bacterial Pathogens? *Tuberculosis* **2002**, 82 (2–3), 85–90. <https://doi.org/10.1054/tube.2002.0328>.
- (71) Chen, P.; Shi, M.; Feng, G. D.; Liu, J. Y.; Wang, B. J.; Shi, X. D.; Ma, L.; Liu, X. D.; Yang, Y. N.; Dai, W.; et al. A Highly Efficient Ziehl-Neelsen Stain: Identifying de Novo Intracellular Mycobacterium Tuberculosis and Improving Detection of Extracellular M. Tuberculosis in Cerebrospinal Fluid. *J. Clin. Microbiol.* **2012**, 50 (4), 1166–1170. <https://doi.org/10.1128/JCM.05756-11>.
- (72) Brennan, P. J.; Nikaido, H. The Envelope of Mycobacteria. *Annu. Rev. Biochem.* **1995**, 64 (1), 29–63. <https://doi.org/10.1146/annurev.bi.64.070195.000333>.
- (73) Brennan, P. J. Structure, Function, and Biogenesis of the Cell Wall of Mycobacterium Tuberculosis. *Tuberculosis* **2003**, 83 (1–3), 91–97. [https://doi.org/10.1016/S1472-9792\(02\)00089-6](https://doi.org/10.1016/S1472-9792(02)00089-6).
- (74) Takayama, K.; Wang, C.; Besra, G. S. Pathway to Synthesis and Processing of Mycolic Acids In. *Society* **2005**, 18 (1), 81–101. <https://doi.org/10.1128/CMR.18.1.81>.
- (75) Hunter, R. L.; Olsen, M. R.; Jagannath, C.; Actor, J. K. Multiple Roles of Cord Factor in the Pathogenesis of Primary, Secondary, and Cavitory Tuberculosis, Including a Revised Description of the Pathology of Secondary Disease. *Ann. Clin. Lab. Sci.* **2006**, 36 (4), 371–386. <https://doi.org/0091-7370/06/0400-0371>.
- (76) Rajni; Rao, N.; Meena, L. S. Biosynthesis and Virulent Behavior of Lipids Produced by Mycobacterium Tuberculosis: LAM and Cord Factor: An Overview. *Biotechnol. Res. Int.* **2011**, 2011, 274693. <https://doi.org/10.4061/2011/274693>.
- (77) Spargo, B. J.; Crowe, L. M.; Ionedo, T.; Beaman, B. L.; Crowe, J. H. Cord Factor (Alpha,Alpha-Trehalose 6,6'-Dimycolate) Inhibits Fusion between Phospholipid Vesicles. *Proc. Natl. Acad. Sci. U. S. A.* **1991**, 88 (3), 737–740. <https://doi.org/10.1016/j.cryobiol.2005.08.003>.
- (78) Tam, P. H.; Lowary, T. L. Recent Advances in Mycobacterial Cell Wall Glycan Biosynthesis. *Curr. Opin. Chem. Biol.* **2009**, 13 (5–6), 618–625.

- <https://doi.org/10.1016/j.cbpa.2009.09.012>.
- (79) Berg, S.; Kaur, D.; Jackson, M.; Brennan, P. J. The Glycosyltransferases of Mycobacterium Tuberculosis - Roles in the Synthesis of Arabinogalactan, Lipoarabinomannan, and Other Glycoconjugates. *Glycobiology* **2007**, *17* (6), 35R–56R. <https://doi.org/10.1093/glycob/cwm010>.
- (80) Alsteens, D.; Verbelen, C.; Dague, E.; Raze, D.; Baulard, A. R.; Dufrêne, Y. F. Organization of the Mycobacterial Cell Wall: A Nanoscale View. *Pflugers Arch. Eur. J. Physiol.* **2008**, *456* (1), 117–125. <https://doi.org/10.1007/s00424-007-0386-0>.
- (81) Robinson, N.; Kolter, T.; Wolke, M.; Rybniker, J.; Hartmann, P.; Plum, G. Mycobacterial Phenolic Glycolipid Inhibits Phagosome Maturation and Subverts the Pro-Inflammatory Cytokine Response. *Traffic* **2008**, *9* (11), 1936–1947. <https://doi.org/10.1111/j.1600-0854.2008.00804.x>.
- (82) Vergne, I.; Fratti, R. A.; Hill, P. J.; Chua, J.; Belisle, J.; Deretic, V. Mycobacterium Tuberculosis Phagosome Maturation Arrest: Mycobacterial Phosphatidylinositol Analog Phosphatidylinositol Mannoside Stimulates Early Endosomal Fusion. *Mol. Biol. Cell* **2004**, *15*, 3751–3737. <https://doi.org/10.1091/mbc.E03>.
- (83) Sacchettini, J. C.; Blanchard, J. S. The Structure and Function of the Isoniazid Target in M. Tuberculosis. *Res. Microbiol.* **1996**, *147* (1–2), 36–43. [https://doi.org/10.1016/0923-2508\(96\)80201-4](https://doi.org/10.1016/0923-2508(96)80201-4).
- (84) Heym, B.; Saint-Joanis, B.; Cole, S. T. The Molecular Basis of Isoniazid Resistance in Mycobacterium Tuberculosis. *Tuber. Lung Dis.* **1999**, *79* (4), 267–271. <https://doi.org/10.1054/tuld.1998.0208>.
- (85) Heym, B.; Alzari, P. M.; Honoré, N.; Cole, S. T. Missense Mutations in the Catalase-Peroxidase Gene, KatG, Are Associated with Isoniazid Resistance in Mycobacterium Tuberculosis. *Mol. Microbiol.* **1995**, *15* (2), 235–245. <https://doi.org/10.1111/j.1365-2958.1995.tb02238.x>.
- (86) Zhang, Y.; Heym, B.; Allen, B.; Young, D.; Cole, S. The Catalase-Peroxidase Gene and Isoniazid Resistance of Mycobacterium Tuberculosis. *Nature* **1992**, *358* (6387), 591–593. <https://doi.org/10.1038/358591a0>.
- (87) Udawadia Amale, R.A., Ajbani, K.K., Rodrigues, C., Z. F. Totally Drug-Resistant Tuberculosis in India. *Clin. Infect. Dis.* **2012**, *54* (4), 579–581. <https://doi.org/10.1093/cid/cir889>.
- (88) Velayati, A. A.; Masjedi, M. R.; Farnia, P.; Tabarsi, P.; Ghanavi, J.; ZiaZarifi, A. H.; Hoffner, S. E. Emergence of New Forms of Totally Drug-Resistant Tuberculosis Bacilli: Super Extensively Drug-Resistant Tuberculosis or Totally Drug-Resistant Strains in Iran. *Chest* **2009**, *136* (2), 420–425. <https://doi.org/10.1378/chest.08-2427>.
- (89) Cole, S. T.; Brosch, R.; Parkhill, J.; Garnier, T.; Churcher, C.; Harris, D.; Gordon, S. V.; Eiglmeier, K.; Gas, S.; Barry, C. E.; et al. Deciphering the Biology of Mycobacterium Tuberculosis from the Complete Genome Sequence. *Nature* **1998**, *393*, 537–544. <https://doi.org/10.1038/29241>.
- (90) Tekaiia, F.; Gordon, S. V.; Garnier, T.; Brosch, R.; Barrell, B. G.; Cole, S. T. Analysis of the Proteome of Mycobacterium Tuberculosis in Silico. *Tuber. Lung Dis.* **1999**, *79* (6), 329–342. <https://doi.org/10.1054/tuld.1999.0220>.
- (91) Souter, A.; Mclean, K. J.; Smith, W. E.; Munro, A. W. The Genome Sequence of Mycobacterium Tuberculosis Reveals Cytochromes P450 as Novel Anti-TB Drug Targets. *J. Chem. Technol. Biotechnol.* **2000**, *75* (May), 933–941. [https://doi.org/10.1002/1097-4660\(200010\)75:10<933::AID-JCTB301>3.0.CO;2-C](https://doi.org/10.1002/1097-4660(200010)75:10<933::AID-JCTB301>3.0.CO;2-C).
- (92) Blattner, F.; Plunkett, G.; Bloch, C.; Perna, N.; Burland, V.; Riley, M.; Collado-Vides, J.; Glasner, J.; Rode, C.; Mayhew, G.; et al. The Complete Genome Sequence of Escherichia Coli K-12. *Science* (80-. ). **1997**, *277* (5331), 1453–1474. <https://doi.org/10.1126/science.277.5331.1453>.

- (93) McLean, K. J.; Clift, D.; Lewis, D. G.; Sabri, M.; Balding, P. R.; Sutcliffe, M. J.; Leys, D.; Munro, A. W. The Preponderance of P450s in the Mycobacterium Tuberculosis Genome. *Trends Microbiol.* **2006**, *14* (5), 220–228. <https://doi.org/10.1016/j.tim.2006.03.002>.
- (94) Bernhardt, R. Cytochromes P450 as Versatile Biocatalysts. *J. Biotechnol.* **2006**, *124* (1), 128–145. <https://doi.org/10.1016/j.jbiotec.2006.01.026>.
- (95) Guengerich, F. P. Common and Uncommon Cytochrome P450 Reactions Related to Metabolism and Chemical Toxicity. *Chem. Res. Toxicol.* **2001**, *14* (6), 611–650. <https://doi.org/10.1021/tx0002583>.
- (96) Sono, M.; Roach, M. P.; Coulter, E. D.; Dawson, J. H. Heme-Containing Oxygenases. *Chem. Rev.* **1996**, *96* (7), 2841–2888. <https://doi.org/10.1021/cr9500500>.
- (97) Ouellet, H.; Johnston, J. B.; Ortiz de Montellano, P. R. The Mycobacterium Tuberculosis Cytochrome P450 System. *Arch. Biochem. Biophys.* **2010**, *493* (1), 82–95. <https://doi.org/10.1016/j.abb.2009.07.011>.
- (98) Guengerich, F. P. Cytochromes P450, Drugs, and Diseases. *Mol. Interv.* **2003**, *3* (4), 194–204. <https://doi.org/10.1124/mi.3.4.194>.
- (99) Guengerich, F. P. Cytochrome P450 and Chemical Toxicology. *Chem. Res. Toxicol.* **2008**, *21* (1), 70–83. <https://doi.org/10.1021/tx700079z>.
- (100) Omura, T. Mitochondrial P450s. *Chem. Biol. Interact.* **2006**, *163* (1–2), 86–93. <https://doi.org/10.1016/j.cbi.2006.06.008>.
- (101) Hudson, S. A.; McLean, K. J.; Munro, A. W.; Abell, C. Mycobacterium Tuberculosis Cytochrome P450 Enzymes: A Cohort of Novel TB Drug Targets. *Biochem. Soc. Trans.* **2012**, *40* (3), 573–579. <https://doi.org/10.1042/BST20120062>.
- (102) Munro, A. W.; Lindsay, J. G. MicroReview Bacterial Cytochromes P-450. **1996**, *20*.
- (103) Como, J. A.; Dismukes, W. E. Oral Azole Drugs as Systemic Antifungal Therapy. *Drug Ther. (NY)*. **1994**, *330* (4), 263–272.
- (104) European Medicines Agency. European Public Assessment Report: Zytiga - Abiraterone Acetate. **2013**, *44* (0).
- (105) Mouridsen, H.; Gershonovich, M.; Sun, Y.; Pérez-Carrión, R.; Boni, C.; Monnier, A.; Apffelstaedt, J.; Smith, R.; Sleeboom, H. P.; Jänicke, F.; et al. Superior Efficacy of Letrozole versus Tamoxifen as First-Line Therapy for Postmenopausal Women with Advanced Breast Cancer: Results of a Phase III Study of the International Letrozole Breast Cancer Group. *J. Clin. Oncol.* **2001**, *19* (10), 2596–2606. <https://doi.org/10.1200/JCO.2001.19.10.2596>.
- (106) McLean, K. J.; Dunford, A. J.; Sabri, M.; Neeli, R.; Girvan, H. M.; Balding, P. R.; Leys, D.; Seward, H. E.; Marshall, K. R.; Munro, A. W. CYP121, CYP51 and Associated Redox Systems in Mycobacterium Tuberculosis: Towards Deconvoluting Enzymology of P450 Systems in a Human Pathogen. *Biochem. Soc. Trans.* **2006**, *34* (Pt 6), 1178–1182. <https://doi.org/10.1042/BST0341178>.
- (107) McLean, K. J.; Dunford, A. J.; Neeli, R.; Driscoll, M. D.; Munro, A. W. Structure, Function and Drug Targeting in Mycobacterium Tuberculosis Cytochrome P450 Systems. *Arch. Biochem. Biophys.* **2007**, *464* (2), 228–240. <https://doi.org/10.1016/j.abb.2007.03.026>.
- (108) McLean, K. J.; Munro, A. W. Structural Biology and Biochemistry of Cytochrome P450 Systems in Mycobacterium Tuberculosis. *Drug Metab. Rev.* **2008**, *40* (3), 427–446. <https://doi.org/10.1080/03602530802186389>.
- (109) McLean, K. J.; Belcher, J.; Driscoll, M. D.; Fernandez, C. C.; Le Van, D.; Bui, S.; Golovanova, M.; Munro, A. W. The Mycobacterium Tuberculosis Cytochromes P450: Physiology, Biochemistry & Molecular Intervention. *Future Med. Chem.* **2010**, *2* (8), 1339–1353. <https://doi.org/10.4155/fmc.10.216>.
- (110) McLean, K. J.; Carroll, P.; Lewis, D. G.; Dunford, A. J.; Seward, H. E.; Neeli, R.;

- Cheesman, M. R.; Marsollier, L.; Douglas, P.; Smith, W. E.; et al. Characterization of Active Site Structure in CYP121: A Cytochrome P450 Essential for Viability of Mycobacterium Tuberculosis H37Rv. *J. Biol. Chem.* **2008**, *283* (48), 33406–33416. <https://doi.org/10.1074/jbc.M802115200>.
- (111) UniProt-Consortium. UniProtKB Protein Knowledgebase <http://www.uniprot.org/> (accessed Jan 31, 2018).
- (112) Belin, P.; Moutiez, M.; Lautru, S.; Seguin, J.; Pernodet, J. L.; Gondry, M. The Nonribosomal Synthesis of Diketopiperazines in TRNA-Dependent Cyclodipeptide Synthase Pathways. *Nat. Prod. Rep.* **2012**, *29* (9), 961–979. <https://doi.org/10.1039/c2np20010d>.
- (113) Leys, D.; Mowat, C. G.; Kirsty, J.; Richmond, A.; Stephen, K.; Walkinshaw, M. D.; Munro, A. W.; Leys, D.; Mowat, C. G.; Mclean, K. J.; et al. Atomic Structure of Mycobacterium Novel Features of Cytochrome P450 Atomic Structure of Mycobacterium Tuberculosis CYP121 to 1.06 Å Reveals Novel Features of Cytochrome P450. *J. Biol. Chem.* **2003**, *278* (7), 5141–5147. <https://doi.org/10.1074/jbc.M209928200>.
- (114) Gondry, M.; Sauguet, L.; Belin, P.; Thai, R.; Amouroux, R.; Tellier, C.; Tuphile, K.; Jacquet, M.; Braud, S.; Courçon, M.; et al. Cyclodipeptide Synthases Are a Family of TRNA-Dependent Peptide Bond-Forming Enzymes. *Nat. Chem. Biol.* **2009**, *5* (6), 414–420. <https://doi.org/10.1038/nchembio.175>.
- (115) Belin, P.; Le Du, M. H.; Fielding, A.; Lequin, O.; Jacquet, M.; Charbonnier, J.-B.; Lecoq, A.; Thai, R.; Courcon, M.; Masson, C. d.; et al. Identification and Structural Basis of the Reaction Catalyzed by CYP121, an Essential Cytochrome P450 in Mycobacterium Tuberculosis. *Proc. Natl. Acad. Sci.* **2009**, *106* (18), 7426–7431.
- (116) Dumas, V. G.; Defelipe, L. A.; Petruk, A. A.; Turjanski, A. G.; Marti, M. A. QM/MM Study of the C-C Coupling Reaction Mechanism of CYP121, an Essential Cytochrome P450 of Mycobacterium Tuberculosis. *Proteins Struct. Funct. Bioinforma.* **2014**, *82* (6), 1004–1021. <https://doi.org/10.1002/prot.24474>.
- (117) Fonvielle, M.; Le Du, M. H.; Lequin, O.; Lecoq, A.; Jacquet, M.; Thai, R.; Dubois, S.; Grach, G.; Gondry, M.; Belin, P. Substrate and Reaction Specificity of Mycobacterium Tuberculosis Cytochrome P450 CYP121: Insights from Biochemical Studies and Crystal Structures. *J. Biol. Chem.* **2013**, *288* (24), 17347–17359. <https://doi.org/10.1074/jbc.M112.443853>.
- (118) Giessen, T. W.; Von Tesmar, A. M.; Marahiel, M. A. Insights into the Generation of Structural Diversity in a TRNA-Dependent Pathway for Highly Modified Bioactive Cyclic Dipeptides. *Chem. Biol.* **2013**, *20* (6), 828–838. <https://doi.org/10.1016/j.chembiol.2013.04.017>.
- (119) Giessen, T. W.; Tesmar, A. M. von; Marahiel, M. A. A TRNA-Dependent Two-Enzyme Pathway for the Generation of Singly and Doubly Methylated Dityryptophan 2,5-Diketopiperazines. *Biochemistry* **2013**, *52*, 4274–4283. <https://doi.org/10.1021/bi4004827>.
- (120) Martins, M. B.; Carvalho, I. Diketopiperazines: Biological Activity and Synthesis. *Tetrahedron* **2007**, *63* (40), 9923–9932. <https://doi.org/10.1016/j.tet.2007.04.105>.
- (121) McLean, K. J.; Marshall, K. R.; Richmond, A.; Hunter, I. S.; Fowler, K.; Kieser, T.; Gurcha, S. S.; Besra, G. S.; Munro, A. W. Azole Antifungals Are Potent Inhibitors of Cytochrome P450 Mono-Oxygenases and Bacterial Growth in Mycobacteria and Streptomyces. *Microbiology* **2002**, *148* (10), 2937–2949.
- (122) McLean, K. J.; Cheesman, M. R.; Rivers, S. L.; Richmond, A.; Leys, D.; Chapman, S. K.; Reid, G. A.; Price, N. C.; Kelly, S. M.; Clarkson, J.; et al. Expression, Purification and Spectroscopic Characterization of the Cytochrome P450 CYP121 from Mycobacterium Tuberculosis. *J. Inorg. Biochem.* **2002**, *91* (4), 527–541.

- [https://doi.org/10.1016/S0162-0134\(02\)00479-8](https://doi.org/10.1016/S0162-0134(02)00479-8).
- (123) Seward, H. E.; Roujeinikova, A.; McLean, K. J.; Munro, A. W.; Leys, D. Crystal Structure of the Mycobacterium Tuberculosis P450 CYP121-Fluconazole Complex Reveals New Azole Drug-P450 Binding Mode. *J. Biol. Chem.* **2006**, *281* (51), 39437–39443. <https://doi.org/10.1074/jbc.M607665200>.
- (124) Hudson, S. A.; McLean, K. J.; Surade, S.; Yang, Y. Q.; Leys, D.; Ciulli, A.; Munro, A. W.; Abell, C. Application of Fragment Screening and Merging to the Discovery of Inhibitors of the Mycobacterium Tuberculosis Cytochrome P450 CYP121. *Angew. Chemie - Int. Ed.* **2012**, *51* (37), 9311–9316. <https://doi.org/10.1002/anie.201202544>.
- (125) Hudson, S. A.; Surade, S.; Coyne, A. G.; Mclean, K. J.; Leys, D.; Munro, A. W.; Abell, C. Overcoming the Limitations of Fragment Merging: Rescuing a Strained Merged Fragment Series Targeting Mycobacterium Tuberculosis CYP121. *ChemMedChem* **2013**, *8* (9), 1451–1456. <https://doi.org/10.1002/cmcd.201300219>.
- (126) Kavanagh, M. E.; Coyne, A. G.; McLean, K. J.; James, G. G.; Levy, C. W.; Marino, L. B.; De Carvalho, L. P. S.; Chan, D. S. H.; Hudson, S. A.; Surade, S.; et al. Fragment-Based Approaches to the Development of Mycobacterium Tuberculosis CYP121 Inhibitors. *J. Med. Chem.* **2016**, *59* (7), 3272–3302. <https://doi.org/10.1021/acs.jmedchem.6b00007>.
- (127) Fonvielle, M.; Le Du, M.-H.; Lequin, O.; Lecoq, A.; Thai, R.; Dubois, S.; Grach, G.; Gondry, M.; Belin, P. Substrate and Reaction Specificity of Mycobacterium Tuberculosis Cytochrome P450 CYP121. *J. Biol. Chem.* **2013**, *288* (24), 17347–17359. <https://doi.org/10.1074/jbc.M112.443853>.
- (128) Kavanagh, M. E.; Gray, J. L.; Gilbert, S. H.; Coyne, A. G.; McLean, K. J.; Davis, H. J.; Munro, A. W.; Abell, C. Substrate Fragmentation for the Design of M. Tuberculosis CYP121 Inhibitors. *ChemMedChem* **2016**, *11* (17), 1924–1935. <https://doi.org/10.1002/cmcd.201600248>.
- (129) El-wahab, H. A. A. A.; Accietto, M.; Marino, L. B.; McLean, K. J.; Levy, C. W.; Abdel-Rahman, H. M.; El-Gendy, M. A.; Munro, A. W.; Aboraia, A. S.; Simons, C. Design, Synthesis and Evaluation against Mycobacterium Tuberculosis of Azole Piperazine Derivatives as Dicycloyrosine (CYY) Mimics. *Bioorganic Med. Chem.* **2018**, *26* (1), 161–176. <https://doi.org/10.1016/j.bmc.2017.11.030>.
- (130) Centers for disease control and Prevention. Pseudomonas aeruginosa in Health Care Settings <https://www.cdc.gov/hai/organisms/pseudomonas.html>.
- (131) Richards, M. J.; Edwards, J. R.; Culver, D. H.; Gaynes, R. P. Nosocomial Infections in Pediatric Intensive Care Units in the United States. National Nosocomial Infections Surveillance System. *Pediatrics* **1999**, *103* (4). <https://doi.org/10.1542/peds.103.4.e39>.
- (132) Sordé, R.; Pahissa, A.; Rello, J. Management of Refractory Pseudomonas Aeruginosa Infection in Cystic Fibrosis. *Infect. Drug Resist.* **2011**, *4* (1), 31–41. <https://doi.org/10.2147/IDR.S16263>.
- (133) Razvi, S.; Quittell, L.; Sewall, A.; Quinton, H.; Marshall, B.; Saiman, L. Respiratory Microbiology of Patients With Cystic Fibrosis in the United States, 1995 to 2005. *Chest* **2009**, *136* (6), 1554–1560. <https://doi.org/10.1378/CHEST.09-0132>.
- (134) Valenza, G.; Tappe, D.; Turnwald, D.; Frosch, M.; König, C.; Hebestreit, H.; Abele-Horn, M. Prevalence and Antimicrobial Susceptibility of Microorganisms Isolated from Sputa of Patients with Cystic Fibrosis. *J. Cyst. Fibros.* **2008**, *7* (2), 123–127. <https://doi.org/10.1016/j.jcf.2007.06.006>.
- (135) Obritsch, M. D.; Fish, D. N.; MacLaren, R.; Jung, R. Nosocomial Infections Due to Multidrug-Resistant Pseudomonas Aeruginosa: Epidemiology and Treatment Options. *Pharmacotherapy* **2005**, *25* (10 I), 1353–1364. <https://doi.org/10.1592/phco.2005.25.10.1353>.
- (136) Lyczak, J. B.; Cannon, C. L.; Pier, G. B. Establishment of Pseudomonas Aeruginosa

- Infection: Lessons from a Versatile Opportunist. *Microbes Infect.* **2000**, 2 (9), 1051–1060. [https://doi.org/10.1016/S1286-4579\(00\)01259-4](https://doi.org/10.1016/S1286-4579(00)01259-4).
- (137) Hazlett, L. D. Corneal Response to *Pseudomonas Aeruginosa* Infection. *Prog. Retin. Eye Res.* **2004**, 23 (1), 1–30. <https://doi.org/10.1016/j.preteyeres.2003.10.002>.
- (138) Oguntibeju, O. O.; Nwobu, R. A. U. Occurrence of *Pseudomonas Aeruginosa* in Post-Operative Wound Infection. *Pakistan J. Med. Sci.* **2004**, 20 (3), 187–191.
- (139) Fong, I. W.; Tomkins, K. B. Review of *Pseudomonas Aeruginosa* Meningitis with Special Emphasis on Treatment with Ceftazidime. *Rev. Infect. Dis.* **1985**, 7 (5), 604–612. <https://doi.org/10.1093/clinids/7.5.604>.
- (140) Mesaros, N.; Nordmann, P.; Plésiat, P.; Roussel-Delvallez, M.; Eldere, J. Van; Glupczynski, Y.; Laethem, Y. Van; Jacobs, F.; Lebecque, P.; Malfroot, A.; et al. *Pseudomonas Aeruginosa*: Resistance and Therapeutic Options at the Turn of the New Millennium. *Clin. Microbiol. Infect.* **2007**, 13 (6), 560–578. <https://doi.org/http://dx.doi.org/10.1111/j.1469-0691.2007.01681.x>.
- (141) Hancock, R. E. W.; Speert, D. P. Antibiotic Resistance in *Pseudomonas Aeruginosa*: Mechanisms and Impact on Treatment. *Drug Resist. Updat.* **2000**, 3 (4), 247–255. <https://doi.org/10.1054/drup.2000.0152>.
- (142) Nikaido, H.; Yoshimura, F. Permeability of *Pseudomonas Aeruginosa* Outer Membrane to Hydrophilic Solutes. *J. Bacteriol.* **1982**, 152 (2), 636–642.
- (143) Moreira, M. A. S.; Souza, E. C. de; Moraes, C. A. de. Multidrug Efflux Systems in Gram-Negative Bacteria. *Brazilian J. Microbiol.* **2004**, 35 (1–2), 19–28. <https://doi.org/10.1590/S1517-83822004000100003>.
- (144) Pos, K. M. Drug Transport Mechanism of the AcrB Efflux Pump. *Biochim. Biophys. Acta - Proteins Proteomics* **2009**, 1794 (5), 782–793. <https://doi.org/10.1016/j.bbapap.2008.12.015>.
- (145) Hancock, R. E. W.; Woodruff, W. A. Roles of Porin and  $\beta$ -Lactamase in  $\beta$ -Lactam Resistance of *Pseudomonas Aeruginosa*. *Clin. Infect. Dis.* **1988**, 10 (4), 770–775. <https://doi.org/10.1093/clinids/10.4.770>.
- (146) Thomson, J. M.; Bonomo, R. A. The Threat of Antibiotic Resistance in Gram-Negative Pathogenic Bacteria:  $\beta$ -Lactams in Peril! *Curr. Opin. Microbiol.* **2005**, 8 (5), 518–524. <https://doi.org/10.1016/j.mib.2005.08.014>.
- (147) Yoon, S. S.; Hennigan, R. F.; Hilliard, G. M.; Ochsner, U. a.; Parvatiyar, K.; Kamani, M. C.; Allen, H. L.; DeKievit, T. R.; Gardner, P. R.; Schwab, U.; et al. *Pseudomonas Aeruginosa* Anaerobic Respiration in Biofilms. *Dev. Cell* **2002**, 3 (4), 593–603. [https://doi.org/10.1016/S1534-5807\(02\)00295-2](https://doi.org/10.1016/S1534-5807(02)00295-2).
- (148) Højby, N.; Krogh Johansen, H.; Moser, C.; Song, Z.; Ciofu, O.; Kharazmi, A. *Pseudomonas Aeruginosa* and the in Vitro and in Vivo Biofilm Mode of Growth. *Microbes Infect.* **2001**, 3 (1), 23–35. [https://doi.org/10.1016/S1286-4579\(00\)01349-6](https://doi.org/10.1016/S1286-4579(00)01349-6).
- (149) Strateva, T.; Mitov, I. Contribution of an Arsenal of Virulence Factors to Pathogenesis of *Pseudomonas Aeruginosa* Infections. *Ann. Microbiol.* **2011**, 61 (4), 717–732. <https://doi.org/10.1007/s13213-011-0273-y>.
- (150) Arnon, S. S.; Schechter, R.; Maslanka, S. E.; Jewell, N. P.; Hatheway, C. L. Human Botulism for the Treatment of Infant Botulism. *N. Engl. J. Med.* **2006**, 354 (5), 462–471.
- (151) Migone, T.-S.; Subramanian, G. M.; Zhong, J.; Healey, L. M.; Corey, A.; Devalaraja, M.; Lo, L.; Ullrich, S.; Zimmerman, J.; Chen, A.; et al. Raxibacumab for the Treatment of Inhalational Anthrax. *N. Engl. J. Med.* **2009**, 361 (2), 135–144. <https://doi.org/10.1056/NEJMoa0810603>.
- (152) Greig, S. L. Obiltoxaximab: First Global Approval. *Drugs* **2016**, 76 (7), 823–830. <https://doi.org/10.1007/s40265-016-0577-0>.
- (153) Lowy, I.; Molrine, D. C.; Leav, B. A.; Blair, B. M.; Baxter, R.; Gerding, D. N.; Nichol,

- G.; Thomas, W. D.; Leney, M.; Sloan, S.; et al. Treatment with Monoclonal Antibodies against Clostridium Difficile Toxins. *N. Engl. J. Med.* **2010**, *362* (3), 197–205. <https://doi.org/10.1056/NEJMoa1402685>.
- (154) Wagner, S.; Sommer, R.; Hinsberger, S.; Lu, C.; Hartmann, R. W.; Empting, M.; Titz, A. Novel Strategies for the Treatment of Pseudomonas Aeruginosa Infections. *J. Med. Chem.* **2016**, *59* (13), 5929–5969. <https://doi.org/10.1021/acs.jmedchem.5b01698>.
- (155) DiGiandomenico, A.; Keller, A. E.; Gao, C.; Rainey, G. J.; Warren, P.; Camara, M. M.; Bonnell, J.; Fleming, R.; Bezabeh, B.; Dimasi, N.; et al. A Multifunctional Bispecific Antibody Protects against Pseudomonas Aeruginosa. *Sci. Transl. Med.* **2014**, *6* (262), 262ra155--262ra155. <https://doi.org/10.1126/scitranslmed.3009655>.
- (156) Baer, M.; Sawa, T.; Flynn, P.; Luehrsen, K.; Martinez, D.; Wiener-Kronish, J. P.; Yarranton, G.; Bebbington, C. An Engineered Human Antibody Fab Fragment Specific for Pseudomonas Aeruginosa PcrV Antigen Has Potent Antibacterial Activity. *Infect. Immun.* **2009**, *77* (3), 1083–1090. <https://doi.org/10.1128/IAI.00815-08>.
- (157) Adekoya, O. A.; Sylte, I. The Thermolysin Family (M4) of Enzymes: Therapeutic and Biotechnological Potential. *Chem. Biol. Drug Des.* **2009**, *73* (1), 7–16. <https://doi.org/10.1111/j.1747-0285.2008.00757.x>.
- (158) Hangauer, D. G.; Monzingo, A. F.; Matthews, B. W. An Interactive Computer Graphics Study of Thermolysin-Catalyzed Peptide Cleavage and Inhibition by N-Carboxymethyl Dipeptides. *Biochemistry* **1984**, *23* (24), 5730–5741.
- (159) Matthews, B. W. Structural Basis of the Action of Thermolysin and Related Zinc Peptidases. *Acc. Chem. Res.* **1988**, *21* (9), 333–340. <https://doi.org/10.1021/ar00153a003>.
- (160) Mock, W. L.; Stanford, D. J. Arazoformyl Dipeptide Substrates for Thermolysin. Confirmation of a Reverse Protonation Catalytic Mechanism. *Biochemistry* **1996**, *35* (23), 7369–7377. <https://doi.org/10.1021/bi952827p>.
- (161) Mock, W. L.; Aksamawati, M. Binding to Thermolysin of Phenolate-Containing Inhibitors Necessitates a Revised Mechanism of Catalysis. *Biochem J* **1994**, *302* ( Pt 1), 57–68. <https://doi.org/10.1042/bj3020057>.
- (162) Thayer, M. M.; Flaherty, K. M.; McKay, D. B. Three-Dimensional Structure of the Elastase of Pseudomonas Aeruginosa at 1.5-Å Resolution. *J. Biol. Chem.* **1991**, *266* (5), 2864–2871.
- (163) McKay, D. B.; Thayer, M. M.; Flaherty, K. M.; Pley, H.; Benvegna, D. Crystallographic Structures of the Elastase of Pseudomonas Aeruginosa. *Matrix Suppl.* **1992**, *1*, 112–115.
- (164) Holland, D. R.; Tronrud, D. E.; Matthews, B. W.; Pley, H. W.; Flaherty, K. M.; McKay, D. B.; Stark, W.; Jansonius, J. N. Structural Comparison Suggests That Thermolysin and Related Neutral Proteases Undergo Hinge-Bending Motion During Catalysis. *Biochemistry* **1992**, *31* (46), 11310–11316. <https://doi.org/10.1021/bi00161a008>.
- (165) Adekoya, O. A.; Sjøli, S.; Wuxiuer, Y.; Bילו, I.; Marques, S. M.; Santos, M. A.; Nuti, E.; Cercignani, G.; Rossello, A.; Winberg, J. O.; et al. Inhibition of Pseudolysin and Thermolysin by Hydroxamate-Based MMP Inhibitors. *Eur. J. Med. Chem.* **2015**, *89*, 340–348. <https://doi.org/10.1016/j.ejmech.2014.10.009>.
- (166) De Kreijf, A.; Venema, G.; Van Den Burg, B. Substrate Specificity in the Highly Heterogeneous M4 Peptidase Family Is Determined by a Small Subset of Amino Acids. *J. Biol. Chem.* **2000**, *275* (40), 31115–31120. <https://doi.org/10.1074/jbc.M003889200>.
- (167) Liu, P. V. Extracellular Toxins of Pseudomonas Aeruginosa. *J. Infect. Dis.* **1974**, *130* (November), S94–S99. <https://doi.org/10.1093/infdis/130.Supplement.S94>.
- (168) Galloway, D. R. Pseudomonas Aeruginosa Elastase and Elastolysis Revisited: Recent Developments. *Mol. Microbiol.* **1991**, *5* (10), 2315–2321.

- <https://doi.org/10.1111/j.1365-2958.1991.tb02076.x>.
- (169) Morihara, K.; Tsuzuki, H.; Oka, T.; Inoue, H.; Ebata, M. Pseudomonas Aeruginosa Elastase: Isolation, Crystallization and Preliminary Characterization. **1965**, *240* (8), 3297–3304.
- (170) Heck, L. W.; Morihara, K.; McRae, W. B.; Miller, E. J. Specific Cleavage of Human Type III and IV Collagens by Pseudomonas Aeruginosa Elastase. *Infect. Immun.* **1986**, *51* (1), 115–118.
- (171) Preston, M. J.; Seed, P. C.; Toder, D. S.; Iglewski, B. H.; Ohman, D. E.; Gustin, J. K.; Goldberg, J. B.; Pier, G. B. Contribution of Proteases and LasR to the Virulence of Pseudomonas Aeruginosa during Corneal Infections. *Infect. Immun.* **1997**, *65* (8), 3086–3090.
- (172) Schmidtchen, A.; Holst, E.; Tapper, H.; Björck, L. Elastase-Producing Pseudomonas Aeruginosa Degrade Plasma Proteins and Extracellular Products of Human Skin and Fibroblasts, and Inhibit Fibroblast Growth. *Microb. Pathog.* **2003**, *34* (1), 47–55. [https://doi.org/10.1016/S0882-4010\(02\)00197-3](https://doi.org/10.1016/S0882-4010(02)00197-3).
- (173) Heck, L. W.; Alarcon, P. G.; Kulhavy, R. M.; Morihara, K.; Mestecky, M. W.; Russell, J. F. Degradation of IgA Proteins by Pseudomonas Aeruginosa Elastase. *J. Immunol.* **1990**, *144*, 2253–2257.
- (174) Holder, I. A.; Wheeler, R. Experimental Studies of the Pathogenesis of Infections Owing to Pseudomonas Aeruginosa: Elastase, an IgG Protease. *Can. J. Microbiol.* **1984**, *30* (9), 1118–1124.
- (175) Parmely, M.; Gale, A.; Clabaugh, M.; Horvat, R.; Zhou, W. Proteolytic Inactivation of Cytokines by Pseudomonas Aeruginosa. *Infect. Immun.* **1990**, *58* (9), 3009–3014.
- (176) Morihara, K.; Tsuzuki, H.; Oda, K. Protease and Elastase of Pseudomonas Aeruginosa: Inactivation of Human Plasma A1-Proteinase Inhibitor. *Infect. Immun.* **1979**, *24* (1), 188–193.
- (177) Johnson, D. A.; Carter-Hamm, B.; Dralle, W. M. Inactivation of Human Bronchial Mucosal Proteinase Inhibitor by Pseudomonas Aeruginosa Elastase. *Am. Rev. Respir. Dis.* **1982**, *126* (6), 1070–1073. <https://doi.org/10.1164/arrd.1982.126.6.1070>.
- (178) Oda, K.; Koyama, T.; Murao, S. Purification and Properties of a Proteinaceous Metallo-Proteinase Inhibitor from Streptomyces Nigrescens TK-23. *Biochim. Biophys. Acta* **1979**, *571*, 147–156.
- (179) Nishino, N.; Powers, J. C. Pseudomonas Aeruginosa Elastase - Development of a New Substrate, Inhibitors and an Affinity Ligand. *J. Biol. Chem.* **1979**, *255* (8), 3482–19.
- (180) Kessler, E.; Israel, M.; Landshman, N.; Chechick, A.; Blumberg, S. In Vitro Inhibition of Pseudomonas Aeruginosa Elastase by Metal-Chelating Peptide Derivatives. *Infect. Immun.* **1982**, *38* (2), 716–723.
- (181) Cathcart, G. R. A.; Quinn, D.; Greer, B.; Harriott, P.; Lynas, J. F.; Gilmore, B. F.; Walker, B. Novel Inhibitors of the Pseudomonas Aeruginosa Virulence Factor LasB: A Potential Therapeutic Approach for the Attenuation of Virulence Mechanisms in Pseudomonas Infection. *Antimicrob. Agents Chemother.* **2011**, *55* (6), 2670–2678. <https://doi.org/10.1128/AAC.00776-10>.
- (182) Burns, F. R.; Paterson, C. A.; Gray, R. D.; Wells, J. T. Inhibition of Pseudomonas Aeruginosa Elastase and Pseudomonas Keratitis Using a Thiol-Based Peptide. *Antimicrob. Agents Chemother.* **1990**, *34* (11), 2065–2069. <https://doi.org/10.1128/AAC.34.11.2065>.
- (183) Fullagar, J. L.; Garner, A. L.; Struss, A. K.; Day, J. A.; Martin, D. P.; Yu, J.; Cai, X.; Janda, K. D.; Cohen, S. M. Antagonism of a Zinc Metalloprotease Using a Unique Metal-Chelating Scaffold: Tropolones as Inhibitors of P. Aeruginosa Elastase. *Chem. Commun.* **2013**, *49* (31), 3197–3199. <https://doi.org/10.1039/c3cc41191e>.
- (184) J., Z.; X., C.; T.L., H.; M., G.; M., W.; M., L. Disarming Pseudomonas Aeruginosa

- Virulence Factor LasB by Leveraging a *Caenorhabditis Elegans* Infection Model. *Chem. Biol.* **2015**, 22, no pagination.
- (185) Kany, A. M.; Sikandar, A.; Hauptenthal, J.; Yahiaoui, S.; Maurer, C. K.; Proschak, E.; Ko, J.; Hartmann, R. W. Binding Mode Characterization and Early in Vivo Evaluation of Fragment-Like Thiols as Inhibitors of the Virulence Factor LasB from *Pseudomonas Aeruginosa*. *ACS Infect. Dis.* **2018**, 4, 988–997. <https://doi.org/10.1021/acsinfecdis.8b00010>.
- (186) Brengel, C.; Thomann, A.; Schiffrin, A.; Allegretta, G.; Kamal, A. A. M.; Hauptenthal, J.; Schnorr, I.; Cho, S. H.; Franzblau, S. G.; Empting, M.; et al. Biophysical Screening of a Focused Library for the Discovery of CYP121 Inhibitors as Novel Antimycobacterials. *ChemMedChem* **2017**, 12 (19), 1616–1626. <https://doi.org/10.1002/cmdc.201700363>.
- (187) Ahmad, Z.; Sharma, S.; Khuller, G. K.; Singh, P.; Faujdar, J.; Katoch, V. M. Antimycobacterial Activity of Econazole against Multidrug-Resistant Strains of *Mycobacterium Tuberculosis*. *Int. J. Antimicrob. Agents* **2006**, 28 (6), 543–544. <https://doi.org/10.1016/j.ijantimicag.2006.07.028>.
- (188) Ahmad, Z.; Sharma, S.; Khuller, G. K. Azole Antifungals as Novel Chemotherapeutic Agents against Murine Tuberculosis. *FEMS Microbiol. Lett.* **2006**, 261 (2), 181–186. <https://doi.org/10.1111/j.1574-6968.2006.00350.x>.
- (189) Ahmad, Z.; Sharma, S.; Khuller, G. K. The Potential of Azole Antifungals against Latent/Persistent Tuberculosis. *FEMS Microbiol. Lett.* **2006**, 258 (2), 200–203. <https://doi.org/10.1111/j.1574-6968.2006.00224.x>.
- (190) Belin, P.; Leqoc, A.; Beaufrepaire Ledu, M.-H.; Gondry, M.; Pernodet, J.-L. Patent EP2088143A1, 2009.
- (191) Chenge, J. T.; Van Duyet, L.; Swami, S.; McLean, K. J.; Kavanagh, M. E.; Coyne, A. G.; Rigby, S. E. J.; Cheesman, M. R.; Girvan, H. M.; Levy, C. W.; et al. Structural Characterization and Ligand/Inhibitor Identification Provide Functional Insights into the *Mycobacterium Tuberculosis* Cytochrome P450 CYP126A1. *J. Biol. Chem.* **2017**, 292 (4), 1310–1329. <https://doi.org/10.1074/jbc.M116.748822>.
- (192) Burlingham, B. T.; Widlanski, T. S. An Intuitive Look at the Relationship of  $K_i$  and  $IC_{50}$ : A More General Use for the Dixon Plot. *J. Chem. Educ.* **2003**, 80 (2), 214–218. <https://doi.org/10.1021/ed080p214>.
- (193) Copeland, R. A. *Evaluation of Enzyme Inhibitors in Drug Discovery: A Guide for Medicinal Chemists and Pharmacologists*, 2nd ed.; Wiley, John, 2013.
- (194) Kurokohchi, K.; Nishioka, M.; Ichikawa, Y. Inhibition Mechanism of Reconstituted Cytochrome P-450<sub>scc</sub>-Linked Monooxygenase System by Antimycotic Reagents and Other Inhibitors. *J. Steroid Biochem. Mol. Biol.* **1992**, 42 (3), 287–292.
- (195) Raab, W.; Högl, F. Zur Enzymaktivitätshemmenden Wirkung Der Antimyzetisch Wirksamen Imidazol-Derivate. *Mycoses* **1981**, 24, 525–533. <https://doi.org/10.1111/j.1439-0507.1981.tb01903.x>.
- (196) Armstrong, J. A.; Hart, P. D. A. Phagosome-Lysosome Interactions in Cultured Macrophages Infected with Virulent Tubercle Bacilli - Reversal of the Usual Nonfusion Pattern and Observations on Bacterial Survival. *J. Exp. Med.* **1975**, 142, 1–16.
- (197) Brengel, C.; Thomann, A.; Schiffrin, A.; Eberhard, J.; Hartmann, R. W. Discovery and Biophysical Evaluation of First Low Nanomolar Hits Targeting CYP125 of *M. Tuberculosis*. *ChemMedChem* **2016**, 11 (21), 2385–2391. <https://doi.org/10.1002/cmdc.201600361>.
- (198) Chang, J. C.; Harik, N. S.; Liao, R. P.; Sherman, D. R. Identification of *Mycobacterial* Genes That Alter Growth and Pathology in Macrophages and in Mice. *J. Infect. Dis.* **2007**, 196 (5), 788–795. <https://doi.org/10.1086/520089>.

- (199) Capyk, J. K.; Kalscheuer, R.; Stewart, G. R.; Liu, J.; Kwon, H.; Zhao, R.; Okamoto, S.; Jacobs, W. R.; Eltis, L. D.; Mohn, W. W. Mycobacterial Cytochrome P450 125 (Cyp125) Catalyzes the Terminal Hydroxylation of C27 Steroids. *J. Biol. Chem.* **2009**, *284* (51), 35534–35542. <https://doi.org/10.1074/jbc.M109.072132>.
- (200) Hong, X.; Hopfinger, A. J. Molecular Modeling and Simulation of Mycobacterium Tuberculosis Cell Wall Permeability. *Biomacromolecules* **2004**, *5* (3), 1066–1077. [https://doi.org/Doi 10.1021/Bm0345155](https://doi.org/Doi%2010.1021/Bm0345155).
- (201) Hong, X.; Hopfinger, A. J. Construction, Molecular Modeling, and Simulation of Mycobacterium Tuberculosis Cell Walls. *Biomacromolecules* **2004**, *5*, 1052–1065. [https://doi.org/Doi 10.1021/Bm034514c](https://doi.org/Doi%2010.1021/Bm034514c).
- (202) Milano, A.; Pasca, M. R.; Provvedi, R.; Lucarelli, A. P.; Manina, G.; Luisa de Jesus Lopes Ribeiro, A.; Manganelli, R.; Riccardi, G. Azole Resistance in Mycobacterium Tuberculosis Is Mediated by the MmpS5-MmpL5 Efflux System. *Tuberculosis* **2009**, *89* (1), 84–90. <https://doi.org/10.1016/j.tube.2008.08.003>.
- (203) Mclean, K. J.; Cheesman, M. R.; Rivers, S. L.; Richmond, A.; Leys, D.; Chapman, S. K.; Reid, G. A.; Price, N. C.; Kelly, S. M.; Clarkson, J.; et al. Expression, Purification and Spectroscopic Characterization of the Cytochrome P450 CYP121 from Mycobacterium Tuberculosis. *J. Inorg. Biochem.* **2002**, *91*, 527–541.
- (204) Franzblau, S. G.; Degroote, M. A.; Cho, S. H.; Andries, K.; Nuermberger, E.; Orme, I. M.; Mdluli, K.; Angulo-Barturen, I. I.; Dick, T.; Dartois, V.; et al. Comprehensive Analysis of Methods Used for the Evaluation of Compounds against Mycobacterium Tuberculosis. *Tuberculosis* **2012**, *92* (6), 453–488. <https://doi.org/10.1016/j.tube.2012.07.003>.
- (205) Cochrane, J. R.; White, J. M.; Wille, U.; Hutton, C. A. Total Synthesis of Mycrocyclosin. *Org. Lett.* **2012**, *14* (9), 2402–2405. <https://doi.org/10.1002/anie.201305822>.
- (206) Strateva, T.; Yordanov, D. Pseudomonas Aeruginosa - A Phenomenon of Bacterial Resistance. *J. Med. Microbiol.* **2009**, *58* (9), 1133–1148. <https://doi.org/10.1099/jmm.0.009142-0>.
- (207) Li, X. Z.; Livermore, D. M.; Nikaido, H. Role of Efflux Pump(s) in Intrinsic Resistance of Pseudomonas Aeruginosa: Resistance to Tetracycline, Chloramphenicol, and Norfloxacin. *Antimicrob. Agents Chemother.* **1994**, *38* (8), 1732–1741. <https://doi.org/10.1128/AAC.38.8.1732>.
- (208) Gasink, L. B.; Fishman, N. O.; Weiner, M. G.; Nachamkin, I.; Bilker, W. B.; Lautenbach, E. Fluoroquinolone-Resistant Pseudomonas Aeruginosa: Assessment of Risk Factors and Clinical Impact. *Am. J. Med.* **2006**, *119* (6), 19–25. <https://doi.org/10.1016/j.amjmed.2005.11.029>.
- (209) Poole, K. Aminoglycoside Resistance in Pseudomonas Aeruginosa. *Antimicrob. Agents Chemother.* **2005**, *49* (2), 479–487. <https://doi.org/10.1128/AAC.49.2.479>.
- (210) ASCP Susceptibility Testing Group. United States Geographic Bacteria Susceptibility Patterns. *Am. J. Clin. Pathol.* **1996**, *106* (3), 275–281. <https://doi.org/10.1093/ajcp/106.3.275>.
- (211) Mariencheck, W. I.; Alcorn, J. F.; Palmer, S. M.; Wright, J. R. Pseudomonas Aeruginosa Elastase Degrades Surfactant Proteins A and D. *Am. J. Respir. Cell Mol. Biol.* **2003**, *28* (4), 528–537. <https://doi.org/10.1165/rcmb.2002-0141OC>.
- (212) Zhu, J.; Cai, X.; Harris, T. L.; Gooyit, M.; Wood, M.; Lardy, M.; Janda, K. D. Disarming Pseudomonas Aeruginosa Virulence Factor LasB by Leveraging a Caenorhabditis Elegans Infection Model. *Chem. Biol.* **2015**, *22* (4), 483–491. <https://doi.org/10.1016/j.chembiol.2015.03.012>.
- (213) Koppenhoefer, B.; Schurig, V. (S)-2-Chloroalkanoic Acids of High Enantiomeric Purity From (S)-2-Amino Acids: (S)-2-Chloropropanoic Acid. *Org. Synth.* **1988**, *66*

- (September), 151. <https://doi.org/10.15227/orgsyn.066.0151>.
- (214) Schönauer, E.; Kany, A. M.; Haupenthal, J.; Hüsecken, K.; Hoppe, I. J.; Voos, K.; Yahiaoui, S.; Elsässer, B.; Ducho, C.; Brandstetter, H.; et al. Discovery of a Potent Inhibitor Class with High Selectivity toward Clostridial Collagenases. *J. Am. Chem. Soc.* **2017**, *139* (36), 12696–12703. <https://doi.org/10.1021/jacs.7b06935>.
- (215) Kany, A. M.; Sikandar, A.; Yahiaoui, S.; Haupenthal, J.; Walter, I.; Empting, M.; Köhnke, J.; Hartmann, R. W. Tackling Pseudomonas Aeruginosa Virulence by a Hydroxamic Acid-Based LasB Inhibitor. *ACS Chem. Biol.* **2018**, *13* (9), 2449–2455. <https://doi.org/10.1021/acscchembio.8b00257>.
- (216) Haupenthal, J.; Baehr, C.; Zeuzem, S.; Piiper, A. RNase A-like Enzymes in Serum Inhibit the Anti-Neoplastic Activity of SiRNA Targeting Polo-like Kinase 1. *Int. J. Cancer* **2007**, *121*, 206–210. <https://doi.org/10.1002/ijc.22665>.
- (217) Winter, G. Xia2: An Expert System for Macromolecular Crystallography Data Reduction. *J. Appl. Crystallogr.* **2010**, *43* (1), 186–190. <https://doi.org/10.1107/S0021889809045701>.
- (218) Kabsch, W. XDS. *Acta Crystallogr. Sect. D Biol. Crystallogr.* **2010**, *66*, 125–132. <https://doi.org/10.1107/S0907444909047337>.
- (219) McCoy, A. J.; Grosse-Kunstleve, R. W.; Adams, P. D.; Winn, M. D.; Storoni, L. C.; Read, R. J. Phaser Crystallographic Software. *J. Appl. Crystallogr.* **2007**, *40*, 658–674. <https://doi.org/10.1107/S0021889807021206>.
- (220) Emsley, P.; Lohkamp, B.; Scott, W. G.; Cowtan, K. Features and Development of Coot. *Acta Crystallogr. D. Biol. Crystallogr.* **2010**, *66* (Pt 4), 486–501. <https://doi.org/10.1107/S0907444910007493>.
- (221) Adams, P. D.; Afonine, P. V.; Bunkóczi, G.; Chen, V. B.; Davis, I. W.; Echols, N.; Headd, J. J.; Hung, L.-W.; Kapral, G. J.; Grosse-Kunstleve, R. W.; et al. PHENIX: A Comprehensive Python-Based System for Macromolecular Structure Solution. *Acta Crystallogr. D. Biol. Crystallogr.* **2010**, *66* (Pt 2), 213–221. <https://doi.org/10.1107/S0907444909052925>.
- (222) Skubák, P.; Murshudov, G. N.; Pannu, N. S. Direct Incorporation of Experimental Phase Information in Model Refinement. *Acta Crystallogr. Sect. D* **2004**, *60* (12 Part 1), 2196–2201. <https://doi.org/10.1107/S0907444904019079>.
- (223) Fukushima, K.; Yazawa, K.; Arai, T. Biological Activities of Albonoursin. *J. Antibiot. (Tokyo)*. **1972**, *26* (3), 175–176.
- (224) Uffen, R. L.; Canale-Parola, E. Synthesis of Pulcherriminic Acid by Bacillus Subtilis. *J. Bacteriol.* **1972**, *111* (1), 86–93.
- (225) Zhang, Q.; Li, S.; Chen, Y.; Tian, X.; Zhang, H.; Zhang, G.; Zhu, Y.; Zhang, S.; Zhang, W.; Zhang, C. New Diketopiperazine Derivatives from a Deep-Sea-Derived Nocardiosis Alba SCSIO 03039. *J. Antibiot. (Tokyo)*. **2012**, *66* (1), 31–36.
- (226) Strieker, M.; Tanović, A.; Marahiel, M. A. Nonribosomal Peptide Synthetases: Structures and Dynamics. *Curr. Opin. Struct. Biol.* **2010**, *20* (2), 234–240. <https://doi.org/10.1016/j.sbi.2010.01.009>.
- (227) King, R. R.; Calhoun, L. A. The Thaxtomin Phytotoxins: Sources, Synthesis, Biosynthesis, Biotransformation and Biological Activity. *Phytochemistry* **2009**, *70* (7), 833–841. <https://doi.org/10.1016/j.phytochem.2009.04.013>.
- (228) Jin, X.; Rao, M.; Wei, W.; Ge, M.; Liu, J.; Chen, D.; Liang, Y. Biosynthesis of New Lipopentapeptides by an Engineered Strain of Streptomyces Sp. *Biotechnol. Lett.* **2012**, *34* (12), 2283–2289. <https://doi.org/10.1007/s10529-012-1032-2>.
- (229) Rudolf, J. D.; Chang, C. Y.; Ma, M.; Shen, B. Cytochromes P450 for Natural Product Biosynthesis in Streptomyces: Sequence, Structure, and Function. *Nat. Prod. Rep.* **2017**, *34* (9), 1141–1172. <https://doi.org/10.1039/c7np00034k>.
- (230) Liu, W. T.; Kersten, R. D.; Yang, Y. L.; Moore, B. S.; Dorrestein, P. C. Imaging Mass

- Spectrometry and Genome Mining via Short Sequence Tagging Identified the Anti-Infective Agent Arylomycin in *Streptomyces Roseosporus*. *J. Am. Chem. Soc.* **2011**, *133* (45), 18010–18013. <https://doi.org/10.1021/ja2040877>.
- (231) Chen, C. I. U.; Schaller-Bals, S.; Paul, K. P.; Wahn, U.; Bals, R.  $\beta$ -Defensins and LL-37 in Bronchoalveolar Lavage Fluid of Patients with Cystic Fibrosis. *J. Cyst. Fibros.* **2004**, *3* (1), 45–50. <https://doi.org/10.1016/j.jcf.2003.12.008>.
- (232) Schmidtchen, A.; Frick, I. M.; Andersson, E.; Tapper, H.; Björck, L. Proteinases of Common Pathogenic Bacteria Degrade and Inactivate the Antibacterial Peptide LL-37. *Mol. Microbiol.* **2002**, *46* (1), 157–168. <https://doi.org/10.1046/j.1365-2958.2002.03146.x>.
- (233) Schenkman, J. B.; Remmer, H.; Estabrook, R. W. Spectral Studies of Drug Interaction with Hepatic Microsomal Cytochrome. *Mol. Pharmacol.* **1967**, *3* (2), 113–123.
- (234) Gatfield, J.; Pieters, J. Essential Role for Cholesterol in Entry of Mycobacteria into Macrophages. *Science* (80-. ). **2000**, *288* (5471), 1647–1651. <https://doi.org/10.1126/science.277.5334.2007>.
- (235) Sbardella, D.; Fasciglione, G. F.; Gioia, M.; Ciaccio, C.; Tundo, G. R.; Marini, S.; Coletta, M. Human Matrix Metalloproteinases: An Ubiquitarian Class of Enzymes Involved in Several Pathological Processes. *Mol. Aspects Med.* **2012**, *33* (2), 119–208. <https://doi.org/10.1016/j.mam.2011.10.015>.
- (236) Dufour, A.; Overall, C. M. Missing the Target: Matrix Metalloproteinase Antitargets in Inflammation and Cancer. *Trends Pharmacol. Sci.* **2013**, *34* (4), 233–242. <https://doi.org/10.1016/j.tips.2013.02.004>.
- (237) Vandenbroucke, R. E.; Libert, C. Is There New Hope for Therapeutic Matrix Metalloproteinase Inhibition? *Nat. Rev. Drug Discov.* **2014**, *13* (12), 904–927. <https://doi.org/10.1038/nrd4390>.
- (238) Turk, B. Targeting Proteases: Successes, Failures and Future Prospects. *Nat. Rev. Drug Discov.* **2006**, *5* (9), 785–799. <https://doi.org/10.1038/nrd2092>.
- (239) Ilies, M.; Banciu, M. D.; Scozzafava, A.; Ilies, M. A.; Caproiu, M. T.; Supuran, C. T. Protease Inhibitors: Synthesis of Bacterial Collagenase and Matrix Metalloproteinase Inhibitors Incorporating Arylsulfonylureido and 5-Dibenzo-Suberenyl/Suberyl Moieties. *Bioorganic Med. Chem.* **2003**, *11* (10), 2227–2239. [https://doi.org/10.1016/S0968-0896\(03\)00113-5](https://doi.org/10.1016/S0968-0896(03)00113-5).
- (240) Sjøli, S.; Nuti, E.; Camodeca, C.; Bilotto, I.; Rossello, A.; Winberg, J. O.; Sylte, I.; Adekoya, O. A. Synthesis, Experimental Evaluation and Molecular Modelling of Hydroxamate Derivatives as Zinc Metalloproteinase Inhibitors. *Eur. J. Med. Chem.* **2016**, *108*, 141–153. <https://doi.org/10.1016/j.ejmech.2015.11.019>.
- (241) Park, H. I.; Jin, Y.; Hurst, D. R.; Monroe, C. A.; Lee, S.; Schwartz, M. A.; Sang, Q. X. A. The Intermediate S1' Pocket of the Endometase/ Matrilysin-2 Active Site Revealed by Enzyme Inhibition Kinetic Studies, Protein Sequence Analyses, and Homology Modeling. *J. Biol. Chem.* **2003**, *278* (51), 51646–51653. <https://doi.org/10.1074/jbc.M310109200>.

## 6 Acknowledgement

Ich möchte mich ganz herzlich bei allen bedanken, die zum Gelingen dieser Arbeit beigetragen haben:

Ein ganz besonderer Dank gilt Prof. Dr. Rolf W. Hartmann für die Möglichkeit der Promotion in den beiden vielseitigen und spannenden Projekten, für die sehr gute Betreuung und die konstruktive Unterstützung sowie die Freiheiten bei der Umsetzung der jeweiligen Ideen.

Prof. Dr. Christian Ducho danke ich für die wissenschaftliche Begleitung und die Übernahme des Zweitgutachtens.

Ein herzlicher Dank geht an Dr. Andreas Thomann und Dr. Christian Brengel für die anfängliche Betreuung des CYP-Projektes und auch die anschließende andauernde Bereitschaft zur Beantwortung aufkommender Fragen.

Weiterer großer Dank gebührt Dr. Andreas Kany für die Einführung in das LasB Projekt und die Unterstützung bei der Ideen-Entwicklung. Ebenfalls danke ich Dr. Jörg Hauptenthal und Dr. Samir Yahiaoui für die Leitung des Projekts und ihre konstruktiven Beiträge.

Des Weiteren gilt mein besonderer Dank den Kooperationspartnern für ihre wesentlichen Beiträge zum Gelingen der jeweiligen Projekte dieser Arbeit:

Ich bedanke mich bei Dr. Jesko Köhnke, Sebastian Adam und Asfandyar Sikandar von HIPS-SBBE für die unkomplizierte und konstruktive Zusammenarbeit. Des Weiteren bei Prof. Dr. Tim Sparwasser und Dr. Maria Virginia Gentilini vom TWINCORE Hannover sowie bei Prof. Dr. Scott Franzblau und Dr. Sang Hyun Cho von der University of Illinois in Chicago. Ebenso möchte ich mich bei Prof. Dr. Christian Ducho und Katrin Voos von der Universität des Saarlandes bedanken.

Ein großer Dank geht an alle ehemaligen und aktuellen Mitglieder der Arbeitskreise Hartmann, Hirsch und Titz für die freundliche Aufnahme in die Gruppe, die gute Zusammenarbeit, für alle hilfreichen Ratschläge und Antworten bezüglich Doktorandenzeit und Promotion sowie die angenehme und abwechslungsreiche gemeinsame Zeit.

Ein besonders herzliches Dankeschön geht hierbei an meine Bürokollegen Philine Kirsch (mit Molly), Andreas Kany und Alwin Hartman für die angenehme, abwechslungsreiche und lustige Zeit. Dasselbe gilt für die stetigen Büro-Besucher Christian Schütz und Valentin Jakob. Vielen

Dank auch an meinen ehemaligen Bürokollegen Dr. Benni Kirsch für die sehr unterhaltsame Zeit.

Ebenso bedanke ich mich bei Dr. Christine Maurer und Dr. Giuseppe Allegretta für Ihre Unterstützung bei analytischen Fragestellungen. Des Weiteren bei Dr. Martin Empting für seine Hilfe bei Computer-basierten Methoden und bei Dr. Mostafa Hamed und Dr. Ahmed Kamal für ihre Hilfe bei chemischen Fragestellungen. Zudem danke ich meinen Nachfolgerinnen im LasB-Projekt Cansu Kaya und Jelena Konstantinovic für die gute Zusammenarbeit.

Vielen Dank an unser tolles TA-Team bestehend aus Simone Amann, Jeannine Jung, Tabea Schramm und Dennis Jenner für die unermüdliche Hilfsbereitschaft und Unterstützung sowie die immer freundliche Gesellschaft im Biolabor. Ebenfalls bedanken möchte ich mich bei Julia Mohr und May Sena Küffner für ihre Hilfe in administrativen Angelegenheiten sowie dem IT-Team und dem Facility Management für ihre Hilfsbereitschaft.

Zu guter Letzt möchte ich mich ganz herzlich bei meiner Familie und meinen Freunden für die nötige Ablenkung von der Arbeit und den unfassbar wertvollen Ausgleich zur Arbeit bedanken. Ein ganz besonderer Dank gilt hierbei meinem Mann Christian für seine immerwährende und unersetzbare Unterstützung. Vielen Dank!

## 7 Appendix

### 7.1 Supporting Information

#### 7.1.1 Supporting Information for Chapter 3.1



### Supporting Information

#### **Biophysical Screening of a Focused Library for the Discovery of CYP121 Inhibitors as Novel Antimycobacterials**

Christian Brengel<sup>+, [a]</sup>, Andreas Thomann<sup>+, [a]</sup>, Alexander Schifrin,<sup>[b]</sup> Giuseppe Allegretta,<sup>[a]</sup>  
Ahmed A. M. Kamal,<sup>[a]</sup> Jörg Hauptenthal,<sup>[a]</sup> Isabell Schnorr,<sup>[a]</sup> Sang Hyun Cho,<sup>[c]</sup>  
Scott G. Franzblau,<sup>[c]</sup> Martin Empting,<sup>[a]</sup> Jens Eberhard,<sup>[a]</sup> and Rolf W. Hartmann<sup>\*, [a, d]</sup>

cmdc\_201700363\_sm\_miscellaneous\_information.pdf

# Content

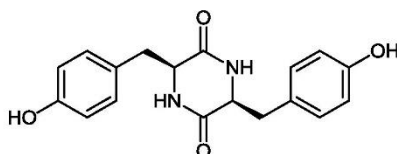
1. Chemical synthesis cYY and Mycocyclosin: .....	2
1.1 Synthesis of cyclo-di-L-tyrosine (cYY) .....	2
1.2 Synthesis of mycocyclosine .....	2
2. SDS-PAGE of His-tagged CYP121 .....	3
3. Activity of CYP121/ CO Spectra .....	4
4. LC-MS analysis of <i>in vitro</i> CYP121 enzyme reaction and effect of I:47 .....	5
5. Surface Plasmon Resonance Sensogram of econazole and I:16 .....	7
6. Screening overview .....	8
7. $K_D$ determination by UV-VIS Heme coordination assay .....	12
8. Protein Blast of Mtb H <sub>37</sub> R <sub>V</sub> CYP121 (Rv2276) and M. bovis BCG Pasteur CYP121 (BCG_2293) .....	13
9. MIC <sub>BCGT</sub> determination against <i>Mycobacterium bovis</i> .....	14
10. Calculation of antimicrobial efficiency .....	16
11. Toxicity assessment against human cancer cell lines HEK293 and HepG2 .....	17
12. MIC against <i>Escherichia coli</i> and <i>Staphylococcus aureus</i> in comparison to growth inhibition against <i>Mycobacterium bovis</i> BCG.....	18
13. Physicochemical data: .....	19
14. References .....	27

## 1. Chemical synthesis cYY and Mycocyclosin:

### 1.1 Synthesis of cyclo-di-L-tyrosine (cYY)

#### cyclo-di-L-tyrosine (cYY):

cYY was synthesized as previously described.<sup>1</sup>



cYY was synthesized as previously described.<sup>[1]</sup> Spectral data is in accordance with the previously published results:<sup>[1]</sup>

<sup>1</sup>H NMR (300 MHz, DMSO-*d*<sub>6</sub>) δ 9.19 (s, 1H), 7.75 (d, *J* = 2.6 Hz, 1H), 7.05 – 6.78 (m, 2H), 6.78 – 6.55 (m, 2H), 3.85 (s, 1H), 2.54 (dd, *J* = 4.6 Hz, 1H), 2.11 (dd, *J* = 13.7, 6.5 Hz, 1H); <sup>13</sup>C NMR (75 MHz, DMSO) δ 166.7, 156.5, 131.2, 127.0, 115.5, 56.2, 39.3; ESI-MS(+) = *m/z* 327.1 [M+H]<sup>+</sup>.

### 1.2 Synthesis of mycocyclosine

#### Mycocyclosine:



Mycocyclosine was synthesized as previously described.<sup>[1,2]</sup> Spectral data is in accordance with the previously published results:<sup>[1]</sup>

<sup>1</sup>H NMR (300 MHz, DMSO-*d*<sub>6</sub>) δ 7.98 (s, 1H), 6.84 (dd, *J* = 2.51, 7.9 Hz, 1H), 6.62 (d, *J* = 8.1 Hz, 1H), 6.58 (d, *J* = 2.4 Hz, 1H), 4.32 (d, *J* = 4.8 Hz, 1H), 3.46 (d, *J* = 15.7 Hz, 1H), 2.64 (dd, *J* = 5.73, 15.6 Hz, 1H).

## 2. SDS-PAGE of His-tagged CYP121

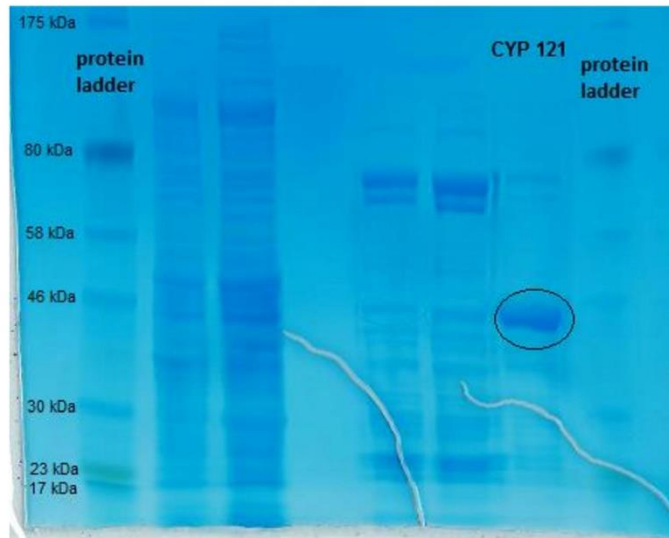


**Figure S1.** SDS-PAGE of Ni-NTA purified heterologous expressed CYP121. The band corresponds to a molecular mass of > 46000 Da which is in good accordance with the calculated protein mass of 43256 Da.

### 3. Activity of CYP121/ CO Spectra

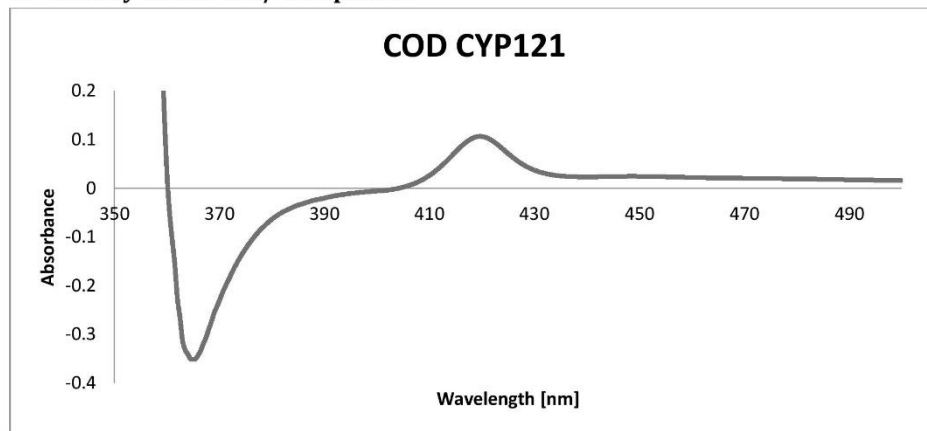


**Figure S2.** UV-VIS carbonmonoxide difference spectra (COD) of CYP121 after treatment with sodium sulfide and carbonmonoxide. The characteristic band at ~420 nm shows CO coordination to the reduced iron-heme.

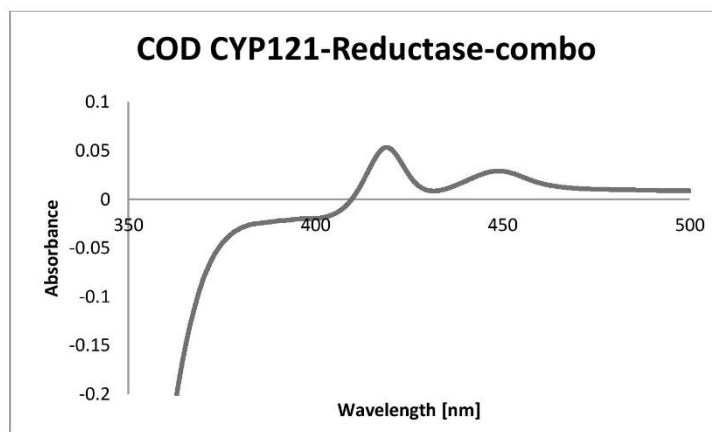


**Figure S3.** UV-VIS carbonmonoxide difference spectra (COD) of CYP121 after incubation with reductase Arh1\_A18G and ferredoxin Etp1fd (516-618) followed by carbonmonoxide treatment. The characteristic band at ~420 nm shows CO coordination to the reduced iron-heme

#### 4. LC-MS analysis of *in vitro* CYP121 enzyme reaction and effect of I:47

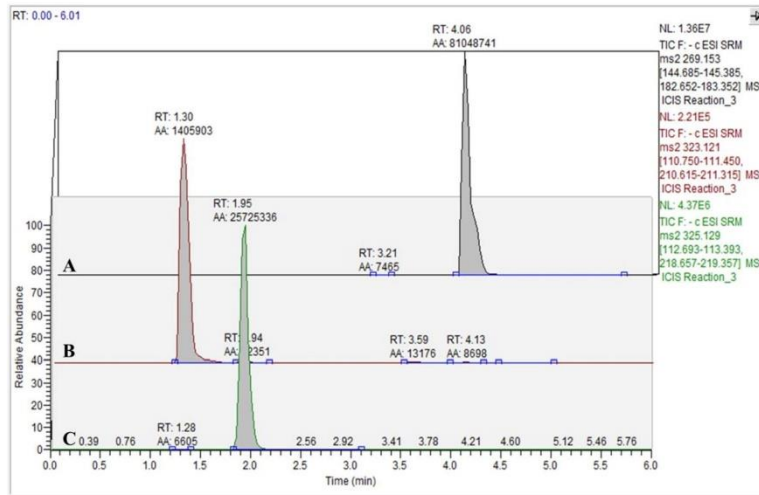


**Figure S4.** LC-MS/MS quantification of CYP121 enzyme reaction: internal standard estrone  $t_R = 4.05$  min (A); mycocyclosin  $t_R = 1.30$  min (B); cYY  $t_R = 1.95$  min (C).

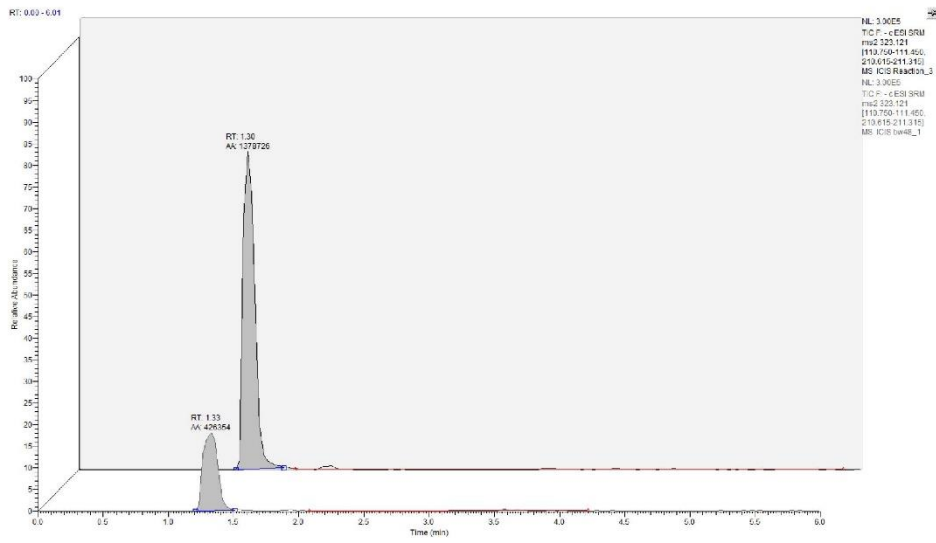


**Figure S5.** LC-MS/MS based quantification of CYP121 *in vitro* enzyme reaction product mycocyclusin with addition of I:47 (100  $\mu$ M, lower chromatogram) and without the presence of the inhibitor (upper chromatogram).

## 5. Surface Plasmon Resonance Sensogram of econazole and I:16

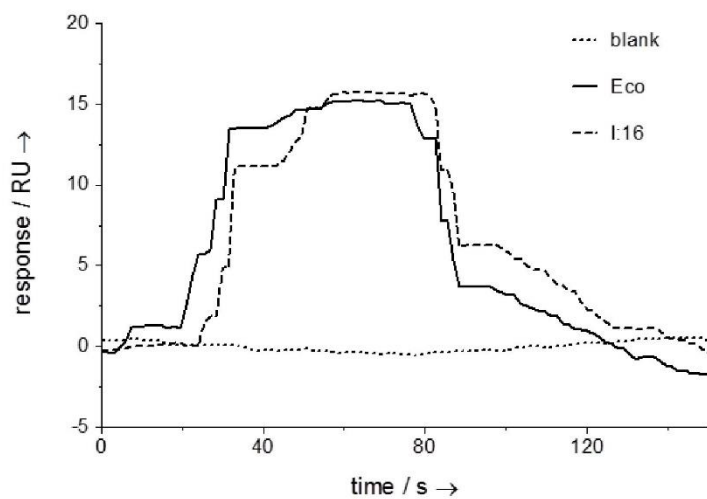


**Figure S6.** Representative example for SPR binding curve of econazole (Eco, bold line) and I:16 (dashed line) to CYP121 injected from 100  $\mu$ M sample in comparison to blank (dotted line).

## 6. Screening overview

**Table S1.** Overview of the results of SPR screening, Heme binding assay, BCG and Mtb growth inhibition and MIC determination

Cmpd	SPR [R/Rpos]	Heme coord. <sup>a</sup>	Heme- K <sub>D</sub> [μM]	BCGT Inhibition @ 100 μM [%]	MIC <sub>BCGT</sub> [μM]	MIC <sub>Mtb</sub> [μM]
I:1	0.4	N		10		
I:2	0					
I:3	0.1					
I:4	0.2					
I:5	0.1					
I:6	0.1					
I:7	0.5					
I:8	0.5					
I:9	0					
I:10	0					
I:11	0.6	N				
I:12	0.4					
I:13	0					
I:14	0.2					
I:15	0.3	Y (T-II)	34	87	41	
I:16	1.2	Y (T-II)	1	78	5	6
I:17	1.9	Y (T-II)	3	65	38	
I:18	0.1					
I:19	0					
I:20	0.4					
I:21	0.1					
I:22	0.1					
I:23	0.1					
I:24	0.3					
I:25	0.5					
I:26	0.1					
I:27	1.0	Y (T-II)	weak			
I:28	0.3					
I:29	0.4					
I:30	1.4	Y (T-II)	11	94	11	48
I:31	1.5	N				
I:32	1.1	Y (T-II)	14	85	30	41
I:33	0.1	N		0		
I:34	0.7	Y (T-II)	29	25		
I:35	0.5					
I:36	0.1					

S8

I:37	0.2					
I:38	0.2					
I:39	0.1					
I:40	0.3					
I:41	0.1					
I:42	0.1					
I:43	0.2					
I:44	0.2					
I:45	0.5					
I:46	0.1					
I:47	0.6	Y (T-II)	5	87	1	1
I:48	0.8	Y (T-II)	5	88	7	12
<hr/>						
II:1	0.3					
II:2	0.3					
II:3	0.5					
II:4	0.2					
II:5	0.2					
II:6	0.1					
II:7	0.0					
II:8	0.3					
II:9	0.2					
II:10	0.1					
II:11	0.3					
II:12	0.2					
II:13	0.1					
II:14	0.5	N				
II:15	0.1					
II:16	0.2					
II:17	0.2					
II:18	0.2					
II:19	0.2					
II:20	1.3	Y (T-II)	9	48		
II:21	0.7	Y (T-II)	31			
II:22	0.2					
II:23	0.6	N				
II:24	0.1					
II:25	0.2					
II:26	0.8	Y (T-II)	16			
II:27	0.9	Y (T-II)	20			
II:28	0.9	Y (T-II)	19			
II:29	0.7	Y (T-II)	62			
II:30	0.8	Y (T-II)	weak			
II:31	0.6	Y (T-II)	weak			
II:32	0.7	Y (T-II)	weak			

II:33	0.3			
II:34	0.7	Y (T-II)	12	0
II:35	1.0	Y (T-II)	weak	
II:36	0.9	Y (T-II)	16	
II:37	1.4	Y (T-II)	50	
II:38	1.2	Y (T-II)	weak	
II:39	1.4	N		
II:40	0.7	Y (T-II)	27	
II:41	0.9	Y (T-II)	13	7
II:42	0.2			
III:1	0.3			
III:2	0.4			
III:3	1.7	Y (T-II)	weak	20
III:4	1.7	N		20
III:5	0.5			
III:6	0.3			
III:7	1.8	N		18
III:8	1.4	Y (T-II)	weak	5
III:9	0.6	Y (T-II)	weak	
III:10	0.4			
III:11	0.3			
III:12	0.2			
III:13	0.1			
III:14	0.3			
III:15	0.4			
III:16	0.2			
III:17	0.2			
III:18	0.4			
III:19	0.4			
III:20	0.2			
III:21	0.3			
IV:1	0.2			
IV:2	0.1			
IV:3	0.1			
IV:4	0.3			
IV:5	0.1	N		
IV:6	0.5			
IV:7	0.6	N		
IV:8	0.5			
IV:9	0.4			
IV:10	0.5			60
IV:11	0.9	Y (T-II)	weak	
IV:12	0.9	N		
IV:13	0.8	Y (T-II)	62	

S10

<b>V:1</b>	0.0					
<b>V:2</b>	0.3					
<b>V:3</b>	0.2					
<b>V:4</b>	0.1					
<b>V:5</b>	0.2					
<b>V:6</b>	0.1					
<b>V:7</b>	0.3					
<b>V:8</b>	0.8	N				
<b>V:9</b>	0.8	N				
<b>VI:1</b>	0.6	N		50		
<b>VI:2</b>	1.2	N				
<b>VI:3</b>	1.5	N				
<b>VI:4</b>	1.3	N				
<b>VI:5</b>	0.4					
<b>VI:6</b>	1.3	N				
<b>Eco<sup>b</sup></b>	1.0	Y (T-II)	3	71	14	11 <sup>3</sup>
<b>cYY<sup>c</sup></b>		Y (T-I)	12			

<sup>a</sup>n= no, y= yes, T-I = type I binding profile, T-II = type II binding profile, <sup>b</sup> Eco = econazole, cYY = cyclo-di-L-tyrosine

## 7. $K_D$ determination by UV-VIS Heme coordination assay

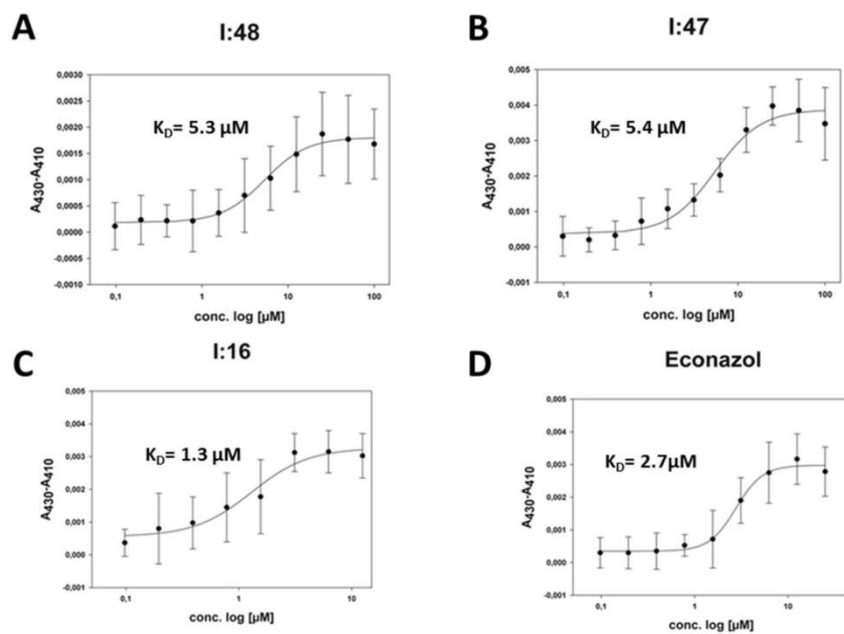


**Figure S7.** Determination of  $K_D$ 's by titration of I:48 (A), I:47 (B), I:16 (C) and econazole (D) and monitoring the difference between the absorption at 430 nm minus absorption at 410 nm in the presence of CYP121. Graphs were plotted with SigmaPlot using Marquardt-Levenberg algorithm.

## 8. Protein Blast of Mtb H<sub>37</sub>R<sub>v</sub> CYP121 (Rv2276) and M. bovis BCG Pasteur CYP121 (BCG\_2293)

Range 1: 1 to 396 [Graphics](#) ▼ Next Match ▲ Previous Match

Score	Expect	Method	Identities	Positives	Gaps
800 bits(2066)	0.0	Compositional matrix adjust.	396/396(100%)	396/396(100%)	0/396(0%)
Query 1	MTATVLLLEVPF SARGDRIPDAVAELRTREPIRKVRTITGAEAWLVSSYALCTQVLEDRRF				60
Sbjct 1	MTATVLLLEVPF SARGDRIPDAVAELRTREPIRKVRTITGAEAWLVSSYALCTQVLEDRRF				60
Query 61	SMKETAAGAPRLNALTVPPEVWNMGNIADAGLRKAVMKAITPKAPGLEQFLRDTANSL				120
Sbjct 61	SMKETAAGAPRLNALTVPPEVWNMGNIADAGLRKAVMKAITPKAPGLEQFLRDTANSL				120
Query 121	LDNLITGAPADLRNDFADPLATALHCKVLGIPQEDGPKLFRSLSI AFMSADPIPAKI				180
Sbjct 121	LDNLITGAPADLRNDFADPLATALHCKVLGIPQEDGPKLFRSLSI AFMSADPIPAKI				180
Query 181	NMDRDIEYMAGILENPNITTTGLMGELSR LRKDPAYSHVSD E L F A T I G V T F F G A G V I S T G S				240
Sbjct 181	NMDRDIEYMAGILENPNITTTGLMGELSR LRKDPAYSHVSD E L F A T I G V T F F G A G V I S T G S				240
Query 241	FLTTALISLIQRPQLRNLLHEKPELIPAGVEELLRINLSFADGLPRLATADIQVGDVLR				300
Sbjct 241	FLTTALISLIQRPQLRNLLHEKPELIPAGVEELLRINLSFADGLPRLATADIQVGDVLR				300
Query 301	KGELVLVLLLEGANFDPEHFPNPGSIELDRPNPTSHLAFGRGQHF CPGSALGRRHAQIGIE				360
Sbjct 301	KGELVLVLLLEGANFDPEHFPNPGSIELDRPNPTSHLAFGRGQHF CPGSALGRRHAQIGIE				360
Query 361	ALLKKMPGVDLAVPIDQLWVTRFQRRIPE RLPVLW		396		
Sbjct 361	ALLKKMPGVDLAVPIDQLWVTRFQRRIPE RLPVLW		396		

**Figure S8.** Results of the Protein Blast of Mtb CYP121 (upper sequence) and BCGT CYP121 (lower sequence) showing 100% amino acid identity between both proteins.

## 9. MIC<sub>BCGT</sub> determination against *Mycobacterium bovis*

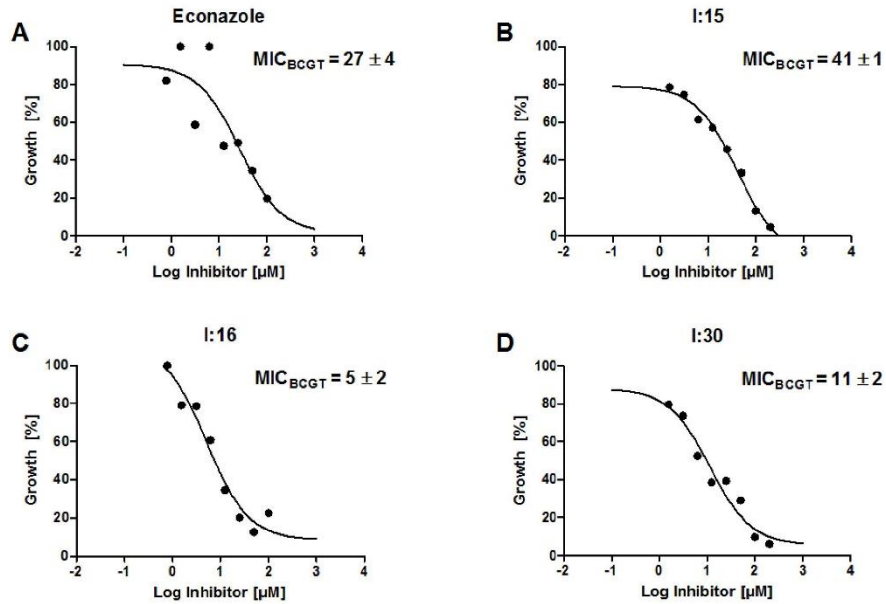


**Figure S9.** Growth inhibition of BCG versus control (%) of econazole (A), I:15 (B), I:16 (C), I:30 (D) of concentrations ranging from 100-1.56 µM of the respective compounds. Endpoint optical density was measured at 600 nm. MIC<sub>BCGT</sub> were determined by GraphPad Prism using OneSite Log IC<sub>50</sub> model provided by the software.

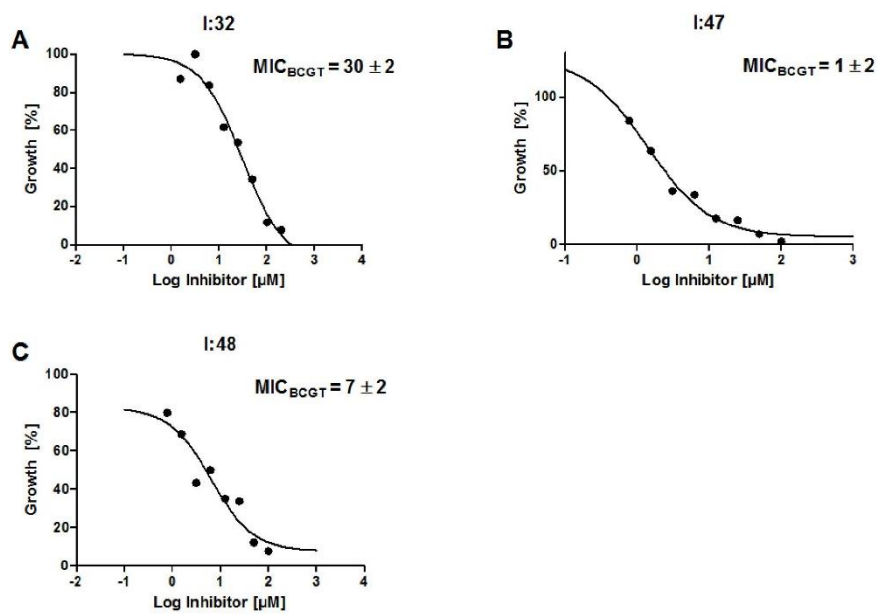


**Figure S10.** Growth inhibition of BCG versus control (%) of I:32 (A), I:47 (B), I:48 (C) of concentrations ranging from 100-1.56  $\mu\text{M}$  of the respective compounds. Endpoint optical density was measured at 600 nm. MIC<sub>BCGT</sub> were determined by GraphPad Prism using OneSite Log IC<sub>50</sub> model provided by the software.

## 10. Calculation of antimicrobial efficiency

$$\text{Antibacterial Efficiency} = -\ln\left(\frac{MIC}{NHA}\right)$$

**Table S2.** Antimicrobial efficiency<sup>[3]</sup> of **I:16, I:30, I:32, I:47, I:48, econazole, isoniazide** and **rifampicine** calculated for effects on *Mycobacterium tuberculosis*.

Cmpd.	MIC [mg/L]	MW	NHA <sup>a</sup>	Antibacterial Efficiency
<b>I:16</b>	1.90	310	24	0.26
<b>I:30</b>	11.20	234	18	0.25
<b>I:32</b>	9.60	234	18	0.26
<b>I:47</b>	0.30	278	21	0.39
<b>I:48</b>	3.50	292	22	0.26
<b>Eco</b>	4.20	382	23	0.24
<b>INH<sup>b</sup></b>	0.05	137	10	0.99
<b>Rif<sup>c</sup></b>	0.11	823	57	0.16

<sup>a</sup>NHA = number of heavy atoms, INH = isoniazide,<sup>[4]</sup> Rif = rifampicine.<sup>[4]</sup>

## 11. Toxicity assessment against human cancer cell lines HEK293 and HepG2

**SI Table 3.** Toxicity data against human cancer cell lines HEK293 and HepG2 of I:47, I:16 and econazole (Eco).

Compounds	LD <sub>50</sub> HEK293 [μM]	SD	LD <sub>50</sub> HEK293 [mg/L]	LD <sub>50</sub> HepG2 [μM]	SD	LD <sub>50</sub> HepG2 [mg/L]
I:47	66.9	5.3	18.6	47.5	8.1	17.1
I:16	19.6	3.8	6.1	12.1	2.8	3.9
Eco	15.6	3.8	6.0	11.8	4.3	3.1

**12. MIC against *Escherichia coli* and *Staphylococcus aureus* in comparison to growth inhibition against *Mycobacterium bovis* BCG**

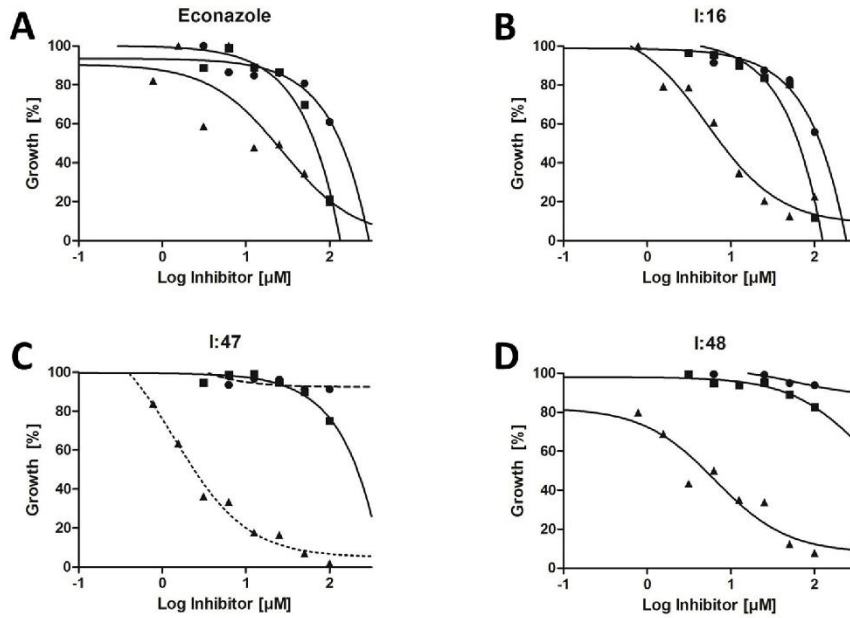


**Figure S11.** Comparison of growth inhibition of econazole (A), I:16 (B), I:47 (C) and I:48 (D) against *M. bovis* ( $\blacktriangle$ ,  $c = 1.56 - 100 \mu\text{M}$ ), *E. coli* ( $\blacksquare$ ,  $c = 3.125 - 100 \mu\text{M}$ ), *S. aureus* ( $\bullet$ ,  $c = 3.125 - 100\mu\text{M}$ ) of concentrations ranging from 100-0.725  $\mu\text{M}$  of the respective compounds. Endpoint optical density was measured at 600 nm. Graphs were plotted with GraphPad Prism using OneSite Log  $\text{IC}_{50}$  model provided by the software.

### 13. Physicochemical data:

1:16



**ACD/Labs**

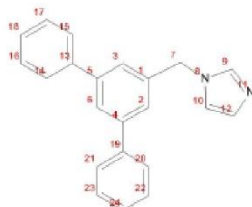
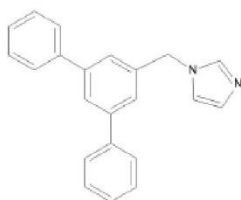
ACD/Labs  
ACD/LogP Classic Module Report

Date: February 17, 2016 9:47 AM

Software name and version: ACD/Percepta 14.0.0 (Build 2203)

Compound name:

Structure:



Calculated LogP: 5.26 ± 0.35

ACD/Labs

ACD/LogP Classic Module Report

S19

**LogP Calculation Protocol:**

Increments of the functional groups:

1. -1.86 (experimental value), atom(s) number: 8, 11, 8

Increments of the Carbon atoms:

2. +0.53 (experimental value), atom(s) number: 7  
3. +0.37 (experimental value), atom(s) number: 10  
4. +0.37 (experimental value), atom(s) number: 12  
5. -0.08 (experimental value), atom(s) number: 1  
6. -0.08 (experimental value), atom(s) number: 5  
7. -0.08 (experimental value), atom(s) number: 4  
8. -0.08 (experimental value), atom(s) number: 19  
9. -0.08 (experimental value), atom(s) number: 13  
10. +0.37 (experimental value), atom(s) number: 3  
11. +0.37 (experimental value), atom(s) number: 2  
12. +0.37 (experimental value), atom(s) number: 6  
13. +0.37 (experimental value), atom(s) number: 21  
14. +0.37 (experimental value), atom(s) number: 20  
15. +0.37 (experimental value), atom(s) number: 15  
16. +0.37 (experimental value), atom(s) number: 14  
17. +0.37 (experimental value), atom(s) number: 23  
18. +0.37 (experimental value), atom(s) number: 22  
19. +0.37 (experimental value), atom(s) number: 17  
20. +0.37 (experimental value), atom(s) number: 16  
21. +0.37 (experimental value), atom(s) number: 24  
22. +0.37 (experimental value), atom(s) number: 18

Interactions through aromatic system:

8-9 +0.29 (experimental value), atom(s) number: 10, 4, 6, 5, 13

Interactions through aliphatic system:

1-5 +0.28 (experimental value), atom(s) number: 1, 7, 8

Increments of the ring interactions

Increments of the ring interactions

Increments of the ring interactions

1:47



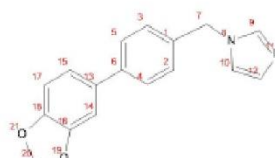
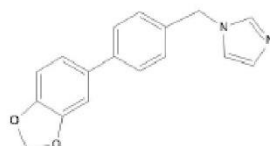
ACD/Labs  
ACD/LogP Classic Module Report

Date: February 17, 2016 9:59 AM

Software name and version: ACD/Percepta 14.0.0 (Build 2203)

Compound name:

Structure:



Calculated LogP: 3.08 ± 0.37

**LogP Calculation Protocol:**

**Increments of the functional groups:**

1. +0,43 (experimental value), atom(s) number: 20, 21, 19
2. -1,86 (experimental value), atom(s) number: 9, 11, 8

**Increments of the Carbon atoms:**

3. +0,53 (experimental value), atom(s) number: 7
4. +0,37 (experimental value), atom(s) number: 10
5. +0,37 (experimental value), atom(s) number: 12
6. +0,08 (experimental value), atom(s) number: 16
7. +0,08 (experimental value), atom(s) number: 18
8. -0,08 (experimental value), atom(s) number: 1
9. -0,08 (experimental value), atom(s) number: 13
10. -0,08 (experimental value), atom(s) number: 6
11. +0,37 (experimental value), atom(s) number: 14
12. +0,37 (experimental value), atom(s) number: 17
13. +0,37 (experimental value), atom(s) number: 3
14. +0,37 (experimental value), atom(s) number: 2
15. +0,37 (experimental value), atom(s) number: 15
16. +0,37 (experimental value), atom(s) number: 5
17. +0,37 (experimental value), atom(s) number: 4

**Interactions through aromatic system:**

- 1-10 0,00 (approximated value), atom(s) number: 19, 16, 14, 13, 8

**Interactions through aliphatic system:**

- 2-8 +0,28 (experimental value), atom(s) number: 1, 7, 8

**Increments of the ring interactions**

**Increments of the ring interactions**

Econazole



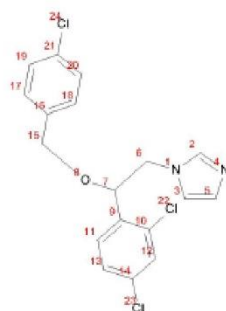
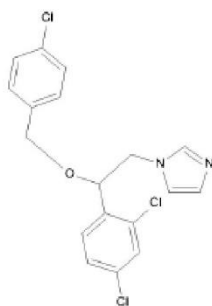
ACD/Labs  
ACD/LogP Classic Module Report

Date: February 17, 2015 10:16 AM

Software name and version: ACD/Percepta 14.0.0 (Build 2203)

Compound name: Econazole

Structure:



Calculated LogP: 5,32 ± 0,55

**LogP Calculation Protocol:**

## Increments of the functional groups:

1. -1.86 (experimental value), atom(s) number: 2, 4, 1
2. +1.04 (experimental value), atom(s) number: 22
3. +1.04 (experimental value), atom(s) number: 23
4. +1.04 (experimental value), atom(s) number: 24
5. -1.00 (experimental value), atom(s) number: 8

## Increments of the Carbon atoms:

6. +0.53 (experimental value), atom(s) number: 15
7. +0.53 (experimental value), atom(s) number: 6
8. -0.03 (experimental value), atom(s) number: 7
9. +0.37 (experimental value), atom(s) number: 3
10. +0.37 (experimental value), atom(s) number: 5
11. -0.08 (experimental value), atom(s) number: 10
12. -0.08 (experimental value), atom(s) number: 14
13. -0.08 (experimental value), atom(s) number: 21
14. -0.08 (experimental value), atom(s) number: 9
15. -0.08 (experimental value), atom(s) number: 16
16. +0.37 (experimental value), atom(s) number: 12
17. +0.37 (experimental value), atom(s) number: 13
18. +0.37 (experimental value), atom(s) number: 20
19. +0.37 (experimental value), atom(s) number: 19
20. +0.37 (experimental value), atom(s) number: 11
21. +0.37 (experimental value), atom(s) number: 18
22. +0.37 (experimental value), atom(s) number: 17

## Interactions through aromatic system:

- 2-3 +0.01 (experimental value), atom(s) number: 22, 10, 12, 14, 23

## Interactions through aliphatic system:

- 14-15 -0.05 (experimental value), atom(s) number: 16, 15, 8, 7, 9
- 1-14 -0.01 (experimental value), atom(s) number: 9, 7, 6, 1
- 1-5 +0.64 (experimental value), atom(s) number: 1, 6, 7, 8
- 5-14 +0.65 (experimental value), atom(s) number: 9, 7, 8
- 5-15 +0.65 (experimental value), atom(s) number: 16, 15, 8
- 1-15 +0.10 (approximated value), atom(s) number: 16, 15, 8, 7, 6, 1

**Referenced data:**

1:48



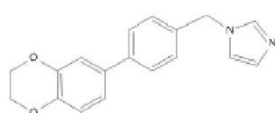
ACD/Labs  
ACD/LogP Classic Module Report

Date: February 17, 2015 10:03 AM

Software name and version: ACD/Percepta 14.0.0 (Build 2203)

Compound name:

Structure:



Calculated LogP: 2.63 ± 0.39

**LogP Calculation Protocol:**

**Increments of the functional groups:**

1. -1.86 (experimental value), atom(s) number: 9, 11, 8
2. -0.55 (experimental value), atom(s) number: 19
3. -0.55 (experimental value), atom(s) number: 21

**Increments of the Carbon atoms:**

4. +0.56 (experimental value), atom(s) number: 20
5. +0.56 (experimental value), atom(s) number: 22
6. +0.53 (experimental value), atom(s) number: 7
7. +0.37 (experimental value), atom(s) number: 10
8. +0.37 (experimental value), atom(s) number: 12
9. +0.08 (experimental value), atom(s) number: 17
10. +0.08 (experimental value), atom(s) number: 18
11. -0.08 (experimental value), atom(s) number: 1
12. -0.08 (experimental value), atom(s) number: 13
13. -0.08 (experimental value), atom(s) number: 6
14. +0.37 (experimental value), atom(s) number: 15
15. +0.37 (experimental value), atom(s) number: 16
16. +0.37 (experimental value), atom(s) number: 3
17. +0.37 (experimental value), atom(s) number: 2
18. +0.37 (experimental value), atom(s) number: 14
19. +0.37 (experimental value), atom(s) number: 5
20. +0.37 (experimental value), atom(s) number: 4

**Interactions through aromatic system:**

- 3-13 -0.10 (experimental value), atom(s) number: 6, 13, 14, 16, 18, 21
- 2-13 -0.15 (experimental value), atom(s) number: 6, 13, 15, 17, 19
- 2-3 -0.09 (experimental value), atom(s) number: 19, 17, 18, 21

**Interactions through aliphatic system:**

- 2-3 +0.29 (experimental value), atom(s) number: 21, 22, 20, 19
- 1-11 +0.28 (experimental value), atom(s) number: 1, 7, 8

**Increments of the ring interactions**

**Increments of the ring interactions**

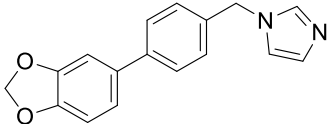
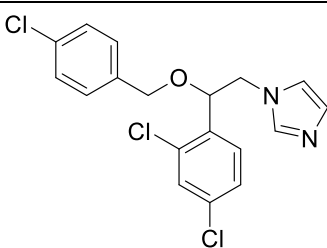
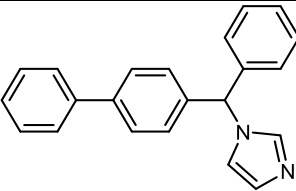
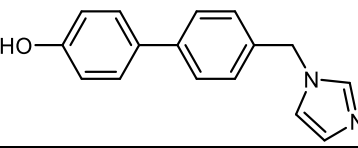
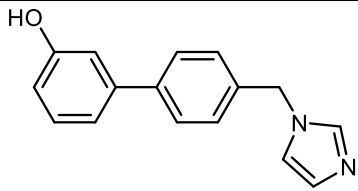
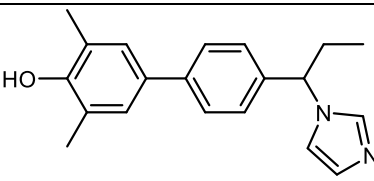
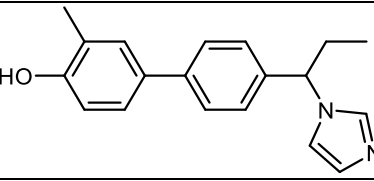
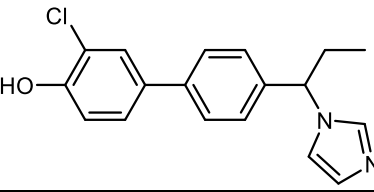
## 14. References

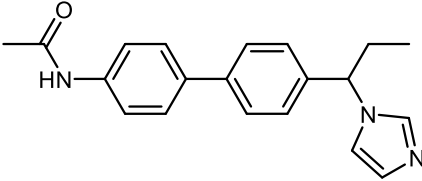
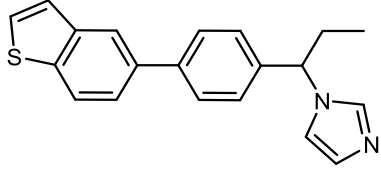
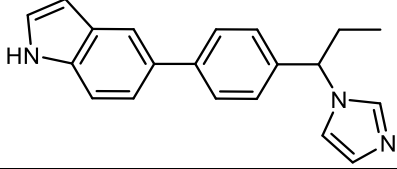
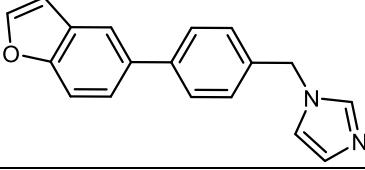
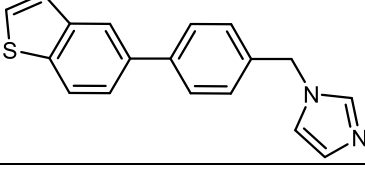
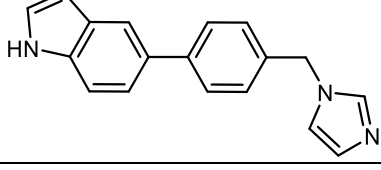
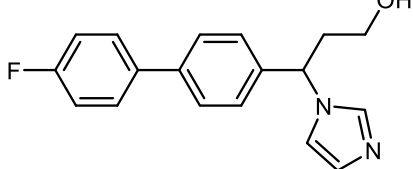
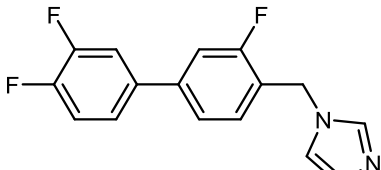
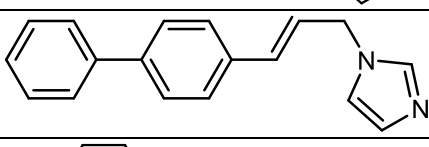
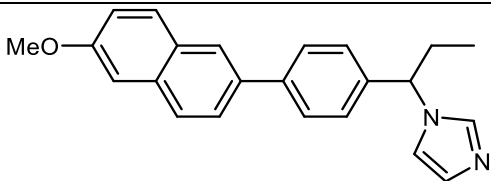
- [1] J. R. Cochrane, J. M. White, U. Wille, C. A. Hutton, *Org. Lett.* **2012**, *14*, 2402–2405.
- [2] M. E. Jung, J. C. Rohlofp, *J. Org. Chem.* **1985**, *2*, 4909–4913.
- [3] A. Brzostek, B. Dziadek, A. Rumijowska-Galewicz, J. Pawelczyk, J. Dziadek, *FEMS Microbiol. Lett.* **2007**, *275*, 106–112.
- [4] S. G. Franzblau, M. A. Degroote, S. H. Cho, K. Andries, E. Nuermberger, I. M. Orme, K. Mdluli, I. Angulo-Barturen, T. Dick, V. Dartois, et al., *Tuberculosis* **2012**, *92*, 453–488.

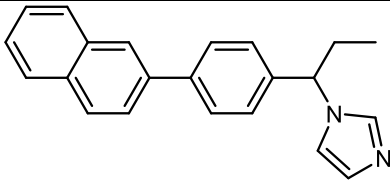
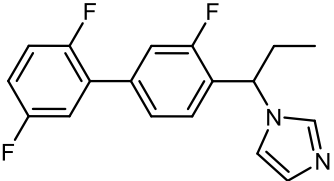
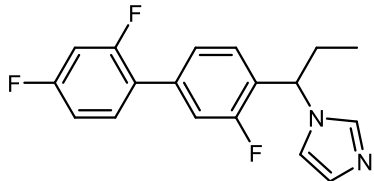
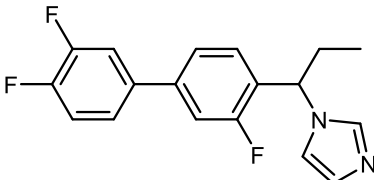
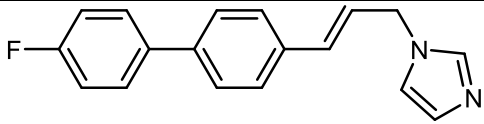
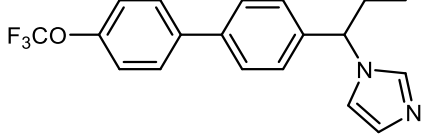
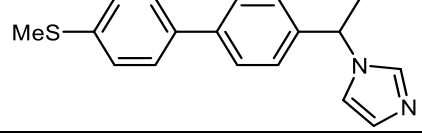
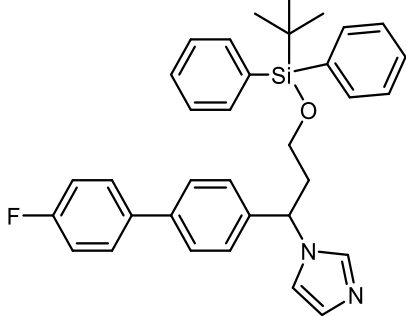
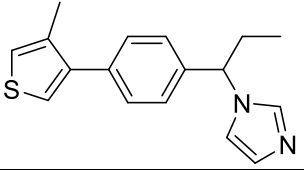
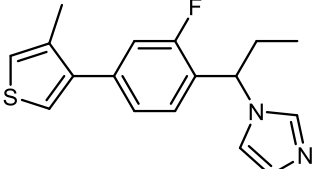
## 7.1.2 Supporting Information for Chapter 3.2

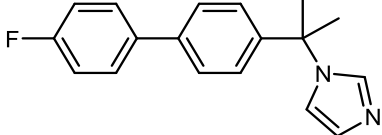
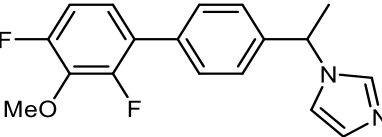
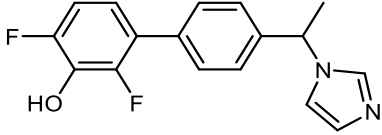
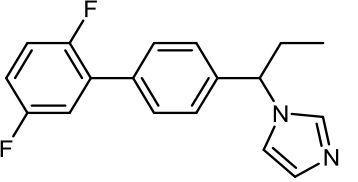
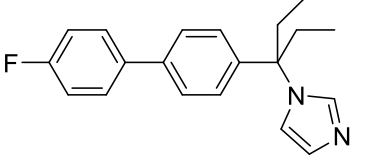
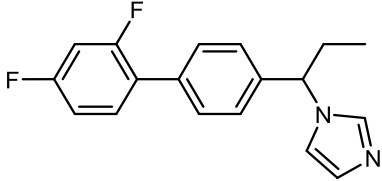
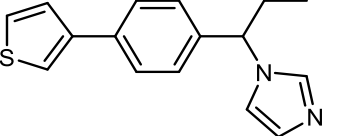
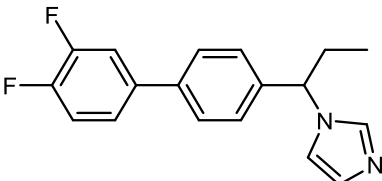
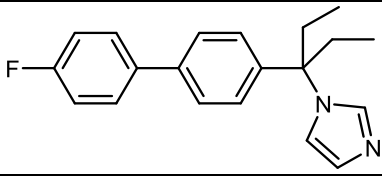
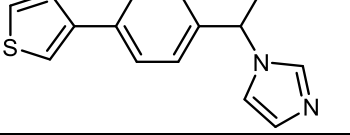
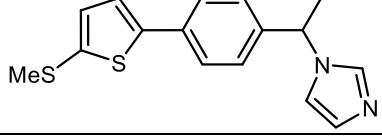
### 1. Screening Overview: $K_D$ and $MIC_{50}$ values

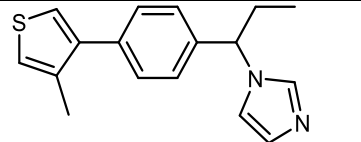
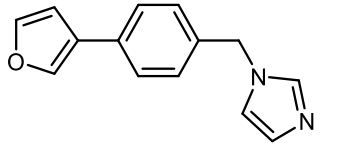
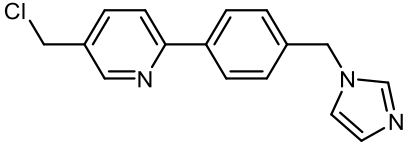
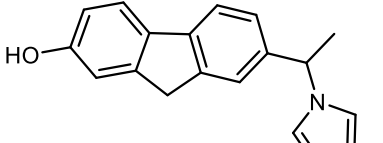
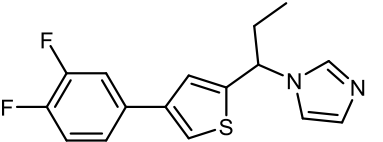
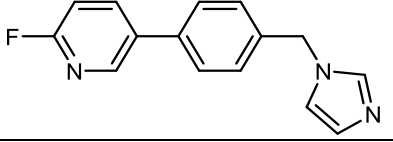
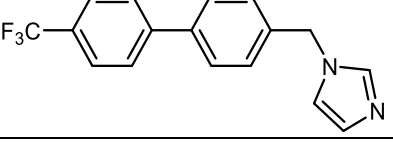
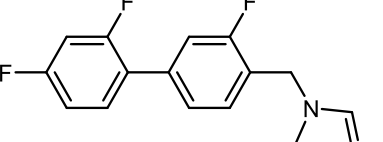
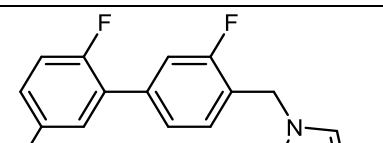
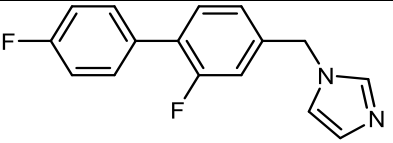
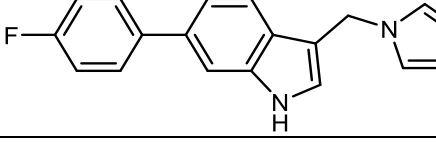
**Table S1:** Determined  $K_D$  values with standard deviation and  $MIC_{50}$  values against *M. bovis* BCG

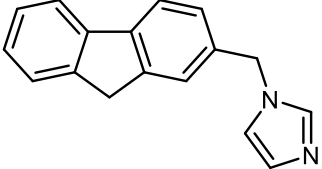
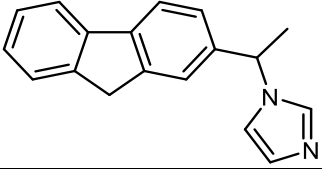
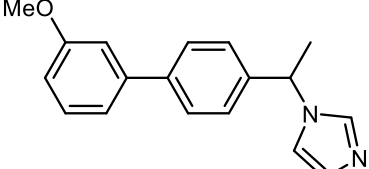
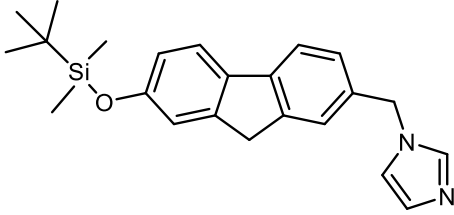
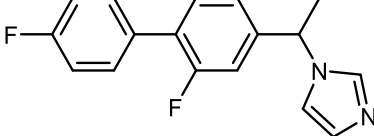
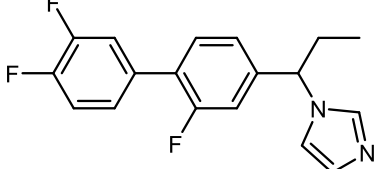
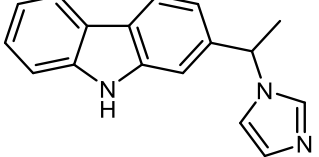
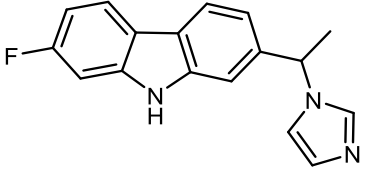
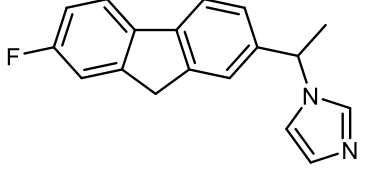
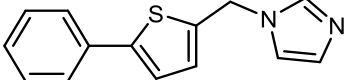
Compound	Structure	$K_D \pm STD$ [ $\mu M$ ]	$MIC_{50}$ [ $\mu M$ ]
I:47		$5.4 \pm 1.0$	4.0
Econazole		$2.8 \pm 0.2$	12.7
L1		$1.4 \pm 0.22$	
L2		$7.4 \pm 2.3$	
L3		$34.0 \pm 8.9$	
L4			
L5		$6.5 \pm 2.7$	
L6		$19.4 \pm 13.4$	

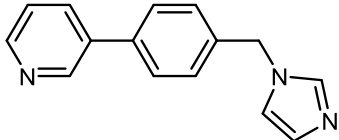
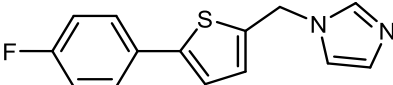
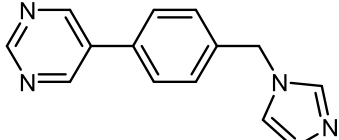
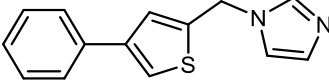
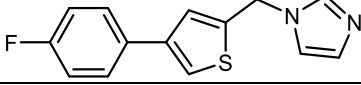
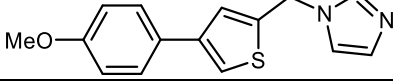
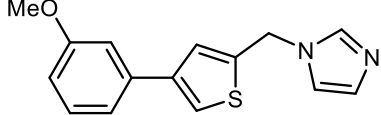
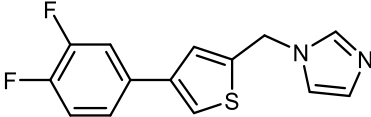
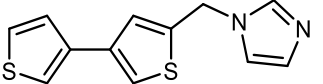
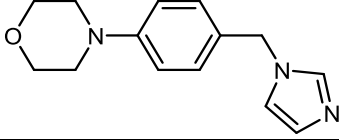
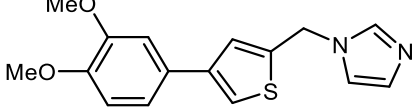
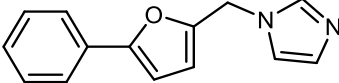
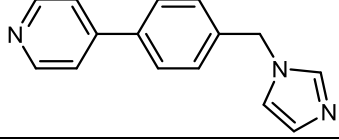
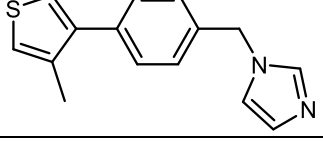
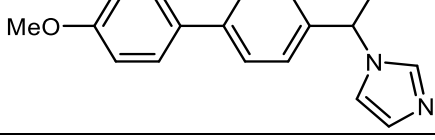
<b>L7</b>		$2.0 \pm 0.44$	
<b>L8</b>		$2.7 \pm 0.52$	18.4
<b>L9</b>		$2.9 \pm 1.2$	36.1
<b>L10</b>		$2.9 \pm 0.38$	2.6
<b>L11</b>		$1.5 \pm 0.46$	
<b>L12</b>		$2.4 \pm 0.19$	7.6
<b>L13</b>		$14.0 \pm 2.0$	
<b>L14</b>		$6.4 \pm 0.85$	2.7
<b>L15</b>		$4.3 \pm 0.78$	1.8
<b>L16</b>		$0.5 \pm 0.09$	7.4

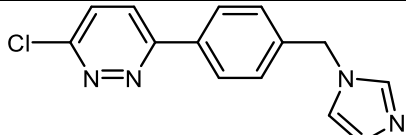
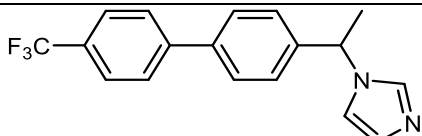
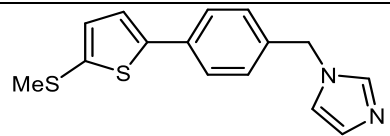
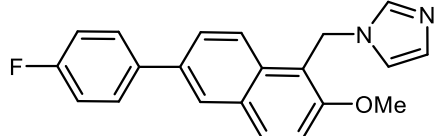
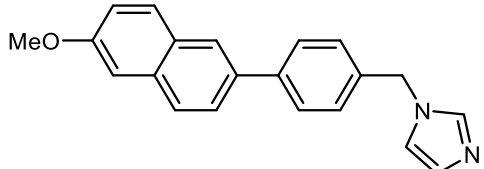
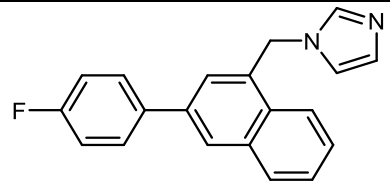
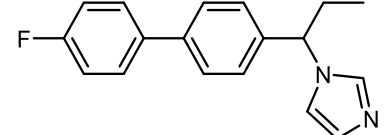
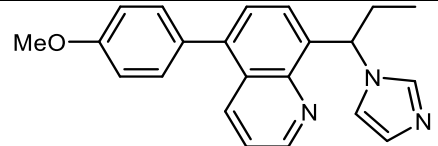
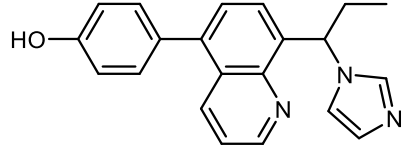
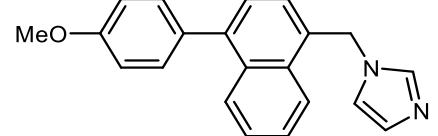
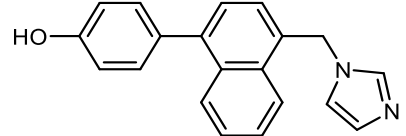
<b>L17</b>		$1.4 \pm 0.20$	
<b>L18</b>		$8.0 \pm 1.3$	
<b>L19</b>		$4.8 \pm 0.84$	20.2
<b>L20</b>		$5.0 \pm 1.5$	
<b>L21</b>		$5.9 \pm 0.55$	1.5
<b>L22</b>		$5.0 \pm 0.49$	
<b>L23</b>		$3.0 \pm 0.74$	
<b>L24</b>		$3.1 \pm 0.73$	
<b>L25</b>			
<b>L26</b>		$9.0 \pm 1.3$	

<b>L27</b>		$8.9 \pm 0.54$	
<b>L28</b>			
<b>L29</b>			
<b>L30</b>		$7.5 \pm 0.86$	
<b>L31</b>			
<b>L32</b>		$8.7 \pm 1.2$	
<b>L33</b>		$18.3 \pm 1.7$	
<b>L34</b>		$4.1 \pm 0.91$	
<b>L35</b>		$2.5 \pm 0.57$	
<b>L36</b>		$16.9 \pm 2.2$	
<b>L37</b>		$4.5 \pm 0.88$	

<b>L38</b>		$9.4 \pm 0.66$	
<b>L39</b>		$32.9 \pm 11.1$	
<b>L40</b>			
<b>L41</b>		$5.3 \pm 0.68$	13.2
<b>L42</b>		$6.3 \pm 1.1$	
<b>L43</b>			
<b>L44</b>		$5.6 \pm 0.93$	2.4
<b>L45</b>		$12.6 \pm 2.0$	3.4
<b>L46</b>		$9.2 \pm 1.5$	2.9
<b>L47</b>		$7.4 \pm 0.80$	6.0
<b>L48</b>		$5.9 \pm 2.0$	6.1

<b>L49</b>		$6.0 \pm 1.1$	6.7
<b>L50</b>		$4.8 \pm 0.78$	
<b>L51</b>			
<b>L52</b>			
<b>L53</b>		$5.3 \pm 1.2$	
<b>L54</b>		$4.6 \pm 0.70$	
<b>L55</b>		$8.7 \pm 1.3$	
<b>L56</b>		$7.5 \pm 0.80$	
<b>L57</b>		$17.0 \pm 2.0$	
<b>L58</b>		$19.6 \pm 4.4$	

<b>L59</b>			
<b>L60</b>		$9.1 \pm 1.5$	7.0
<b>L61</b>			
<b>L62</b>		$28.3 \pm 3.7$	
<b>L63</b>		$18.9 \pm 3.1$	
<b>L64</b>		$16.0 \pm 3.9$	
<b>L65</b>		$11.2 \pm 1.9$	
<b>L66</b>		$5.3 \pm 1.1$	5.1
<b>L67</b>			
<b>L68</b>			
<b>L69</b>		$62.7 \pm 12.4$	
<b>L70</b>		$33.7 \pm 5.6$	
<b>L71</b>			
<b>L72</b>		$21.7 \pm 2.0$	
<b>L73</b>		$10.9 \pm 2.0$	4.5

<b>L74</b>			
<b>L75</b>		$8.6 \pm 2.0$	8.6
<b>L76</b>		$6.6 \pm 0.97$	3.2
<b>L77</b>		$1.4 \pm 0.23$	14.7
<b>L78</b>		$0.6 \pm 0.17$	2.4
<b>L79</b>		$1.3 \pm 0.27$	29.8
<b>L80</b>		$10.1 \pm 1.5$	
<b>L81</b>		$2.5 \pm 0.70$	
<b>L82</b>		$1.7 \pm 0.37$	
<b>L83</b>		$1.3 \pm 0.11$	
<b>L84</b>		$1.1 \pm 0.22$	36.4

<b>L85</b>		$1.5 \pm 0.18$	
<b>L86</b>		$4.0 \pm 0.61$	
<b>L87</b>		$1.8 \pm 0.32$	
<b>L88</b>		$3.8 \pm 0.85$	
<b>L89</b>		$0.3 \pm 0.09$	21.7
<b>L90</b>		$5.5 \pm 0.9$	6.9
<b>L91</b>		$7.3 \pm 1.8$	10.9
<b>L92</b>		$2.9 \pm 0.59$	
<b>L93</b>		$1.9 \pm 0.39$	
<b>L94</b>		$4.7 \pm 0.8$	3.3

## 2. Chemical Synthesis

### 2.1. Method A: Suzuki coupling

2.1.1: 4'-methoxy-3'-methyl-[1,1'-biphenyl]-4-carbaldehyde (**S4b**): Synthesized according to method A using 4-bromobenzaldehyde (1.35 mmol; 250 mg) and 4-Methoxy-3-methylphenylboronic acid (1.75 mmol; 291 mg). Yield: 317 mg (100 %) of a white solid.  $R_f = 0.54$  (hexane : EtOAc = 9 : 1).  $^1\text{H-NMR}$  (300 MHz, CHLOROFORM- $d_3$ ):  $\delta$  (ppm) = 2.31 (s, 3 H); 3.90 (d,  $J=1.2$  Hz, 3 H); 6.94 (d,  $J=8.1$  Hz, 1 H); 7.41 - 7.52 (m, 2 H); 7.65 - 7.77 (m, 2 H); 7.87 - 7.97 (m, 2 H); 10.04 (s, 1 H).  $^{13}\text{C-NMR}$  (300 MHz, CHLOROFORM- $d_3$ ):  $\delta$  (ppm) = 16.4; 55.4; 110.3; 125.8; 127.0; 127.3; 129.6; 130.3; 131.6; 134.6; 147.0; 158.4; 191.9. LC-MS (ESI):  $R_t = 9.04$  min;  $m/z = 227.04$  [M+H] $^+$ .

2.1.2: 4-(benzo[d][1,3]dioxol-5-yl)benzaldehyde (**S5b**): Synthesized according to method A using 4-bromobenzaldehyde (1.35 mmol; 250 mg) and 3,4-methylenedioxyphenylboronic acid (1.75 mmol; 290 mg). Yield: 322 mg (100 %) of a white solid.  $R_f = 0.66$  (hexane : EtOAc = 8 : 2).  $^1\text{H-NMR}$  (300 MHz, CHLOROFORM- $d_3$ ):  $\delta$  (ppm) = 6.04 (s, 2 H); 6.92 (dd,  $J=7.7, 0.7$  Hz, 1 H); 7.10 - 7.17 (m, 2 H); 7.64 - 7.71 (m, 2 H); 7.88 - 7.97 (m, 2 H); 10.04 (s, 1 H).  $^{13}\text{C-NMR}$  (300 MHz, CHLOROFORM- $d_3$ ):  $\delta$  (ppm) = 101.4; 107.6; 108.8; 121.3; 127.3; 130.3; 133.9; 134.9; 146.8; 148.1; 148.4; 191.8. LC-MS (ESI):  $R_t = 8.20$  min;  $m/z = 227.01$  [M+H] $^+$ .

2.1.3: 3'-fluoro-4'-methoxy-[1,1'-biphenyl]-4-carbaldehyde (**S6b**): Synthesized according to method A using 4-bromobenzaldehyde (1.35 mmol; 250 mg) and 3-Fluoro-4-methoxybenzeneboronic acid (1.75 mmol; 297 mg). Yield: 289 mg (93 %) of a white solid.  $R_f = 0.46$  (hexane : EtOAc = 8 : 2).  $^1\text{H-NMR}$  (300 MHz, CHLOROFORM- $d_3$ ):  $\delta$  (ppm) = 3.96 (s, 3 H); 7.01 - 7.13 (m, 1 H); 7.34 - 7.45 (m, 2 H); 7.70 (d,  $J=8.5$  Hz, 2 H); 7.91 - 7.99 (m, 2 H); 10.05 (s, 1 H).  $^{13}\text{C-NMR}$  (300 MHz, CHLOROFORM- $d_3$ ):  $\delta$  (ppm) = 56.4 (s); 113.7 (d,  $J=2.2$  Hz); 115.0 (d,  $J=18.6$  Hz); 123.1 (d,  $J=3.7$  Hz); 127.1 (s); 130.3 (s); 132.7 (d,  $J=6.7$  Hz); 135.1 (s); 145.6 (d,  $J=1.5$  Hz); 148.1 (d,  $J=10.4$  Hz); 152.6 (d,  $J=246.6$  Hz); 191.8 (s). LC-MS (ESI):  $R_t = 8.50$  min;  $m/z = 231.05$  [M+H] $^+$ .

2.1.4: 4'-formyl-[1,1'-biphenyl]-4-carbonitrile (**S7b**): Synthesized according to method A using 4-bromobenzaldehyde (1.35 mmol; 250 mg) and 4-Cyanophenylboronic acid (1.75 mmol; 257 mg). Yield: 263 mg (94 %) of a white solid.  $R_f = 0.78$  (hexane : EtOAc = 7 : 3).  $^1\text{H-NMR}$  (300 MHz, CHLOROFORM- $d_3$ ):  $\delta$  (ppm) = 7.70 - 7.83 (m, 6 H); 7.97 - 8.05 (m, 2 H); 10.10 (s, 1 H).  $^{13}\text{C-NMR}$  (300 MHz, CHLOROFORM- $d_3$ ):  $\delta$  (ppm) = 112.2; 118.5; 127.9; 128.0; 130.4; 132.8; 136.1; 144.1; 144.9; 191.6. LC-MS (ESI):  $R_t = 8.39$  min;  $m/z = 415.28$  [2M+H] $^+$ .

2.1.5: 4-(benzo[d][1,3]dioxol-5-yl)-2-fluorobenzaldehyde (**S8b**): Synthesized according to method A using 4-bromo-2-fluorobenzaldehyde (1.35 mmol; 274 mg) and 3,4-methylenedioxyphenyl boronic acid (1.75 mmol; 290 mg). Yield: 311 mg (94 %) of a white-yellow solid.  $R_f = 0.47$  (hexane : EtOAc = 95 : 5).  $^1\text{H-NMR}$  (300 MHz, CHLOROFORM- $d_3$ ):  $\delta$  (ppm) = 6.05 (s, 2 H); 6.92 (d,  $J=8.1$  Hz, 1 H); 7.07 - 7.15 (m, 2 H); 7.32 (dd,  $J=11.8, 1.6$  Hz, 1 H); 7.43 (dd,  $J=8.1, 1.0$  Hz, 1 H); 7.87 - 7.94 (m, 1 H); 10.37 (s, 1 H).  $^{13}\text{C-NMR}$  (300 MHz, CHLOROFORM- $d_3$ ):  $\delta$  (ppm) = 101.6 (s); 107.4 (s); 108.9 (s); 114.3 (d,  $J=22.35$  Hz); 121.3 (s); 122.4 (d,  $J=8.9$  Hz); 122.9 (d,  $J=2.9$  Hz); 129.1 (d,  $J=2.9$  Hz); 132.7 (d,  $J=2.2$  Hz); 148.5 (s); 148.6 (s); 149.3 (d,  $J=8.9$  Hz); 164.9 (d,  $J=257.8$  Hz); 186.7 (d,  $J=5.9$  Hz). LC-MS (ESI):  $R_t = 8.38$  min;  $m/z = 244.98$  [M+H] $^+$ .

### 2.2 Method B: Grignard reaction

2.2.1: 1-(3'-fluoro-4'-methoxy-[1,1'-biphenyl]-4-yl)prop-2-en-1-ol (**S6a**): Synthesized according to method B using **S6b** (1.17 mmol; 270 mg) and vinylmagnesium bromide (0.7 M in THF; 1.40 mmol; 2.0 mL). Yield: 182 mg (60 %) of a yellow solid.  $R_f = 0.29$  (hexane : EtOAc = 8 : 2).  $^1\text{H-NMR}$  (300 MHz, CHLOROFORM- $d_3$ ):  $\delta$  (ppm) = 3.94 (s, 3 H); 5.21 - 5.29 (m, 2 H); 5.40 (d,  $J=17.0$  Hz, 1 H); 6.09 (ddd,  $J=16.8, 10.4, 6.0$  Hz, 1 H); 7.00 - 7.07 (m, 1 H); 7.29 - 7.37 (m, 2 H); 7.42 - 7.47 (m, 2 H); 7.50 - 7.57 (m, 2 H).  $^{13}\text{C-NMR}$  (300 MHz, CHLOROFORM- $d_3$ ):  $\delta$  (ppm) = 56.4 (s); 75.09 (s); 113.7 (d,  $J=2.2$  Hz); 114.7 (d,  $J=19.4$  Hz); 115.3 (s); 122.6 (d,  $J=3.0$  Hz); 126.8 (s); 126.9 (s); 134.0 (d,  $J=6.0$  Hz); 139.2 (d,  $J=1.5$  Hz); 140.1 (s); 141.6 (s); 147.1 (d,  $J=10.4$  Hz); 152.6 (d,  $J=244.4$  Hz). LC-MS (ESI):  $R_t = 7.21$  min;  $m/z = 241.14$  [M-OH] $^+$ .

2.2.2: 4'-(1-hydroxyallyl)-[1,1'-biphenyl]-4-carbonitrile (**S7a**): Synthesized according to method B using **S7b** (1.21 mmol; 250 mg) and vinylmagnesium bromide (0.7 M in THF; 1.45 mmol; 2.1 mL). Yield: 168 mg (59 %) of a yellow solid.  $R_f = 0.27$  (hexane : EtOAc = 8 : 2).  $^1\text{H-NMR}$  (300 MHz, CHLOROFORM- $d_3$ ):  $\delta$  (ppm) = 5.22 - 5.32 (m, 2 H); 5.41 (d,  $J=17.0$  Hz, 1 H); 6.08 (ddd,  $J=16.9, 10.4, 6.1$  Hz, 1 H); 7.51 (d,  $J=8.2$  Hz, 2 H); 7.60 (d,  $J=8.2$  Hz, 2 H); 7.71 (dd,  $J=15.1, 8.2$  Hz, 4 H).  $^{13}\text{C-NMR}$  (300 MHz, CHLOROFORM- $d_3$ ):  $\delta$  (ppm) = 75.0; 110.9; 115.6; 118.9; 127.0; 127.4; 127.7; 132.6; 138.5; 140.0; 143.1; 145.3. LC-MS (ESI):  $R_t = 7.10$  min;  $m/z = 218.15$  [M-OH] $^+$ .

2.2.3: 1-(4-(benzo[d][1,3]dioxol-5-yl)-2-fluorophenyl)prop-2-en-1-ol (**S8a**): Synthesized according to method B using **S8b** (1.23 mmol; 300 mg) and vinylmagnesium bromide (0.7 M in THF; 1.47 mmol; 2.1 mL). Yield: 127 mg (38 %) of a yellow solid.  $R_f = 0.38$  (hexane : EtOAc = 85 : 15).  $^1\text{H-NMR}$  (300 MHz, CHLOROFORM- $d_3$ ):  $\delta$  (ppm) = 2.14 (br. s., 1 H); 5.24 (d,  $J=10.3$  Hz, 1 H); 5.40 (dd,  $J=17.1, 0.6$  Hz, 1 H); 5.55 (d,  $J=5.3$  Hz, 1 H); 6.05 - 6.18 (m, 1 H); 6.85 - 6.92 (m, 1 H); 7.01 - 7.08 (m, 2 H); 7.20 (dd,  $J=11.6, 1.7$  Hz, 1 H); 7.31 (dd,  $J=8.0, 1.7$  Hz, 1 H); 7.43 - 7.52 (m, 1 H).  $^{13}\text{C-NMR}$  (300 MHz, CHLOROFORM- $d_3$ ):  $\delta$  (ppm) = 69.1 (s); 101.3 (s); 107.5 (s); 108.6 (s); 113.7 (d,  $J=23.1$  Hz); 115.4 (s); 120.6 (s); 122.6 (d,  $J=3.0$  Hz); 127.7 - 128.3 (m); 133.9 (d,  $J=2.2$  Hz); 138.8 (s); 142.4 (d,  $J=8.2$  Hz); 147.5 (s); 148.2 (s); 160.2 (d,  $J=248.1$  Hz).

2.2.4: 1-(4'-((tert-butyldimethylsilyloxy)-[1,1'-biphenyl]-4-yl)prop-2-en-1-ol (**S9b**): Synthesized according to method B using **S9c** (1.14 mmol; 357 mg) and vinylmagnesium bromide (0.7 M in THF; 1.37 mmol; 2.0 mL). Yield: 47 mg (47 %) of a yellow oil.  $R_f = 0.32$  (hexane : EtOAc = 9 : 1).  $^1\text{H-NMR}$  (300 MHz, CHLOROFORM- $d_3$ ):  $\delta$  (ppm) = 0.21 - 0.26 (m, 6 H); 0.98 - 1.03 (m, 9 H); 5.21 - 5.28 (m, 2 H); 5.40 (dt,  $J=17.1, 1.4$  Hz, 1 H); 6.10 (ddd,  $J=17.1, 10.3, 6.0$  Hz, 1 H); 6.88 - 6.94 (m, 2 H); 7.40 - 7.48 (m, 4 H); 7.53 - 7.58 (m, 2 H).  $^{13}\text{C-NMR}$  (300 MHz, CHLOROFORM- $d_3$ ):  $\delta$  (ppm) = -4.4; 18.2; 25.7; 75.2; 115.2; 120.3; 126.7; 126.9; 128.0; 133.8; 140.2; 140.5; 140.9; 155.3.

2.2.5: 1-(4-(1-(tert-butyldimethylsilyl)-1H-indol-5-yl)phenyl)prop-2-en-1-ol (**S10b**): Synthesized according to method B using **S10c** (1.18 mmol; 397 mg) and vinylmagnesium bromide (0.7 M in THF; 1.42 mmol; 2.0 mL). Yield: 302 mg (70 %) of a yellow oil.  $R_f = 0.43$  (hexane : EtOAc = 8 : 2).  $^1\text{H-NMR}$  (300 MHz, CHLOROFORM- $d_3$ ):  $\delta$  (ppm) = 0.63 (d,  $J=1.1$  Hz, 6 H); 0.96 (s, 9 H); 5.19 - 5.31 (m, 2 H); 5.42 (dd,  $J=17.1, 1.4$  Hz, 1 H); 6.06 - 6.20 (m, 1 H); 6.67 (d,  $J=3.2$  Hz, 1 H); 7.20 - 7.24 (m, 1 H); 7.37 - 7.49 (m, 3 H); 7.57 (d,  $J=8.6$  Hz, 1 H); 7.66 (d,  $J=7.5$  Hz, 2 H); 7.84 (s, 1 H). LC-MS (ESI):  $R_t = 10.82$  min;  $m/z = 346.27$  [M-OH] $^+$ .

### 2.3 Method C: CDI reaction

2.3.1 1-(1-(3'-fluoro-4'-methoxy-[1,1'-biphenyl]-4-yl)allyl)-1H-imidazole (**S6**): Synthesized according to method C using **S6a** (160 mg, 0.62 mmol) and CDI (301 mg, 1.86 mmol). Yield: 44 mg (23 %) of a colorless oil.  $R_f = 0.44$  (EtOAc : MeOH = 98 : 2).  $^1\text{H-NMR}$  (300 MHz, CHLOROFORM- $d_3$ ):  $\delta$ [ppm] = 3.94 (s, 3 H) 5.19 (d,  $J=17.04$  Hz, 1 H) 5.47 (d,  $J=10.24$  Hz, 1 H) 5.84 (d,  $J=6.24$  Hz, 1 H) 6.31 (ddd,  $J=16.86, 10.34, 6.33$  Hz, 1 H) 6.93 (s, 1 H) 7.00 - 7.09 (m, 1 H) 7.13 (s, 1 H) 7.22 - 7.38 (m, 4 H) 7.54 (d,  $J=8.20$  Hz, 2 H) 7.61 (s, 1 H).  $^{13}\text{C-NMR}$  (75 MHz, CHLOROFORM- $d_3$ ):  $\delta$ [ppm] = 56.3 (s), 63.3 (s), 113.7 (d,  $J=2.24$  Hz), 114.7 (d,  $J=18.63$  Hz), 118.6 (s), 119.5 (s), 122.6 (d,  $J=2.9$  Hz), 127.2 (s), 127.9 (s), 129.0 (s), 133.3 (d,  $J=5.9$  Hz), 135.5 (s), 136.6 (s), 136.9 (s), 139.9 (s), 147.3 (d,  $J=11.2$  Hz), 152.6 (d,  $J=248.1$  Hz). LC-MS (ESI):  $R_t = 2.73$  min,  $m/z = 309.18$  [M+H] $^+$ , 241.14 [M-Imidazole] $^+$ .

2.3.2 4'-(1-(1H-imidazol-1-yl)allyl)-[1,1'-biphenyl]-4-carbonitrile (**S7**): Synthesized according to method C using **S7a** (150 mg, 0.64 mmol) and CDI (310 mg, 1.92 mmol). Yield: 22 mg (34 %) of an orange oil.  $R_f = 0.22$  (100% EtOAc).  $^1\text{H-NMR}$  (300 MHz, CHLOROFORM- $d_3$ ):  $\delta$ [ppm] = 5.20 (dd,  $J=17.00, 0.61$  Hz, 1 H) 5.48 (d,  $J=10.24$  Hz, 1 H) 5.85 (d,  $J=6.24$  Hz, 1 H) 6.31 (ddd,  $J=16.90, 10.38, 6.33$  Hz, 1 H) 6.93 (s, 1 H) 7.12 (s, 1 H) 7.30 (d,  $J=8.38$  Hz, 2 H) 7.54 - 7.63 (m, 3 H) 7.64 - 7.78 (m, 4 H).  $^{13}\text{C-NMR}$  (75 MHz, CHLOROFORM- $d_3$ ):  $\delta$ [ppm] = 63.1, 111.3, 118.5, 118.7, 119.8, 127.7, 127.8, 128.2, 129.5, 132.7, 135.35, 136.6, 138.8, 139.4, 144.7. LC-MS (ESI):  $R_t = 7.70$  min,  $m/z = 286.08$  [M+H] $^+$ , 218.01 [M-Imidazole] $^+$ .

2.3.3 1-(1-(4-(benzo[d][1,3]dioxol-5-yl)-2-fluorophenyl)allyl)-1H-imidazole (**S8**): Synthesized according to method C using **S8a** (125 mg, 0.46 mmol) and CDI (224 mg, 1.38 mmol). Yield: 43 mg (29 %) of a colorless oil.  $R_f = 0.39$  (100% EtOAc).  $^1\text{H-NMR}$  (300 MHz, METHANOL- $d_4$ ):  $\delta$ [ppm] =

5.16 (d,  $J=16.86$  Hz, 1 H) 5.43 - 5.51 (m, 1 H) 5.99 (s, 2 H) 6.31 (d,  $J=6.05$  Hz, 1 H) 6.36 - 6.50 (m, 1 H) 6.87 - 6.93 (m, 1 H) 7.02 (t,  $J=1.12$  Hz, 1 H) 7.10 - 7.16 (m, 3 H) 7.27 - 7.40 (m, 2 H) 7.40 - 7.46 (m, 1 H) 7.74 (s, 1 H).  $^{13}\text{C-NMR}$  (75 MHz, METHANOL- $d_4$ ):  $\delta$ [ppm] = 58.7 (d,  $J=2.9$  Hz), 102.9 (s), 108.4 (s), 109.8 (s), 115.0 (d,  $J=22.4$  Hz), 119.8 (s), 120.3 (s), 122.0 (s), 124.1 (d,  $J=2.9$  Hz), 125.4 (d,  $J=14.2$  Hz), 129.1 (s), 130.5 (d,  $J=3.7$  Hz), 134.7 (d,  $J=1.5$  Hz), 136.2 (s), 138.0 (s), 145.3 (d,  $J=8.2$  Hz), 149.5 (s), 150.0 (s), 163.8 (s). LC-MS (ESI):  $R_t$  = 2.95 min,  $m/z$  = 323.12 [M+H] $^+$ , 254.99 [M-Imidazole] $^+$ .

2.3.4 1-(1-(4'-((tert-butyldimethylsilyl)oxy)-[1,1'-biphenyl]-4-yl)allyl)-1H-imidazole (**S9a**): Synthesized according to method C using **S9b** (175 mg, 0.51 mmol) and CDI (249 mg, 1.53 mmol). Yield: 58 mg (29 %) of a colorless oil.  $R_f$  = 0.31 (100% EtOAc).  $^1\text{H-NMR}$  (300 MHz, CHLOROFORM- $d_3$ ):  $\delta$ [ppm] = 0.24 (s, 6 H); 1.01 (s, 9 H) 5.18 (d,  $J=17.0$  Hz, 1 H); 5.45 (d,  $J=10.2$  Hz, 1 H); 5.81 (d,  $J=6.3$  Hz, 1 H); 6.31 (ddd,  $J=16.9, 10.4, 6.3$  Hz, 1 H); 6.88 - 6.94 (m, 3 H); 7.11 (s, 1 H); 7.24 (d,  $J=8.4$  Hz, 2 H); 7.43 - 7.48 (m, 2 H); 7.53 - 7.58 (m, 3 H).

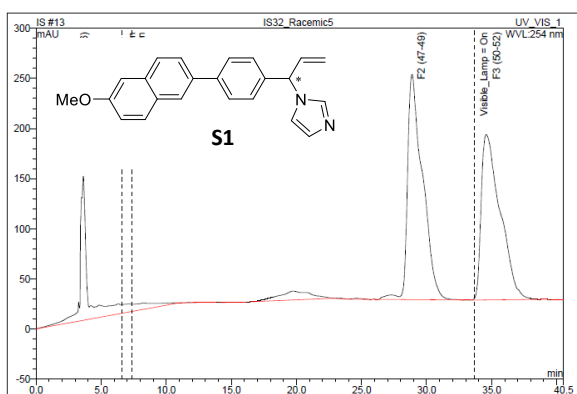
3.10 5-(4-(1-(1H-imidazol-1-yl)allyl)phenyl)-1-(tert-butyldimethylsilyl)-1H-indole (**S10a**): Synthesized according to method C using **S10b** (302 mg, 0.83 mmol) and CDI (404 mg, 2.49 mmol). Yield: 106 mg (31 %) of a yellow oil.  $R_f$  = 0.31 (100% EtOAc).

### 3. Synthesized Compounds: $K_D$ and $\text{MIC}_{50}$ values

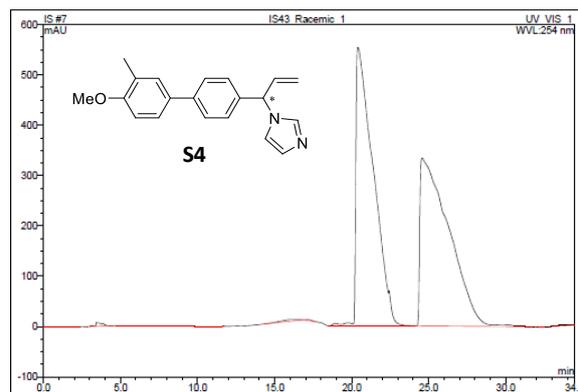
**Table S3:** Determined  $K_D$  values with standard deviation and  $\text{MIC}_{50}$  values against *M. bovis* BCG

Compound	$K_D \pm \text{STD}$ [ $\mu\text{M}$ ]	$\text{MIC}_{50}$ [ $\mu\text{M}$ ]
<b>S1</b>	$0.8 \pm 0.8$	9.7
<b>S2</b>	$8.3 \pm 1.7$	49.9
<b>S3</b>	$21.3 \pm 1.1$	>100
<b>S4</b>	$5.8 \pm 0.5$	17.3
<b>S5</b>	$6.7 \pm 0.6$	20.0
<b>S6</b>	$7.1 \pm 0.7$	14.5
<b>S7</b>	$10.0 \pm 1.4$	9.2
<b>S8</b>	$4.2 \pm 0.3$	>30
<b>S9</b>	$7.2 \pm 0.5$	>50
<b>S10</b>	$3.5 \pm 0.4$	41.0
<b>S11</b>	$5.9 \pm 0.5$	5.8

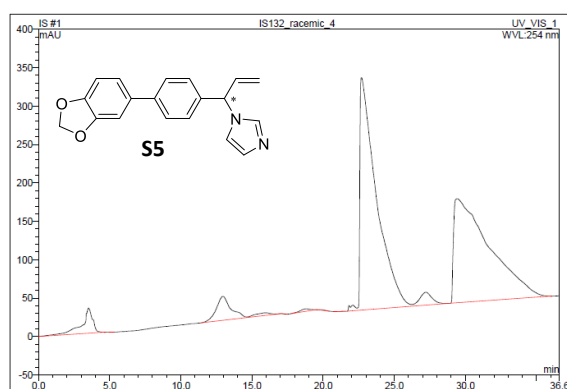
#### 4. Enantiomer Separation and affinities of enantiomers



MtBE : Ethanol = 98 : 2



MtBE : Ethanol = 98 : 2



MtBE : Ethanol = 96 : 4

**Figure S4:** Chromatograms of enantiomer separation with a chiral column and used solvent composition.

**Table S4:** Determined  $K_D$  values for the separated enantiomers.

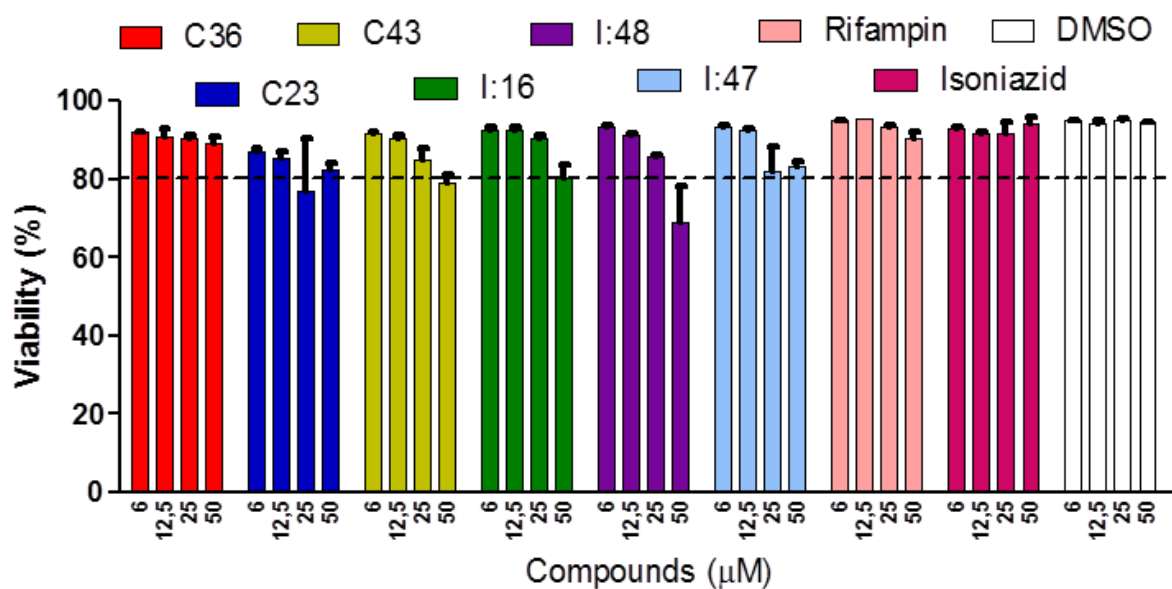
	$K_D$ [ $\mu$ M]		
	Rac.	E1	E2
<b>S1</b>	0.8	0.9	0.7
<b>S4</b>	5.8	6.1	2.6
<b>S5</b>	6.7	9.6	4.6

## 5. *In vitro* inhibition of cYY conversion: IC<sub>50</sub> values

**Table S5:** IC<sub>50</sub> values for reference compound econazole, hit compound **I:47** and the identified potent inhibitors **L10**, **L21** and **L15**.

Compound	IC <sub>50</sub> [μM]	
	Product formation	Substrate depletion
Econazole	11	8
<b>I:47</b>	36	34
<b>L10</b>	23	19
<b>L21</b>	24	21
<b>L15</b>	26	21

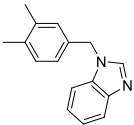
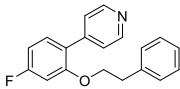
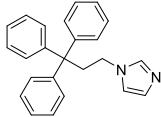
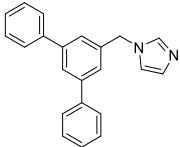
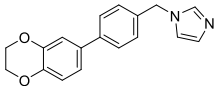
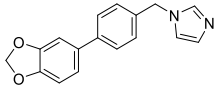
## 6. Cytotoxicity toward Macrophages



**Figure S6:** Cytotoxicity toward macrophages at compound concentrations of 50, 25, 12.5 and 6 μM after 48 h.

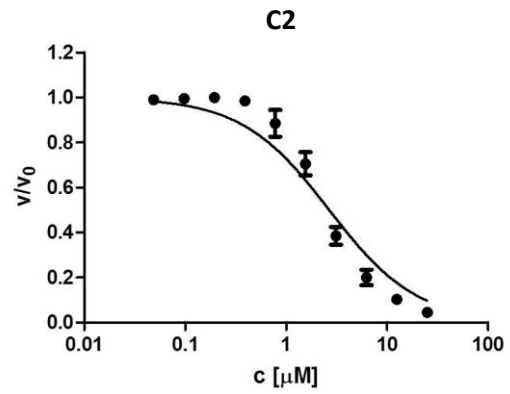
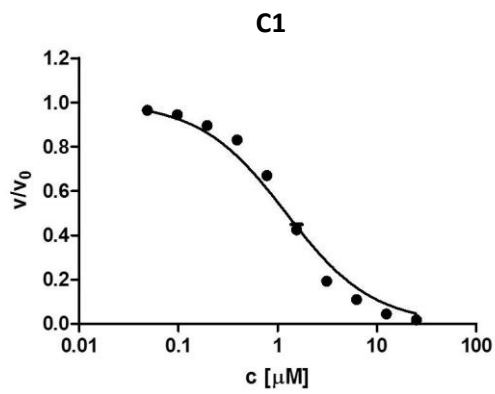
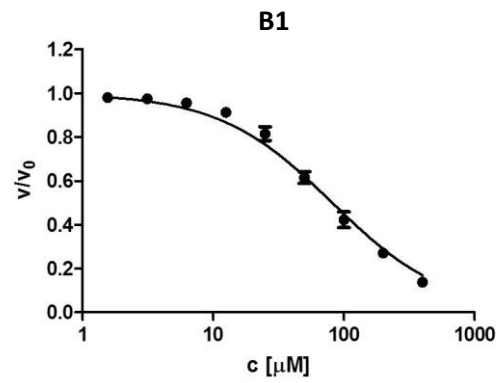
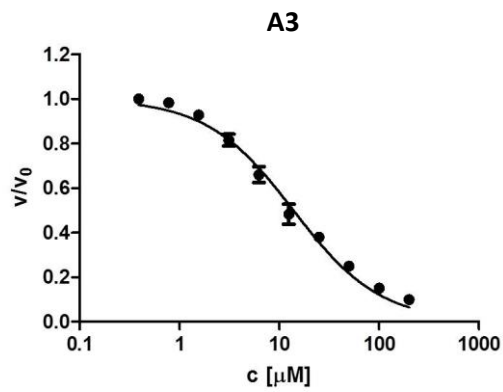
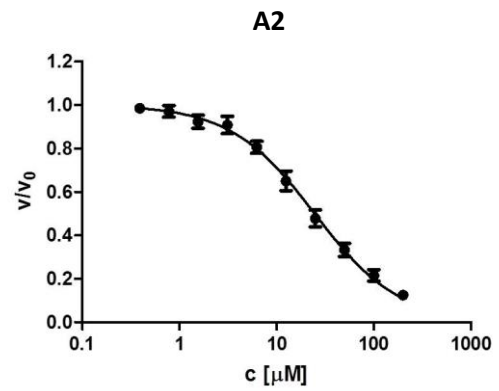
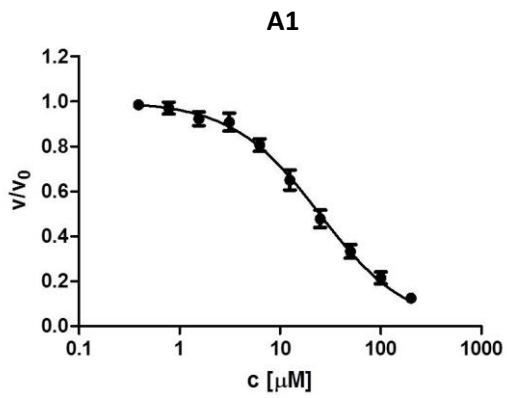
## 7. Intracellular Replication in Macrophages: Affinities toward CYP121 and CYP125

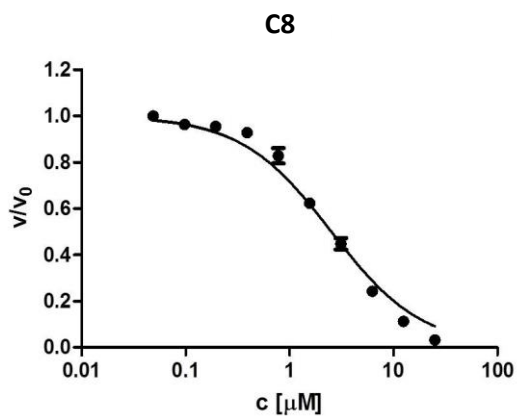
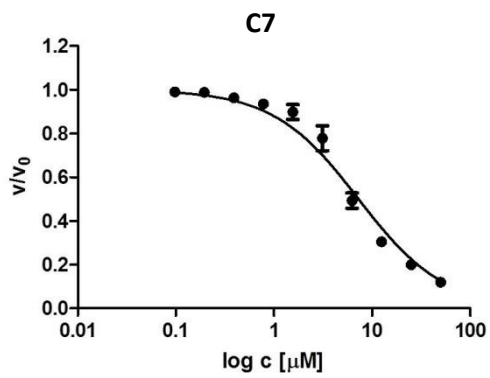
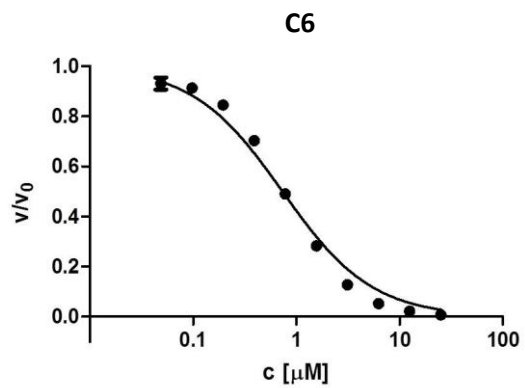
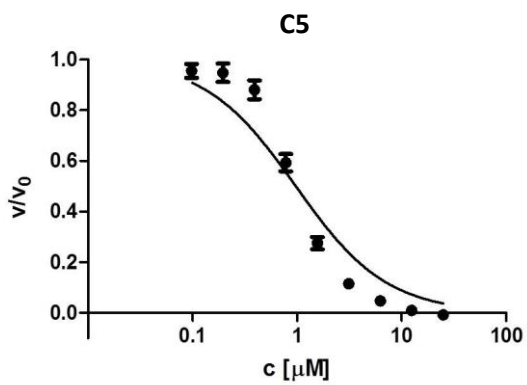
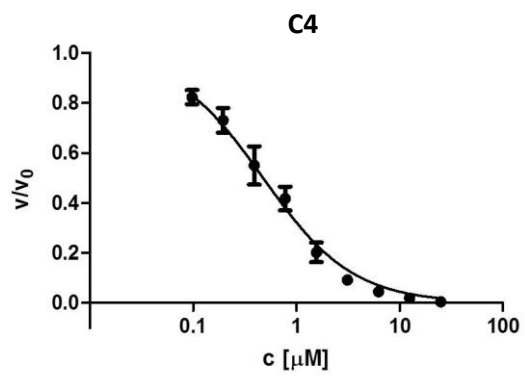
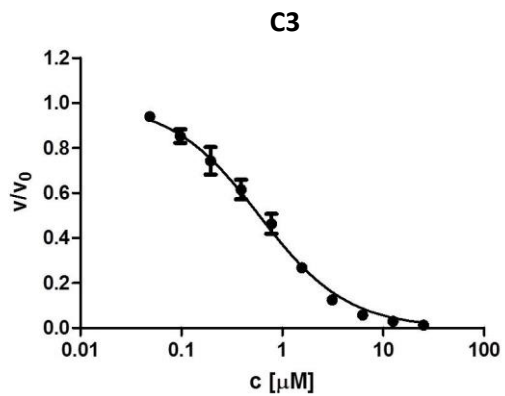
**Table S7:** Affinities toward CYP121 and CYP125 of compounds evaluated against intracellular replication in macrophages.<sup>186,197</sup>

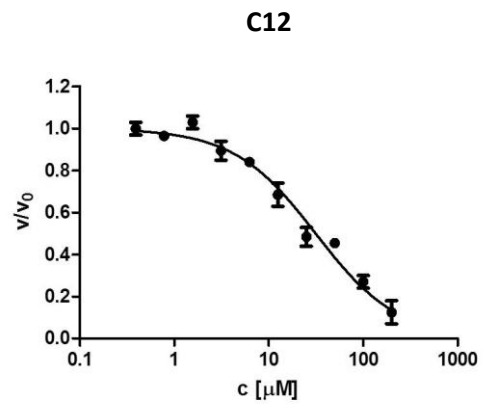
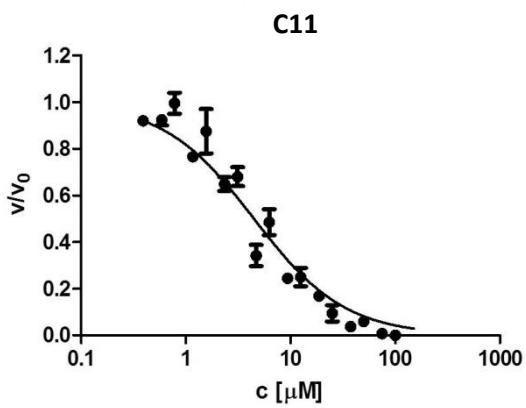
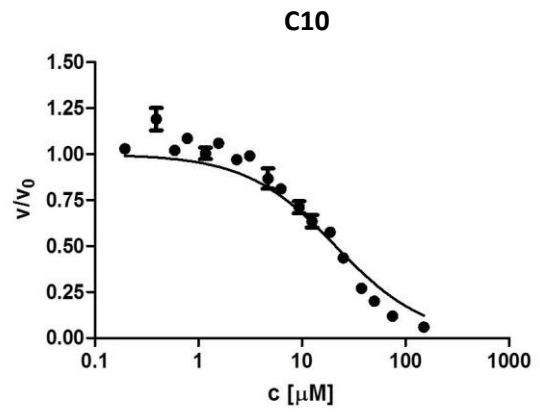
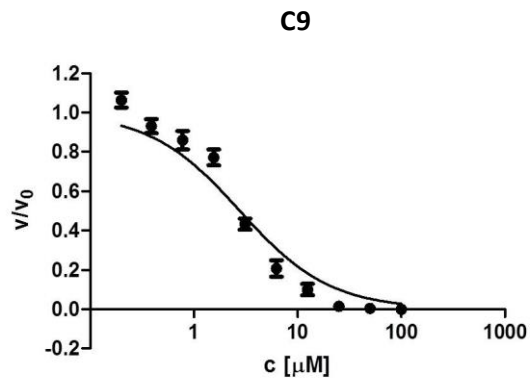
Compound	Structure	K <sub>D</sub> CYP121 [μM]	K <sub>D</sub> CYP125 [μM]
C36		>100	1.3 ± 0.7
C23		7.2 ± 0.5	1.5 ± 0.6
C43		8.8 ± 3.0	13.1 ± 0.9
I:16		1.3 ± 0.4	no SPR response
I:48		5.3 ± 0.6	Not tested
I:47		5.4 ± 1.0	Not tested

## 7.1.3 Supporting Information for Chapter 3.3

### 1. IC<sub>50</sub> Determination

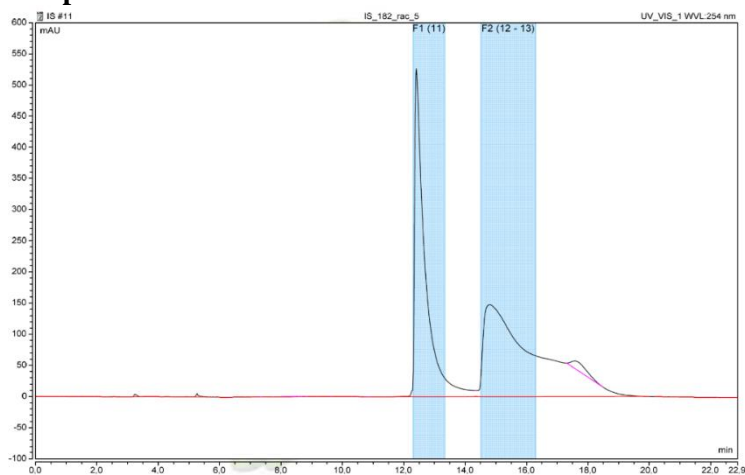




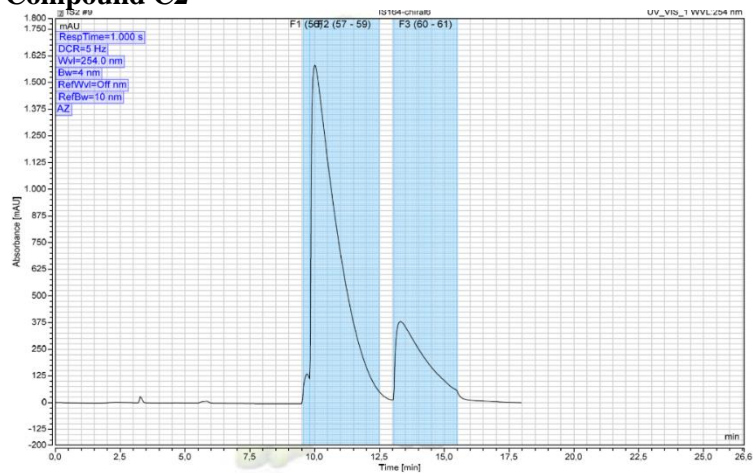


## 2. Enantiomer Separation

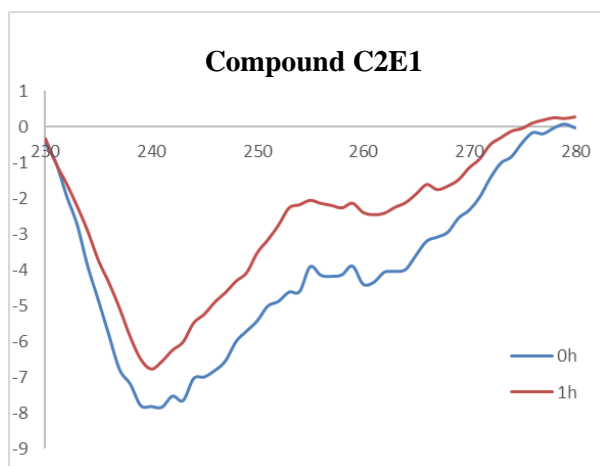
### Compound C1



## Compound C2



## 3. CD Spectra



#### 4. Crystallographic Data

Table 1. Data collection and refinement statistics.

	Compound <b>C1</b>
Resolution range	33.62 - 1.65 (1.709 - 1.65)
Space group	P 1 21 1
Unit cell	39.428 92.603 40.771 90 114.058 90
Total reflections	60992 (6122)
Unique reflections	30874 (3072)
Multiplicity	2.0 (2.0)
Completeness (%)	92.45 (96.48)
Mean I/sigma(I)	18.09 (5.02)
R-merge	0.03211 (0.15)
R-work	0.2019 (0.2131)
R-free	0.2176 (0.2399)
Number of non-hydrogen atoms	2717
macromolecules	2291
ligands	38
solvent	388
Protein residues	298
RMS(bonds)	0.003
RMS(angles)	0.60
Ramachandran favored (%)	95.95
Ramachandran allowed (%)	3.72
Ramachandran outliers (%)	0.34
Rotamer outliers (%)	0.86
Clashscore	3.17
Average B-factor	19.54
macromolecules	17.47
ligands	37.30
solvent	30.02

Statistics for the highest-resolution shell are shown in parentheses.

## 7.1.4 Supporting Information for Chapter 3.4

### SUPPORTING INFORMATION TO THE PUBLICATION

#### Tackling *Pseudomonas aeruginosa* Virulence by a Hydroxamic Acid Based LasB Inhibitor

Andreas M. Kany<sup>†</sup>, Asfandyar Sikandar<sup>‡</sup>, Samir Yahiaoui<sup>†</sup>, Jörg Haupenthal<sup>†</sup>, Isabell Walter<sup>†</sup>, Martin Empting<sup>†</sup>, Jesko Köhnke<sup>‡</sup>, Rolf W. Hartmann<sup>\*,†,§</sup>

<sup>†</sup> Department of Drug Design and Optimization, Helmholtz Institute for Pharmaceutical Research Saarland (HIPS), Campus E8.1, 66123, Saarbrücken, Germany

<sup>‡</sup> Workgroup Structural Biology of Biosynthetic Enzymes, Helmholtz Institute for Pharmaceutical Research Saarland (HIPS), Campus E8.1, 66123, Saarbrücken, Germany

<sup>§</sup> Department of Pharmacy, Pharmaceutical and Medicinal Chemistry, Saarland University, Campus E8.1, 66123 Saarbrücken, Germany

\* Rolf.Hartmann@helmholtz-hzi.de

**Table of Contents**

1 Supporting Tables and Figures..... S3

2 Synthesis..... S5

3 References .....**SError! Bookmark not defined.**

S2

## 1 Supporting Tables and Figures

Table S1. Data collection and refinement statistics.

<b>LasB-7</b>	
Resolution range	61.26 - 2.1 (2.175 - 2.1)
Space group	P 21 21 21
Unit cell	43.7 53.0 122.5 90 90 90
Total reflections	88777
Unique reflections	16581 (1575)
Multiplicity	5.3 (5.4)
Completeness (%)	95.88 (93.64)
Mean I/sigma(I)	4.3 (1.9)
R-merge	0.257 (0.689)
R-work	0.1828 (0.2210)
R-free	0.2102 (0.3084)
Number of non-hydrogen atoms	2641
macromolecules	2317
ligands	29
solvent	295
Protein residues	300
RMS(bonds)	0.004
RMS(angles)	0.94
Ramachandran favored (%)	95.27
Ramachandran allowed (%)	4.39
Ramachandran outliers (%)	0.34
Rotamer outliers (%)	0.00
Clashscore	2.00
Average B-factor	17.59
macromolecules	16.44
ligands	24.71
solvent	25.92

Statistics for the highest-resolution shell are shown in parentheses.

Table S2. Residual LasB activity at each tested concentration of **7** in the in vitro inhibition assay. Mean and SD of four independent measurements are shown.

<b>7</b> [ $\mu\text{M}$ ]	350	175	87,5	43,75	21,88	10,94	5,47	2,73	1,37	0,68
Residual activity [%]	4.0 $\pm$ 2.0	9.3 $\pm$ 2.8	16.9 $\pm$ 2.7	30.9 $\pm$ 3.6	45.9 $\pm$ 5.2	62.3 $\pm$ 6.6	74.6 $\pm$ 7.5	82.4 $\pm$ 9.6	87.7 $\pm$ 9.9	93.1 $\pm$ 8.0

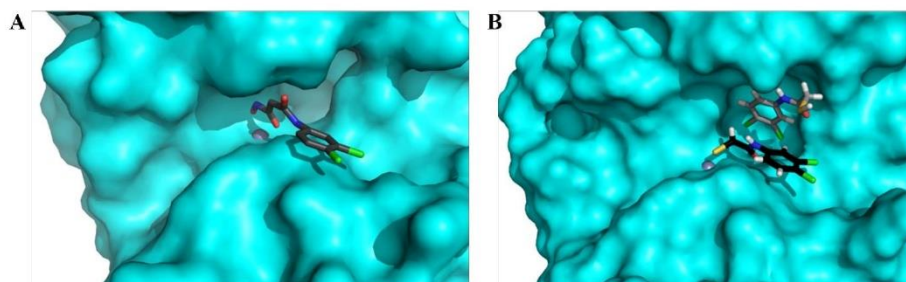


Figure S1. (A) Binding of the hydroxamate compound **7** leads to a closed conformation of the LasB active site. (B) In contrast, binding of the recently reported thiol inhibitor of LasB (**1**) arrests the enzyme in an open conformation. LasB is shown as a cyan surface representation, the active-site Zinc ion as a grey sphere and ligand molecules as grey/black sticks.

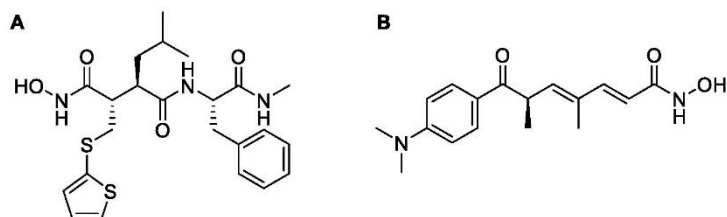


Figure S2. Structure of MMP inhibitor Batimastat<sup>1</sup> (A) and HDAC inhibitor Trichostatin A<sup>2</sup> (B).

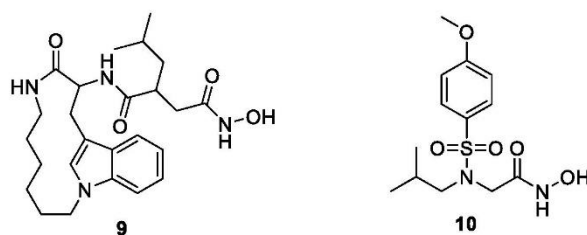


Figure S3. Structures of published hydroxamate-based MMP-7 inhibitor **9**<sup>3</sup> and MMP-3 inhibitor **10**<sup>4</sup>.

## 2 Synthesis

*4-((3,4-dichlorophenyl)amino)-4-oxobutanoic acid (3)*. 3,4-dichloroaniline (160 mg, 0.99 mmol) was placed in a crimp vial and dissolved in 5 mL of dioxane at 70°C. Succinic anhydride (105 mg, 1.05 mmol) was added. The reaction was stirred at 70°C for 6 hours. Hydrochloric acid (2 M, 2 mL) was added and the aqueous phase was extracted with ethyl acetate, washed with brine and dried over magnesium sulfate and concentrated under reduced pressure. The crude was purified using automated flash chromatography (reversed-phase: acetonitrile + 0.1% formic acid:water + 0.1% formic acid 15:85 to 65:35) to yield the title compound as a white powder (152 mg, 59%). <sup>1</sup>H NMR (300 MHz, DMSO-d<sub>6</sub>) δ ppm 2.37 - 2.49 (m, 4 H), 7.36 - 7.44 (dd, *J* = 8.8, 2.3 Hz, 1 H), 7.48 (d, *J* = 8.8 Hz, 1 H), 7.93 (d, *J* = 2.2 Hz, 1 H), 10.21 (s, 1 H), 11.57 - 12.75 (br. s, 2 H); <sup>13</sup>C NMR (75 MHz, DMSO-d<sub>6</sub>) δ ppm 28.6, 31.1, 118.9, 120.1, 124.3, 130.6, 131.0, 139.3, 170.7, 173.7; MS (ESI<sup>+</sup>) *m/z* 262 (M+H)<sup>+</sup>

*(Z)-4-((3,4-dichlorophenyl)amino)-4-oxobut-2-enoic acid (4)*. 3,4-dichloroaniline (170 mg, 1.05 mmol) was placed in a crimp vial and dissolved in 5 mL of dioxane at 70°C. Maleic anhydride (103 mg, 1.05 mmol) was added. The reaction was stirred at 70°C for 6 hours. Filtration of the formed precipitate gave the title compound as a white powder (151 mg, 55%). <sup>1</sup>H NMR (300 MHz, DMSO-d<sub>6</sub>) δ ppm 6.32 (d, *J* = 11.9 Hz, 1 H), 6.48 (d, *J* = 11.9 Hz, 1 H), 7.50 (dd, *J* = 8.9, 2.4 Hz, 1 H), 7.59 (d, *J* = 8.8 Hz, 1 H), 8.01 (d, *J* = 2.3 Hz, 1 H), 10.6 (s, 1 H), 12.76 - 13.04 (br s., 1 H); <sup>13</sup>C NMR (75 MHz, DMSO-d<sub>6</sub>) δ ppm 119.4, 120.5, 125.1, 130.1, 130.7, 131.0, 131.6, 138.8, 163.7, 166.8; MS (ESI<sup>+</sup>) *m/z* 260 (M+H)<sup>+</sup>

*Methyl-3-((3,4-dichlorophenyl)amino)-3-oxopropanoate (5)*. 3,4-dichloroaniline (500 mg, 3.1 mmol) was dissolved in 10 mL of dichloromethane under cooling on ice. Triethylamine (850 μL, 6.2 mmol) were added, followed stepwise by methyl malonyl chloride (520 μL, 4.9 mmol). The mixture was warmed to room temperature and stirred for 4 hours. The organic phase was washed with saturated ammonium bicarbonate solution. The crude was purified automated flash chromatography (petroleum ether:ethyl acetate 80:20 to 5:95) to yield the title compound as a white powder (548 mg, 67%). <sup>1</sup>H NMR (300 MHz, DMSO-d<sub>6</sub>) δ ppm 3.49 (s, 2 H), 3.66 (s, 3 H), 7.45 (dd, *J* = 8.9, 2.4 Hz, 1 H), 7.58 (d, *J* = 8.8 Hz, 1 H), 7.96 (d, *J* = 2.4 Hz, 1 H), 10.49 (s, 1 H); <sup>13</sup>C NMR (75 MHz, DMSO-d<sub>6</sub>) δ ppm 43.5, 52.0, 119.1, 120.3, 125.0, 130.8, 131.0, 138.8, 164.5, 167.8; MS (ESI<sup>+</sup>) *m/z* 262 (M+H)<sup>+</sup>

*3-((3,4-dichlorophenyl)amino)-3-oxopropanoic acid (6)*. **5** (150 mg, 0.57 mmol) was dissolved in 4 mL of tetrahydrofuran. Sodium hydroxide solution (2 M, 570 μL) was added, followed stepwise by 1.43 mL of water. The mixture was stirred at room temperature for 24 hours. The aqueous phase was extracted with diethyl ether. After addition of 5 mL of water, the aqueous phase was extracted with ethyl acetate, dried over magnesium sulfate and concentrated under reduced pressure to yield the title compound as a white powder (115 mg, 81%). <sup>1</sup>H NMR (300 MHz, DMSO-d<sub>6</sub>) δ ppm 3.36 (s, 2 H), 7.46 (dd, *J* = 8.9, 2.4 Hz, 1 H), 7.58 (d, *J* = 8.8 Hz, 1 H), 7.98 (d, *J* = 2.3 Hz, 1 H), 10.43 (s, 1 H),

12.48 - 12.94 (br. s, 1 H);  $^{13}\text{C}$  NMR (75 MHz,  $\text{DMSO-d}_6$ )  $\delta$  ppm 44.0, 119.1, 120.2, 124.8, 130.8, 131.0, 139.0, 165.1, 168.9; MS (ESI $^+$ )  $m/z$  248 (M+H) $^+$

*N*<sup>1</sup>-(3,4-dichlorophenyl)-*N*<sup>3</sup>-hydroxymalonamide (**7**). Hydroxylamine hydrochloride (106 mg, 1.52 mmol) was dissolved in 10 mL of methanol. *N,N*-Diisopropylethylamine (280  $\mu\text{l}$ , 1.68 mmol) was added. The mixture was stirred at room temperature for 30 minutes. **5** (100 mg, 0.84 mmol) was added and the reaction refluxed for 8 hours, followed by 16 hours at room temperature. The mixture was acidified with hydrochloric acid until pH 1 and extracted with ethyl acetate. The organic phase was washed with brine, dried over magnesium sulfate and concentrated under reduced pressure. The crude was purified using automated flash chromatography (reversed-phase: acetonitrile + 0.1% formic acid:water + 0.1% formic acid 20:80 to 100:0) to yield the title compound as a white powder (27 mg, 27%).  $^1\text{H}$  NMR (300 MHz,  $\text{DMSO-d}_6$ )  $\delta$  ppm 3.12 (s, 2 H), 7.48 (dd,  $J = 8.9, 2.4$  Hz, 1 H), 7.57 (d,  $J = 8.9$  Hz, 1 H), 7.98 (d,  $J = 2.3$  Hz, 1 H), 8.99 (s, 1 H), 10.42 (s, 1 H), 10.62 (s, 1 H);  $^{13}\text{C}$  NMR (75 MHz,  $\text{DMSO-d}_6$ )  $\delta$  ppm 44.5, 119.6, 120.7, 125.3, 131.3, 131.5, 139.5, 165.6, 169.4; MS (ESI $^+$ )  $m/z$  263 (M+H) $^+$

*N*-(3,4-dichlorophenyl)-2-hydroxyacetamide (**8**). 3,4-dichloroaniline (200 mg, 1.23 mmol) and glycolic acid (94 mg, 1.24 mmol) were placed in a crimp vial. The vial was sealed and heated to 130°C for 24 hours. The crude was purified using flash chromatography (petroleum ether:ethyl acetate 70:30 to 60:40) to yield the title compound as a white powder (156 mg, 58%).  $^1\text{H}$  NMR (300 MHz,  $\text{DMSO-d}_6$ )  $\delta$  ppm 4.00 (s, 2 H) 5.50 – 6.00 (br. s, 1 H) 7.56 (d,  $J = 8.9$  Hz, 1 H) 7.70 (dd,  $J = 8.8, 2.5$  Hz, 1 H) 8.11 (d,  $J = 2.4$  Hz, 1 H) 9.76 – 10.23 (br. s, 1 H);  $^{13}\text{C}$  NMR (75 MHz,  $\text{DMSO-d}_6$ )  $\delta$  ppm 61.9, 119.7, 120.8, 124.8, 130.5, 130.8, 138.7, 171.5; MS (ESI $^+$ )  $m/z$  220 (M+H) $^+$

## References

- 1 Rasmussen, H. S., McCann, P. P. (1997) Matrix metalloproteinase inhibition as a novel anticancer strategy. A review with special focus on batimastat and marimastat. *Pharmacol. Ther.* 75, 69–75.
- 2 Drummond, D. C., Noble, C. O., Kirpotin, D. B., Guo, Z., Scott, G. K., Benz, C. C. (2005) Clinical development of histone deacetylase inhibitors as anticancer agents. *Annu. Rev. Pharmacol. Toxicol.* 45, 495–528. DOI: 10.1146/annurev.pharmtox.45.120403.095825.
- 3 Browner, M. F., Smith, W. W., Castelhana, A. L. (1995) Matrilysin-inhibitor complexes. Common themes among metalloproteases. *Biochemistry.* 34, 6602–6610.
- 4 Belviso, B. D., Caliandro, R., Siliqi, D., Calderone, V., Arnesano, F., Natile, G. (2013) Structure of matrix metalloproteinase-3 with a platinum-based inhibitor. *Chem. Commun. (Cambridge, U. K.)*. 49, 5492–5494. DOI: 10.1039/c3cc41278d.

## 7.2 Conference Contributions

### Poster presentations:

#### **Topic: “Biophysical Screening of a Focused Library for the Discovery of Novel Antimycobacterials targeting CYP121”**

Schnorr, Isabell, Thomann, Andreas, Brengel, Christian, Schifrin, Alexander, Bernhard, Rita, Allegretta, Giuseppe, Kamal, Ahmed, Haupenthal, Jörg, Eberhard, Jens, Empting, Martin, Cho, Sang Hyun, Franzblau, Scott G. Hartmann, Rolf W

6th International HIPS Symposium, June 2016, Saarbrücken, Germany

Doktorandentag der Fakultät NT Universität des Saarlandes, November 2016, Saarbrücken, Germany

Frontiers in Medicinal Chemistry, February 2017, Bern, Switzerland

7th International HIPS Symposium, June 2017, Saarbrücken, Germany

#### **Topic: “CYP121 and CYP125 as Targets for Novel Antimycobacterials”**

Schnorr, Isabell, Thomann, Andreas, Brengel, Christian, Schifrin, Alexander, Allegretta, Giuseppe, Kamal, Ahmed, Eberhard, Jens, Empting, Martin, Cho, Sang Hyun, Franzblau, Scott G., Hartmann, Rolf W

DPhG Jahrestagung, September 2017, Saarbrücken, Germany

#### **Topic: “Biophysical Screening of a CYP-Inhibitor Library for the Discovery of Novel Antimycobacterials targeting CYP121 and CYP125”**

Walter, Isabell, Thomann, Andreas, Brengel, Christian, Schifrin, Alexander, Allegretta, Giuseppe, Empting, Martin, Cho, Sang Hyun, Franzblau, Scott G. Hartmann, Rolf W

Frontiers in Medicinal Chemistry, March 2018, Jena, Germany

8th International HIPS Symposium, June 2018, Saarbrücken, Germany